R-9315

EXPERIMENTAL INVESTIGATION OF COMBUSTOR EFFECTS ON ROCKET THRUST CHAMBER PERFORMANCE

Final Report

Prepared by

W. H. Nurick

W. S. Hines

Members of Technical Staff

Advanced Programs

Approved by

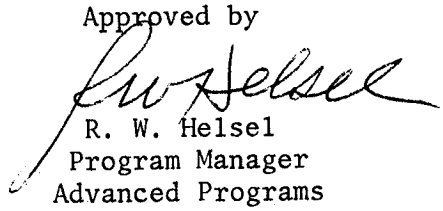

R. W. Helsel
Program Manager
Advanced Programs

Prepared For

National Aeronautics and Space Administration
Lyndon B. Johnson Spacecraft Center
Houston, Texas

September 1973

Contract NASw-2106

Rocketdyne Division,
Rockwell International
6633 Canoga Avenue
Canoga Park, California 91304

FOREWORD

This report was prepared for the National Aeronautics and Space Administration, Lyndon B. Johnson Spacecraft Center, by Rocketdyne Division, Rockwell International. The study was conducted in accordance with Contract NASw-2106 during the period 16 October 1970 to 15 September 1973. The NASA technical monitor was Mr. R. Kahl. At Rocketdyne, Mr. R. W. Helsel was the program manager; Mr. W. H. Nurick was the project engineer, reporting to Dr. D. T. Campbell. Mr. Nurick was assisted by Mr. A. W. Huebner in the engine firing program, Dr. V. H. Dayan, who performed the chemical analysis of the rocket nozzle exhaust species, and Messrs. W. D. Chadwick, R. D. Tobin, and W. S. Hines in the analysis of the experimental data and their correlation to the theoretical predictions of the JANNAF system of computer programs.

This report has been assigned Rocketdyne Report Number R-9315.

ABSTRACT

This report presents the results of a program to develop special instrumentation systems and engine hardware, conduct tests using LOX/GH_2 propellants wherein radial mixture ratio stratification was controlled, and subsequently compare the results of four selected tests with the predictions of the JANNAF performance-prediction computer programs. During the experiments, the overall propellant mixture ratio was varied from 4.4 to 6.6, while the mixture ratios in the core and outer zone were varied from 5.7 to 8.8 and from 3.7 to 7.2, respectively. A nominal 10 percent of the total fuel flow was used as boundary layer coolant in a majority of the firings. Nominal chamber pressure was either 225 or 250 psia, with nozzle expansion ratios of either 25:1 or 4:1. Measurements of the axial chamber pressure and wall heat flux profiles, together with samples of the exhaust gas, were obtained. The corrected experimental specific impulse and characteristic exhaust velocity efficiencies were approximately 97.5 and 98.5 percent, respectively. Although the accuracy of the exhaust gas sampling was limited by valve leakage in the sampling system and by apparently incomplete purging of startup contaminents in the short duration tests, the data and analysis indicate that injected mixture ratio bias persists to the nozzle exit. Satisfactory correlation was obtained between the experimental results and calculations made with the computer programs of the JANNAF Performance Standardization Working Group when a limited mixing criterion was applied to the interaction of the outer zone and boundary layer coolant flows.

CONTENTS

ILLUSTRATIONS

TABLES

NOMENCLATURE

A	=	area
C_D	=	discharge coefficient
C_p	=	specific heat
c^*	=	characteristic exhaust velocity
D	=	diameter of drop, jet, or orifice
$\overline{D}$	=	mass median drop diameter
E_M	=	Rupe mixing parameter
F	=	force
F_M	=	fraction mixed
g	=	force/mass conversion factor
h	=	heat transfer coefficient
H	=	enthalpy
I_s	=	specific impulse
K	=	correlation coefficient
L^*	=	characteristic chamber length equal to the chamber volume divided by the throat area
MR	=	mixture ratio
n	=	number of moles
P	=	pressure
ΔP	=	pressure difference
Pr	=	Prandtl number
q/A	=	heat flux
R, r	=	radius
ΔR	=	annular space
T	=	temperature

U_∞ = free-stream velocity

V = injection velocity, volume

$\dot{w}$ = weight flowrate

X_p = penetration distance

z = axial coordinate

GREEK

α = expansion angle

δ^* = displacement thickness

ε = eddy diffusivity, expansion ratio

η = efficiency, coordinate normal to wall

θ = angle between injector face and liquid jet, momentum boundary layer thickness

μ = viscosity

ρ = density

σ = Bartz property correction factor, surface tension

SUBSCRIPTS

BL = boundary layer

C = chamber

c* = characteristic exhaust velocity

CF = cold flow

E = nozzle exit

ER = energy release

f = final, film

FC = film coolant

g = gas

HF = hot fire

HL = heat loss

I_s = specific impulse

L = liquid

LOX = liquid oxygen

max = maximum

min = minimum

mix = mixing

OZ = outer zone

R = recovery

s = shifting

t = throat, turbulent

TDK = calculated by TDK

VAP = vaporization

w = wall

wax = wax

0 = stagnation

1 = first determination

r = energy boundary layer

∞ = outside the boundary

SUPERSCRIPTS

* = throat conditions

INTRODUCTION AND SUMMARY

An analytical, design, and experimental program has been conducted to document the effects of combustor flow striations on rocket thrust chamber performance. The overall project was designed to complement several current analytical programs in support of the goals of the JANNAF Sub-Committee on Liquid Rocket Thrust Chamber Performance.

For the case of efficient homogeneous combustion, analytical techniques for predicting performance of rocket engine nozzles have reached a high degree of perfection over the past several years. The JANNAF Performance Standardization Working Group has created a methodology and a group of computer programs that represent the best analytical techniques available in the industry for bell nozzle engines and show encouraging results when compared with experimental data (only bell nozzle rocket engines have been considered thus far by the JANNAF working group).

However, many rocket engines have neither efficient combustion nor uniformly distributed combustion products. The effects of these two conditions on nozzle performance, which can total several percent, are only now becoming the subject of rigorous analytical studies and, as yet, have not been well documented experimentally. The objectives of this program are:

1. To develop special instrumentation systems and engine hardware, and conduct tests using LOX/GH_2 propellants wherein the flow stratification is controlled
2. To obtain sufficient experimental measurements to show that the quality and completeness of experimental data are sufficient to characterize the major physical processes occurring in the rocket thrust chamber from injection to the exit plane
3. To use the data as a check on the accuracy of JANNAF combustion models at nonhomogeneous conditions

To meet these objectives, a 35-month program, divided into the following five tasks was conducted:

Task I: Design and fabrication effort to obtain an injector containing provisions for three separate flow zones and a heavily instrumented copper thrust chamber/nozzle assembly

Task II: Cold flow experimental effort to characterize the injection elements

Task III: Development of a gas sampling system

Task IV: Conducting hot fire experimental performance testing at altitude conditions

Task V: Analysis of selected tests using the JANNAF computer programs and comparison of the theoretical and experimental results.

The engine firings were made at nominal chamber pressures of 225 and 250 psia, nozzle expansion ratios of 25:1 and 4:1, and overall mixture ratios from 4.4 to 6.6. Stratified flow conditions were obtained by varying the outer zone mixture ratio from 3.7 to 7.2 for core mixture ratios of 5.7 to 8.8; a film coolant nominally equal to 10 percent of the total fuel flowrate was used in most of the tests. Nominal test durations were either 2.0 or 2.5 seconds. Multiple measurements of wall heat flux and chamber pressure were taken at a sufficient number of axial stations to establish the axial profiles.

Samples of the exhaust gas were obtained at either two or three radial stations. These were analyzed by a combination of pressure and volume measurements at two temperature levels to determine the relative amounts of condensible and noncondensible gases, followed by gas chromatography to characterize the noncondensible fraction. Problems were encountered with excessive valve leakage during the early tests. Anomalous results in later tests were attributed to insufficient combustion gas purging of the sample lines in the short duration tests. Despite these problems, the results of the gas sampling experiments indicate a significant radial stratification of the exhaust mixture ratio was produced by propellant mixture ratio bias at the injector.

A theoretical prediction of performance, wall heat flux, and axial chamber pressure profile was made for the conditions of four of the test firings using the STC, TDK, and BLIMP computer programs of the recommended JANNAF methodology. A satisfactory correlation of theoretical and experimental results was obtained if the film coolant was considered to mix with approximately one half of the outer zone flow. This mixing was assumed to be accomplished close to the injector primarily by penetration of the liquid/oxidizer spray into the film coolant layer, rather than by gas-gas mixing over considerable axial distance, as is usually assumed in film cooling application.

The correlation between the theoretical predictions and experimental data indicates that the JANNAF methodology can be used satisfactorily.

The analytical and experimental results of the five program tasks are detailed in the subsequent sections of this report.

TASK I: INJECTOR AND THRUST CHAMBER DESIGN AND FABRICATION

Because the primary objective of this program was to develop the capability for acquiring high quality data, the engine design and operating parameters were selected primarily to support that goal; however, thrust chamber simplicity and durability considerations also exerted a restraining influence on the final choice. For example, both water cooled and heat sink chamber designs were initially considered. Since accurate thrust measurements were crucial to the program objective, a water cooled design was rejected because it required a large number of water lines resulting in an unacceptable thrust bias. A heat sink design was, therefore, selected.

The heat sink thrust chamber design placed limits on chamber pressure and test duration. Since tests of 2 second duration were needed, the chamber pressure was limited to a maximum of 300 psia. Consideration of performance, heat transfer and sampling accuracy resulted in selection of the following nominal design operating conditions for the engine:

Propellants	= LOX/GH_2
Chamber pressure	= 250 psia
Mixture ratio	= 5
Boundary layer cooling	= 0-10 percent
Expansion ratio	= 4 and 25
Test duration	= 2 seconds

INJECTOR DESIGN

To provide meaningful documentation over a range of mass and mixture ratio distributions, the injector was designed for precision control of the oxidizer and fuel flow in several individually supplied radial zones (i.e., "core," "outer ring," and "film coolant ring"). By variation of the individual mixture ratios and total flowrates within each zone, striated flows of differing mass

and mixture ratio were created*. An injector assembly drawing showing the element arrangement on the face and the manifold design is shown in Fig. 1. The major features are:

1. A 96-element injector arranged in four rings with the outer ring propellant feed controlled separately from that of the inner three rings. The element type is an impinging triplet (oxidizer/fuel/oxidizer).
2. A 96-orifice film coolant ring with flow controlled separately from the rest of the injector.
3. Very low velocities in the manifolds feeding the elements to ensure uniform feed to all elements within each zone.
4. A brazed assembly chosen to allow access for contouring the entrances of all orifices (except the film coolant orifices).
5. Element and row spacing selected so that the mass flux will be constant across the injector face if the elements of both zones are run at the same mixture ratio and element flowrate.
6. The film coolant orifices spaced so that every other one is directly outboard of a corresponding outer row element.

Multiple inlets were selected for all but the core fuel to reduce the size of the manifolds. The four injector rings have their respective number of elements and relative spacing designed to produce uniform mass flux across the injector face. All of the rings contain identical triplet elements which are divided 48 in the core (inner three rings) and 48 in the outer ring. When the total flows

---

*Considerable emphasis was placed on designing the injector such that injection uniformity was maintained within each zone, i.e., equal fuel and oxidizer flow rates to each element and elements spaced to provide uniform flow per unit injector face area. It was recognized, however, that any real injection element produces local inhomogeneities of mass flux and mixture ratio. Therefore the Task II cold flow characterization (see later discussion) was conducted (1) to obtain element design criteria for minimizing such non-uniformities and (2) to acquire a quantitative measure of the "mixing" actually achieved.

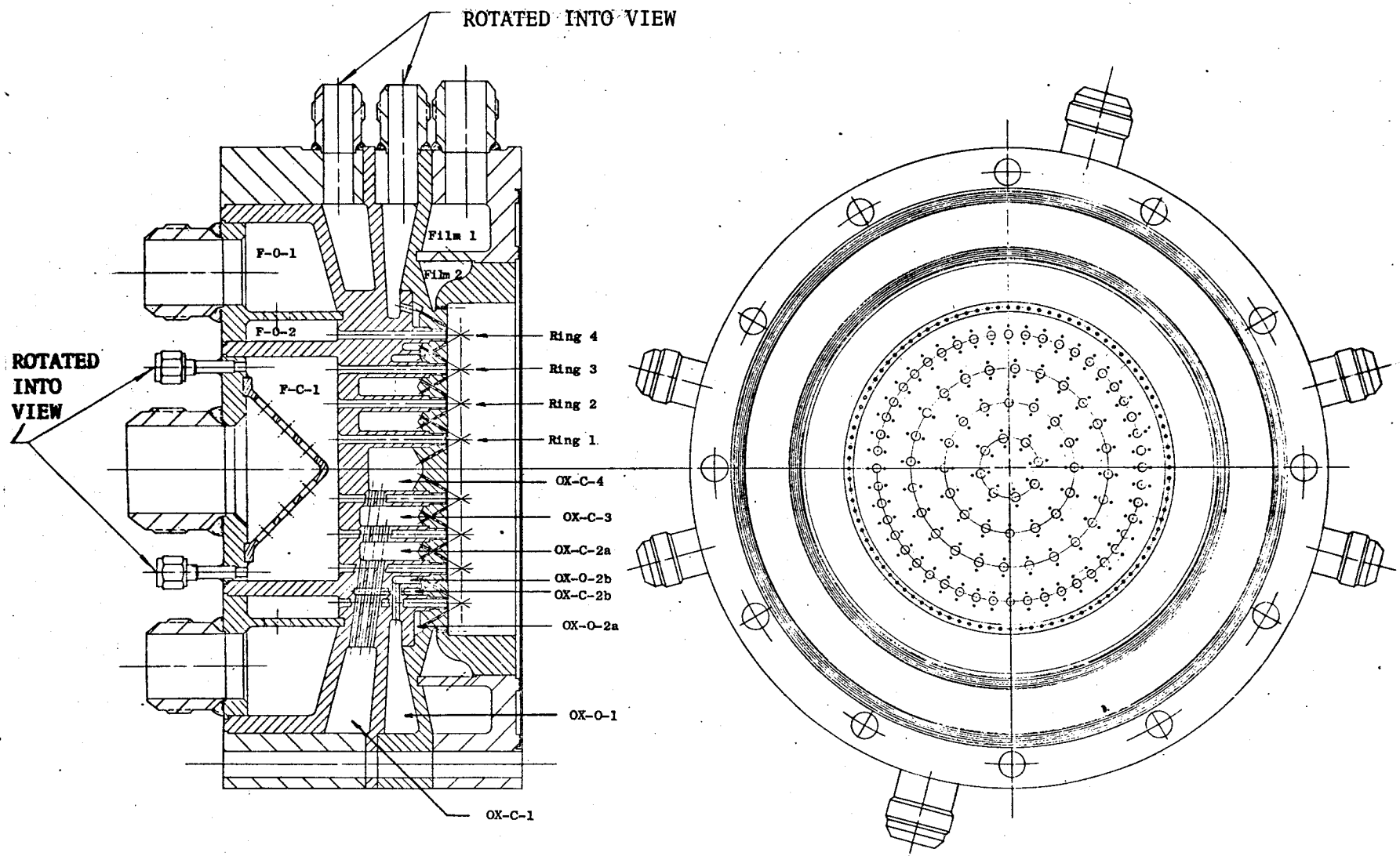

Figure 1. Injector Assembly Drawing

to the core and outer region are equal, the average mass flux for each ring is uniform within 0.6 percent (see Table 1).

The (triplet) injector element is described in Fig. 2 and Table 2. The centerlines of the three (coplanar) streams describe an included impingement angle of 60 degrees and their impingement point is 0.3 inch from the injector face. The orifices have length-to-diameter ratios of 14:1 and contoured inlets were sized to maintain reasonable velocities, Mach numbers, and pressure drops throughout the test range. The nominal orifice flow conditions for the oxidizer and fuel are also summarized in Table 2.

THRUST CHAMBER DESIGN

The thrust chamber was designed as a heat sink calorimeter unit with provisions for extensive instrumentation and for cooling between tests. The combustion chamber design and the attached nozzle skirt are presented in Fig. 3. The chamber material is OFHC copper. The chamber is secured to the injector by 12 bolts which screw into the threaded holes; the nozzle is attached in a similar manner. The combustor L* is 20 inches and the contraction ratio is 2.0 (chamber area divided by nozzle throat area). The water cooling system, used between tests, is not shown in the figure. With low pressure water supply, the heat input to the chamber in a 2-second test can be completely removed in 15 to 20 seconds of cooling time.

The wall radius of curvature upstream of the throat was set equal to 1.5 times the throat radius. This value was selected as being representative of many engine designs and is large enough to facilitate a more accurate theoretical transonic analysis. The large radius used to form the transition from the cylindrical combustion section to the throat circlet was selected to make the turn gradual enough to prevent flow separation, while providing sufficient constant area cylindrical length to simplify the interpretation of chamber pressure measurements. The transition circlet from the throat to the conical nozzle has a radius equal to the throat radius in order to minimize the shock at the tangent

TABLE 1. INJECTOR NOMINAL MASS DISTRIBUTION

Ring Number	Ring Diameter, inches	Ring Area, $in.^2$	Number of Elements	Flow Area**, $lb/sec/in.^2$
1	1.940	2.956	8	0.515
2	3.355	5.885	16	0.516
3	4.7455	8.846	24	0.516
4	6.763	18.236	48	0.518

*Defined at triplet element impingement points

**For equal element flow.

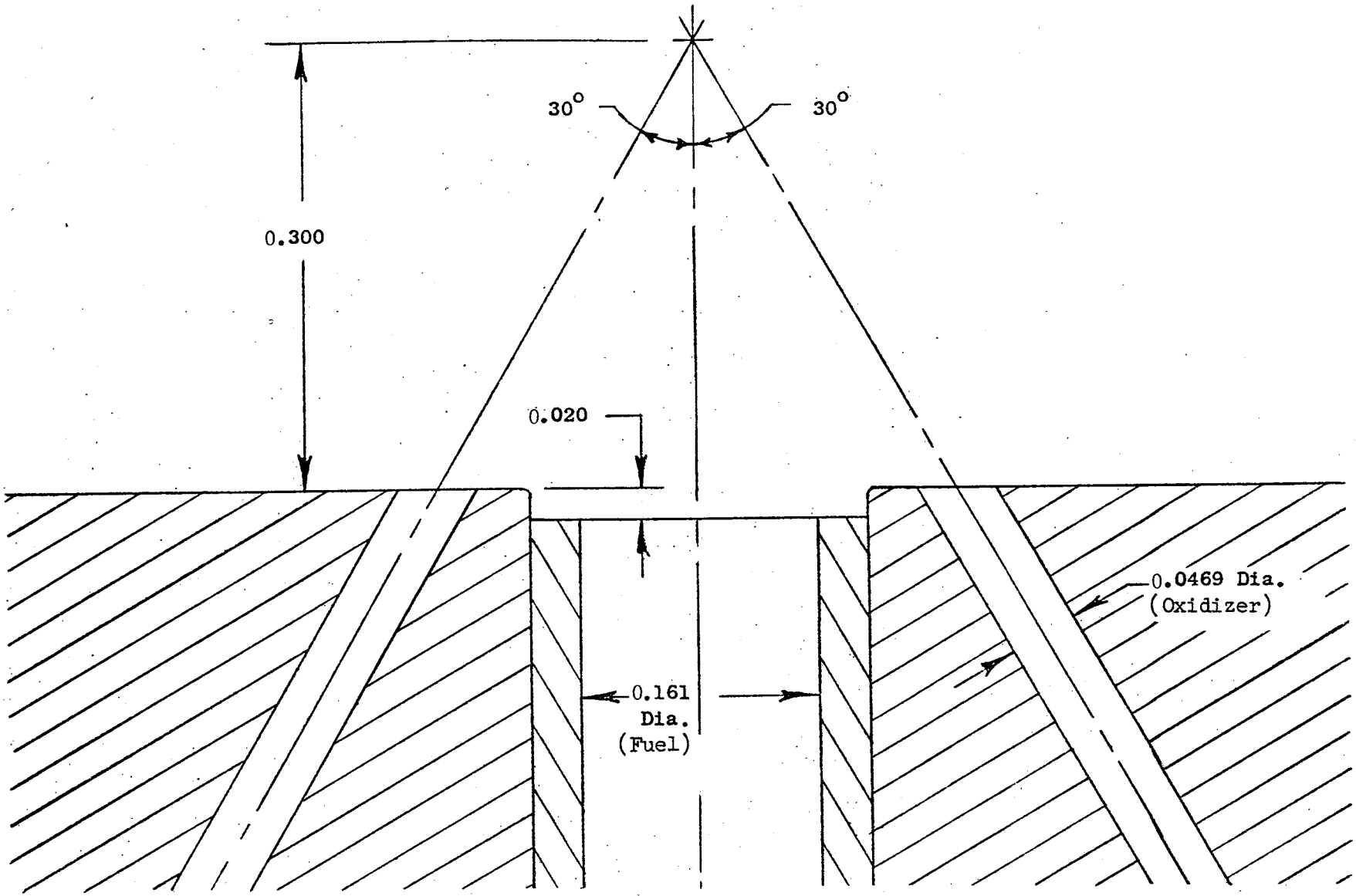

Figure 2 . Injector Element Geometry

TABLE 2. NOMINAL INJECTOR PARAMETERS

	Orifice Diameter, inches	Number of Orifices	Orifice ΔP, psi	Percent Mass	Velocity, ft/sec	Mach Number	L/D
Fuel							
Core	0.161	48	72	8.2	2690	0.620	13.6
Outer	0.161	48	72	8.2	2690	0.620	13.6
Film Coolant	0.052	96	82	1.8	2800	0.645	
Oxidizer							
Core	0.0469	96	141	40.9	126	--	13.5
Outer	0.0469	96	141	40.9	126	--	13.5

Impingement Angle	60 degrees
Impingement Distance	0.30 inch
Chamber Diameter	6.763 inches
Mixture Ratio	
Core	5.0
Outer	5.0
Film Coolant	
Percent of Fuel	10.0

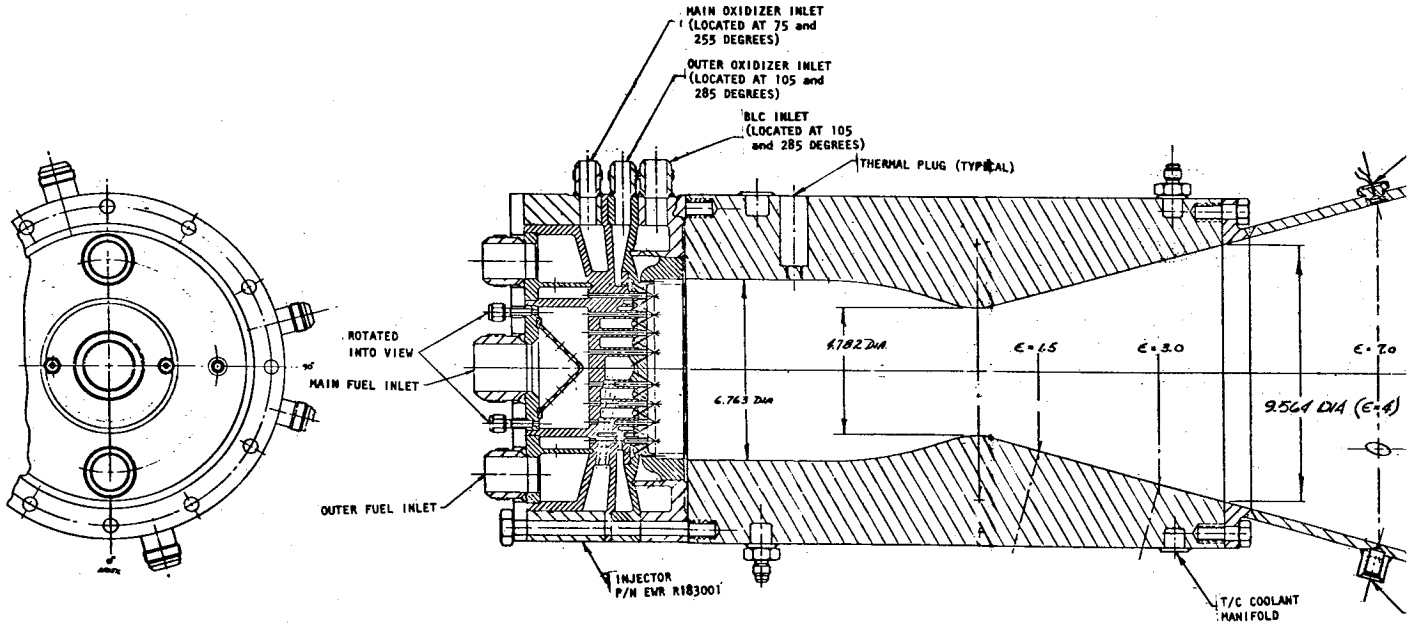
MAIN OXIDIZER INLET
(LOCATED AT 75 and
255 DEGREES)
OUTER OXIDIZER INLET
(LOCATED AT 105 and
285 DEGREES)
BLC INLET
(LOCATED AT 105
and 285 DEGREES)
THERMAL PLUG (TYPICAL)
ROTATED
INTO VIEW
MAIN FUEL INLET
OUTER FUEL INLET
INJECTOR
P/N EWR R183001
T/C COOLANT
MANIFOLD
4.782 DIA
6.763 DIA
ε=1.5
ε=3.0
ε=7.0
9.564 DIA (ε=4)

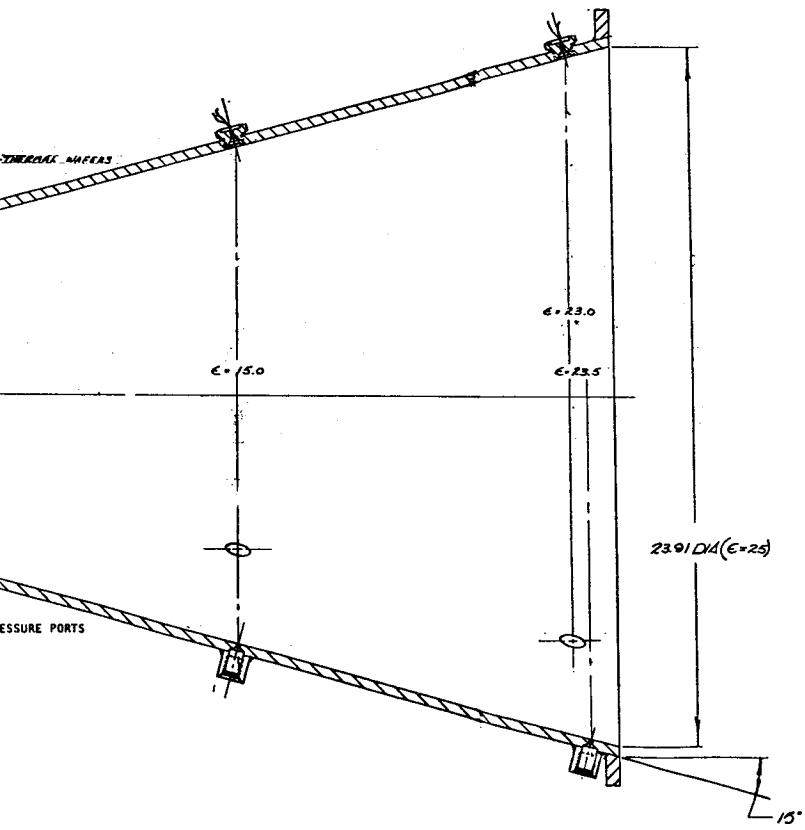

Figure 3. Overall Engine Assembly

point. A 15-degree conical nozzle expansion angle was selected to minimize contour related flow nonuniformities and to simplify interpretation of flow stratification results. The nozzle extension shown in Fig. 3 is made of mild steel. This extension is also a 15-degree conical section starting at an expansion ratio of 4 and terminating at 25.

The chamber and nozzle were fully instrumented for wall pressure and temperature measurements. Tables 3 and 4 list the axial locations of all pressure taps and heat flux gages, and Fig. 4 shows the corresponding circumferential location of these transducers.

Thermal isolation plugs are incorporated into the copper combustion section (T_1 to T_{24}) by machining an annular groove in the bottom of a counter-sunk hole, leaving only a thin supporting web at the inner surface. The groove effectively limits heat conduction to a radial path through the wall. A schematic of this type of isolation slot is shown in Fig. 5. The radial path length (t) for all of these isolation segments is 0.5 inch.

The thermal plugs used in the steel nozzle extension are also shown in Fig. 5. They consist of small copper disks suspended in an insulating environment resulting in fast response and reliable operation. The radial path lengths for these isolation slots are listed in Table 5. Note that the radial path length is considerably shorter for these plugs than for the isolation segments in order to provide desired response at lower anticipated heat flux.

TABLE 3. LOCATION OF PRESSURE TAPS ON CHAMBER/NOZZLE ASSEMBLY

Pressure Tap	Axial Distance from Injector Face* inch	Area Ratio ε
1	1.125	2.0 (Constant Area)
2	"	"
3	3.30	"
4	"	"
5	5.10	"
6	"	"
7	6.85	"
8	"	"
9	14.82	1.5 (Divergent)
10	"	"
11	19.34	3.0 "
12	"	"
13	24.63	5.44 "
14	28.13	7.47 "
15	34.15	11.71 "
16	38.7	15.54 "
17	46.78	23.70 "
18	47.08	24.04 "

*Throat at 12.5 inches

TABLE 4. LOCATION OF TEMPERATURE MEASUREMENTS ON CHAMBER/NOZZLE ASSEMBLY

Temperature Measurement (Thermal Isolation Plugs)	Axial Distance from Injector Face* inch	Area Ratio, ε
T-1	1.125	2.0 (Constant Area)
2	"	"
3	2.84	"
4	"	"
5	5.51	"
6	"	"
7	6.85	"
8	"	"
9	8.18	Convergent
10	"	"
11	9.52	"
12	"	"
13	10.86	"
14	"	"
15	12.19	"
16	"	"
17	"	"
18	12.8	Divergent
19	"	"
20	"	"
21	14.82	"
22	"	"
23	19.34	"
24	"	"
25+	24.6	5.44
26+	"	"
27+	34.2	11.71
28+	"	"
29+	46.8	23.70
30+	"	23.58

*Throat at 12.5 inches
+Heat flux wafers

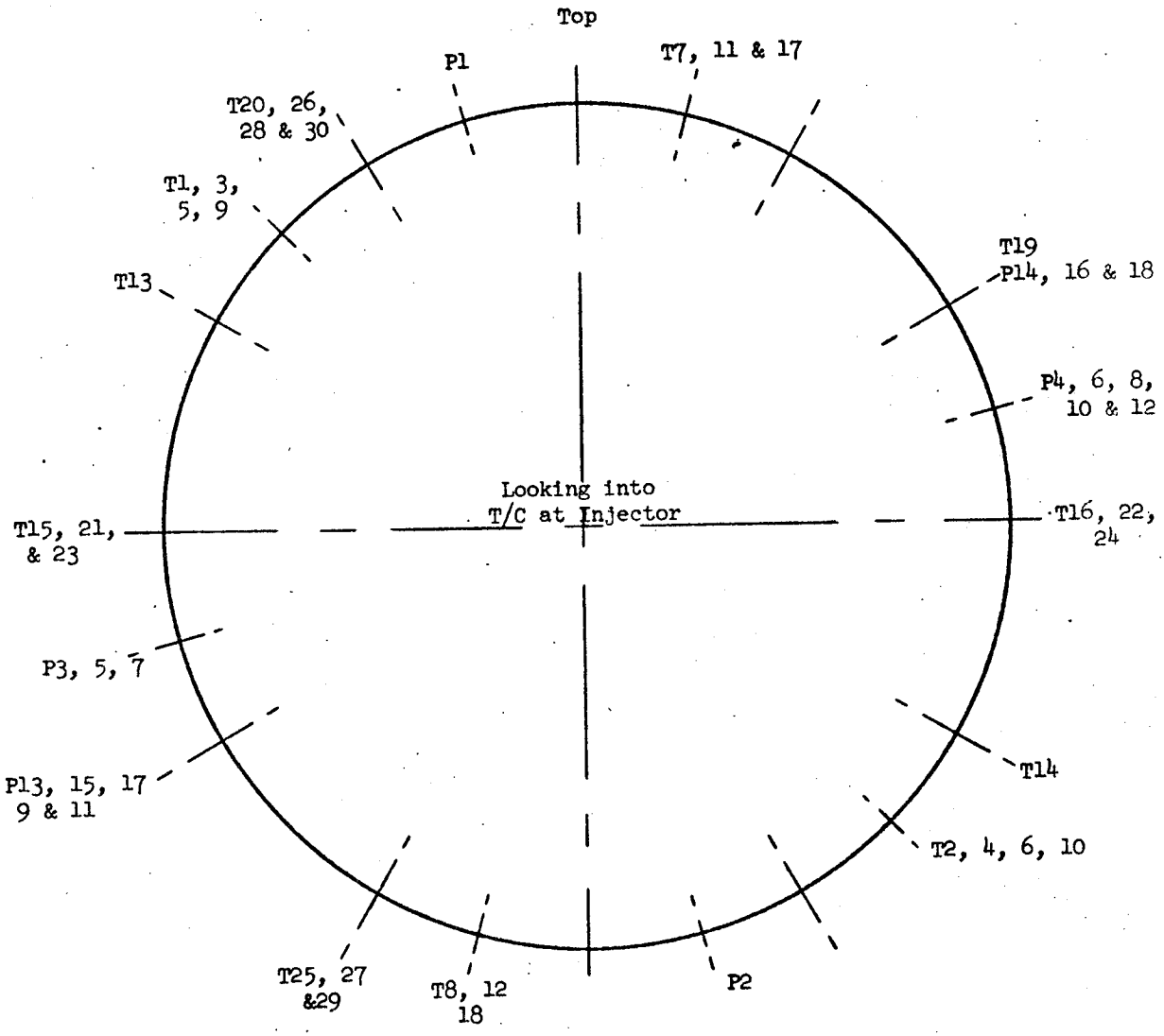

Figure 4. Circumferential Location of Pressure Taps and Wall Temperature Thermocouples

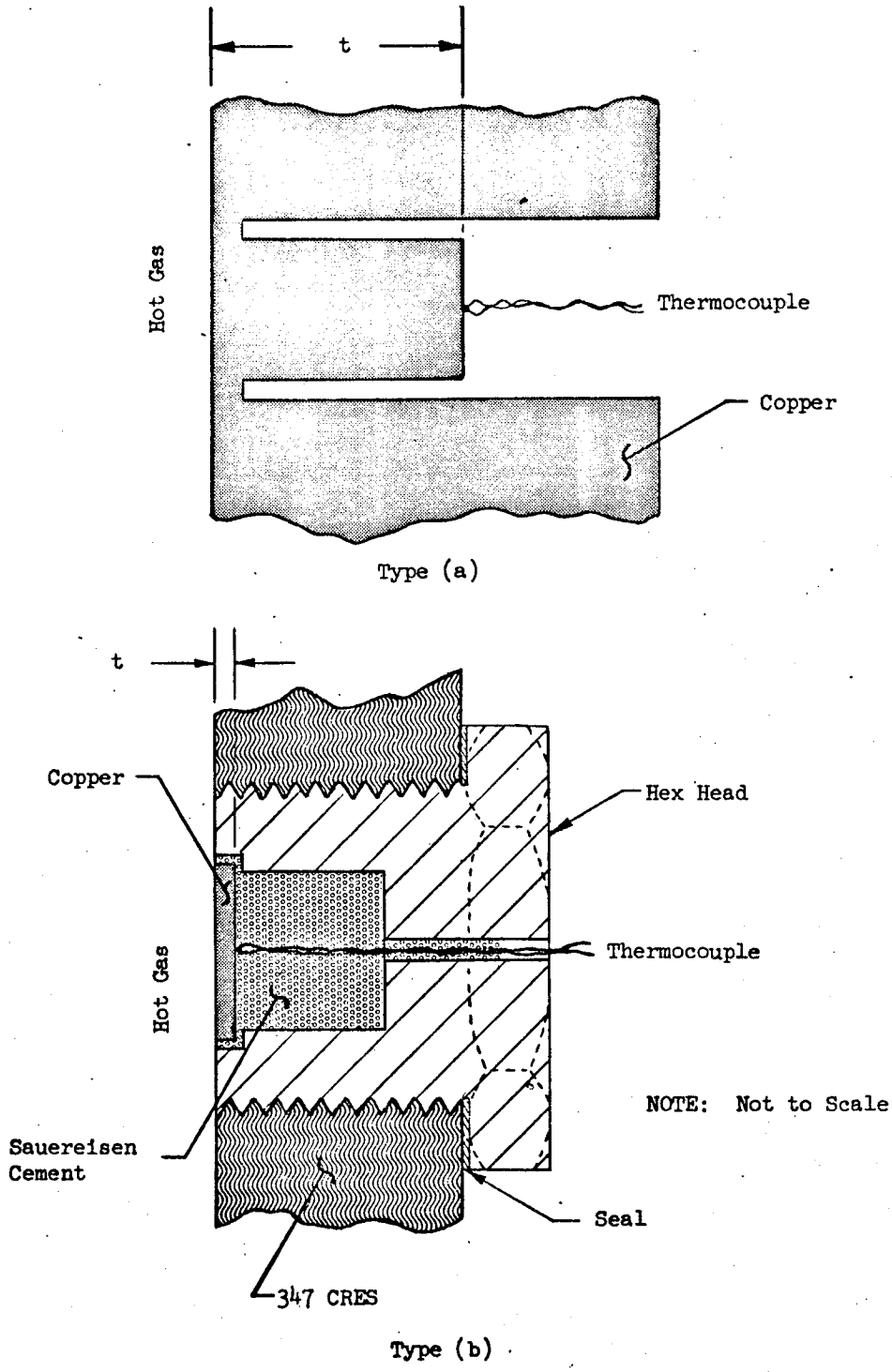

Figure 5. Schematic Cross Sections of Heat Transfer Isolation Segments

TABLE 5. RADIAL PATH LENGTHS FOR THERMAL PLUGS IN NOZZLE

Thermal Plug Designation*	Radial Path Length, inch
25	0.021
26	0.020
27	0.016
28	0.021
29	0.035
30	0.028

*Refer to Table 4 for the corresponding axial location of each thermal plug.

TASK II - INJECTOR COLD-FLOW CHARACTERISTICS

Cold-flow characterization of the injector was performed to provide an experimental description of the actual mass flux and mixture ratio distributions produced by the injector for comparison with the results of gas sampling and zone radiometric analysis in the nozzle exhaust. It also serves to provide input for theoretical combustion model analyses. In particular, the Distributed Energy Release (DER) JANNAF combustion model computer program requires a description of the propellant mass and mixture ratio distribution, and dropsize distribution at a start plane near the injector. These can be obtained from either (1) a description of the mixing and atomization characteristics of a single injection element suitable for inclusion into the Liquid Injector Spray Pattern (LISP) subprogram, which then defines the overall distributions, or (2) definition of the overall mixing and dropsize distributions obtained from cold-flow experiments using the full-scale injectors. Due to facility limitations at the time this program was initiated, testing to determine the mixing characteristics using the full-scale injector was not possible.

Experimental characterization of a single element was conducted in two areas:

1. Mixing tests: to study the degree of mixing between the liquid and gas streams
2. Atomization tests: to establish the initial droplet size distribution

In addition, manifold flow distribution tests were made using the full-scale injector to establish the degree of uniformity of flow to each element achieved with the final injector assembly.

SINGLE-ELEMENT COLD-FLOW TEST FACILITY

Mixing

In order to describe the flowfield produced by a given injection element, the mass fraction of the total fuel and oxidizer present at each point in this flow

field must be determined. A specially designed, two-phase impact probe (Fig. 6) and pressurized test section were employed to accomplish this task. Development of the test procedure is described in Ref. 1 and the probe development is described in Ref. 2. A schematic of the overall facility is presented in Fig. 7. Basically, the impact probe serves the function of stagnating the gas component at the probe tip while allowing the liquid droplets to proceed down the length of the probe. By measuring the stagnation pressure at the probe tip (with a Baratron pressure indicator) and by collecting liquid in the probe for a known interval of time, both gas and liquid flowrates can be determined at each point in the flow field. An oxygen/nitrogen mixture is used to simulate the injected fuel gas while water simulates the liquid oxidizer. As the gas/liquid flow packet moves through the surrounding environment on its way from the injector to the probe location, much of the gas in the environment* is ingested into the flow field. Therefore, the gas flowrate measured at the probe is composed of gas which was injected (nitrogen/oxygen mixture) and gas which was ingested (nitrogen). These two components must be segregated to determine the injected portion. To accomplish this, the gas sample which arrives at the probe is processed through an oxygen sampler. The concentration of oxygen in the sample can then be used to determine the concentration of the original injectant. Finally, to provide a constant chamber pressure, a gas/liquid separator tank (see schematic) is employed to maintain single-phase gas and single-phase liquid exhaust flows.

Atomization

Atomization was measured by the molten wax technique utilized and refined extensively at Rocketdyne over the past five years (see Ref. 1 for some detailed descriptions). Basically, the molten wax which is injected as the simulant of a liquid propellant forms a spray which freezes as it falls to a collection

*The environmental gas consists of pure nitrogen injected through a porous plate at a very low velocity base bleed around the injection element. This base bleed prevents excessive recirculation, allowing a much better simulation of the near-injector region under hot-firing conditions.

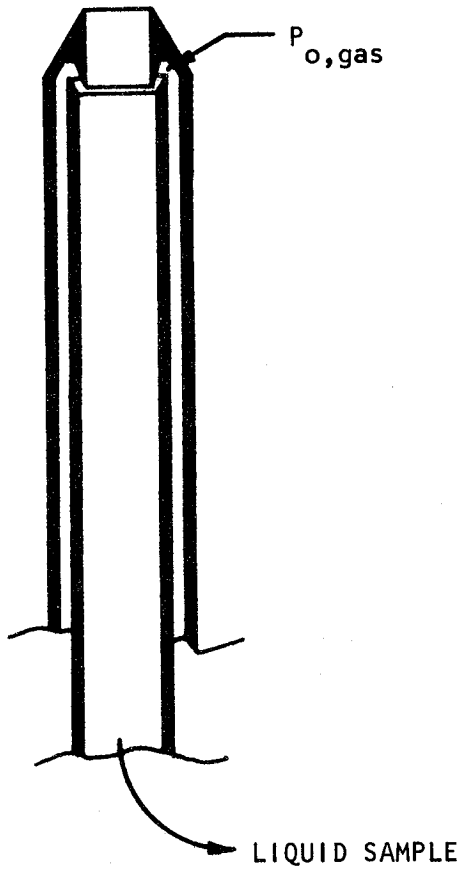

Figure 6. Schematic of Concentric Tube Two-Phase Impact Probe

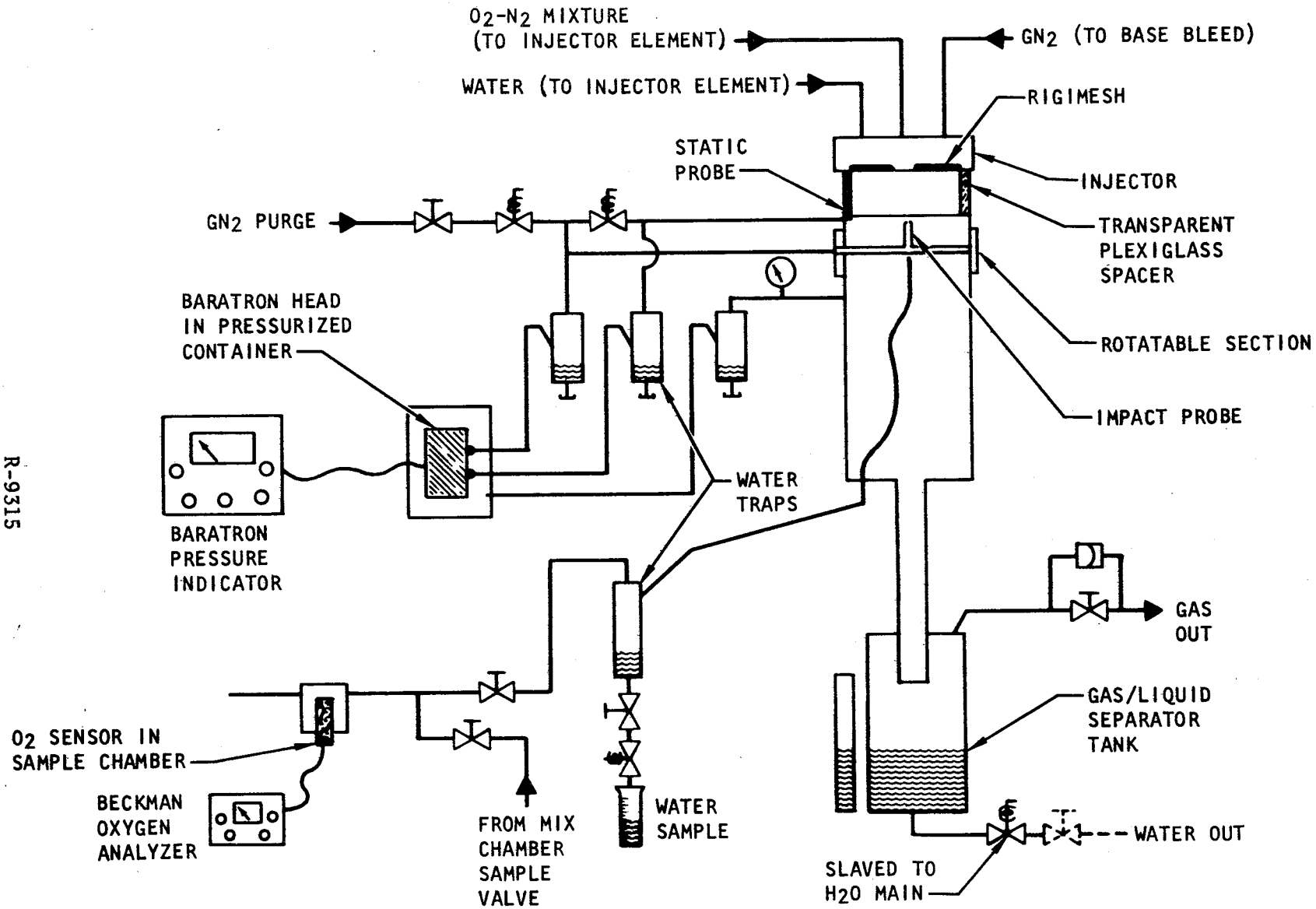

Figure 7. Cold Flow Apparatus

surface, thereby preserving its liquid dropsize distribution. The frozen wax sample is washed down with water, collected, vacuum dried, and finally subjected to a sieve analysis determining the mass distribution as a function of droplet diameter.

Under the present program, atomization experiments with single-element gas/liquid injector elements were performed in the apparatus shown schematically in Fig. 8. The apparatus consists of a large (600-gallon) pressurized tank with an associated water injector to prevent hot wax from impinging on the tank walls. The single-element gas/liquid injector is mounted at the top of the tank and propellant simulants (hot wax, He or GN_2) are supplied from the hot wax supply facility. Hot wax and gas flows are made for approximately 20 seconds and the resulting wax droplets are drained and washed from the tank following tank depressurization. The droplet sample is then vacuum-dried and subjected to sieve analysis in order to determine the dropsize distribution and a mass median dropsize, $\overline{D}$.

INJECTOR ELEMENT DESIGN

Successful cold flow modeling requires that the cold flow injector element be an exact duplicate of the hot fire element geometry. Therefore, the single element cold flow hardware was designed to match the hot fire element geometry, including orifice and free stream L/D and orifice inlet curvature. While the gas and liquid feed manifolds are not exact duplicates of the full scale injector, all feed velocities are similar to those of the hot fire injector. As an added measure to insure cold flow and hot fire similarity, the cold flow and hot fire hardware were fabricated from the same material, using the same tooling.

Figure 9 shows the cold flow hardware assembly used for the mixing tests. In this case, the injector flows into the center of the mixing chamber and is surrounded by a uniform base bleed gas flow (GN_2), which prevents recirculation of the injected simulant gases. The same element hardware was used for

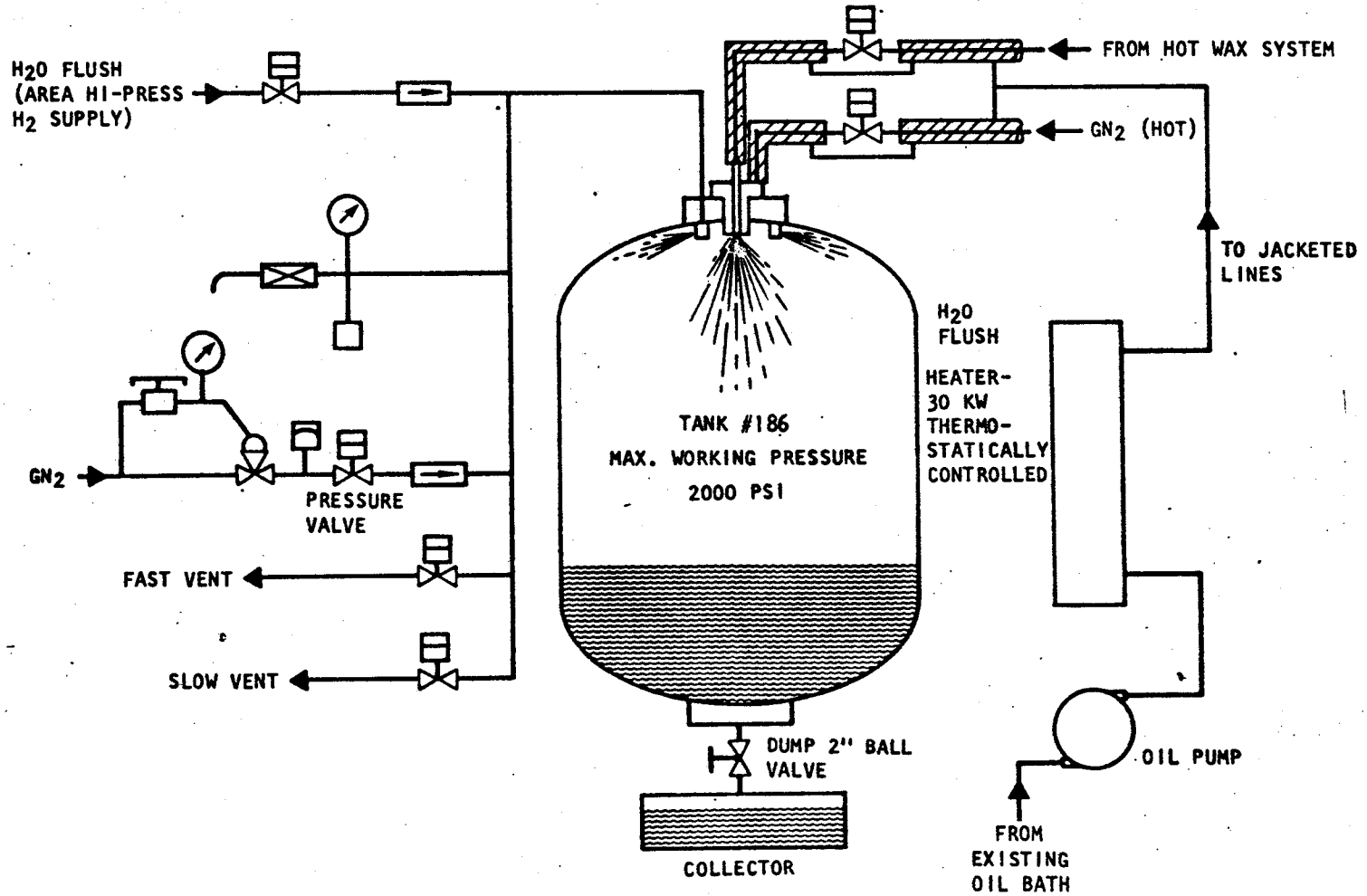

Figure 8. Pressurized Atomization Facility

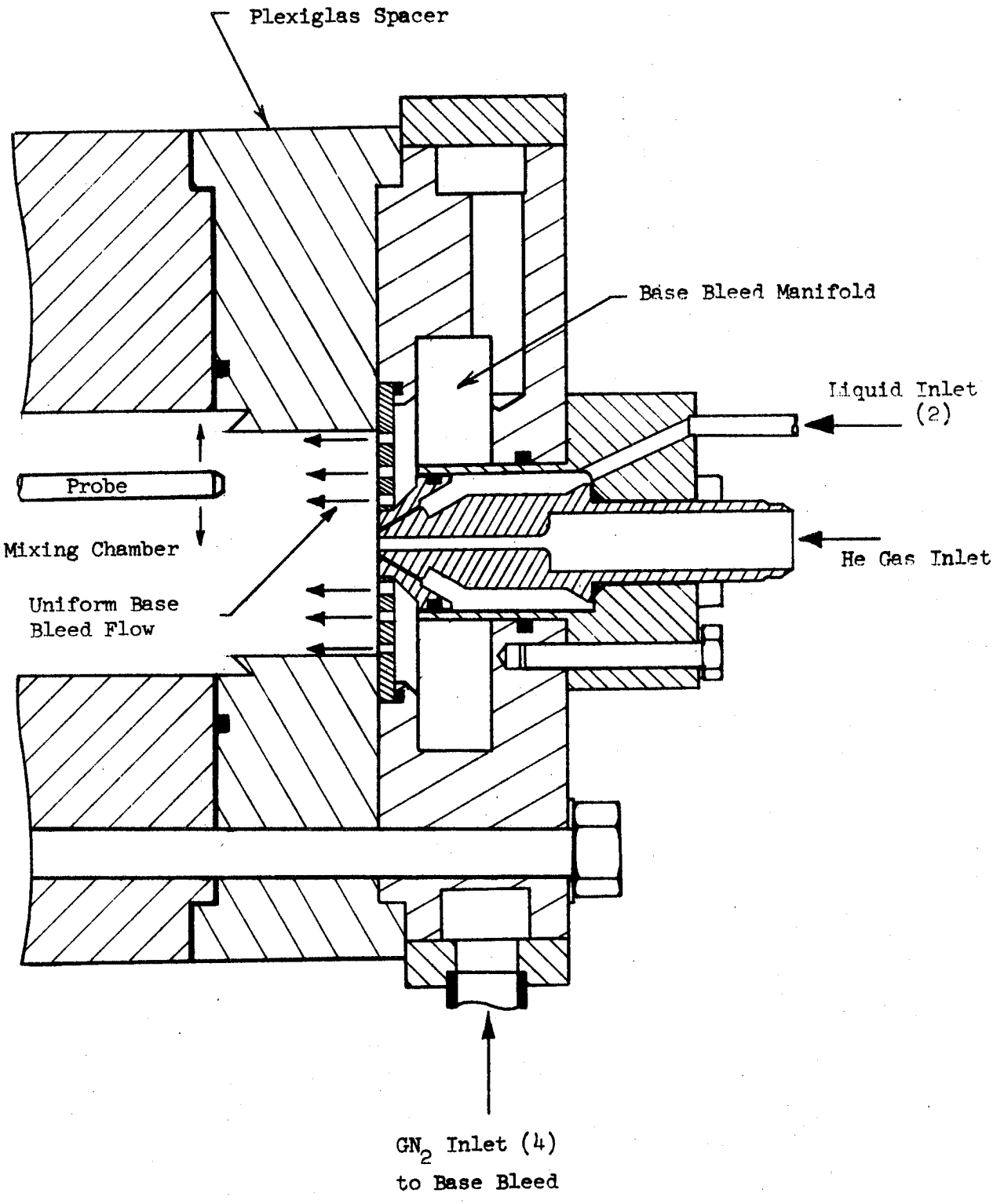

Figure 9. Cold Flow Injector Assembly (Mixing)

the atomization tests. However, for the atomization tests, the mixing chamber is replaced by a 600-gallon pressurized vessel (Fig. 8), which collects the simulant (wax) droplets.

SINGLE ELEMENT COLD FLOW EXPERIMENTS

Selection of Cold Flow Modeling Technique

Mathematical analysis of gas/liquid impinging stream modeling criteria suggests, for fixed element geometry, that a gas dynamic parameter ($\rho_g V_g^2$) and a liquid/gas penetration parameter (X_p/D_g) should control element spray formation processes. The liquid/gas penetration parameter, which may be physically interpreted as an index of the ability of the injected liquid stream to penetrate the gas (fuel) stream, is defined as follows:

$$\frac{X_p}{D_g} = 1.25\left(\frac{MR}{D_L/D_g}\right)\left(\frac{\rho_g}{\rho_L}\right)^{\frac{1}{2}} \cos\theta$$

where θ = angle between injector face and the liquid jet
D = orifice diameter
ρ = density
MR = O/F mixture ratio

Since mixing and atomization processes are inherently related, the same set of variables is thought to control both mixing and atomization (dropsize).

Experiments have demonstrated that the variables X_p/D_g, ρ_g, and V_g can be used to characterize the sprays from gas/liquid impinging type elements. Atomization tests using gaseous nitrogen and helium have shown that the parameter ($\rho_g V_g^2$) does correlate mass median dropsize data in terms of both ρ_g and V_g over the experimental range: $2.5 \leq \rho_g V_g^2 \leq 18$ psi. However, prior to this program, no gas/liquid impinging elements had been cold flowed with the gas dynamic parameter in the 60 to 260 psi range planned for the Task IV

hot fire testing. Furthermore, the dependence of mixing on the $\rho_g V_g^2$ grouping had not yet been confirmed due to insufficient test data. Therefore, as a conservative approach to modeling, it was evident that all of the cold flow variables (X_p/D_g), ρ_g, and V_g should be set equal to their respective hot-fire values. Where it is not possible to experimentally match all of these variables, cold flow modeling can still be accomplished using the parameters (X_p/D_g) and $(\rho_g V_g^2)$, but this latter method of modeling should be used only when the deviation of ρ_g and V_g from the hot-fire values is not great.

In this program cold flow modeling was conducted at equivalent mixture ratios of 3.0, 5.0, and 8.0. The hot-fire values of V_g and $(\rho_g V_g^2)$ at these conditions are much greater than those that can be attained using GN_2 (due to sonic velocity limitations); therefore, the injector characterization program was conducted using gaseous helium as the fuel (GH_2) simulant. The back pressure was selected so that the cold flow simulation tests matched the hot-fire values of (X_p/D_g), ρ_g and V_g for the mixture ratio range of 5.0 to 8.0. However, since the hot-fire gas velocity for the 3.0 mixture ratio case exceeds the subsonic range of helium, cold flow simulation for this mixture ratio was accomplished by matching hot-fire and cold flow (X_p/D_g) and $(\rho_g V_g^2)$.

Experiments

The single-element hot-fire test conditions are presented in Table 6. Also presented in this table are the conditions of the corresponding atomization and mixing tests. Note that the two major modeling variables, $\rho_g V_g^2$ and X_p/D_g, are nearly identical for both the expected hot-fire conditions and the cold flow tests. The results of the single-element tests are discussed below.

Atomization Test Results. Each of the atomization tests was run for a duration of approximately 15 seconds of steady-state flow. Wax samples were analyzed using the standard sieving technique. The data are presented in

TABLE 6. SINGLE-ELEMENT COLD-FLOW TEST MATRIX

HOT-FIRE ELEMENT FLOW CONDITIONS (OXYGEN/HYDROGEN)

MR	P_c psia	$\rho_g V_g^2$ psi	X_p/D_g	V_g fps	V_L fps	ρ_g lbm/ft^3	$\dot{w}_g$/element lbm/sec	$\dot{w}_L$/element lbm/sec
3	250	253	0.248	3450	90	0.099	0.048	0.144
5	250	121	0.400	2460	100	0.093	0.032	0.160
8	250	55.3	0.625	1700	106	0.088	0.021	0.171

ATOMIZATION COLD FLOW TEST CONDITIONS (SHELL WAX 270/HELIUM)

2.13	184	259	0.246	2970	107	0.136	0.057	0.121
4.07	149	117	0.403	2330	119	0.100	0.033	0.134
6.81	144	53.9	0.635	1690	127	0.087	0.021	0.143

COLD-FLOW MIXING TEST CONDITIONS (WATER/HELIUM)

2.29	187	252	0.249	2700	93	0.160	0.061	0.140
4.89	110	118	0.400	2450	103	0.091	0.032	0.154
7.76	116	55.0	0.622	1710	109	0.087	0.021	0.164

non-dimensional form in Fig. 10. The data show that the mass weighted droplet diameter distribution is essentially invariant when normalized by $\overline{D}$; therefore $\overline{D}$ provides a good index of the dropsize distribution. It is also significant that this normalized dropsize distribution curve is similar to the data presented in Ref. 1 for large thrust-per-element gas/liquid triplet injectors. Figure 11 shows the variation of mass median dropsize, $\overline{D}$, with element mixture ratio. The overall range in $\overline{D}$ is from about 100μ to 225μ.

The dropsize data of Fig. 11 are replotted in Fig. 12, in which $\overline{D}$ is shown as a function of the gas dynamic parameter, $\rho_g V_g^2$. Mehegan, et al, (Ref. 1) found that the mass median dropsize for impinging type elements ($1.5<\rho_g V_g^2<17$ psi) was inversely proportional to a power of $\rho_g V_g^2$. Although the penetration parameter, X_p/D_g, is also a variable for the data shown in Fig. 12, additional data presented in Ref. 1 show that the mass median dropsize is insensitive to X_p/D_g over the range 0.2 to 0.7. Because the subject tests fall within this range of penetration, the inverse power relationship shown in Fig. 12 should provide a complete characterization of dropsize for the range $50\leq\rho_g V_g^2\leq260$ psi.

Mixing Test Results. Four mixing tests were conducted. All three of the conditions listed in Table 6 were run at a collection distance of 2 inches (Runs 5,6, and 7), and the low mixture ratio case conditions were repeated at a collection distance of 5 inches (Run 4). Measurement at two distances was made for possible correlation in the GLISP version of the LISP computer program*, which requires knowledge of variation of spray patterns with axial distance (Ref. 3).

Mixing data can be presented in several useful forms. Normalized mass flux profiles (local mass flux/total injected flowrate) are particularly valuable when comparing data from several tests in which the injected mixture ratio

*Data from the mixing tests were reduced to a form which may be used for the development of the Gas Liquid Injection Spray Pattern (GLISP) program, which is part of the overall DER program.

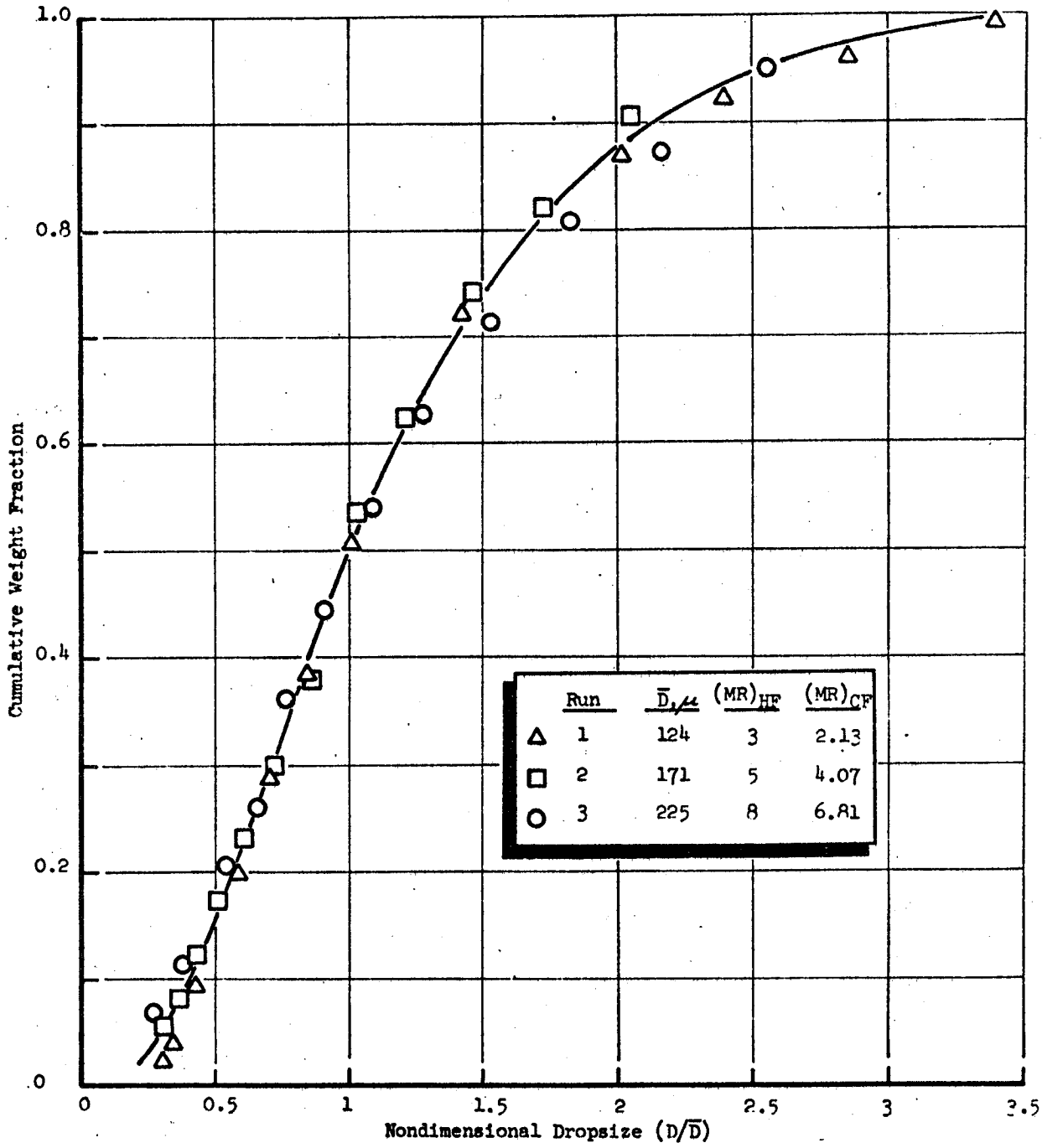

Figure 10. Atomization Test Results: Dropsize Distribution Curve

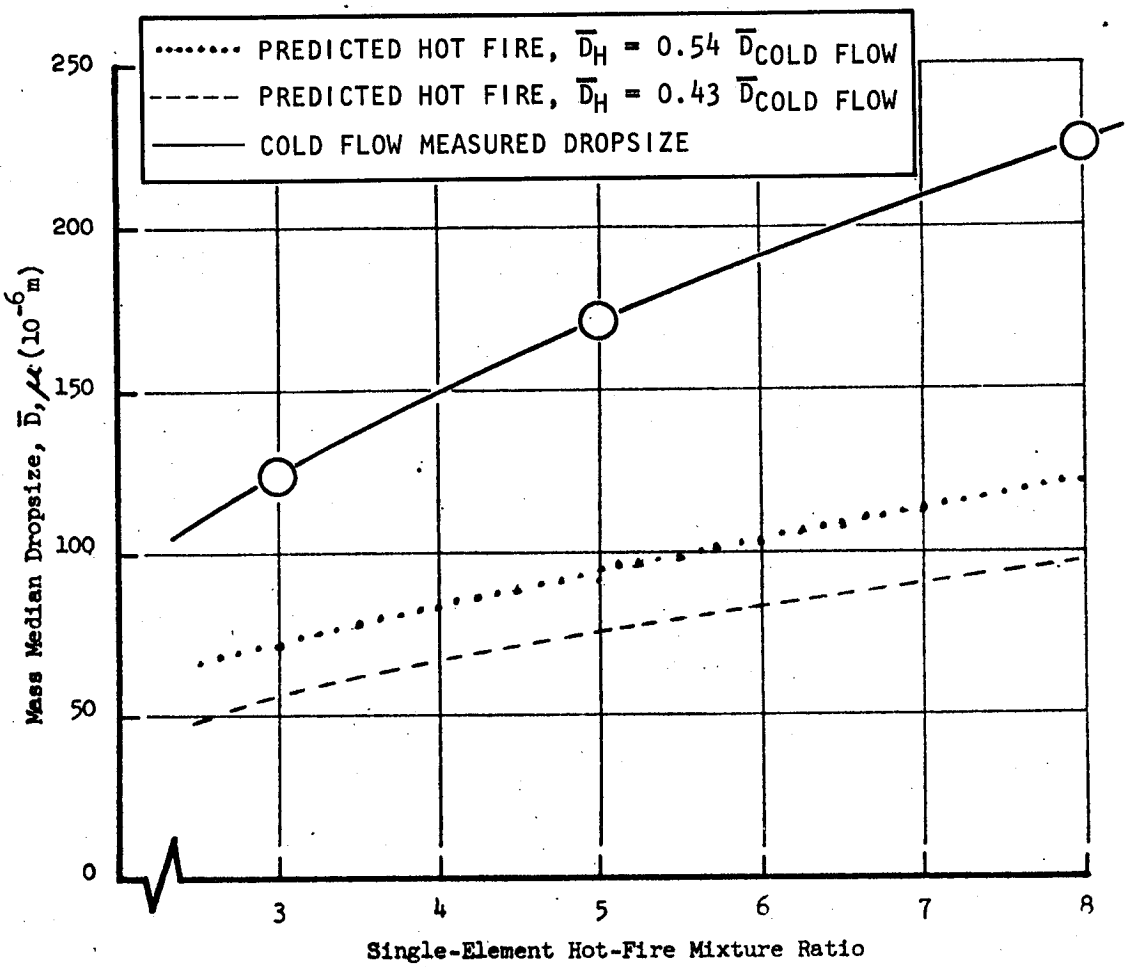

Figure 11. Mass Median Dropsize, $\overline{D}$, as a Function of Single-Element Mixture Ratio

Run No.	$\bar{D}, \mu$	$\rho_g V_g^2$, psi	X_p/D_g	$(MR)_{HF}$	$(MR)_{CF}$
1	124	259	0.25	3	2.13
2	171	117	0.40	5	4.07
3	225	53.9	0.64	8	6.81

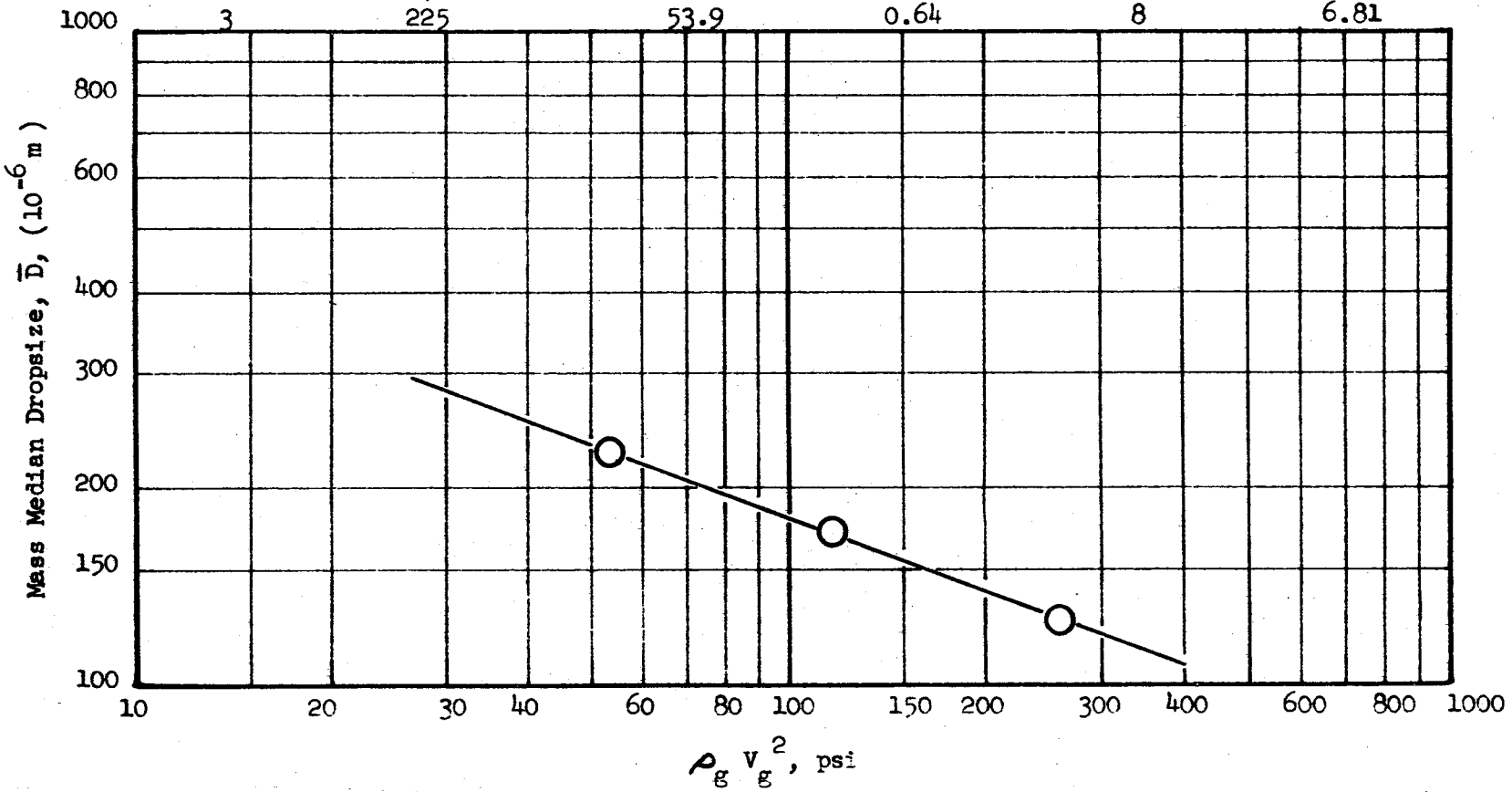

Figure 12. Mass Median Dropsize ($\bar{D}$) vs Gas Dynamic Parameter ($\rho_g V_g^2$)

is varied. This follows because the total volume under each profile (extended to three dimensions) is equal to unity; therefore, changes in the distribution of gas and liquid flux concentrations can be easily seen by direct comparison of normalized mass flux profiles.

Figures 13 through 16 present the normalized profiles measured during the four tests. On each of these figures, the four separate graphs represent cross-sections taken at 11, 33, 56, and 79 degrees from the diameter containing the two oxidizer orifices. Note that the intersections of the gas and liquid curves correspond to locations where the local mixture ratio is equal to the injected ratio. Where the liquid mass flux curve is higher, the local mixture ratio is above that injected and vice versa. For example, in Fig. 13 where the liquid penetration parameter is low, the center portion of the flow field is a region of low (below injected) mixture ratio. For radial positions greater than approximately 0.4 inch, the mixture ratio is above the injected value (liquid curve above gas curve).

Comparing Figures 13, 14, and 15, the effects of increasing penetration parameter (increasing X_p/D_g) and decreasing gas dynamic parameter ($\rho_g V_g^2$) can be seen. As would be expected, the increase in liquid penetration (with corresponding decrease in gas dynamic pressure) results in a splitting of the gas stream close to the injector as the gas flows around the liquid jets. In all cases the location of maximum normalized liquid flux is along the injector axis; however, the effect of increasing the liquid penetration parameter (X_p/D_g) is shown by the increasing value of this maximum; and they approach (at high penetration) the elliptical pattern of the liquid-like doublet injector element.

Since optimum mixing occurs when the normalized gas and liquid profiles are equal, a comparison of Fig. 13 through 15 shows that the best single element mixing probably occurs between equivalent hot-fire mixture ratios of 3 and 5. This conclusion is verified by Fig. 17, in which the mixing efficiency

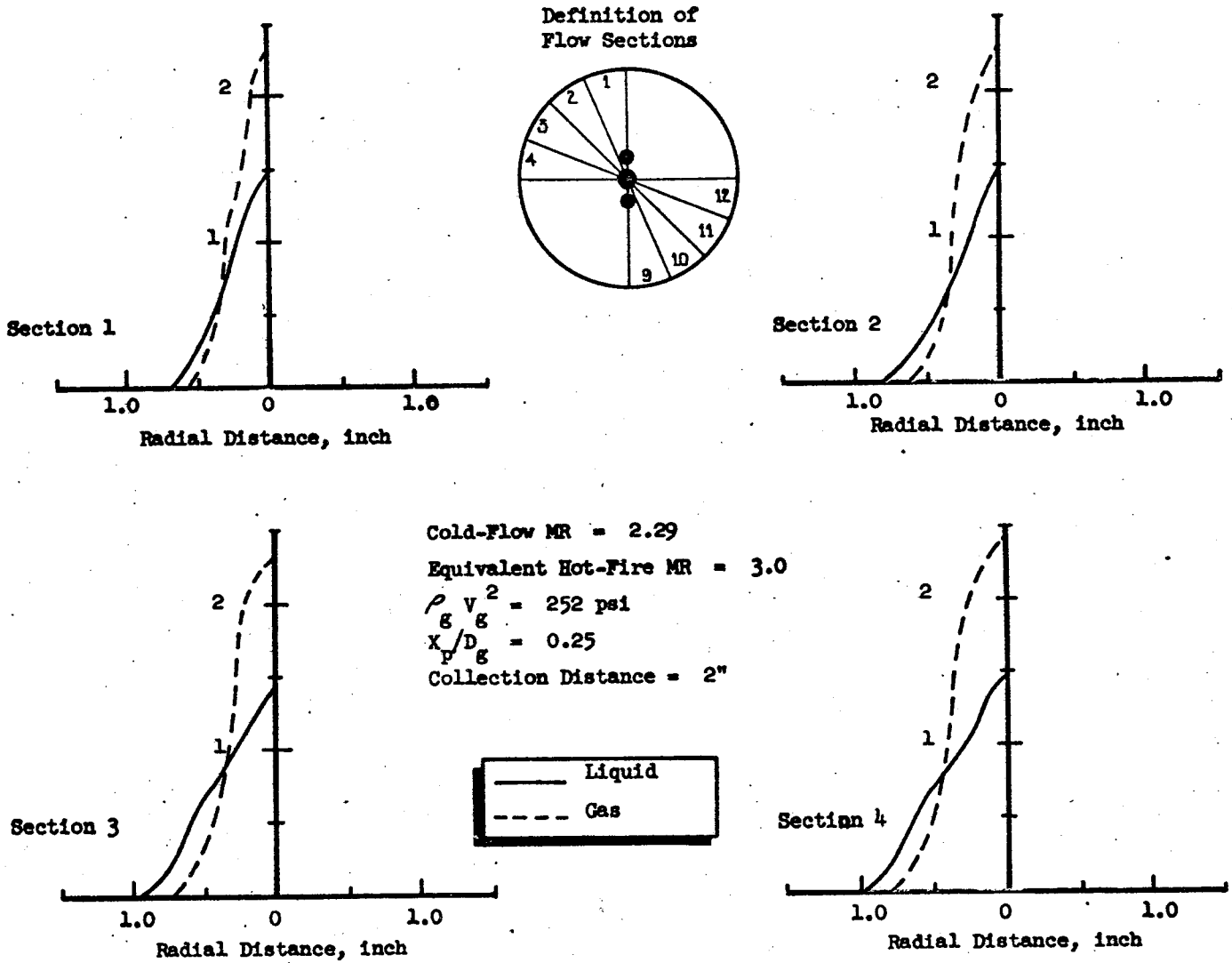

Figure 13. Normalized Mass Flux Profiles for Run No. 7: High Gas Dynamic Parameter, Low Liquid Penetration, 2-inch Collection Distance

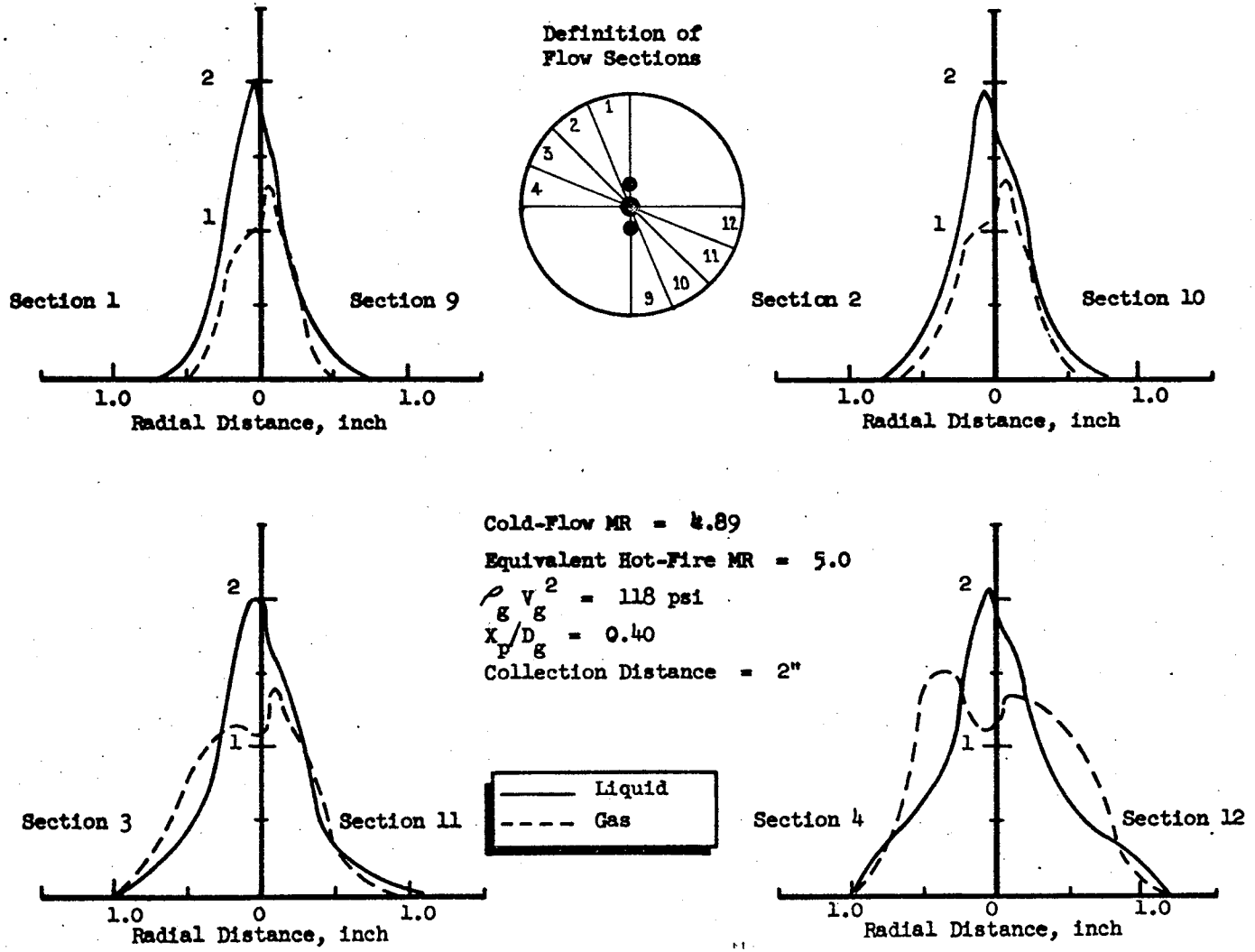

Figure 14. Normalized Mass Flux Profiles for Run No. 5: Medium Gas Dynamic Parameter, Medium Liquid Penetration, 2-inch Collection Distance

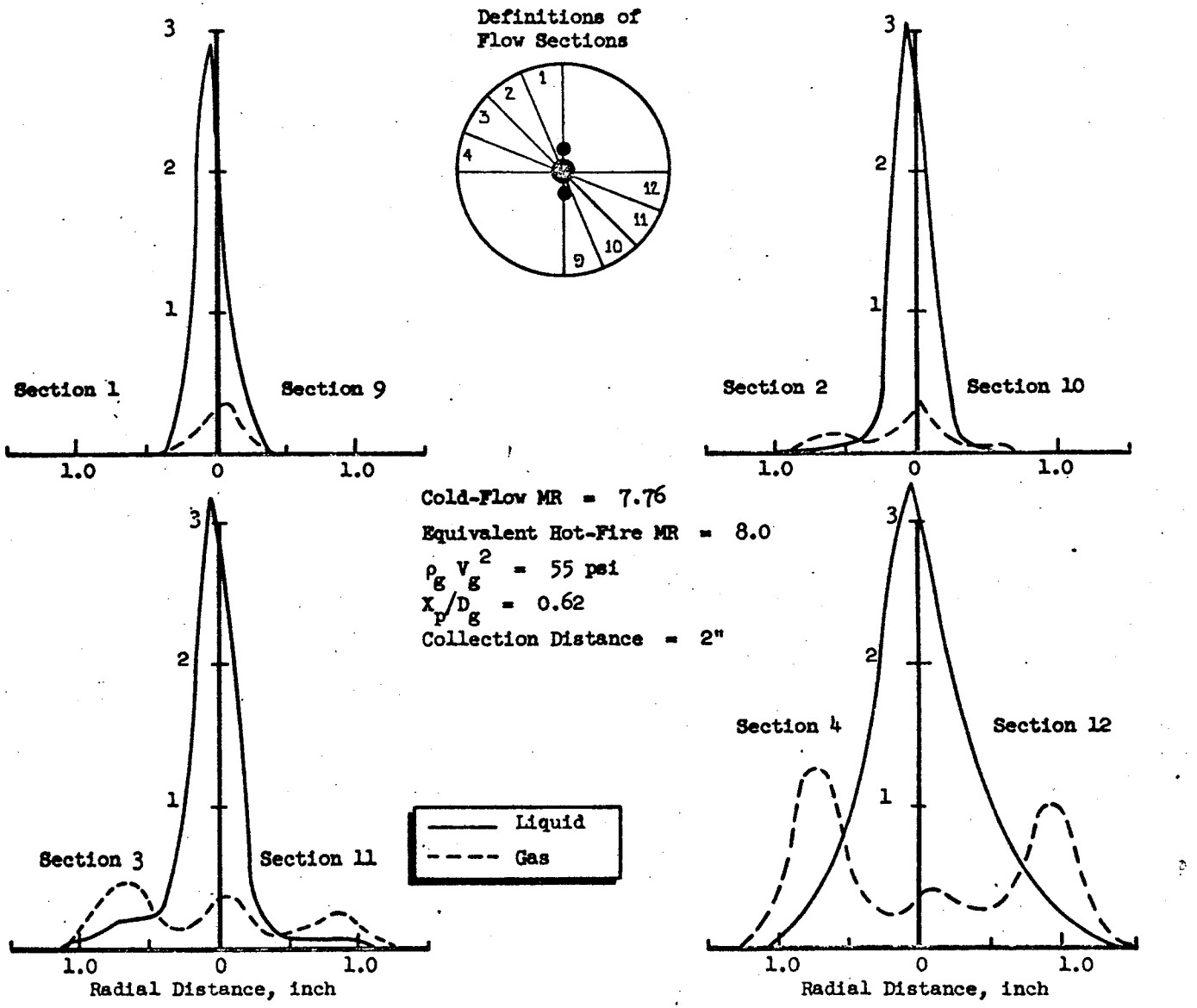

Figure 15. Normalized Mass Flux Profiles for Run No. 6: Low-Gas Dynamic Parameter, High Liquid Penetration, 2-inch Collection Distance

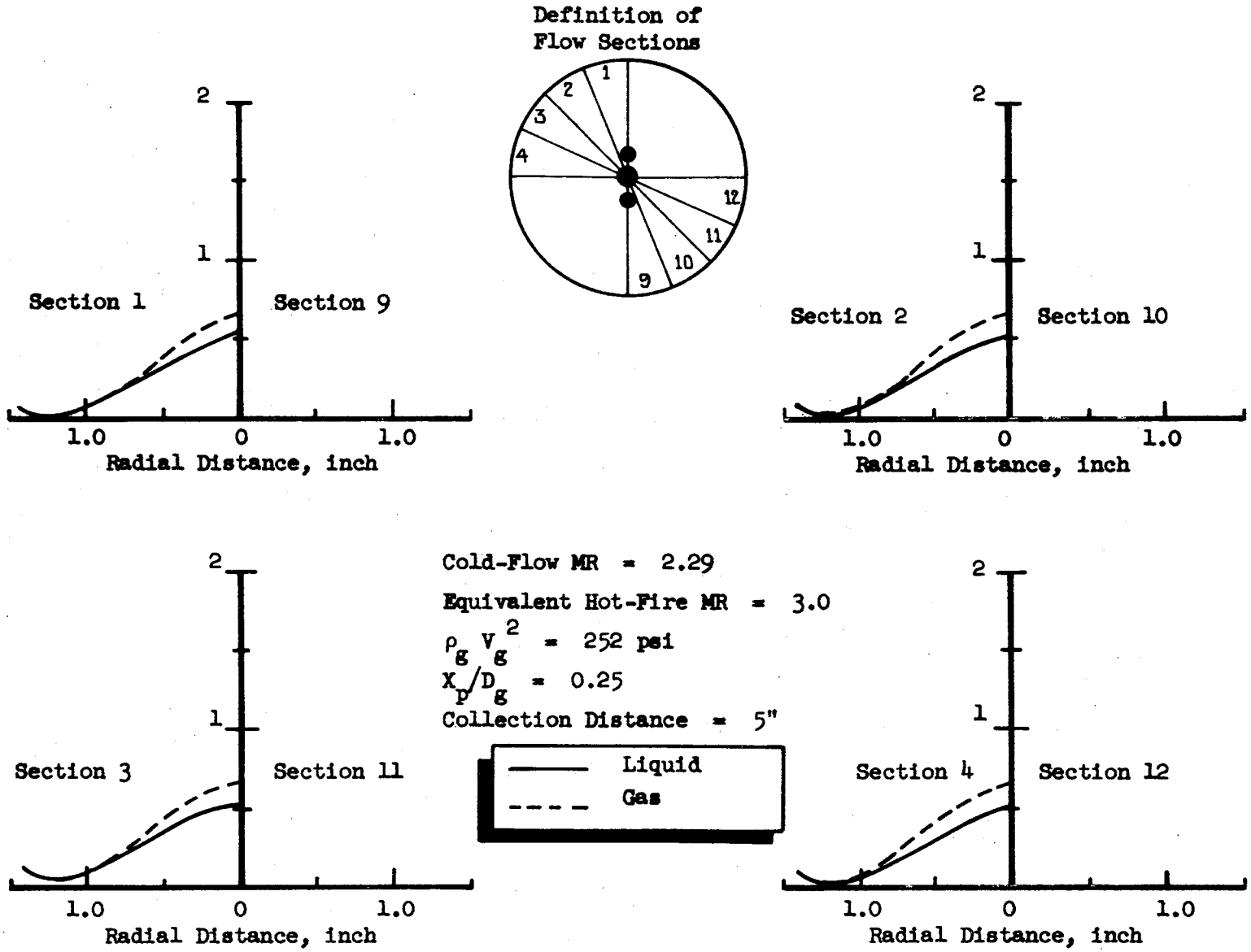

Figure 16. Normalized Mass Flux Profiles for Run No. 4: High Gas Dynamic Parameter, Low Liquid Penetration, 5-inch Collection Distance

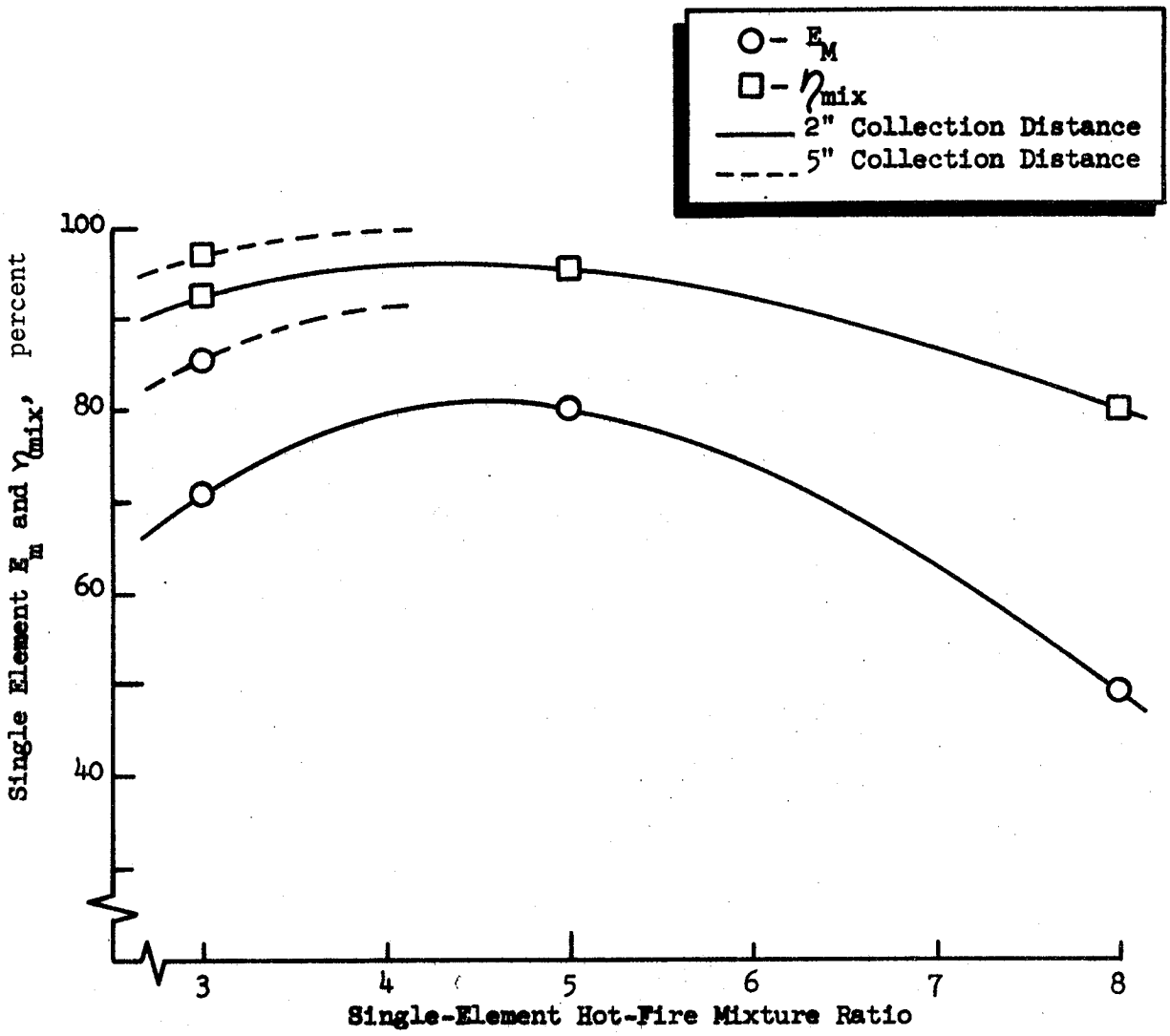

Figure 17. Single-Element Mixing Index (E_M) and Mixing Efficiency (η_{mix}) as a Function of Hot Fire Mixture Ratio

(η_{mix}) and the Rupe mixing parameter (E_m) have been plotted for the four tests. Also shown in this figure is the increase in both η_{mix} and E_m with increasing collection distance at the mixture ratio of 3.0. Figures 13 and 16 show that this improvement is the result of the gas flow field expanding more rapidly than the liquid spray, partially counteracting the initial high concentration of gas near the center.

An alternate presentation of the data is given in Fig. 18 through 21, wherein lines of constant mixture ratio and total mass flux have been plotted at the collection plane.

Comments on the Single-Element Cold-Flow Test Results. The single-element cold-flow testing results indicate that the mixing and atomization of the propellants vary significantly over the range of anticipated hot-fire test conditions. All of the observed trends were expected and can be explained by considering the variation of the liquid penetration (X_p/D_g) and gas momentum flux ($\rho_g V_g^2$) parameters.

Because the single-element, cold-flow data were run to model a specific hot-fire test matrix, all of the data have been presented as a function of single-element hot-fire mixture ratio. For the purpose of physical understanding of the flow field, the same data can be replotted as a function of the two modeling parameters ($\rho_g V_g^2$ and X_p/D_g).

FULL SCALE INJECTOR MANIFOLD TESTS

Manifold Flow Distribution Sampling Facility

The manifold flow distribution tests were designed to experimentally evaluate how uniformly the various fuel and oxidizer manifolds in the full scale injector distribute the propellants to each injection element. It should be noted that this is not the same as measuring the gas/liquid flow field produced by the full scale injector. Also, as a matter of clarification, it is

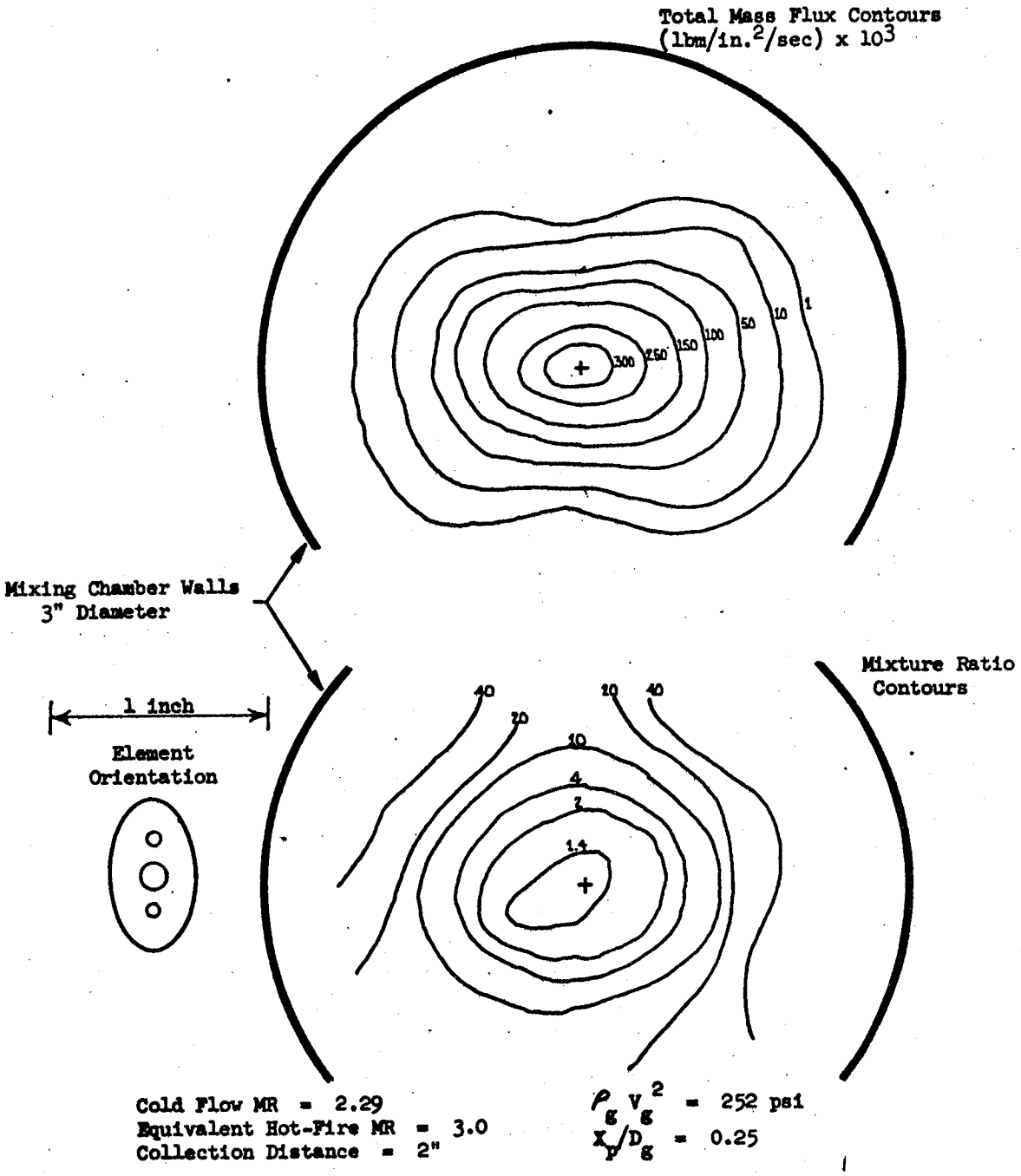

Figure 18. Total Mass Flux and Mixture Ratio Contours for Run No. 7: High Gas Dynamic Parameter, Low Liquid Penetration, 2-inch Collection Distance

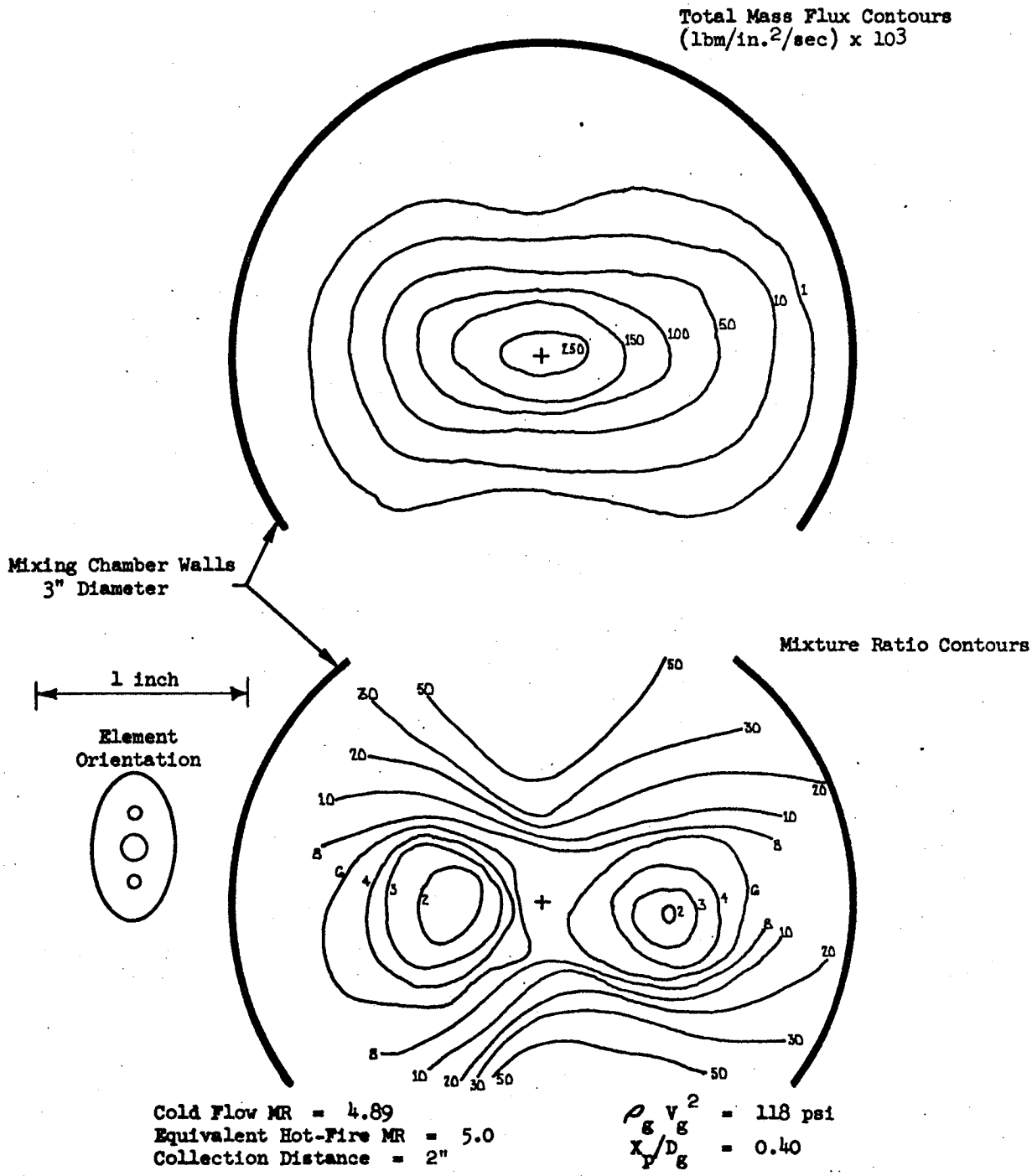

Figure 19. Total Mass Flux and Mixture Ratio Contours for Run No. 5: Medium Gas Dynamic Parameter, Medium Liquid Penetration, 2-inch Collection Distance

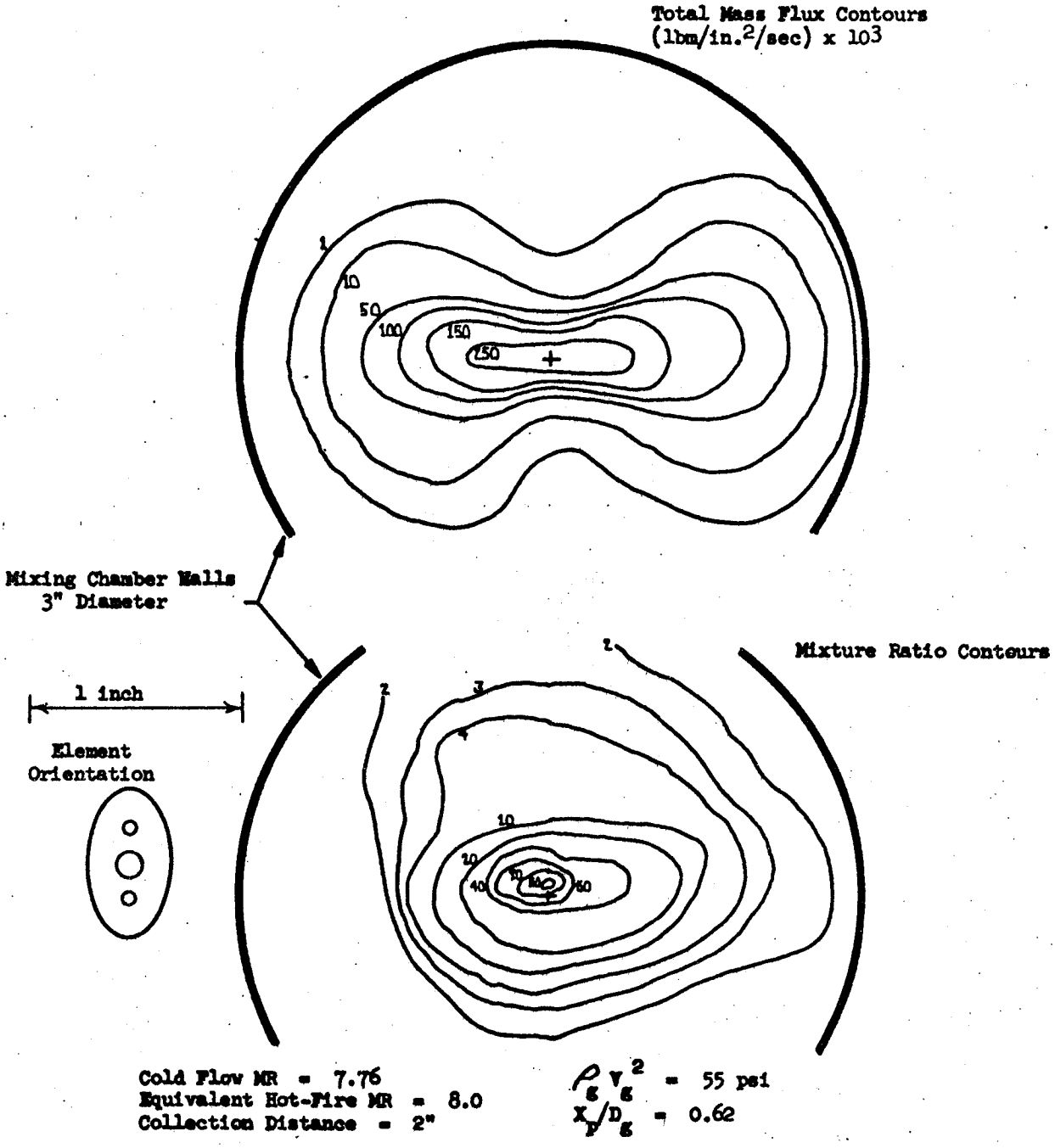

Figure 20. Total Mass Flux and Mixture Ratio Contours for Run No. 6: Low Gas Dynamic Parameter, High Liquid Penetration, 2-inch Collection Distance

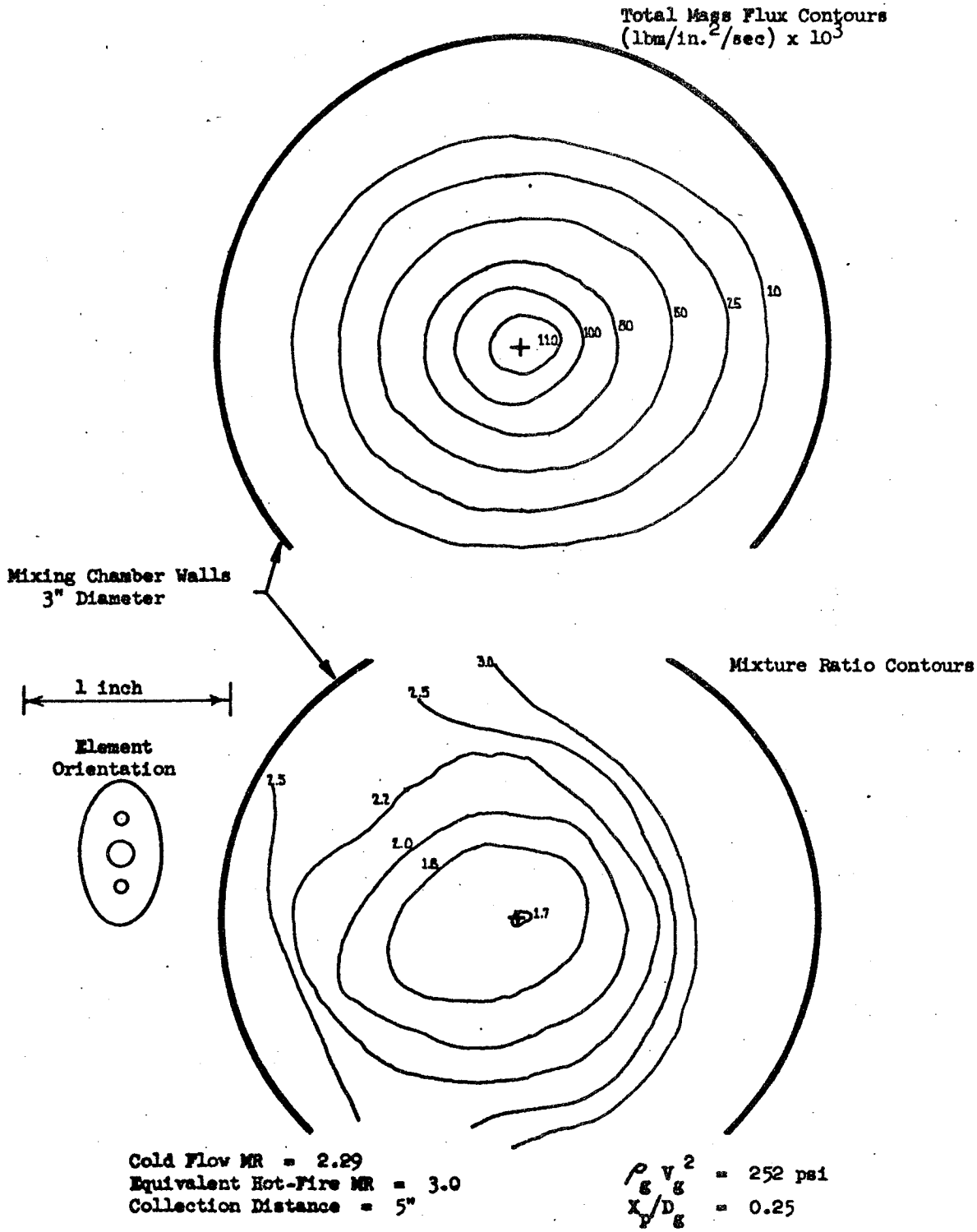

Figure 21. Total Mass Flux and Mixture Ratio Contours for Run No. 4 High Gas Dynamic Parameter, Low Liquid Penetration, 5-inch Collection Distance

pointed out that gas flow measurements were used to evaluate both fuel and oxidizer manifold flows.

A schematic of the test apparatus used to determine the gaseous flowrate through each orifice is shown in Fig. 22. The gas flowrate through each element was determined using the venturi shown downstream of the injector. A Baratron pressure gage was used to measure upstream and throat pressures of the venturi. The total injector flowrate was determined using the upstream venturi shown in Fig. 22. A sectional view of the sampling head for determination of the flowrate through the oxidizer orifices of an element is shown in Fig. 23. The head fits over a triplet element and the central jet is plugged. The flow through the sample head is that coming through the two impinging oxidizer orifice jets. For the fuel orifice, a single tube was used incorporating a seal at the end which fits over the fuel orifice.

Full Scale Injector Manifold Test Results

Measurements were made of the flows through each orifice to determine the maximum flow variation between elements. It was desirable that the injector be designed such that all orifices flowed full and the overall pressure drops (including manifold pressure drops) for each element be identical. This would ensure that the overall distributions in each zone would be equal to that specified by orifice area and manifold pressure.

The results of the tests are presented in Table 7. The data are separated into zone and propellant. The element numbers start in the inner ring and are successively numbered as listed below.

Ring	Orifice Numbers
1*	1 through 8
2	9 through 24
3	25 through 48
4	1 through 48
5**	1 through 48

* 1 is the inner ring containing 8 elements
** 5 is the film coolant (BLC) ring

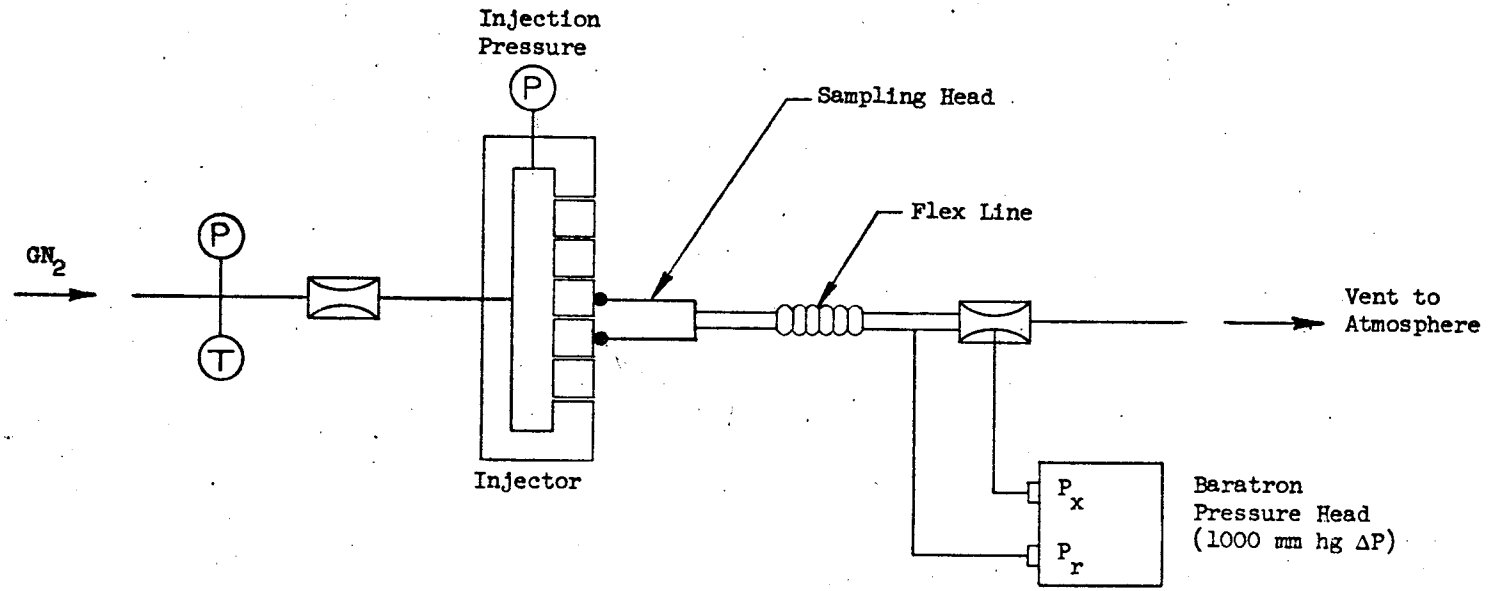

Figure 22. Schematic of Test Apparatus for Manifold Flow Distribution Measurements

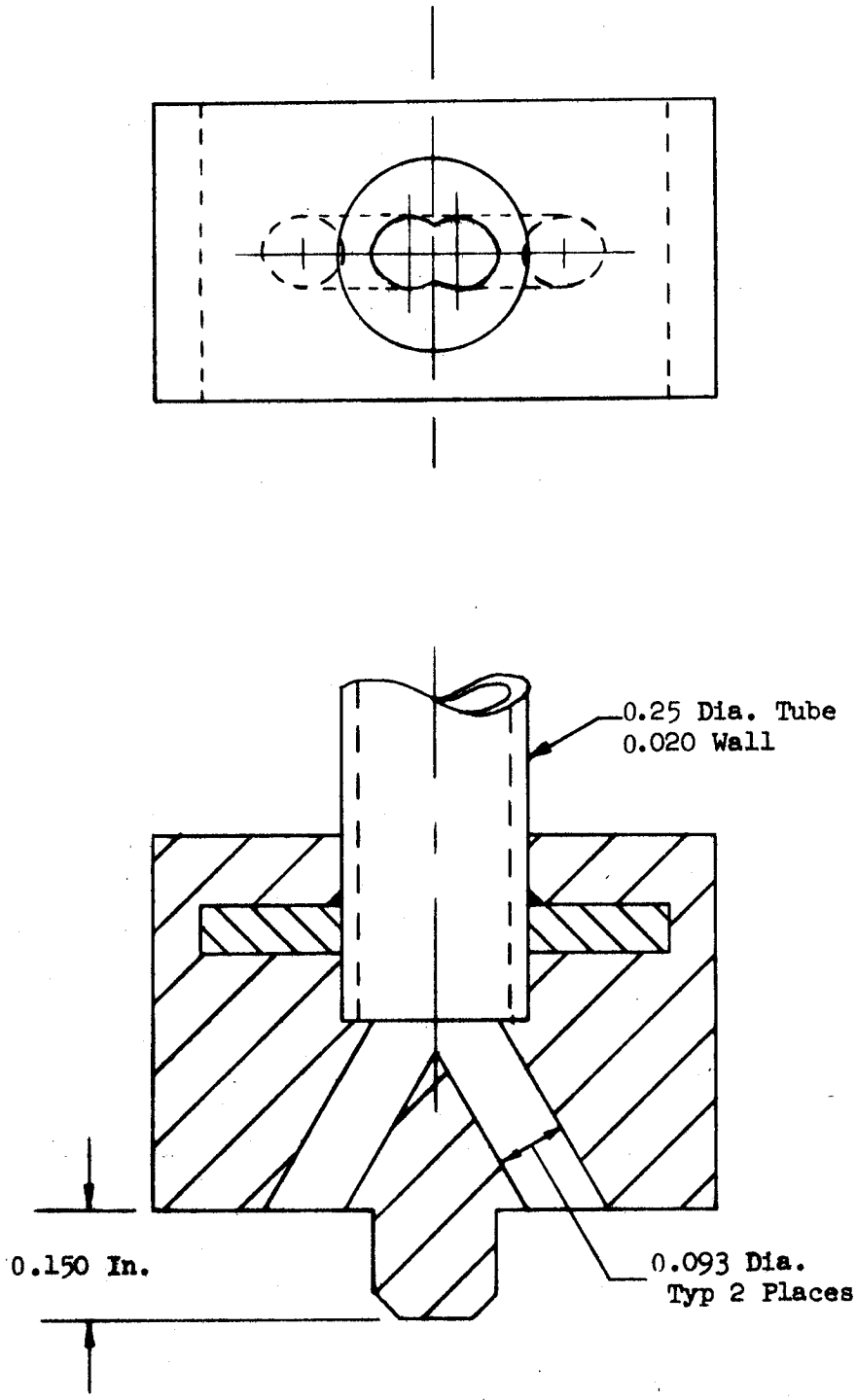

Figure 23. Injector Plug for Sampling Two Impinging LOX Jets

TABLE 7. SUMMARY OF MANIFOLD DISTRIBUTION MEASUREMENTS

Element Number	Main Fuel Manifold* (core) ΔP, mm H_g	Outer Fuel Manifold** ΔP, mm H_g	BLC Manifold*** ΔP, mm H_g	Oxidizer Core**** Manifold ΔP, mm H_g	Outer Oxidizer Manifold ΔP, mm H_g
1	81.3	66.4	76.0	103.2	99.5
2	92.0	65.0	78.4	101.8	98.5
3	82.0	69.2	74.1	102.5	94.0
4	98.0	67.1	76.4	101.3	94.0
5	74.0	69.2	79.7	102.1	94.4
6	89.0	66.4	75.5	100.1	94.8
7	76.0	69.7	72.2	101.2	99.8
8	88.0	69.9	82.1	100.3	107.6
9	72.0	65.6	77.6	100.0	116.2
10	71.0	67.6	83.1	104.3	102.3
11	79.1	70.1	79.3	102.8	108.4
12	82.1	71.5	109.0	101.3	100.5
13	71.5	71.0	60.2	99.0	100.0
14	70.5	72.0	80.2	102.0	103.0
15	76.3	64.0	90.3	104.0	100.2
16	78.4	72.0	86.5	101.5	103.3
17	72.3	69.5	95.5	100.8	108.4
18	70.1	70.0	82.2	103.0	94.5
19	72.5	71.0	85.3	107.7	105.3
20	73.4	70.0	84.3	101.5	99.5
21	65.5	65.6	70.1	101.2	103.5
22	70.5	67.0	94.2	104.3	101.4
23	79.3	69.5	85.2	101.0	101.2
24	80.3	67.5	114.2	100.0	100.0
25	66.3	67.2	99.8	100.7	87.0
26	69.0	68.2	98.9	101.2	101.4
27	66.4	67.5	74.4	100.0	100.6
28	67.3	69.8	96.5	99.5	104.0
29	66.3	70.1	97.5	104.2	100.0
30	67.2	69.5	70.0	102.8	104.1
31	69.0	68.2	80.0	102.5	99.5
32	67.4	70.0	100.0	106.3	105.2
33	67.2	70.5	98.2	104.1	104.2
34	69.2	70.5	86.4	102.1	99.5
35	72.4	70.5	96.5	101.4	103.5
36	67.4	70.5	72.3	105.0	101.4
37	64.3	69.5	79.3	106.8	106.4
38	68.4	69.4	82.4	101.1	99.5
39	67.6	69.9	84.5	103.3	92.4
40	66.4	69.5	72.4	101.1	101.2
41	67.6	68.4	92.4	109.5	109.5
42	66.5	69.0	81.4	104.0	102.4
43	66.5	69.8	90.3	103.2	99.5
44	66.4	69.0	90.0	100.5	100.0
45	65.0	68.0	88.5	103.3	101.0
46	68.3	69.6	99.0	102.6	100.1
47	69.4	68.5	82.5	106.8	90.0
48	66.4	69.0	99.6	102.1	93.1

*Inj. Press. 12.4 psig
**Inj. Press. 13.2 psig
***Inj. Press. 15.6 psig
****Inj. Press. 13.6 psig

Note that the pressure difference between that upstream of the venturi and that at the venturi throat is listed. The injector manifold pressure was 2.72 psig, which results in a pressure ratio that is less than critical.

For constant total pressure upstream of the venturi, the maximum deviation in flows are defined approximately by:

$$\frac{\dot{w}_{min}}{\dot{w}_{max}} \equiv \sqrt{\frac{\Delta P_{min}}{\Delta P_{max}}} \qquad (1)$$

The percent deviation from the maximum value is defined as:

$$\% \text{ Dev} = \left(1 - \sqrt{\frac{\Delta P_{min}}{\Delta P_{max}}}\right) \times 100 \qquad (2)$$

Using Eq. (2) the maximum flow deviation for each manifold is listed below:

Manifold	Percent Deviation
Outer oxidizer	11
Core oxidizer	4
Outer fuel	3
Core fuel	18
BLC	16

It should be noted that the average deviation is much less than the values listed above. Those represent only the maximum value measured. Comparing all the average deviations for all manifolds, the overall average deviation for the entire injector is about 5 percent. This value is considered to be acceptable both for the purposes of the program and for ordinary injector design practice.

TASK III - EXHAUST GAS SAMPLING SYSTEM DEVELOPMENT

SAMPLING SYSTEM DESIGN

The exhaust gas sampling and analysis system consists of exhaust gas sampling probes, sample collection banks, and the sample analysis unit. The function of the probe is to collect a sample of the combustion gas in a supersonic rocket exhaust environment. The sample collection bank stores the samples for later analysis and has provisions for both heating and cooling to maintain the gas sample at any desired temperature during analysis. The analysis unit consists of pressure gages and a gas chromatograph.

Probe Design

Three probes of the same type were designed by the Greyrad Corporation. A sketch of the design is shown in Fig. 24. The tip is able to reach any point in the nozzle exit plane. Two water cooling circuits are included, one for the centerbody and one for the cowl. The probe has sufficient strength to support itself in the exhaust stream when mounted by the terminal block.

The probe capabilities are:

1. Location: All three probes are capable of sampling any streamline from the nozzle centerline to a radius of 13.1 inches.
2. Orientation: Each probe tip is capable of being oriented parallel to the local theoretical streamlines.
3. Traversing: The probes are not designed to be traversed during a test but may be moved, repositioned, and fastened manually between tests.
4. Recovery: At a chamber pressure of 250 psia and nozzle expansion ratio of $\varepsilon = 25$, the steady-state pressure recovery of the probe is approximately 15 psia when the gas collection system is filled.

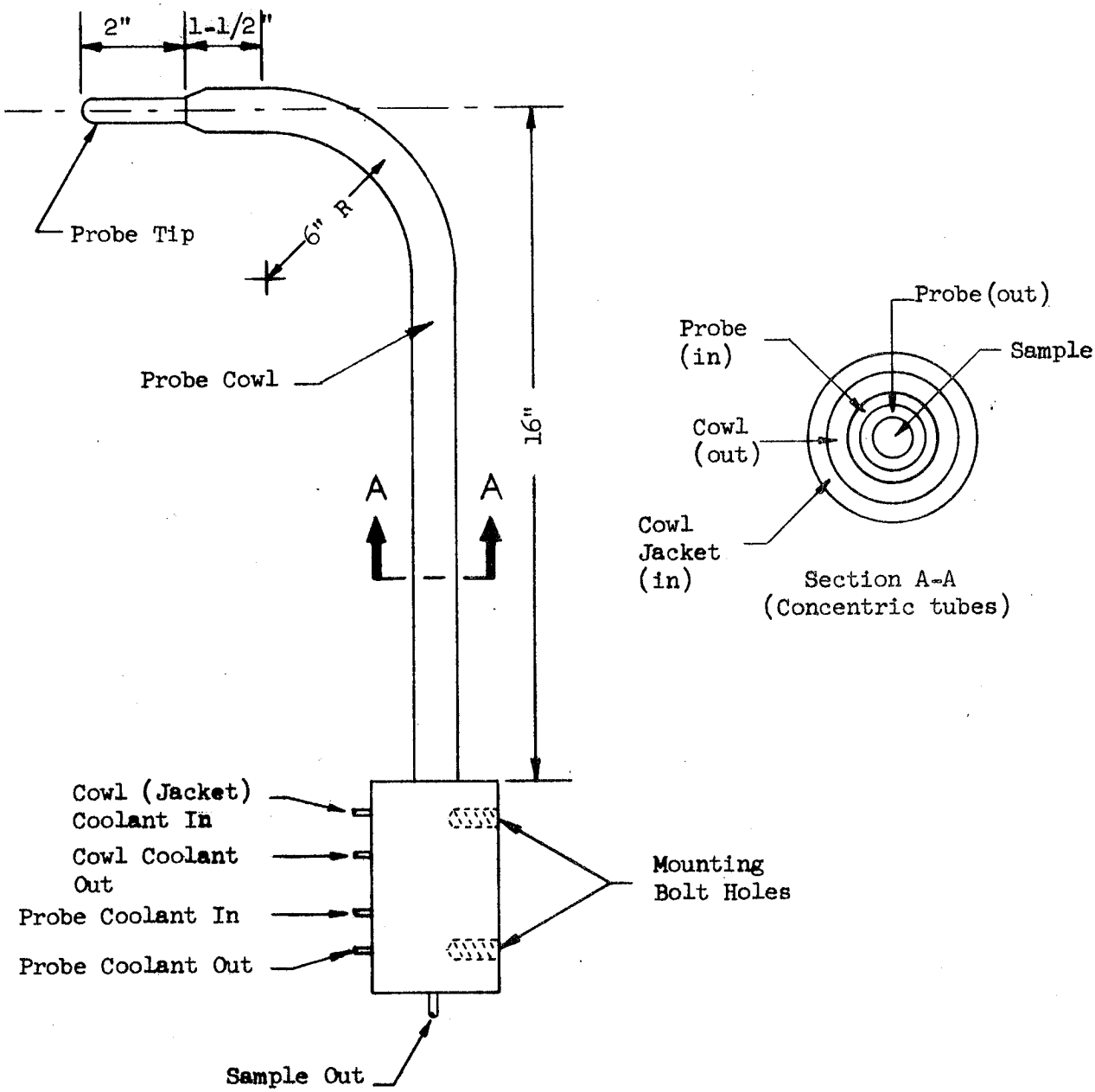

Figure 24. Selected Overall Probe Configuration

5. Response: A sample volume of 20 cubic inches is filled in one second or less.

The size of the probe was determined by two considerations. First, an adequate size sample had to be acquired in 1 second of sampling time. Second, the unit had to be large enough to have space for the internal water cooling passages.

The captured streamtube has a maximum diameter of approximately 0.28 inch. Because of the overall diameter of the probe, the centerline of the captured streamtube can be within 0.35 inch of the wall. For the case of film cooling equal to 5 percent total flow and with the assumption of no mixing between the film and core (as a worst case), the film at the exit of the 25:1 area ratio nozzle would occupy a zone approximately 0.5-inch thick. (For more realistic mixing assumptions, the zone will be much thicker.) Therefore, the dimensions of the probe allow meaningful sampling of the film/core interaction at the 25:1 area ratio. Mixing between the two controlled mixture ratio zones within the core can be studied at an area ratio of either 25:1 or 4:1.

The key heat transfer areas in the probe are the tip and shank, which must be protected from the impinging hot gas stream, and the gas sample extraction tube, which must cool the sample while preventing condensation of the water.

In the probe design, cold incoming coolant is fed up the outside of the shank and returns through the inner passage. Hot water is used to cool the sample to ensure that its temperature cannot be reduced below the temperature at which condensation would occur in the lines. The same heated water protects the probe leading edge.

Hot gas and coolant side heat transfer analyses were conducted to select the coolant conditions required to ensure survivability of the probe's leading edge. From the results of the analyses, the flow conditions summarized in Table 8 were selected. In addition to the inlet conditions, the resulting

TABLE 8. SAMPLING PROBE HEAT TRANSFER SUMMARY

	$\epsilon = 4:1$	$\epsilon = 25:1$
Assumed Probe Inlet Temperature, F	200	250
Assumed Probe Inlet Pressure, psig	500	500
Calculated Tip Temperature, F	1465	654
Calculated Tip Heat Flux, Btu/in.^{2}-sec	7.85	2.31
Calculated Tip Inner Passage Flowrate, lbm/sec	0.25	0.25
Calculated Cowl Temperature, F	1600	360
Calculated Cowl Flowrate, lbm/sec	0.7	0.35
Assumed Cowl Inlet Temperature, F	50-80	50-80
Assumed Cowl Inlet Pressure, psig	500	500

temperature at various locations on the probe is presented. It is seen that modest coolant flowrates and pressures maintain peak temperatures at acceptable levels. Coolant bulk temperature rise is small in each case, on the order of 100 F. Although cooling seems to pose no particular problems for the probe, it is clear from the heat flux levels that cooling is essential.

As noted above, the simplest method for assuring non-condensation of the combustion-generated water was to preheat the coolant so that its temperature was above that of the sample saturation temperature. Assuming a maximum sample water content of 100 percent and a maximum pressure of 30 psia, the minimum wall temperature at the probe exit must be held above 250 F. Since there was no heat transfer difficulty for the 25:1 nozzle, the coolant water was preheated to 250 F to completely avoid condensation problems. For the 4:1 expansion ratio, however, the water inlet could not be 250 F due to excessive heat loads. For this condition the water can be preheated to only 200 F.

The probe support structure is shown in Fig. 25. It provides continuously adjustable probe-tip location at any point between the centerline and the $\varepsilon = 25$ nozzle exit boundary and can keep the probe aligned with the theoretical (conical-flow) streamlines.

After the probes were received from Greyrad, they were water flowed to determine the Δp versus $\dot{w}$ characteristics. The results of these tests are presented in Fig. 26. Note that probes No. 1 and No. 3 had similar characteristics, while probe No. 2 yielded a much higher pressure drop for the same flowrate (approximately 40 percent). Subsequent testing at higher pressure (approximately 1100 psi) resulted in a crack in the tip weld on probe No. 2. Therefore, probes No. 1 and No. 3 were used in the initial series of hot firings. The probe, however, was required in time for the third series of tests. To ensure that the probes would not experience heat transfer problems, the actual flowrates selected for the initial test series were higher than those listed

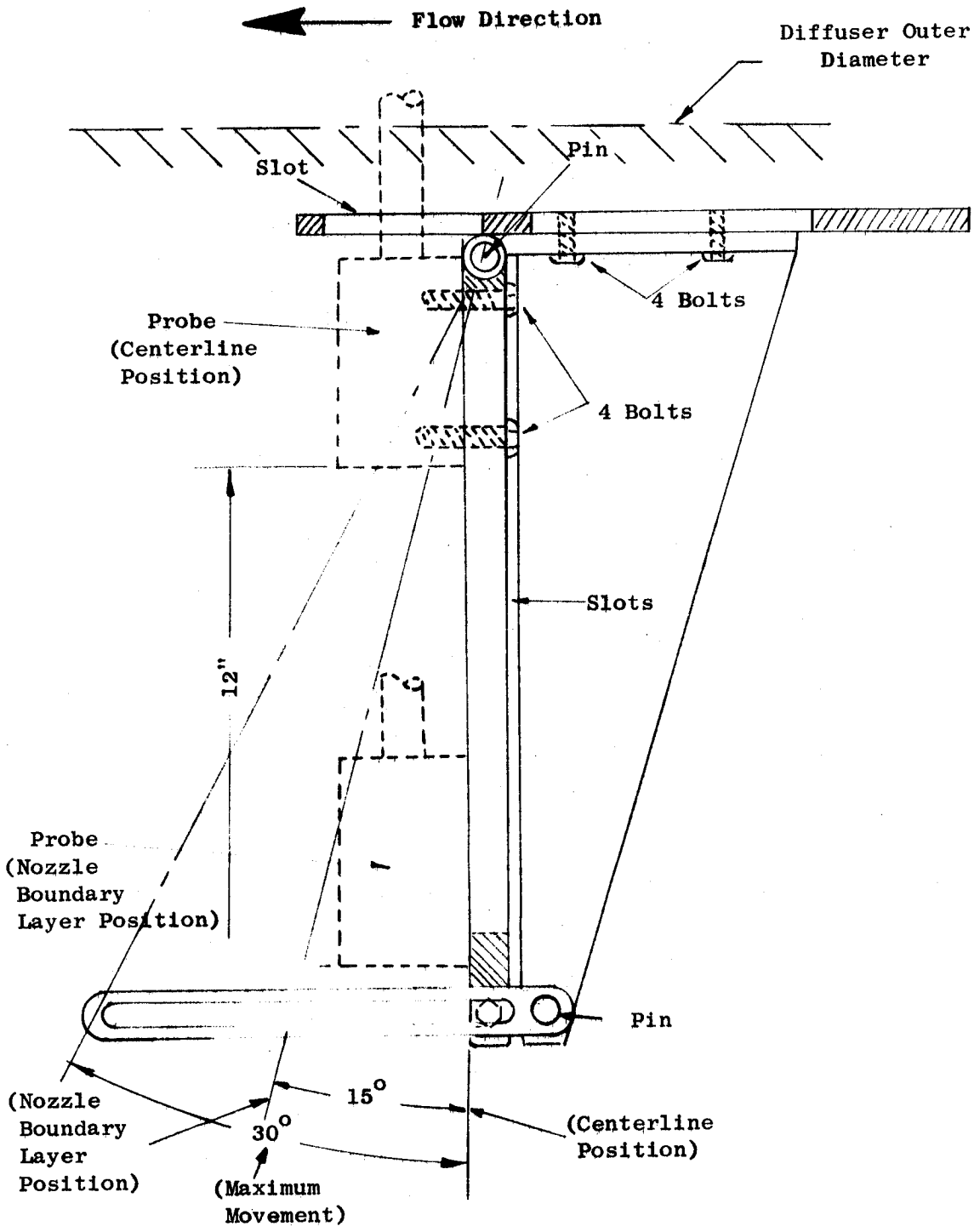

Figure 25. Probe Mounting Bracket

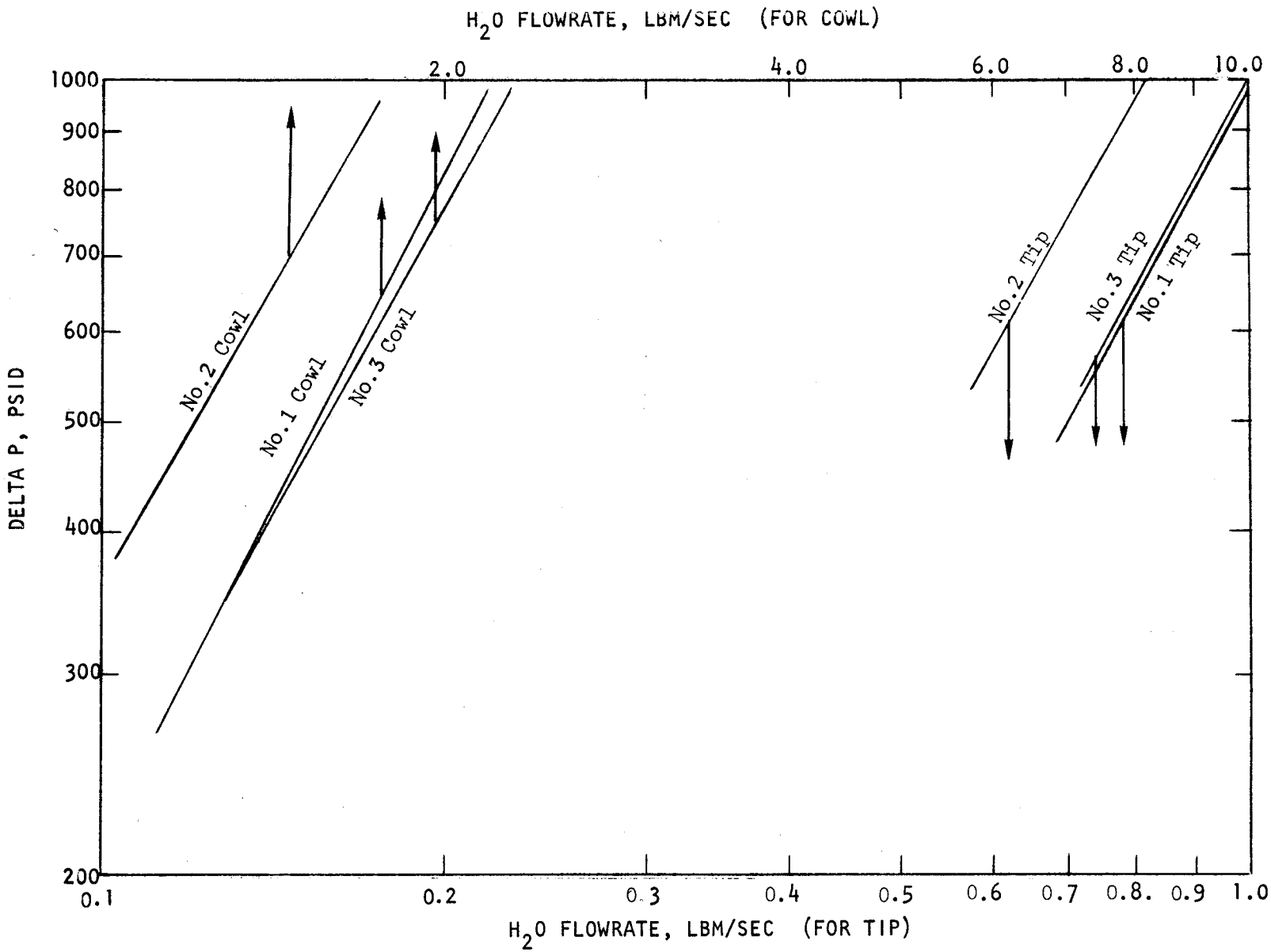

Figure 26. Flow Characteristics of the Greyrad Probes

in Table 8. For the actual tests the nominal coolant flowrates were

$$\dot{w}_{tip} = 0.98 \text{ lb/sec}$$

$$\dot{w}_{cowl} = 2.1 \text{ lb/sec}$$

Sample Block Design

The sample collection unit is shown in Fig. 27. Each of the three units is constructed from a solid block of aluminum and contains 10 sample cylinders. Heating was provided by six 2-kw heaters capable of raising the block temperature by 400 F in approximately 15 minutes. Cooling was provided by LN_2 flow through 6 passages capable of reducing the block temperature by 400 F in less than 10 minutes. The temperature range of 0 F to 400 F allows freezing or full vaporization of the water in the samples. A photograph showing an assembly view of the sample blocks is shown in Fig. 28.

Sample Procedure for Analysis of Hydrogen, Oxygen, and Water Combustion Products

The analysis of hydrogen, oxygen, and water was accomplished by a two-step procedure of P, V, T measurements and gas chromatography.

In the first step, the pressure of an individual sample was measured as it was drawn into a calibrated volume at a known elevated temperature. Assuming ideal gas relationships, the total number of moles of gas in the sample vessel was calculated from PV = nRT.

Secondly, the sample vessel was cooled to a known temperature, permitting condensation of water. The remaining gases were then expanded into the pre-calibrated analyzer system. A portion of the expanded samples was injected into a gas chromatograph for determination of the hydrogen/oxygen concentrations.

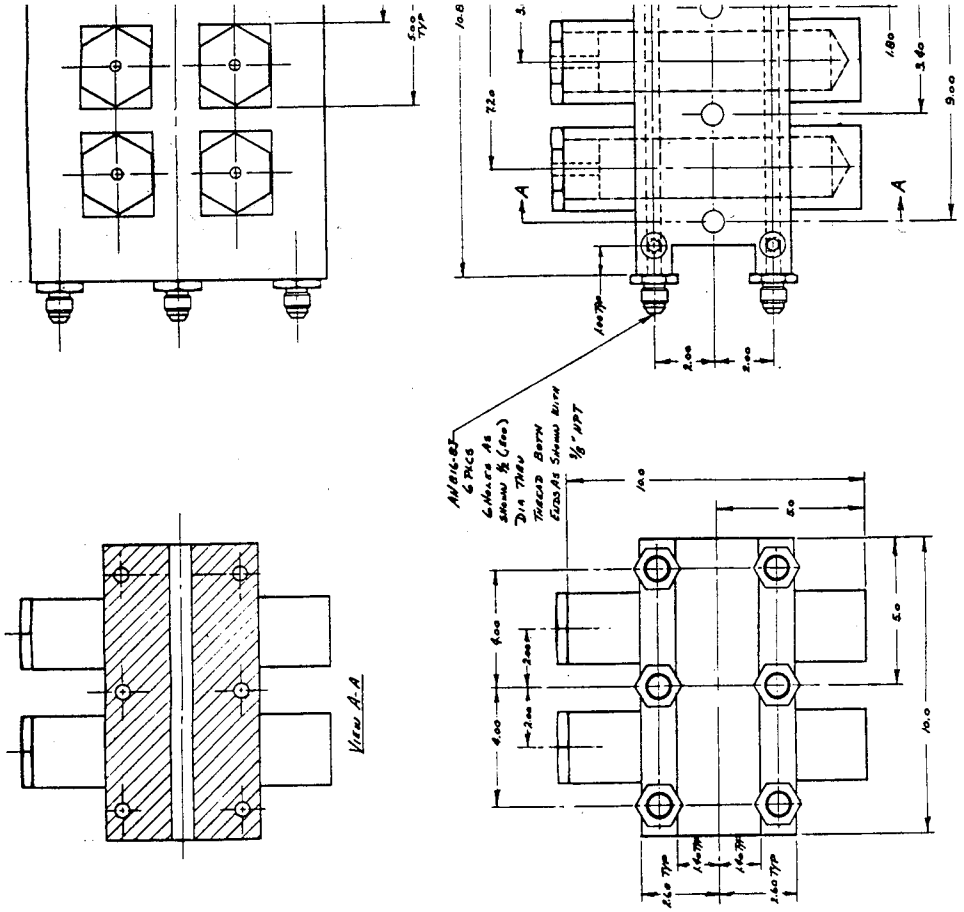
5.00 TYP
10.8
7.20
3.
1.80
3.60
9.00
A
A
1.00 TYP
2.00
2.00
M1616-82
6 PLCS
6 HOLES AS
SHOWN ⅜ (Ø10)
DIA THRU
THREAD BOTH
ENDS AS SHOWN WITH
⅜" NPT
10.0
5.0
5.0
4.00
2.00
2.00
4.00
10.0
1.60 TYP
1.60 TYP
1.60 TYP
VIEW A-A

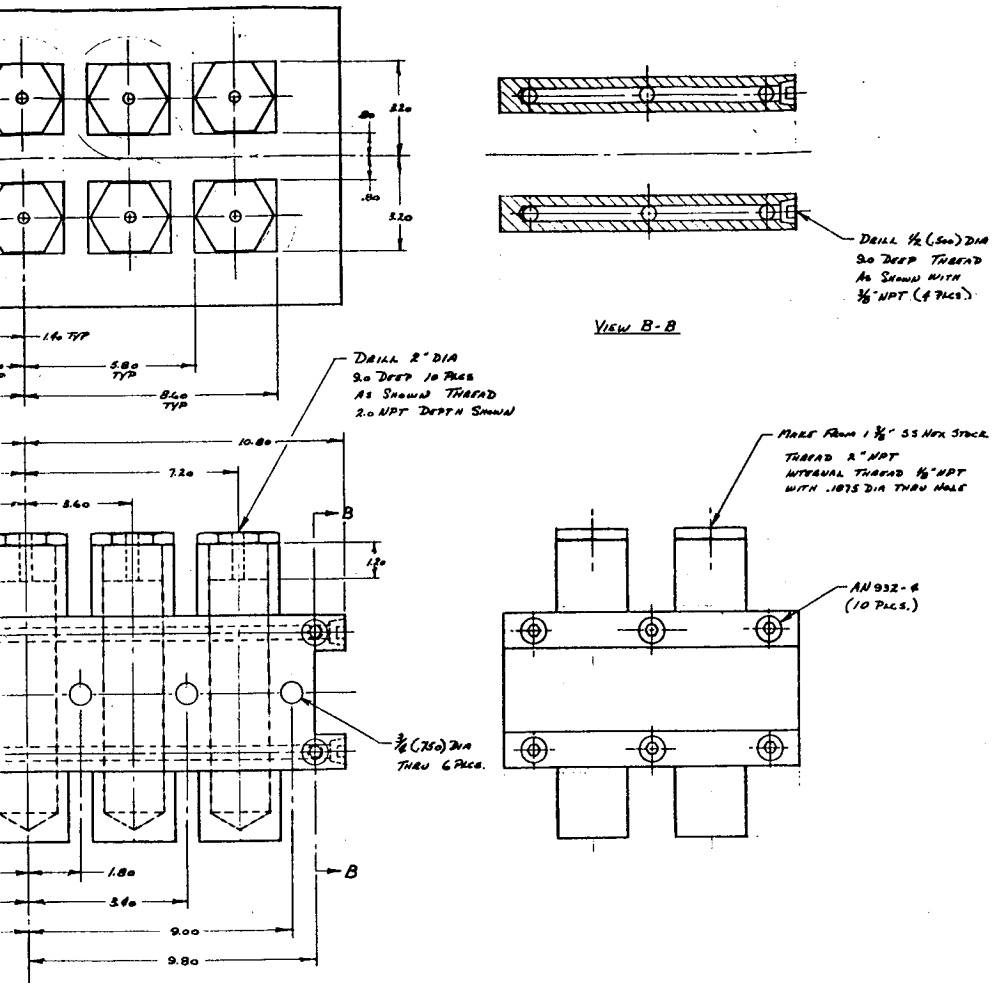

Figure 27. Sample Collection Unit Preliminary Design

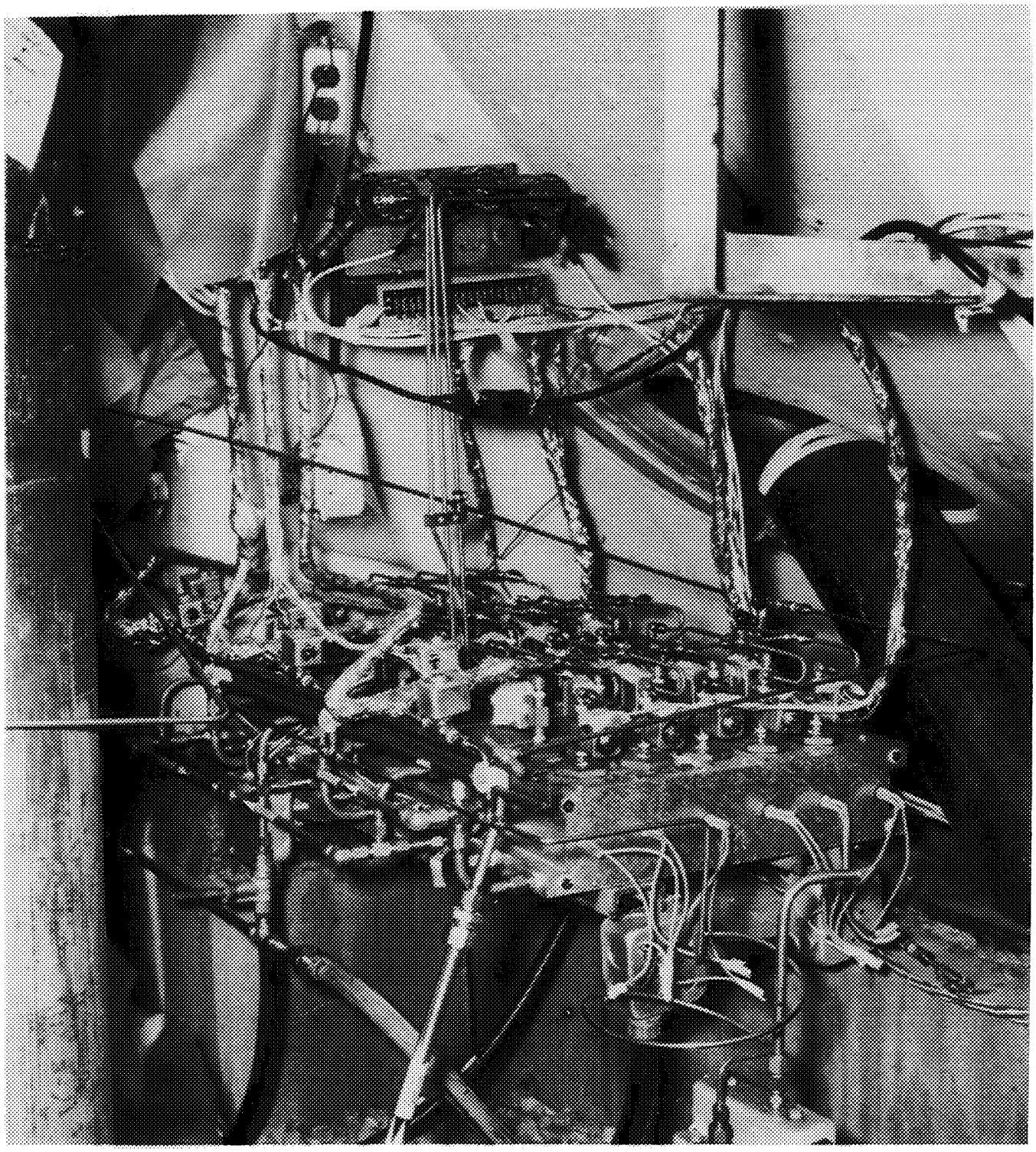

Figure 28. Sample Collection Unit

Given the system temperature, the concentrations of all three species were then calculated for the original sample, again using PVT relationships shown below:

1. Total moles of combustion gases were defined by the pressure measured at known elevated temperature:

$$n_{Total} = \frac{P_1 V_1}{RT_1} \tag{3}$$

2. Moles of hydrogen and/or oxygen were calculated from the calibrated gas chromatographic pressure value (P_{H_2}) and the final system temperature (T_f):

$$n_{H_2} = \frac{P_{H_2} V_1}{RT_f} \qquad n_{O_2} = \frac{P_{O_2} V_1}{RT_f} \tag{4}$$

3. Water was calculated by difference:

$$n_{H_2O} = n_{Total} - (n_{H_2} + n_{O_2}) \tag{5}$$

The gas chromatographic analysis system shown in Fig. 29 was utilized for examination of gaseous propellant residuals in post-combustion samples. The system used a Beckman gas sampling valve and Heise gage. A silica gel pre-column was installed to remove water in the sample. All system components, including the recorder, were mounted on a large cart for portability at the test site (CTL 4). Checkout tests demonstrated that instrument sensitivity and separations for hydrogen, oxygen, and nitrogen were adequate. It was found, however, that peak height measurements could not be used for quantification because of spreading of the hydrogen peak at high concentrations, requiring use of slower integration methods. Response ratio calibrations were performed in the laboratory to minimize the final calibration requirements at the test site.

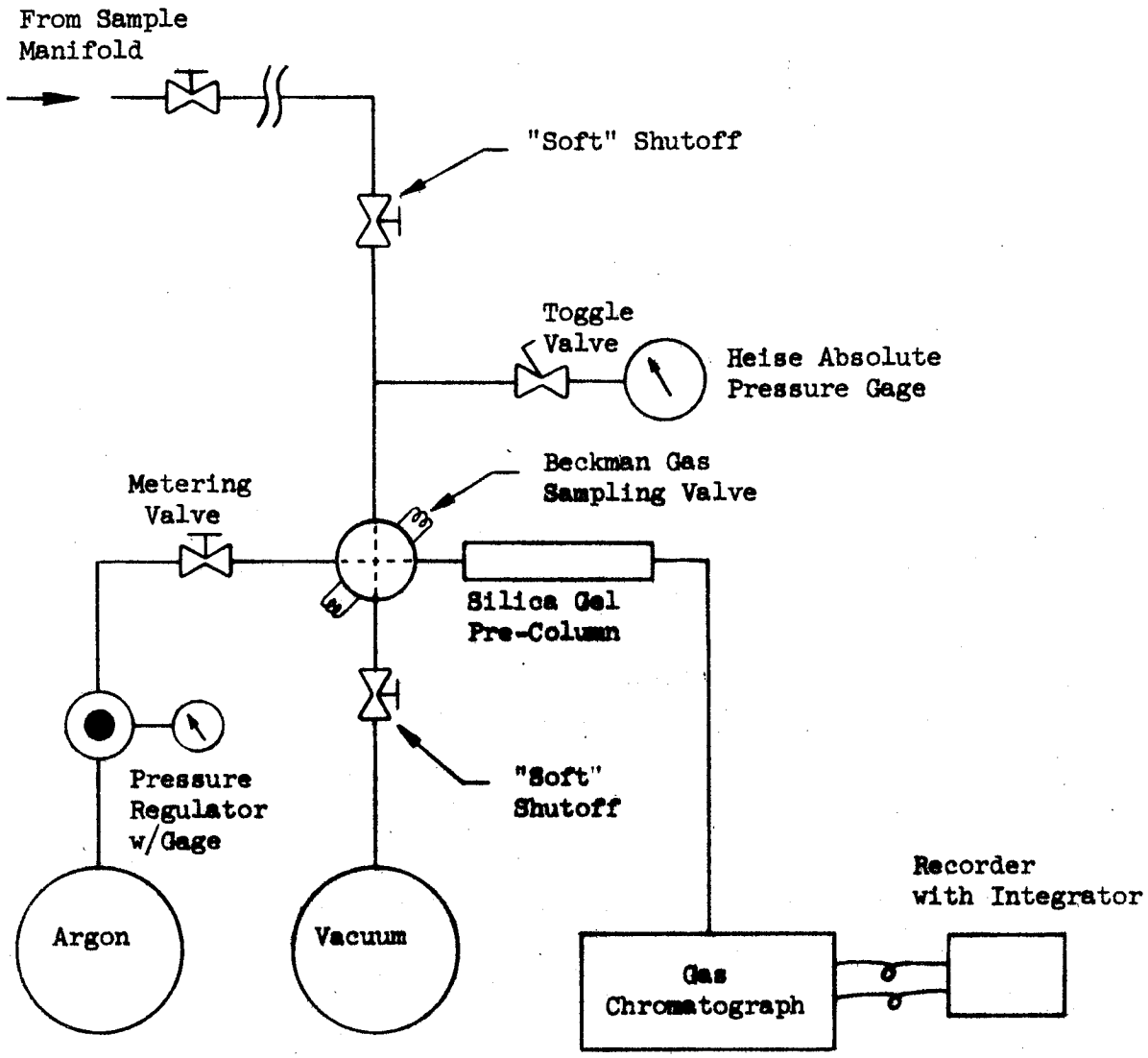

Figure 29. Schematic of Gas Chromatograph Analyzer for H_2 and O_2

Calibration of Sample Blocks

Volumes of the 10 sampling cylinders in each block and of the manifold associated with the blocks were determined manometrically using a calibrated volume and a vacuum system. Separate determinations were made before the initial firings in 1971 (denoted by test numbers 538-552) and later firings in 1972 (denoted by test numbers 238-253) because of a change in valves and short sections of line from the valves to the block. The volumes of blocks No. 1 and 3 used in the first firings are listed in Table 9; the data for block No. 2 are omitted because this unit was not employed during the first set of tests. The volumes measured prior to the later firings are listed in Table 10. Note that differences occurred between the first and second set of volume measurements. As discussed below, the valves were changed because of the unacceptable amount of leakage encountered through the seats of the first model used.

Re-Work and Checkout of Exhaust Analysis Method

The analysis of exhaust gas samples collected during the initial series of motor firings in 1971 resulted in calculated gas compositions which showed no correlation with the injected gas mixture ratios; in addition, the samples were contaminated with considerable quantities of air. Both problems were attributed to leaky sample valves and to insufficient heating of the sample lines. As a result of the latter condition, condensation of some of the water vapor occurred prior to entrapment of the exhaust sample in its bottle.

In the case of the valve leakage, the first valves were typically found to lose approximately 2 mm Hg pressure per minute from a sampling cylinder and 50 to 100 mm Hg per minute from a manifold at atmospheric pressure into an evaculated cylinder. To correct this problem before start of the later program firings in 1972, all sampling bottle valves were replaced by Model MV74P Marotta valves and the entire system leak-checked. With the new valves, the leak rate for the system was reduced to less than 1mm Hg per hour at both ambient and 300 F temperatures in demonstration tests. To determine if sufficient heating of the lines was being provided to ensure that water vapor in the gas sample would not

TABLE 9. MEASURED VOLUMES OF SAMPLING SYSTEM USED DURING INITIAL FIRINGS

SAMPLER NUMBER	VOLUME, cc
SAMPLERS AND MANIFOLD OF BLOCK NO. 1	
1-1	230
1-2	226
1-3	225
1-4	232
1-5	230
1-6	228
1-7	242
1-8	232
1-9	230
1-10	229
Manifold	83
SAMPLERS AND MANIFOLD OF BLOCK NO. 3	
3-1	229
3-2*	224
3-3*	215
3-4	229
3-5	230
3-6	228
3-7	230
3-8	228
3-9	228
3-10	230
Manifold	70

*Valve leaks badly from manifold into sampler.

TABLE 10. MEASURED VOLUMES OF SAMPLING SYSTEM USED DURING LATER FIRINGS

SAMPLER NUMBER	VOLUME, cc
SAMPLERS AND MANIFOLD OF BLOCK NO. 1	
1-1	215
1-2	222
1-3	216
1-4	225
1-5	220
1-6	220
1-7	226
1-8	207
Manifold	
SAMPLERS AND MANIFOLD OF BLOCK NO. 2	
2-1	220
2-2	222
2-3	225
2-4	220
2-5	227
2-6	233
2-7	233
2-8	225
Manifold	
SAMPLERS AND MANIFOLD OF BLOCK NO. 3	
3-1	220
3-2	227
3-3	225
3-4	226
3-5	220
3-6	231
3-7	224
3-8	226
Manifold	

condense, a known sample of air and water vapor mixture was flowed through the entire sampling system while it was heated in an identical manner to that employed during the engine tests. In this test, condensation occurred in the manifold inlet lines. The lines were then wrapped with additional insulation tape and the test repeated. With the extra heating, no condensation was observed. The additional heating was therefore incorporated in the test apparatus.

To determine whether the overall system, including the gas chromatograph, could adequately sample and analyze a mixture of hot gases consisting of noncondensibles (oxygen and/or hydrogen) and condensibles (water vapor), an overall procedure verification was performed. This demonstration consisted of two tests. In one test, an equimolar mixture of air and water vapor was used to simulate the hydrogen/oxygen/water vapor sample that would be obtained from an engine firing. In the second test, the sample contained only air at the same initial pressure as used in the first sample. In each test, samples were prepared in a 1.8 liter container heated to vaporize the water. The container was hooked to the manifold* of the hot sample block and allowed to expand into one of the ten individual cells contained in the sample block. The sample was then entrapped within the cell by shutting the inlet valve and the resulting pressure in the sample cell was measured. The sample block was then cooled to a known temperature to condense any water vapor contained in the sample. Finally, the remaining gases were expanded to the inlet of the gas chromatograph and the pressure was again measured. Knowing the temperature and pressure at the heated and cooled conditions in addition to the gas chromatograph analysis is sufficient to determine the specie concentrations and the amount of water vapor. The results from the two tests are shown in Table 11. Note that the removal of the considerable water vapor molecules from the first sample should result in a ratio between its initial and final pressures (32/341) that is twice the pressure ratio of the second sample (17/310).

*The manifold was maintained at 300 F with heating tapes.

TABLE 11. DEMONSTRATION OF PROCEDURE FOR DETERMINING CONDENSIBLE FRACTION OF NOZZLE EXHAUST GAS

Checkout Mixture	Hot Sample Block Pressure	Cold Sample Block Pressure
Air-Water	32 psia	341 mm Hg*
Air	17 psia	310 mm

*Corrected vapor pressure of water and differential initial pressures

The sample concentrations were selected such that the cold block expansion pressure of the air/water mixture (after correction for the vapor pressure of water and the Charles Law effect of the hot block initial temperature) should match that of the air sample. However, as shown in Table 11, the pressures differed by approximately 10 percent. This difference may be due to imperfect temperature control upon the various parts of the system.

It can be shown that the apparent possible error of 10 percent in the non-condensible fraction (assumed to be all hydrogen) will not introduce serious errors in the computed propellant mixture ratio. For a true mixture ratio of 4.0, an apparent mixture ratio of 3.6 will be calculated. For a true mixture ratio of 5.3, an apparent mixture ratio of 5.1 will be calculated. This level of accuracy is more than adequate to accomplish the objectives of the project, namely to determine the approximate level of mixture ratio striation in the rocket engine exhaust. Consequently the demonstration tests indicated that useful samples could be obtained and analyzed in the second set of firings made in 1972.

TASK IV - STRATIFIED FLOW ENGINE FIRINGS

TEST FACILITY

The hot firing experiments for characterizing the effects of controlled mixture ratio stratification were made at Cell 29B of Component Test Lab IV at the Rocketdyne Santa Susana Field Laboratory, Chatsworth, California. The experiments required an altitude chamber capable of discharging flows at a 25:1 expansion ratio and a total pressure of 250 psia. The installation of the combustor nozzle assembly, with the environmental chamber, is shown in Fig. 30.

Propellant and Water Systems

The 29B test position consists of LOX, GO_2, and GH_2 propellant supply systems, altitude simulation systems, and instrumentation systems.

The test hardware is located in a 16-foot diameter by 30-foot long vacuum chamber which exhausts horizontally. A single-stage steam-driven ejector system is piped to the capsule. This ejector system is capable of sustaining simulated altitude in excess of 23 kilometers in the vacuum chamber.

The propellant supply systems include the temperature, pressure, and flow controls necessary for testing. LOX is supplied to the injector from a 3000-psia, 600-gal uninsulated tank in the tank and feed system shown in Fig. 31. Note that the LOX flows through a flowmeter in the main line before dividing into two branches. One branch feeds LOX to the core of the injector, while the other provides propellant to the outer zone. Each branch is fitted with a flowmeter. In this way, redundant measurements are made. The flowrates through each branch are controlled with orifices as shown. The LOX core feed has a 7/16-inch (0.4375-inch diameter) orifice upstream of the main valve. Two other orifices are a No. 29 (0.136-inch diameter) in the outer zone through-line and a 25/64-inch (0.3906-inch diameter) in the outer zone bypass line (with the shutoff valve). The nitrogen purge, as part of this system is plumbed downstream of all main valves. This system provides both

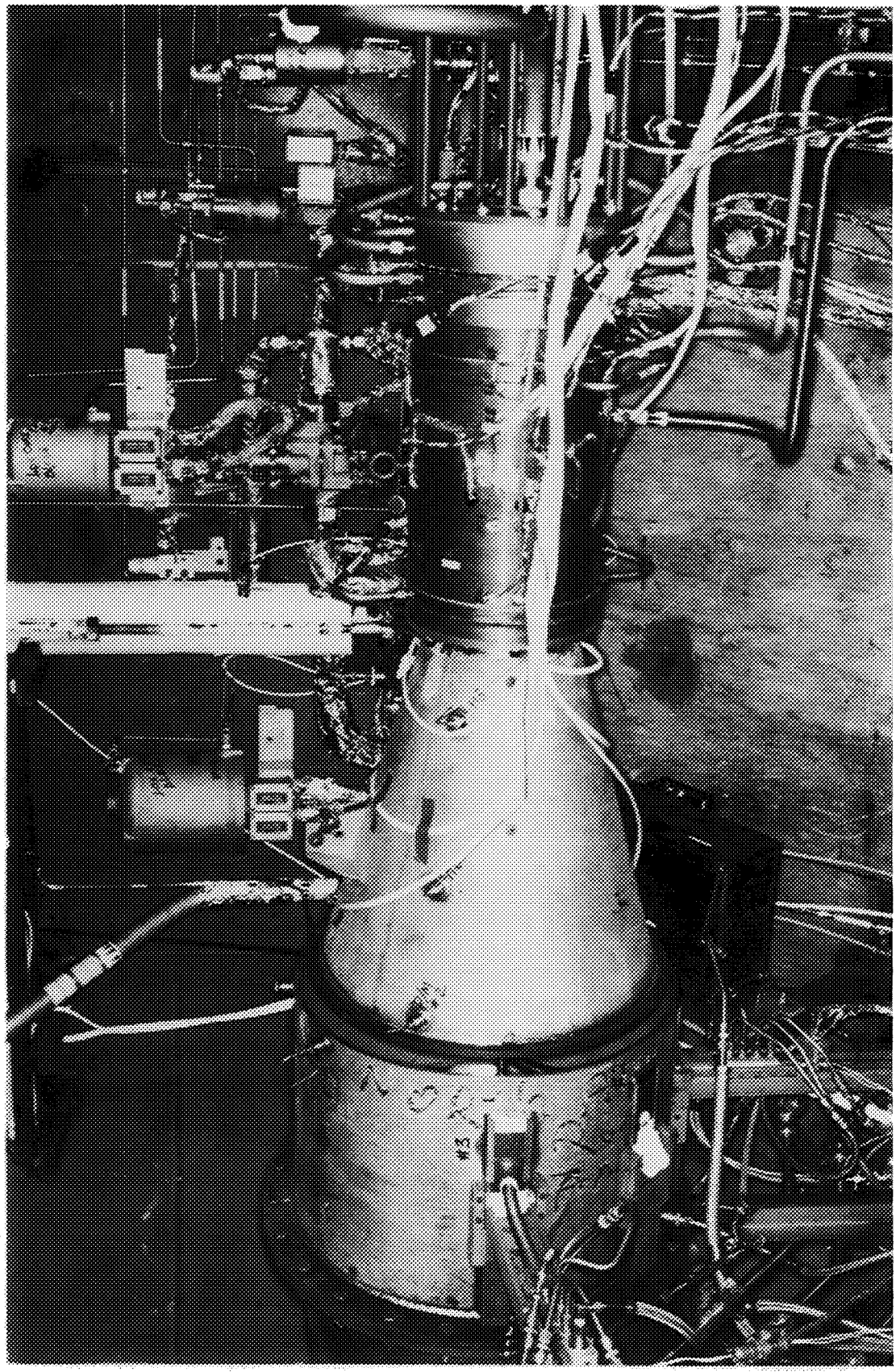

Figure 30. Engine Assembly

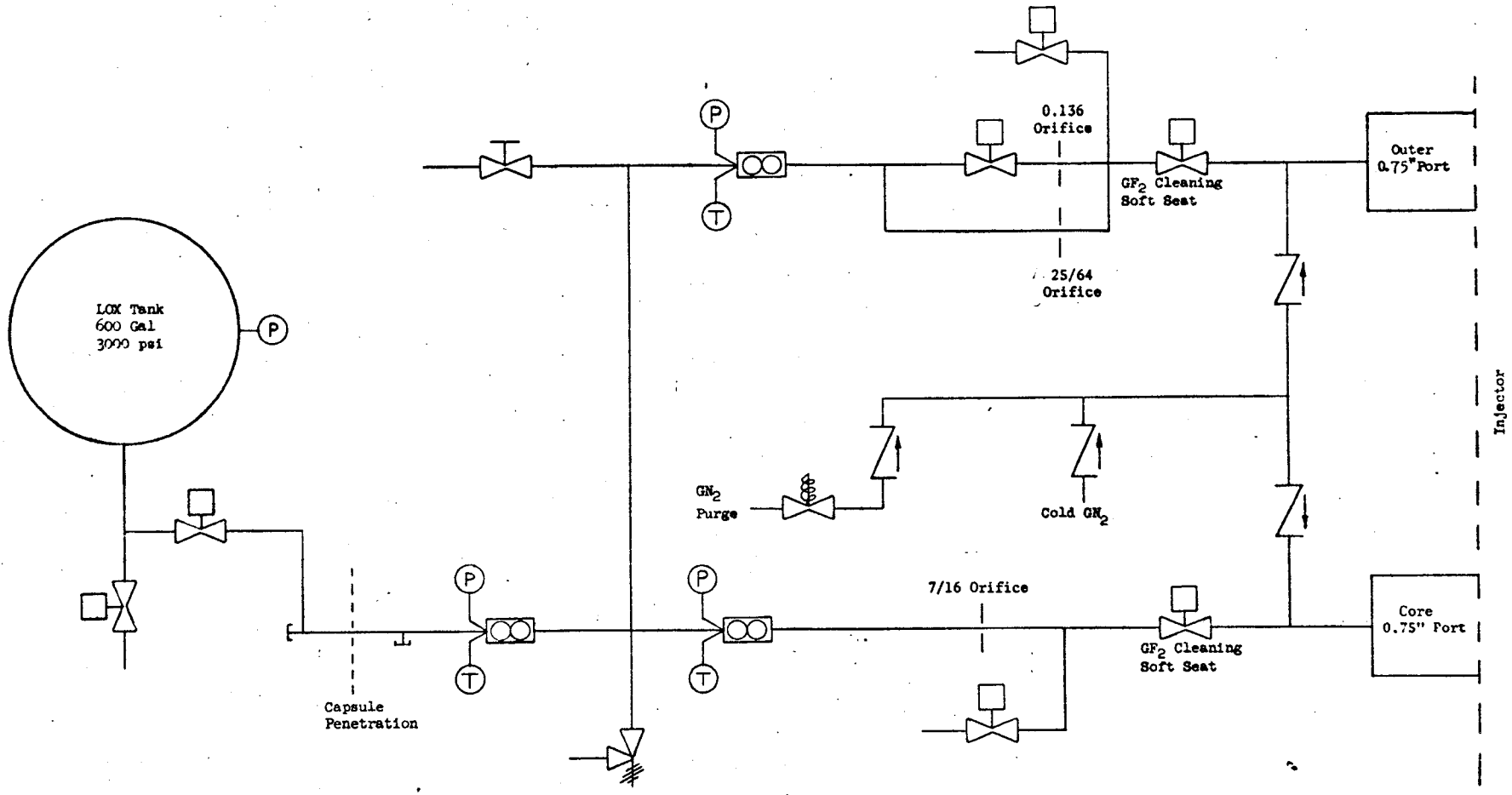

Figure 31. Stratified Injector LOX System

liquid and gaseous nitrogen. The liquid nitrogen is utilized to condition the hardware before firing to ensure the LOX will not boil before injection into the combustion chamber.

The GH_2 is supplied from a 470-ft^3, 3000-psi storage vessel as shown in Fig. 32. For this system, the total propellant flow is divided into three zones, feeding (1) the BLC, (2) the core, and (3) the outer zone of the injector. The initial temperature of the hydrogen gas is ambient.

The chamber is water-cooled between tests and water is required to cool the probes. The entire water system is shown in Fig. 33. Note that two tanks are used. The tank that supplies water to the cowl passages of the probes comes from a 360-gal, 2000-psi tank flowing ambient water, which also supplies water for cooling the chamber between runs. The other system is also a 360-gal, 2000-psi tank; however, the water from this tank is heated by means of the heater shown in the sketch to about 250 F prior to its use in cooling the probe center body annuli.

Finally, the propellants were ignited with gaseous fluorine from the system shown in Fig. 34. One fluorine K bottle was used which was plumbed directly to the LOX system downstream of the LOX main valves. The pressure at the bottle is approximately 250 psia, and the nominal flowrate is 0.17 lb/sec.

The overall instrumentation for the various systems is shown in their respective schematics. The instrumentation within the blockhouse control center is listed in Table 12.

Sampling System

The probes were supplied with high pressure water in the manner illustrated in Fig. 35. The heated water was supplied at a temperature of approximately 250 F at the probe inlet and at the maximum allowable system pressure. This pressure requirement was a result of choked flow areas in the probe tip flow

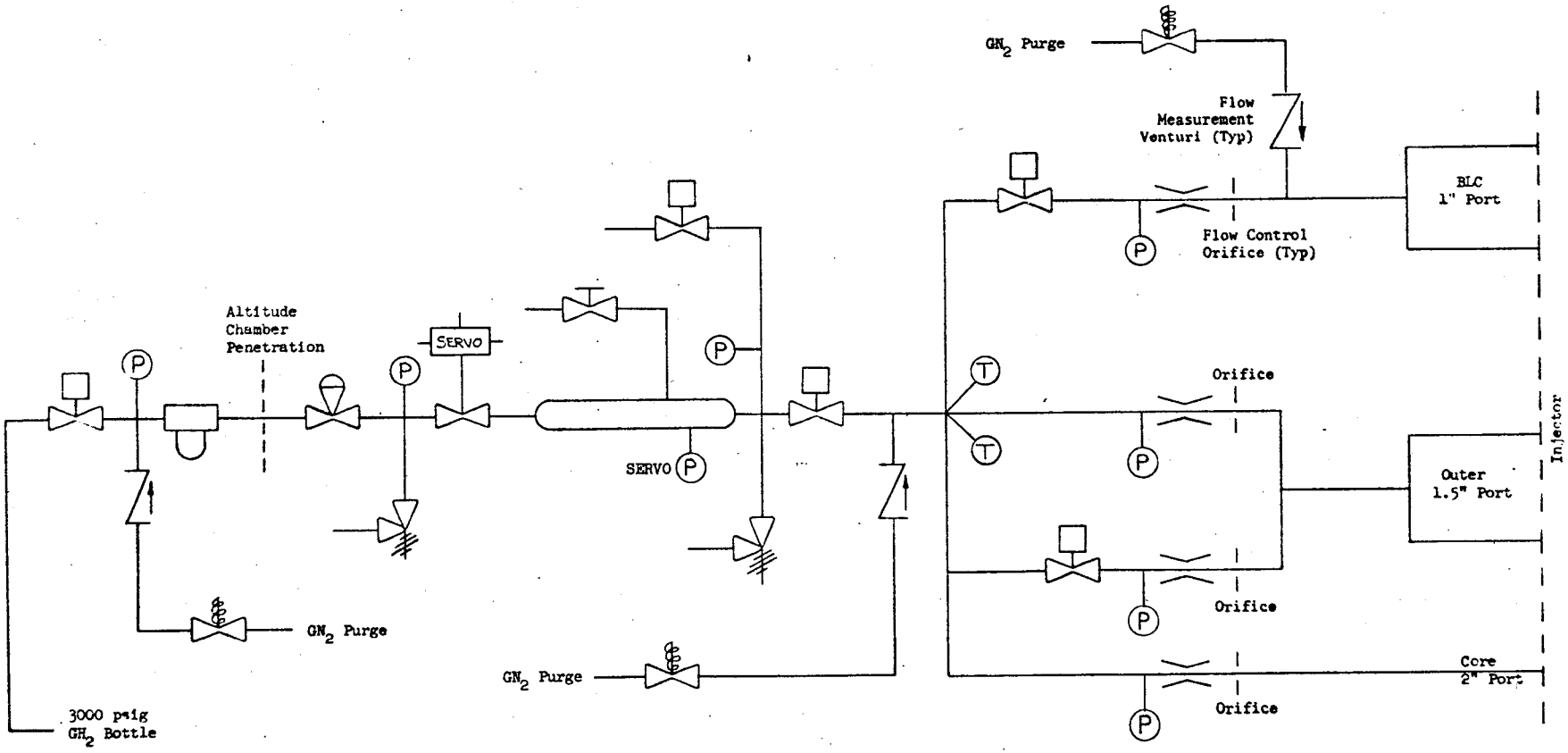

Figure 32. Stratified Injector GH_2 System

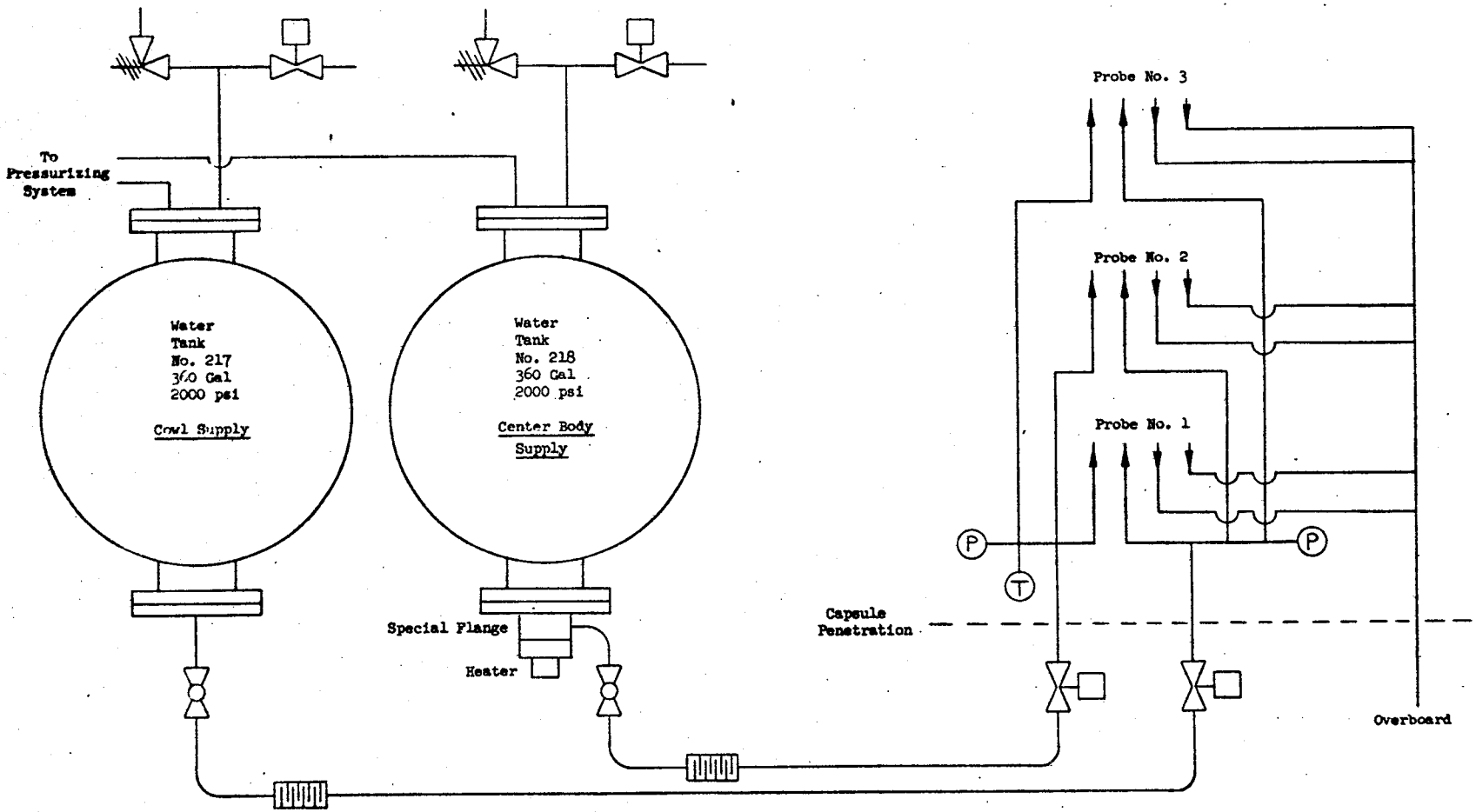

Figure 33. Stratified Injector Exhaust Sampling Probe Water System

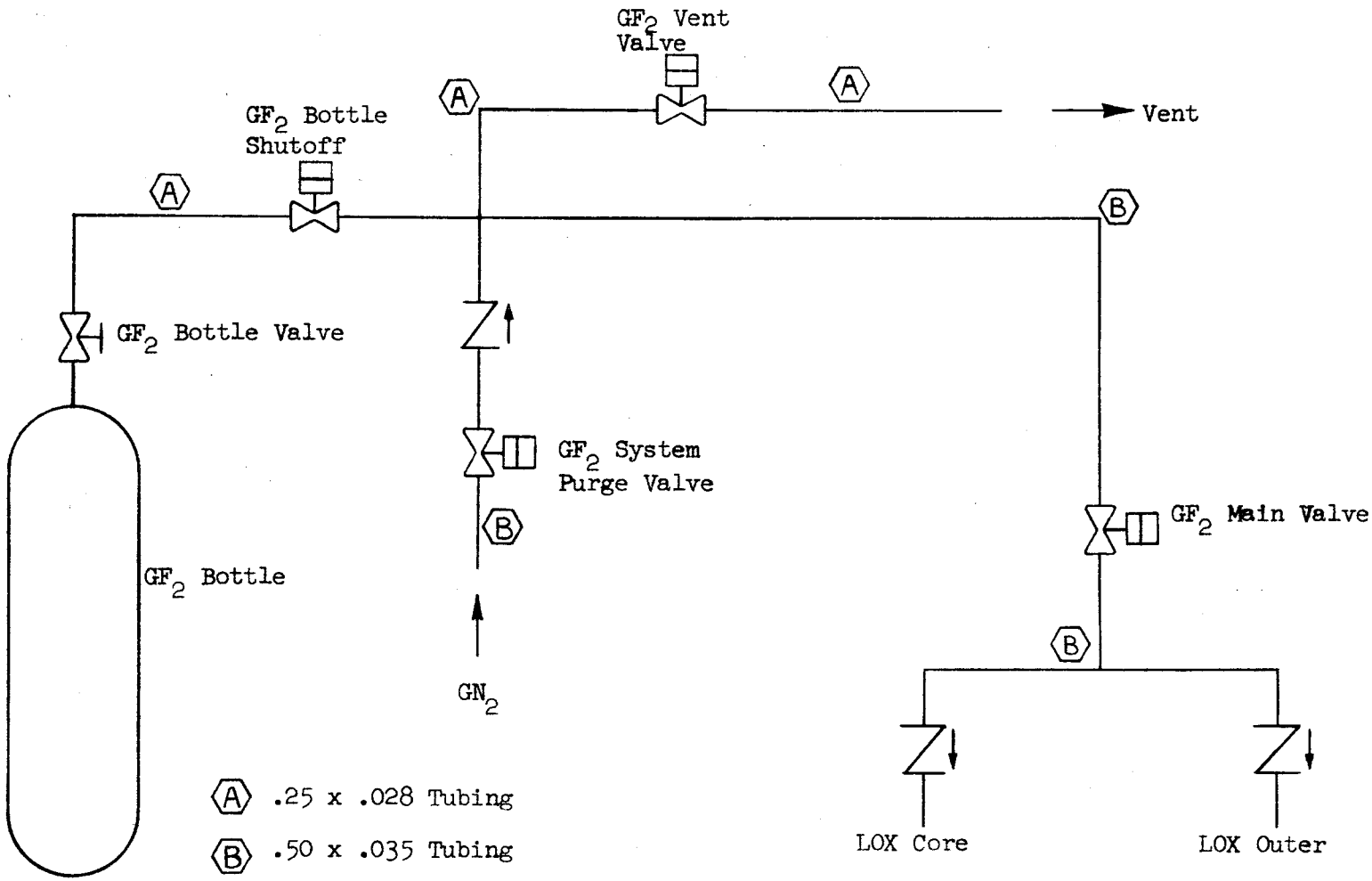

Figure 34. Stratified Injector GF_2 System

TABLE 12. INSTRUMENTATION CAPABILITIES AT CELL 29A

Location	Instrumentation
Instrumentation inside of altitude can	56 channels for pressure, thrust, RTD, flow 6 channels for accelerometers 34 channels iron/constantan only 12 channels iron/constantan or chromel/alumel 3 channels 2 psia pressure systems
Instrumentation outside of altitude can	12 channels for pressure, thrust, RTD, flow 20 channels iron/constantan or chromel/alumel
Recording capabilities	100 channels digital system with sample rate up to 40 KC 36 channels direct write oscillograph frequency response 240 cps 15% 8 channels Brush recording, 80 mm full scale frequency response of 30 cps. 200 cps at reduced amplitude 8 channels Brush recording, 40 mm full scale frequency response of 55 cps. 200 cps at reduced amplitude 54 channels direct inking graphic recorders frequency response of 1 cps 40 channels 28 VDC event; Signal recordings frequency response 10 cps 24 channels 28 VDC event; Signal recordings on 8 channels of direct write oscillograph 48 channels 28 VDC event; Signal recordings on digital system 42 channels of high frequency analog recording up to 20 KC

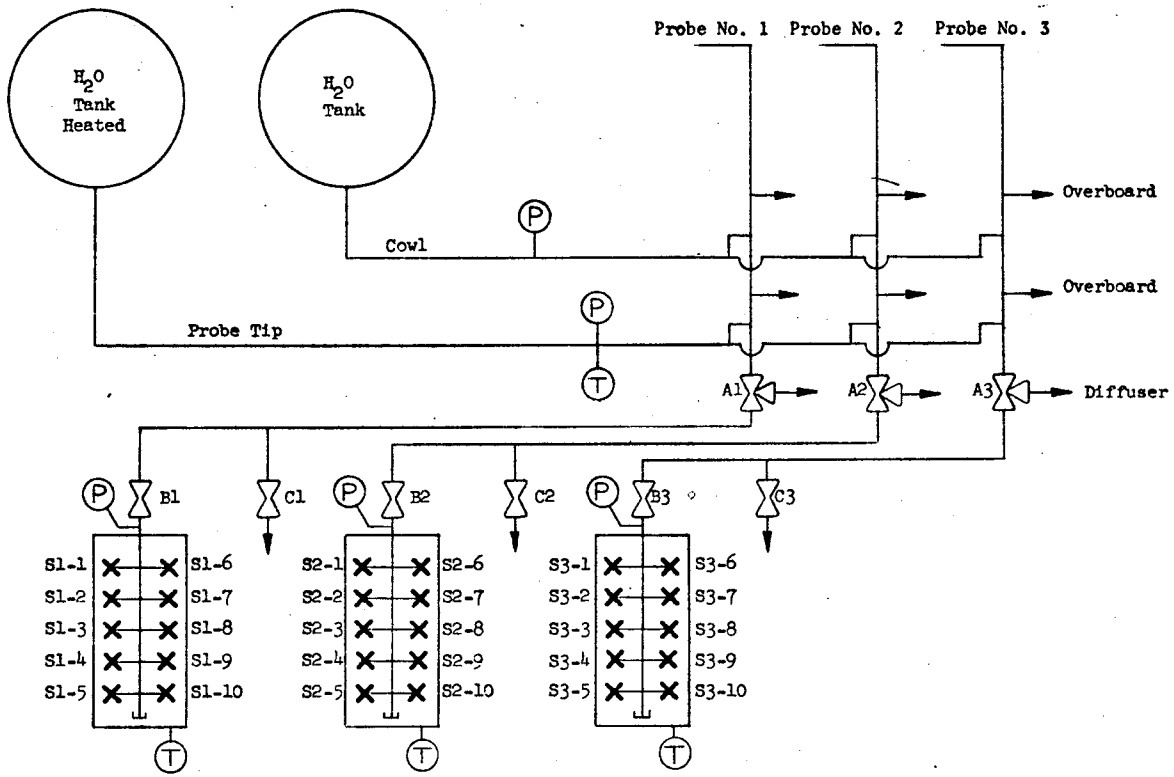

Figure 35. Sample Flow System Schematic

passages. The cowl water supply pressure was 800 to 840 psi. Design water flow through the cowl and tip of each probe was 1.65 lb/sec and 1.38 lb/sec, respectively.

The sample blocks utilized to capture the probe samples are also illustrated in Fig. 35. The sequencing required during test operation is as follows:

1. Probe line heaters and block heaters on - off at 350 F; 300 F steady-state anticipated.
2. All sample valves and B&C identified valves open - evacuate system by vacuum pumping - then close all valves.
3. Pressurize water system and establish flow.
4. Hyperflow system start and brought to stable operation.
5. Open B1 - 3 and S1 - 1, S2 - 1, and S3 - 1
6. Engine start + 850 msecs, close A1 - A3
7. Engine start + 1850 msecs, open A1 - A3 and close S1 - 1, S2 - 1 and S3 - 1
8. Open C1 - C3 and S1 - 2, S2 - 2, and S3 - 2
9. Repeat steps 6, 7, and 8, increasing sample number until test series is complete.

The sample blocks each employed six heaters. It required approximately 15 minutes to heat each block to 350 F. Control of this heating circuit and DIGR* readout to monitor the respective temperatures in each block were available in the control blockhouse. A manually controlled firex water supply was also used to cool the sample blocks for posttest analysis and to condense the water from the sample specimens.

*Digital Readout display system

Valve Sequence

Using the line lengths and sizes for the individual systems shown in the various schematics, the individual line volumes were calculated to differ by a factor of 5. The fuel side line volume is much larger, such that it primed in approximately 15 msec, while the oxidizer side required about 330 msec. Therefore, a typical operational sequence was:

1. Probe water supply on - both coolants
2. Engine start
3. LOX purge on (pressure check off)
4. +100 msec GH_2 main open
5. +130 msec GF_2 main open
6. +200 msec LOX main open - GF_2 main closed
7. +600 msec P_c verification (75 psi)
8. +850 msec record gas samples to +1850 msec
9. +2000 msec engine cut. - all purges on approximately 5 seconds
10. Engine coolant water supply on

This operation is repeated throughout the test series until all scheduled tests are completed.

TEST PROGRAM

A total of 31 engine firings were performed in two major phases. The first phase, consisting of 15 tests, designated by run numbers 538 through 552, included 4 checkout tests of the overall system, followed by 11 successive firings made to measure performance, chamber and nozzle pressure profiles, wall heat flux, and exhaust gas composition. Useful data in all areas except

nozzle gas composition were obtained in 10 of these firings*. Leakage of atmospheric contaminants through valves in the sampling system precluded obtaining accurate composition data in the first tests. During the second phase, consisting of 16 tests, designated by run numbers 238 through 253, the exhaust sampling technique was improved and additional gas composition data were obtained, together with further performance and heat transfer measurements. The test conditions (chamber pressure, overall and zonal mixture ratios, and percent film coolant), together with the uncorrected c* efficiency for the various firings, are summarized in Table 13. Details of operating conditions and performance for the individual firings are presented in Appendix A.

In the first series, the nominal mainstage duration of each firing was 2.0 seconds, although the overall firing duration was 3.0 seconds. In later tests, the mainstage duration was increased to 3.0 seconds. The accuracy of the data obtained in the test program is contingent upon how closely the measured operating conditions during the firings approximated their eventual steady-state values. Typical histories of several key operating parameters are presented in Fig. 36 through 39 for the initial firing series. Figure 36 shows that the total LOX flowrate was just achieving steady-state at test termination. Consequently, both the chamber pressure and the thrust were also varying during the entire run, as shown on Fig. 37 and 38. However, during the last 400 msec of the run, the variation is minimal, such that data evaluated during this period can be considered applicable to steady-state conditions. For the latter firing series increasing the firing duration by 1.0 second insures steady-state operation. I_s and c* performance accordingly were calculated for each test, based upon flowrate, chamber pressure and thrust near the end of the run. Although the system showed a tendency for hard starts, the time-variant data in Fig. 36 through 38 also indicate that the tests were sufficiently stable to permit accurate performance and heat transfer data to be obtained. A typical transient temperature response of one of the throat-region wall-heat flux transducers is shown in Fig. 39. The almost linear rise in temperature,

*One test, Run 543, was terminated before achieving mainstage because of icing in the probe water coolant passages.

TABLE 13. SUMMARY OF STRATIFIED FLOW ENGINE FIRINGS

Test	Expansion Ratio	Chamber Pressure	Mixture Ratio			Percent* Film Coolant	η_{c^*}	Remarks
			Overall	Core	Outer Zone			
538	25:1	---	---	---	---	---	---	Checkout System
539	25:1	---	---	---	---	---	---	Checkout System
540	25:1	---	---	---	---	---	---	Checkout System
541	25:1	---	---	---	---	---	---	Checkout System
542	25:1	232	5.48	7.98	4.71	9.65	0.982	
543	25:1	---	---	---	---	---	---	Cut before Mainstage
544	25:1	232	5.77	6.94	6.17	11.97	0.958	
545	25:1	217	5.09	7.70	4.20	10.02	0.976	
546	25:1	217	5.06	6.90	3.76	0.00	0.988	
547	25:1	223	5.65	6.00	5.28	0.00	1.012	
548	25:1	216	4.85	7.28	4.04	9.82	0.971	
549	25:1	216	5.17	6.16	5.59	12.09	0.990	
550	25:1	207	4.68	6.89	3.97	9.71	0.975	
551	25:1	229	5.39	7.83	4.65	9.70	0.977	
552	25:1	224	5.32	7.29	3.92	0.00	0.986	
238	25:1	217	4.78	7.02	3.94	9.70	0.983	
239	25:1	137	6.64	8.75	5.15	0.00	0.901	
240	25:1	219	5.31	6.16	5.67	11.79	0.999	
241	25:1	215	5.21	6.33	5.27	11.80	0.995	
242	25:1	213	4.79	7.13	3.89	9.70	0.976	
243	25:1	212	5.33	5.69	4.81	0.00	1.009	
244	25:1	205	4.71	7.18	3.94	9.70	0.963	
245	4:1	210	4.94	7.38	4.05	9.69	0.973	
246	4:1	254	5.56	8.08	4.80	9.70	0.984	
247	4:1	269	4.42	6.67	3.66	9.72	0.992	
248	4:1	250	6.73	8.04	7.21	11.81	1.005	
249	4:1	264	4.92	7.35	4.09	9.73	1.006	
250	4:1	274	5.41	6.45	5.81	11.82	1.007	
251	4:1	269	6.24	6.55	5.90	0.00	1.022	
252	4:1	265	4.93	6.00	4.18	0.00	0.982	
253	4:1	258	5.14	7.53	4.40	9.71	0.988	

* Percent of total fuel flow

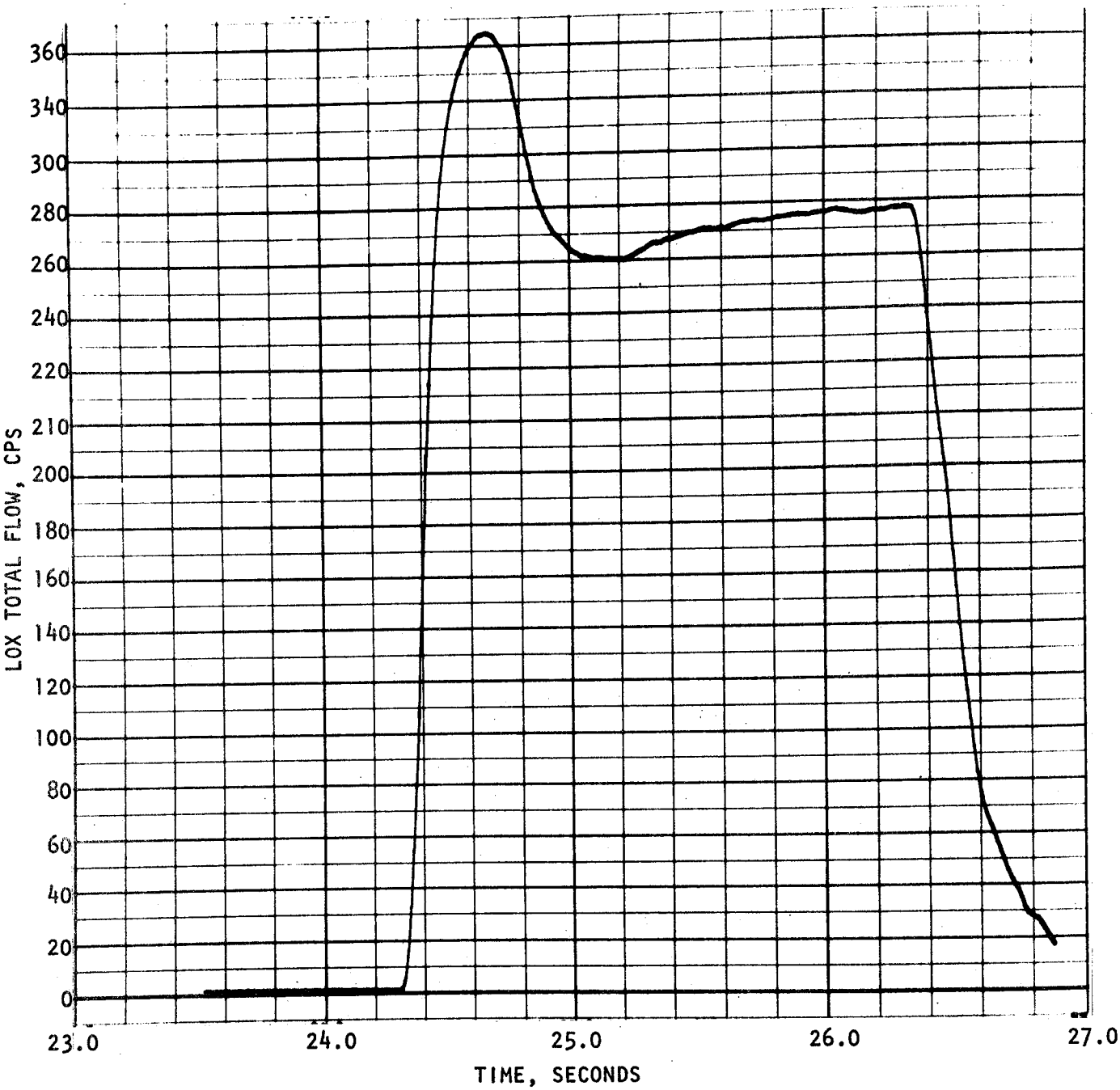

Figure 36. Total LOX Flowrate-Time History for Run 547

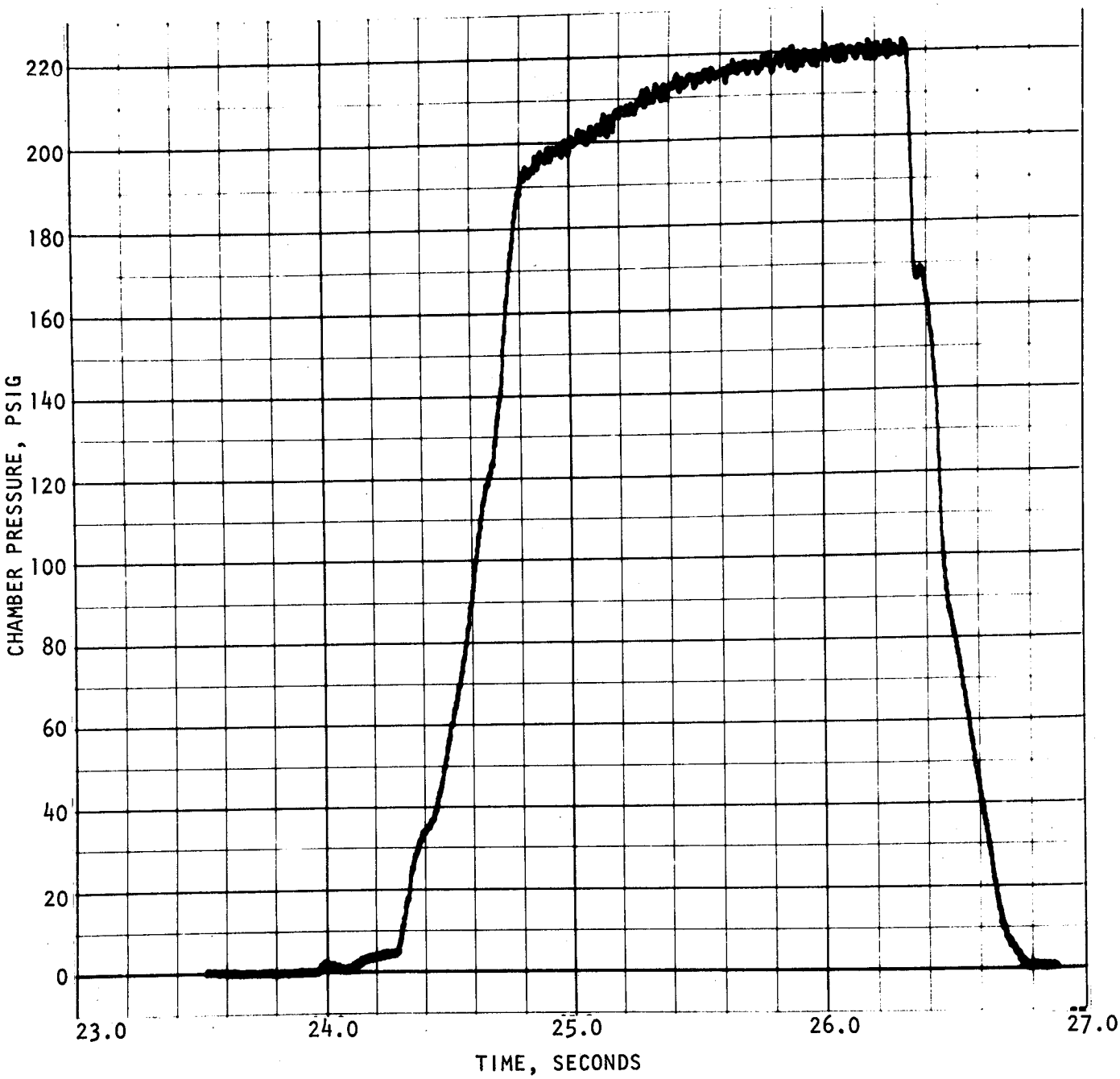

Figure 37. Chamber Pressure-Time History for Run 547

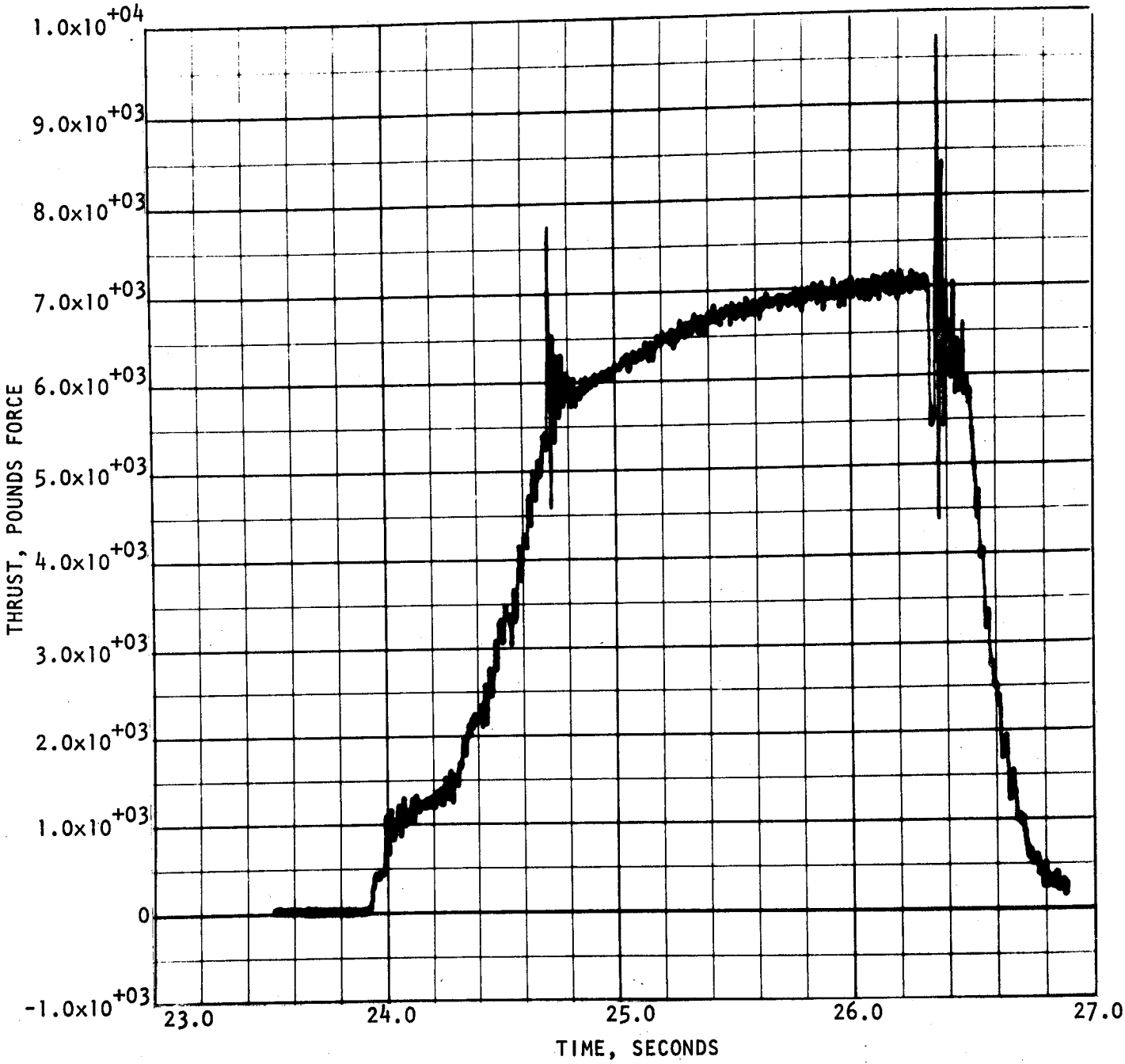

Figure 38. Thrust-Time History for Run 547

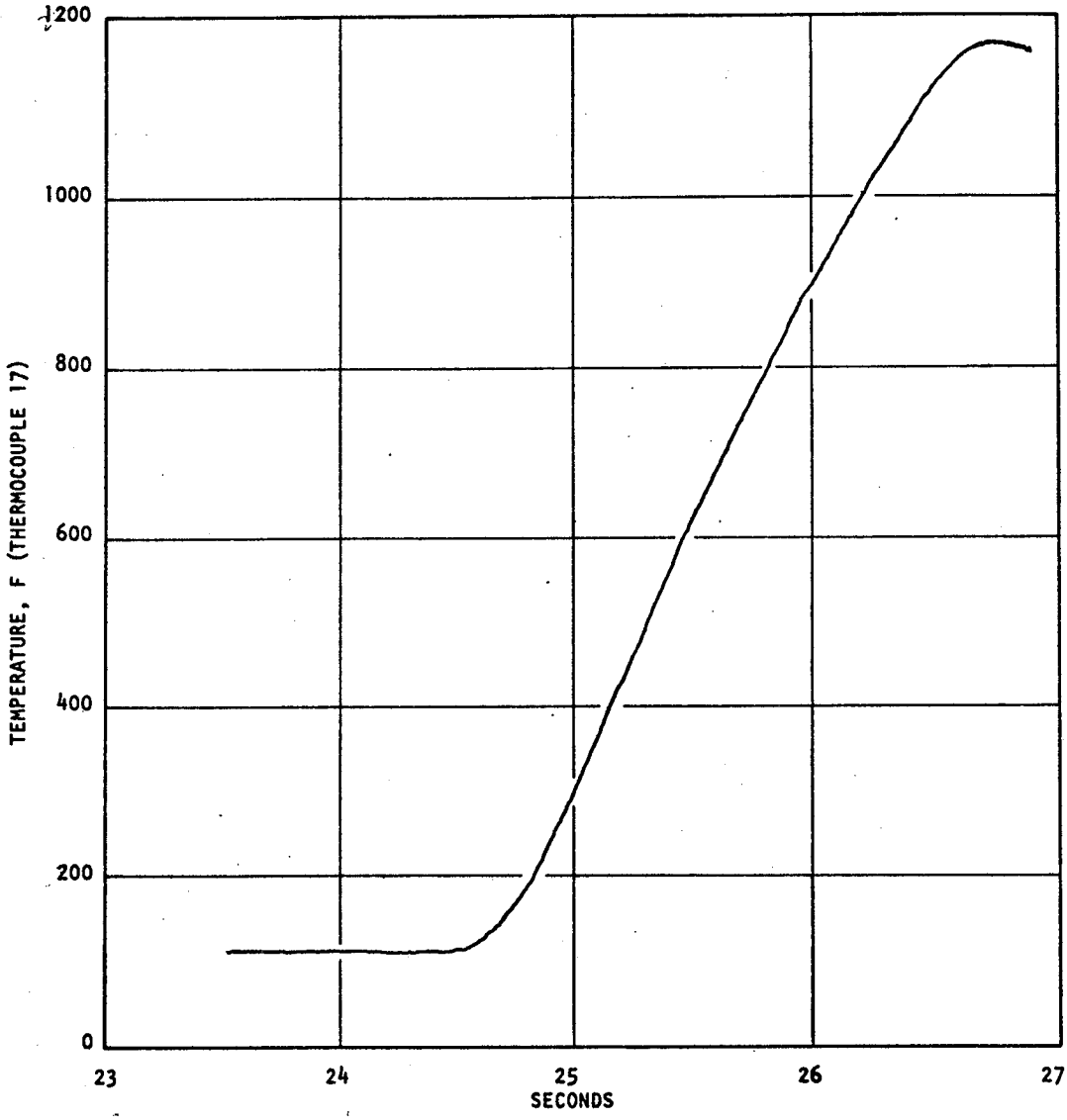

Figure 39. Temperature History of Throat Region Heat Flux Transducer No. 17 During Test 547

together with the low wall temperature relative to the combustion gas stagnation temperature, indicates that the wall heat transfer measurements were also representative of steady-state conditions for cooled wall thrust chamber.

Performance Results

Examination of the c* efficiencies listed in Table 13 shows that, with only four exceptions, η_{c^*} ranged from 0.97 to 1.015, with an average value of 0.985 and an estimated uncertainty of ±0.01 (based upon an analysis of the variance in duplicate measurements of chamber pressure and flow). The listed value of η_{c^*} is based upon the usual definition:

$$c^* = \frac{P_0^* A_g^*}{\dot{w}}$$

when the nozzle stagnation pressure P_0^* is defined from the average of the static pressures measured at pressure taps 7 and 8 as listed in Table 3, together with the appropriate Mach number correction for an area ratio of 2:1. If complete combustion is assumed at the axial location of the two taps (located 6.85 inches downstream of the injector), then no additional corrections are necessary to this prescribed definition of P_0^*.

The high c* efficiency indicates that both combustion and mixing are essentially completed upstream of the nozzle throat. It should also be noted from the data in Table 13 that combustion efficiency is not degraded either by mixture ratio stratification in the main gas stream or by use of as much as 12 percent of the fuel as film coolant.

With complete combustion and mixing, the specific impulse efficiency, η_{I_s}, is defined essentially by the nozzle expansion ratio and the nozzle exhaust pressure, with minor corrections for boundary layer losses and nozzle divergence angle. Table 14 compares the values of η_{I_s} based upon measured thrust to η_{c^*} for those tests in which the more meaningful data were obtained. The uncorrected vacuum η_{I_s}, listed in the third column of Table 14, is defined

TABLE 14. CALCULATED PERFORMANCE OF STRATIFIED FLOW ENGINE WITH CORRECTIONS

Test	η_{c^*}	Uncorrected Vacuum η_{I_s}	Corrected Vacuum η_{I_s}	Expansion Ratio	Remarks
542	0.982	0.920	0.960	25:1	
543	---	---	---	25:1	
544	0.958	0.937	0.978	25:1	
545	0.976	0.909	0.987	25:1	
546	0.988	0.919	0.949	25:1	
547	1.012	0.937	0.979	25:1	
548	0.971	0.907	0.947	25:1	
549	0.990	0.907	0.947	25:1	
550	0.975	0.931	0.972	25:1	
551	0.977	0.894	0.934	25:1	
552	0.986	0.654	0.682	25:1	Thrust measurement suspect
238	0.983	0.914	0.954	25:1	
239	0.901	1.115	1.164	25:1	P_C and $\dot{w}$ measurement suspect
240	0.999	0.956	0.999	25:1	
241	0.995	0.996	1.041	25:1	
242	0.976	1.018	1.043	25:1	
243	1.009	1.055	1.102	25:1	
244	0.963	0.967	1.009	25:1	
245	0.973	0.905	0.957	4:1	
246	0.984	0.802	0.828	4:1	$\eta_{I_s} = 0.952$ for $P_0/P_E = 19$
247	0.992	0.822	0.849	4:1	$\eta_{I_s} = 0.975$ for $P_0/P_E = 19$
248	1.005	0.796	0.852	4:1	$\eta_{I_s} = 0.979$ for $P_0/P_E = 19$
249	1.006	0.810	0.836	4:1	$\eta_{I_s} = 0.962$ for $P_0/P_E = 19$
250	1.007	0.832	0.858	4:1	$\eta_{I_s} = 0.986$ for $P_0/P_E = 19$
251	1.022	0.823	0.849	4:1	$\eta_{I_s} = 0.976$ for $P_0/P_E = 19$
252	0.982	0.808	0.833	4:1	$\eta_{I_s} = 0.958$ for $P_0/P_E = 19$
253	0.988	0.812	0.838	4:1	$\eta_{I_s} = 0.963$ for $P_0/P_E = 19$

from the measured thrust and nozzle exit pressure and from the theoretical full shifting specific impulse from

$$I_s \Big|_{\substack{\text{Uncorrected} \\ \text{Vacuum}}} = \frac{F + P_E A_E}{\dot{w}}$$

$$\eta_{I_s} \Big|_{\substack{\text{Uncorrected} \\ \text{Vacuum}}} = \frac{I_s \Big|_{\substack{\text{Uncorrected} \\ \text{Vacuum}}}}{I_s \Big|_{\substack{\text{Theoretical} \\ \text{Vacuum}}}}$$

The corrected vacuum η_{I_s} listed in the fourth column is defined from the uncorrected specific impulse by application of corrections for boundary layer losses and for nozzle divergence angle. Based upon the detailed theoretical analysis of tests 547, 238, 250, and 252 in Task V, using the JANNAF computer programs, a boundary layer loss of 11.0 seconds was applied to firings with a nozzle expansion ratio of 25:1, while a loss of 6.0 seconds was applied to firings with a nozzle expansion ratio of 4:1. For the 15-degree conical nozzle, a nozzle divergence angle correction factor of 0.983 was applied to the theoretical vacuum I_s. This was based upon the values recommended by Sutton in Ref. 4. A simplified analysis based upon measured wall heat fluxes near the injector indicated that heat losses upstream of the starting point of the boundary layer analysis would introduce impulse losses of less than 0.5 second; consequently, this JANNAF-recommended correction was not applied.

Examination of the corrected η_{I_s} values in Table 14 indicates that the equivalent vacuum, I_s, performance of the stratified flow engine was generally excellent for the 25:1 nozzle (although several of the calculated efficiencies in excess of unity must represent measurement errors in either thrust or propellant flowrate). For those tests with the 4:1 expansion ratio nozzle exhausting to atmospheric pressure, the corrected equivalent vacuum η_{I_s} is only 0.82 through 0.85. In these tests, however, the more appropriate definition of thrust efficiency is one referenced to the theoretical thrust coefficient at the exhaust pressure ratio (P_0/P_E) and nozzle expansion ratio actually tested. Using the chamber pressures listed in Table 13 to define a

mean exhaust pressure ratio of 19, together with the nozzle expansion ratio of 4:1 and the graphical correlation presented in Fig. 3 through 9 of Ref. 4, results in a correction factor of 1.15. This factor is applied to the corrected vacuum η_{I_s} to determine the corresponding efficiency at the real exhaust pressure. These calculated efficiencies are presented in the Remarks column of Table 14 for the final tests at non-vacuum exhaust conditions. Examination of the latter data indicates that a realistically defined thrust efficiency for these tests is essentially equivalent (0.95 to 0.98) to that obtained in the vacuum exhaust tests.

Pressure Profiles

The local static pressures measured at the tap locations presented in Table 3 are listed in Table 15. In Fig. 40, a typical measured pressure profile in the supersonic portion of the nozzle (for test 547 with the 25:1 expansion ratio skirt) is compared to the pressure profile predicted by the Rocketdyne N-element thermodynamic equilibrium model. The experimental data are seen to closely follow the theoretical predictions for a one-dimensional full-shifting chemical equilibrium gas flow. A discussion of the measured static pressure profiles in the subsonic combustion chamber which require analysis of burning rates and stagnation pressure losses is made in the Task V section of the report.

Heat Transfer Results

The transient temperature response of the heat flux transducers listed in Table 4 and depicted in Fig. 5 was utilized to calculate local values of wall heat transfer during the engine firing tests. Thermocouple histories, as typified by the curve shown in Fig. 39, were converted into local values of wall heat flux by the computerized one-dimensional transient conduction analysis described in Appendix B. The results of this analysis are summarized in Table 16. The calculated heat fluxes ($BTU/in^2 sec\ F$) shown in Table 16 represent a standardization of the instantaneous values actually

TABLE 15. MEASURED LOCAL CHAMBER WALL PRESSURES DURING STRATIFIED FLOW ENGINE FIRINGS (IN PSIA)

Pressure Tap Number	Distance From Injector	Expansion Ratio	Test Number									
			542	544	545	546	547	548	549	550	551	552
1	1.125	Not Applicable Subsonic	243.1	---	227.2	228.0	231.5	221.8	226.8	216.7	240.0	239.4
2	1.125		242.0	---	226.7	---	232.9	224.5	226.3	217.1	240.7	235.1
3	3.30		230.3	230.9	215.4	216.3	221.7	210.0	214.8	205.6	227.6	222.8
4	3.30		232.0	232.8	217.5	218.6	224.2	212.6	217.4	208.4	230.6	226.0
5	5.10		235.1	236.1	220.0	220.8	226.7	215.5	220.5	211.4	233.8	228.8
6	5.10		232.1	233.1	217.1	217.9	223.8	212.7	217.7	208.8	231.1	226.1
7	6.85		230.2	230.9	215.1	215.6	221.4	210.0	214.7	205.6	227.5	222.4
8	6.85		233.2	234.0	218.2	218.8	224.5	213.3	218.1	209.0	230.9	225.8
9	14.82	1.5	48.47	49.14	44.71	44.61	46.57	43.26	44.67	42.11	47.52	40.29
10	14.82	1.5	48.30	49.00	44.76	44.71	46.57	43.40	44.81	42.29	47.61	46.40
11	19.34	3.0	16.78	17.24	15.55	15.54	16.33	15.12	15.72	14.74	16.76	16.33
12	19.34	3.0	16.52	17.00	14.65	15.29	16.03	14.87	15.42	14.49	16.53	16.12
13	24.63	5.44	6.22	6.48	5.53	5.66	6.04	5.49	5.71	5.31	6.13	5.93
14	28.13	7.47	4.58	---	4.14	---	---	---	---	---	4.32	3.96
15	34.15	11.71	2.504	2.672	2.291	2.309	2.466	2.239	2.365	2.216	2.574	2.481
16	38.7	15.54	1.755	1.862	1.636	1.652	1.726	1.607	1.651	1.903	1.804	1.745
17	46.78	23.70	1.532	0.463	0.596	0.499	0.461	0.562	0.527	0.685	0.497	0.514
18	47.08	24.04	1.218	1.041	1.415	1.144	1.056	1.281	1.199	1.511	1.130	1.171

TABLE 15. (Continued)

Pressure Tap Number	Distance From Injector	Expansion Ratio	Test Number							
			238	239	240	241	242	243	244	245
1	1.125	Not Applicable Subsonic	229.2	193.6	232.1	228.7	226.2	225.7	218.8	224.0
2	1.125		226.0	162.9	228.1	223.8	221.2	220.3	212.7	217.2
3	3.30		218.9	136.7	220.6	216.7	213.9	213.3	205.7	210.5
4	3.30		218.7	146.7	220.2	216.5	213.7	213.1	205.6	210.2
5	5.10		219.9	137.9	222.0	218.1	215.3	214.7	207.4	212.1
6	5.10		217.6	137.6	219.4	215.7	212.8	212.1	205.0	209.4
7	6.85		216.0	134.6	218.0	214.1	211.4	210.7	203.5	208.3
8	6.85		217.9	138.4	220.3	216.2	213.8	213.1	206.2	210.9
9	14.82	1.5	29.3	45.3	44.4	43.2	43.7	41.6	42.7	52.6
10	14.82	1.5	28.8	45.1	44.2	43.0	43.4	41.2	42.5	52.8
11	19.34	3.0	11.1	15.7	15.4	14.9	15.1	14.3	14.8	18.0
12	19.34	3.0	11.7	16.0	15.8	15.3	15.4	14.7	15.2	18.4
13	24.63	5.44	6.2	5.7	5.6	5.4	5.5	5.0	5.3	DNA[1]
14	28.13	7.47	4.6	3.7	3.6	3.5	3.5	3.3	3.3	DNA
15	34.15	11.71	3.75	2.49	2.44	2.32	2.38	2.44	2.34	DNA
16	38.7	15.54	2.77	1.74	1.71	1.66	1.66	2.35	1.70	DNA
17	46.78	23.70	0.69	0.52	0.57	0.63	0.63	2.23	0.90	DNA
18	47.08	24.04	1.66	1.4	1.66	1.97	2.04	3.28	2.73	DNA

TABLE 15. (Concluded)

Pressure Tap Number	Distance From Injector	Expansion Ratio	Test Number							
			246	247	248	249	250	251	252	253
1	1.125	Not Applicable Subsonic	226.5	281.1	262.0	276.1	287.1	281.2	276.1	270.7
2	1.125		---	---	---	272.7	---	---	273.2	268.0
3	3.20		258.4	273.0	254.8	268.1	278.2	273.1	268.9	262.3
4	3.20		259.5	273.5	256.8	268.7	278.5	273.6	268.8	262.2
5	5.10		257.6	272.0	254.2	267.1	277.2	272.3	267.8	261.5
6	5.10		258.6	273.2	256.3	268.3	278.4	273.6	269.0	262.6
7	6.85		253.8	268.3	249.9	263.5	273.5	268.6	264.1	257.8
8	6.85		254.6	269.2	250.9	264.6	274.6	269.9	265.4	259.1
9	14.82	1.5	54.2	52.5	53.5	56.4	56.0	53.2	52.4	52.4
10	14.52	1.5	54.2	52.6	53.5	56.2	55.6	53.2	51.6	51.5
11	19.34	3.0	18.4	18.1	18.4	19.4	19.4	18.1	18.1	18.1
12	19.34	3.0	18.7	18.4	18.7	19.7	19.8	18.6	18.2	18.2
13-18[2]		>4.0	---	---	---	---	---	---	---	---

1 Does not apply. Nozzle of 4:1 expansion ratio was used for tests 245 through 253.

2 Not used for 4:1 area ratio nozzle

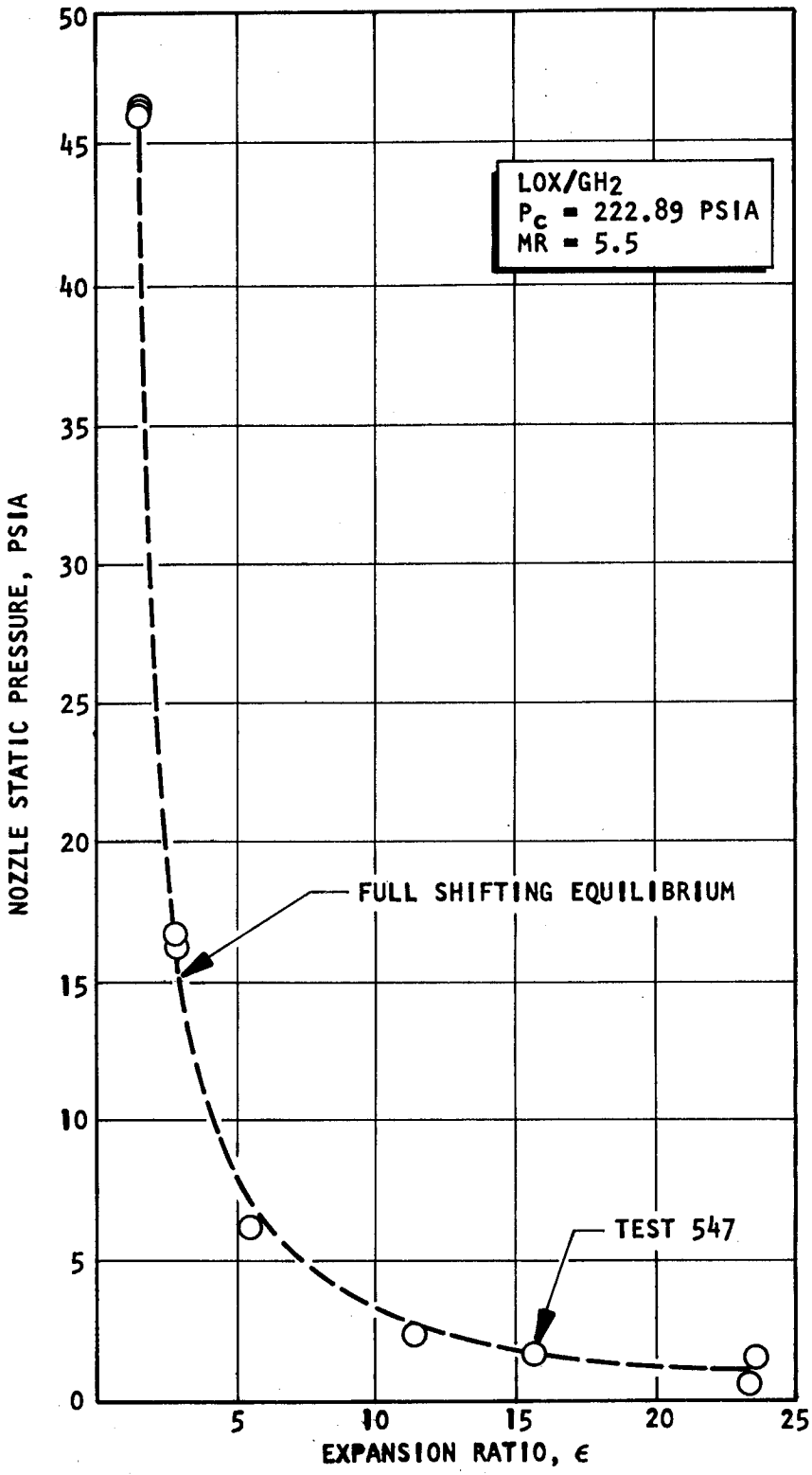

Figure 40. Nozzle Static Pressure as a Function of Expansion Ratio for Full Shifting Equilibrium

TABLE 16. MEASURED LOCAL CHAMBER WALL HEAT FLUXES STANDARDIZED TO A 800 F WALL TEMPERATURE (In Btu/in.^{2}-sec-F)

Test No.	P_c, psia	Overall MR	TC-1	TC-2	TC-3	TC-4	TC-5	TC-6	TC-7	TC-8	TC-9	TC-10	TC-11	TC-12	TC-13	TC-14	TC-15	TC-16	TC-17	TC-18	TC-19	TC-20	TC-21	TC-22	TC-23	TC-24
542	232	5.48	7.33	6.37	7.03	7.61	7.20	6.91	6.79	6.64	5.90	5.98	7.05	6.77	7.55	7.76	9.24	9.17	9.94	8.18	8.19	7.62	5.66	5.32	3.35	3.24
544	232	5.78	5.75	4.67	6.03	6.29	5.84	5.97	5.96	5.78	5.12	5.51	6.17	5.97	6.82	6.92	8.33	8.33	8.96	7.33	7.35	6.84	4.98	4.73	2.85	2.78
545	217	5.09	8.22	5.93	-	7.30	6.76	6.60	6.30	6.23	5.55	5.58	6.62	6.55	7.17	7.45	8.73	8.68	9.05	7.82	7.28	6.93	5.29	4.94	2.97	2.86
546	217	5.06	9.11	5.51	7.79	7.84	7.31	7.35	6.87	6.98	5.92	5.87	6.92	6.88	7.32	7.80	9.13	8.98	9.65	8.03	7.57	7.05	5.32	5.04	2.94	2.82
547	223	5.65	10.43	-	7.86	8.04	6.97	6.99	6.82	6.81	5.67	5.99	6.98	6.87	-	7.51	9.06	8.90	9.97	8.27	7.75	7.50	5.24	4.95	2.90	2.79
548	212	4.86	6.44	3.69	6.00	5.94	5.79	5.60	5.96	5.70	4.91	4.81	6.11	5.83	-	6.09	6.88	6.92	8.28	6.81	6.19	5.70	4.11	3.86	2.34	2.31
549	216	5.17	5.18	3.38	5.51	5.54	5.33	5.21	5.71	5.62	4.61	4.37	5.93	5.76	-	5.95	6.65	6.78	8.42	6.95	6.15	5.86	4.16	3.88	2.36	2.31
550	207	4.68	6.30	3.88	5.86	5.80	5.65	5.49	5.89	5.74	4.85	4.81	5.90	5.85	-	6.10	6.54	6.71	8.09	6.73	5.96	5.59	3.94	3.73	2.29	2.25
551	229	5.39	6.68	3.81	6.49	6.26	6.17	5.74	5.94	5.76	4.76	4.68	6.15	5.95	-	6.58	7.63	7.49	8.63	7.00	6.97	6.36	4.37	4.19	2.50	2.40
552	224	5.32	10.93	5.90	8.12	8.10	6.79	6.78	6.68	6.63	5.50	5.42	6.67	6.52	-	7.50	8.60	8.35	9.36	7.92	7.06	6.46	4.82	4.57	2.71	2.58
238	217	4.78	5.68	4.71	6.20	6.27	-	5.71	5.65	5.53	5.10	5.11	5.89	5.80	-	6.33	6.97	-	7.68	6.51	6.36	-	4.39	4.15	2.59	2.56
239*	137	6.64	9.38	6.15	7.06	7.41	-	6.18	5.98	5.96	5.10	4.87	6.09	6.21	-	6.53	7.20	7.21	7.98	6.86	6.27	-	4.27	4.01	2.37	2.34
240	219	5.31	4.44	3.34	5.44	5.34	4.36	4.86	5.06	5.16	4.36	4.19	5.26	5.47	-	5.58	6.34	6.39	7.36	6.31	5.75	-	3.68	3.68	1.96	2.08
241	215	5.21	4.45	3.60	5.03	4.98	4.13	4.61	4.88	4.72	4.08	3.91	5.07	5.10	-	5.29	5.92	6.00	7.14	5.82	5.40	-	3.50	3.45	1.95	1.96
242	213	4.79	4.57	3.63	4.81	4.82	3.88	4.45	4.63	4.31	3.86	3.62	4.81	4.70	-	4.89	5.38	5.50	6.34	5.09	4.78	-	3.18	2.99	1.76	1.80
243	212	5.33	6.66	4.57	5.89	6.05	4.38	5.14	5.05	4.85	4.30	3.92	5.15	5.13	-	5.55	6.29	6.21	7.09	5.83	5.42	-	3.65	3.52	1.97	1.97
244*	205	4.71	4.42	3.79	3.55	3.55	3.06	3.30	3.15	3.16	2.92	3.10	3.48	3.35	-	3.33	3.37	3.39	3.87	3.23	3.06	-	2.13	1.98	-	1.38
245	210	4.94	4.47	3.72	4.47	4.41	3.71	4.13	4.19	4.10	3.63	3.52	4.33	4.35	-	4.23	4.65	4.64	5.56	4.62	4.29	-	2.88	2.73	1.56	1.71
246	254	5.56	6.10	-	7.56	7.83	7.00	6.91	6.98	6.65	5.99	6.21	6.99	6.97	-	7.86	-	9.56	10.32	8.70	8.36	-	5.18	5.47	3.01	2.98
247	269	4.42	5.65	-	5.93	6.47	5.82	5.87	5.89	5.80	4.59	5.35	5.85	6.19	-	6.63	6.92	-	8.27	7.19	6.36	-	4.06	4.17	2.28	2.25
248	250	6.73	5.27	-	6.97	6.92	6.92	6.70	6.69	6.10	4.67	6.25	5.75	6.91	-	7.91	-	-	10.23	8.83	7.90	-	5.40	5.64	3.09	2.93
249	264	4.92	5.79	-	6.62	7.19	6.46	6.65	6.45	6.08	5.32	5.93	6.14	6.63	-	7.22	-	7.63	8.68	7.96	6.91	-	4.42	4.59	2.55	-
250	274	5.41	5.45	-	-	7.44	7.06	6.96	6.81	6.57	5.78	6.41	5.89	7.20	-	7.94	-	-	10.11	8.70	8.42	-	5.28	5.56	2.97	-
251	269	6.24	10.14	-	-	9.34	8.32	8.02	7.82	7.40	6.41	7.18	6.33	7.72	-	9.03	-	-	10.91	9.47	9.41	-	-	6.11	3.30	-
252	265	4.93	8.25	8.91	9.06	8.59	7.33	7.28	7.28	3.50	5.90	6.43	-	4.55	-	8.03	-	9.19	10.07	6.91	7.73	-	-	5.06	2.91	-
253	259	5.14	3.36	-	6.58	5.88	5.78	5.47	6.53	5.92	5.30	5.05	-	6.57	-	6.14	-	7.30	9.67	7.70	7.03	-	-	4.10	2.17	-

*All data are suspect because of unusually high (Run 239) or low (Run 244) values

calculated at transducer back surface temperatures of 400 to 900 F to a nominal combustion gas side wall temperature of 800 F, according to the formula

$$\frac{q/A\,|_{800}}{q/A\,|_{T_w}} = \frac{T_g - 800}{T_g - T_w}$$

The above formula assumes a heat transfer coefficient which is independent of moderate changes in wall temperature and chamber pressure during the 2-second firings. The relatively linear variation of transducer temperature with time in Fig. 39 is indicative of the validity of these assumptions. It should also be noted that the value of calculated heat flux is also relatively independent of wall temperature changes from 500 to 1000 F for gas temperatures above approximately 4500 F, i.e., for mixture ratios above 3.0 with the H_2/O_2 propellant combination.

It is difficult to assess the absolute accuracy of the heat flux data obtained. Locations in Table 16, where no heat flux values are listed represent not only instances in which no measurements were obtained, but also situations in which the output of the thermocouples and associated electronic recording was erratic or otherwise suspicious. Similarly, a notation has been made in the table for the two tests (runs 239 and 244) in which the data represent a set of consistently high or low heat fluxes. To estimate the accuracy of the remaining data, an analysis of variance was made for measurements obtained at thermocouples 15, 16, and 17, and at 18, 19, and 20, respectively, where triplicate measurements of nominally similar heat transfer situations* were made during Tests 542 through 552. For the individual firings, the standard deviations in heat flux ranged from 3 to 9 percent of the average heat flux at the two axial stations of the six above thermocouples. Based upon these statistical data and upon the comparison between heat flux

* With an injector designed to provide a circumferentially uniform gas flow field, the wall heat flux at or beyond the nozzle throat should be axisymmetric.

measurements made by both the transient conduction technique and steady-state calorimetry (Ref. 5); the accuracy of the average heat flux for multiple measurements is estimated to be ±10 percent, while the accuracy for single thermocouple measurement is estimated to be ±15 percent.

Discussion of Heat Transfer Results

The analysis of the measured chamber wall heat flux was made with the following objectives:

1. To determine how well the heat transfer results were predicted by the usual rocket nozzle convection correlations
2. To correlate the effects of mixture ratio bias and film cooling upon wall heat transfer
3. To relate the heat transfer results to the performance results
4. To lay the basis for subsequent theoretical analysis by the BLIMP computer program of the JANNAF analytical procedure

Axial chamber wall heat flux profiles of tests which illustrate the four general sets of conditions studied are presented in Fig. 41 through 45. The tests represent, respectively:

Tests 547 and 251: effectively uniform main flow, no film cooling

Test 252: striated main flow, no film cooling

Test 252: effectively uniform main flow, nominal 10 percent film cooling

Test 238: striated main flow, nominal 10 percent film cooling

In each of these figures, the experimental points are compared to the predictions of the simplified Bartz correlation for rocket nozzle

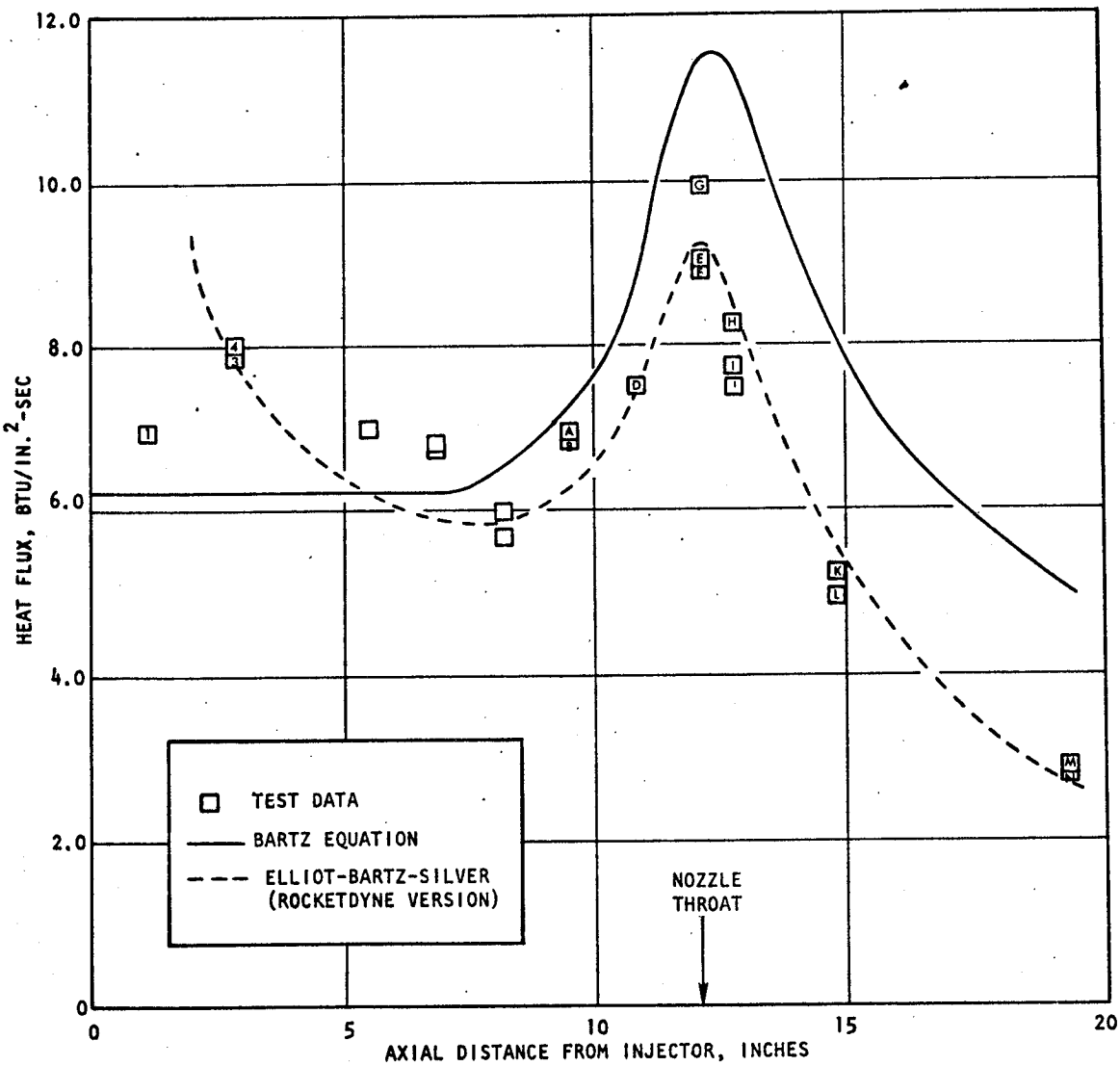

Figure 41. Chamber Wall Heat Flux in Test 547 Made With Essentially Uniform Combustion Gas Flow and No Film Cooling

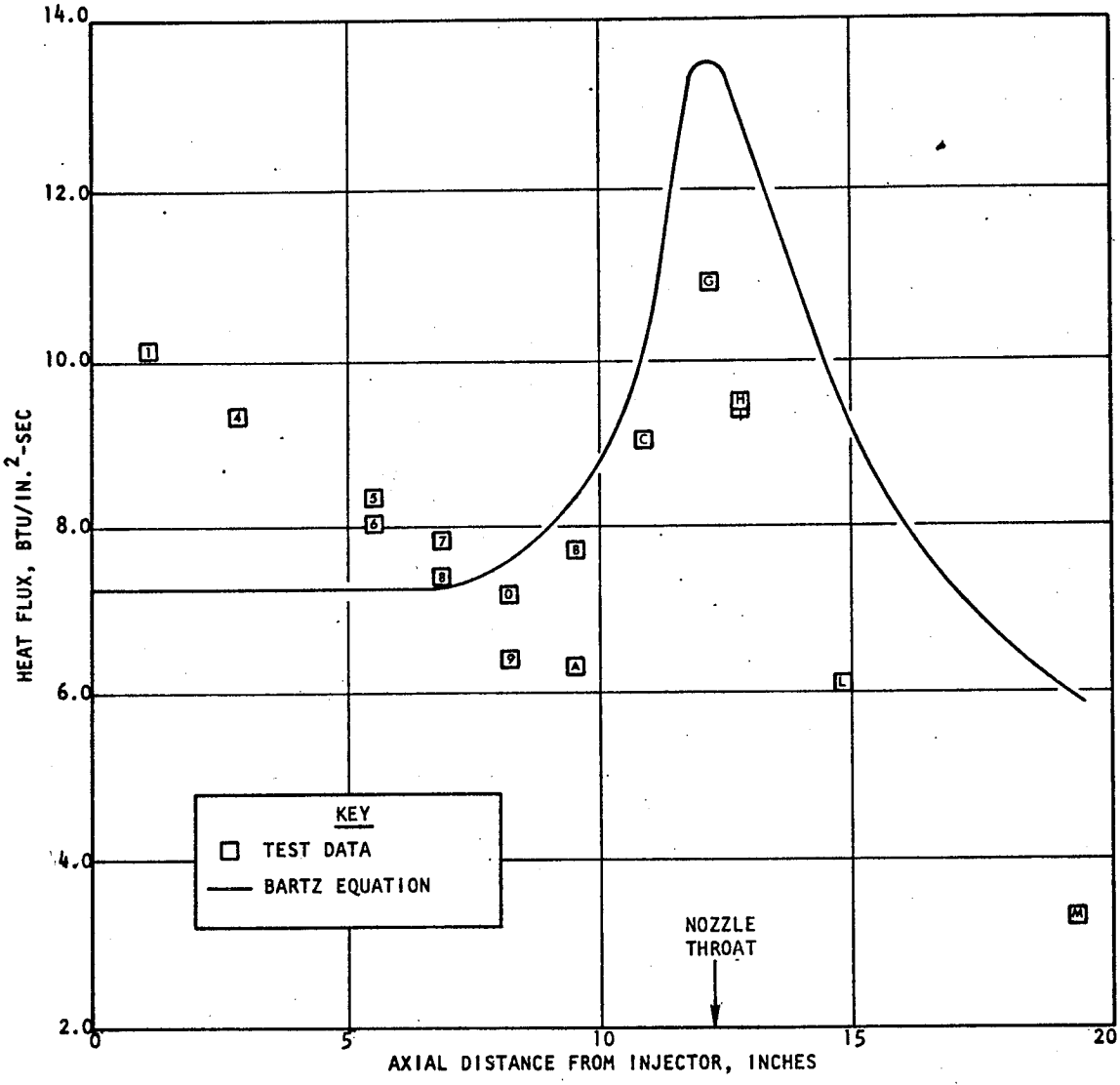

Figure 42. Chamber Wall Heat Flux in Test 251 Made With Essentially Uniform Combustion Gas Flow and No Film Cooling

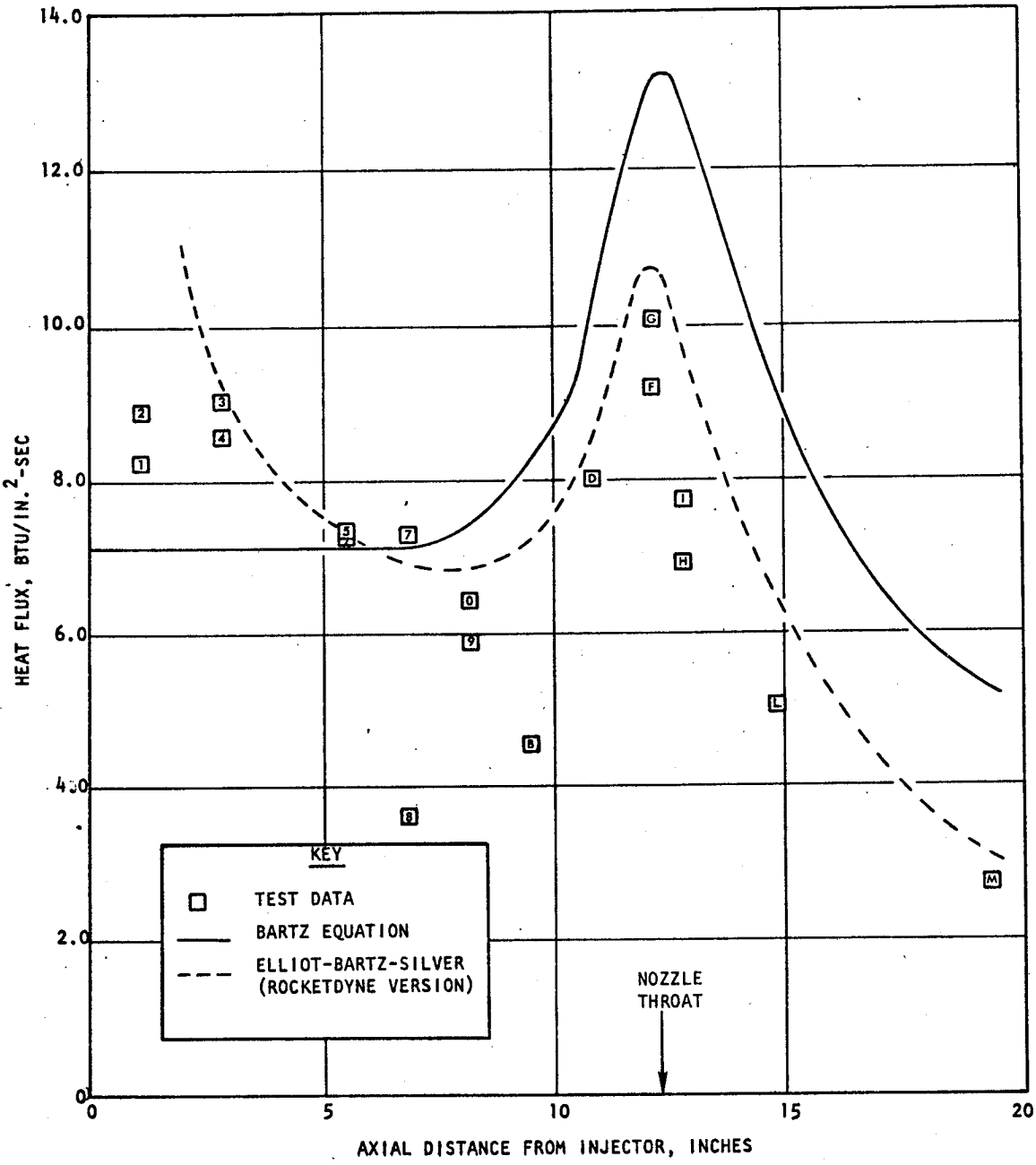

Figure 43. Chamber Wall Heat Flux in Test 252 Made With Striated Mixture Ratio in the Main Gas Stream and No Film Cooling

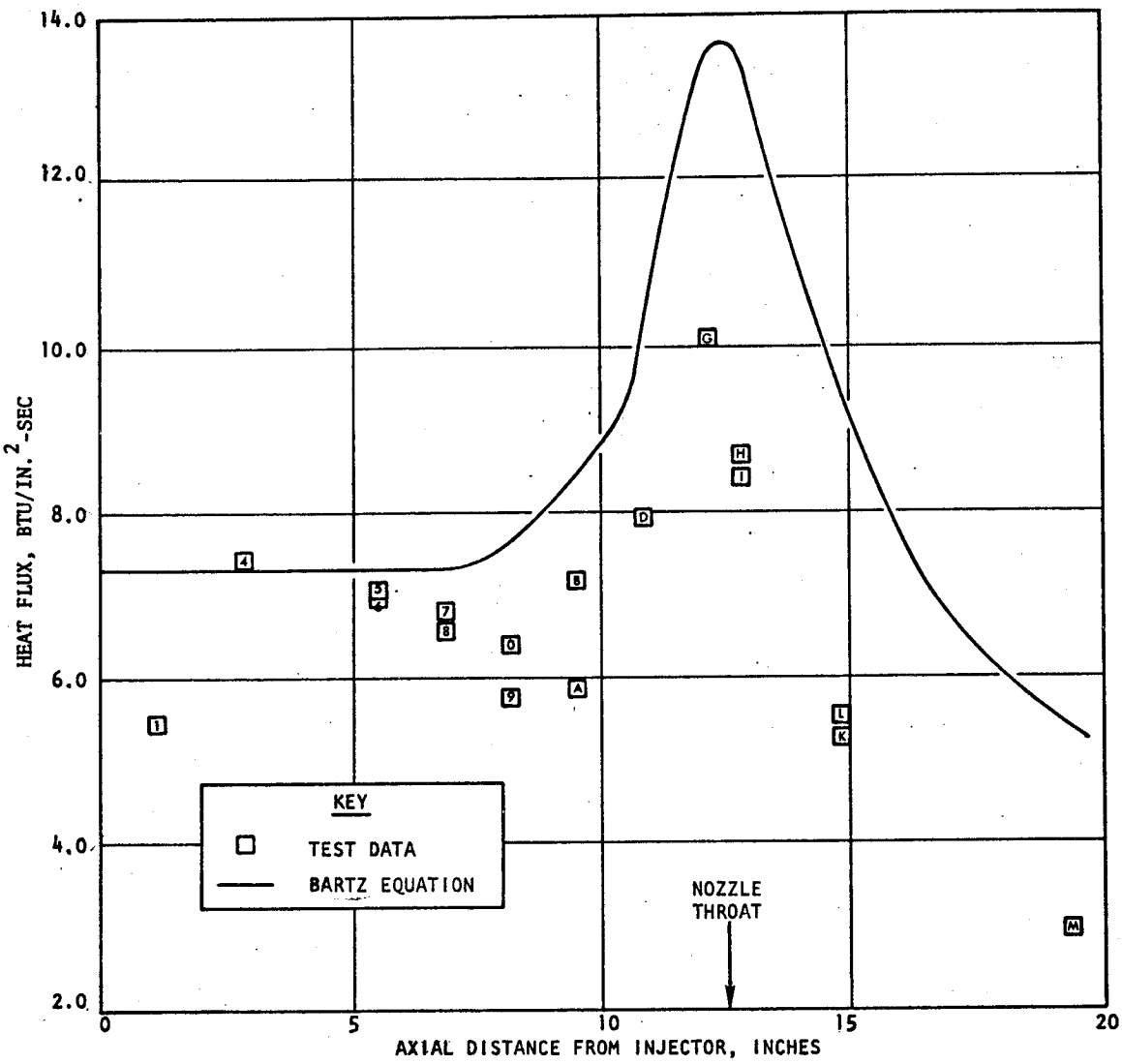

Figure 44. Chamber Wall Heat Flux in Test 250 Made With Essentially Uniform Combustion Gas Flow and 11.8 Percent of the Fuel Used as Film Coolant

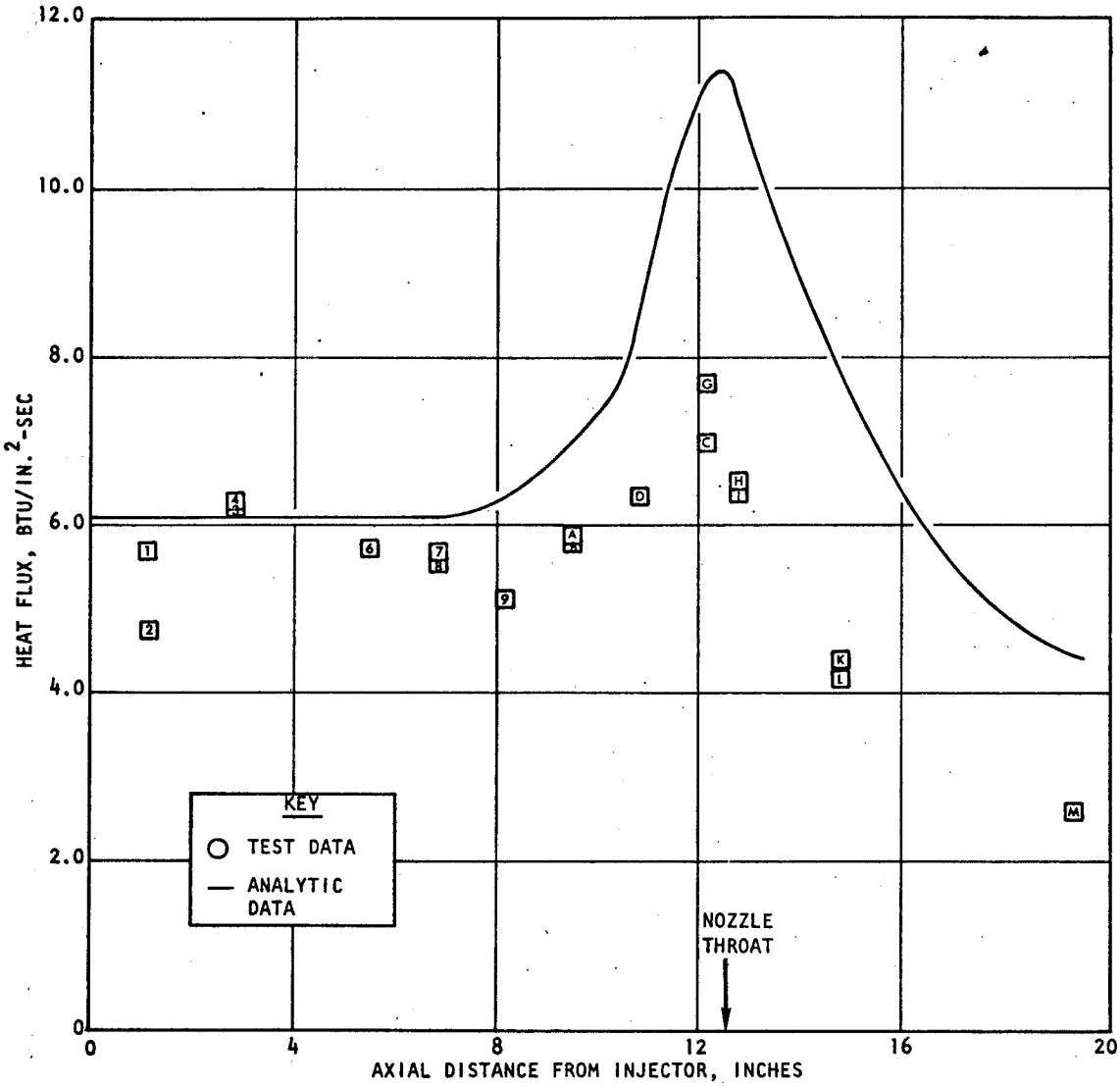

Figure 45. Chamber Wall Heat Flux in Test 238 Made With Striated Combustion Gas Flow and With 9.7 Percent of the Fuel Used as Film Coolant

convective heat transfer coefficient (Ref. 6)

$$h_g = 0.026\, C_p \left(\frac{\mu}{D^*}\right)^{.2}\left(\frac{A^*}{A}\right)^{.9}\left(\frac{P_C g}{c^*}\right)^{.8} \sigma Pr^{-.6} \qquad (6)$$

The simplified Bartz correlation, which is based upon the assumption that thrust chamber heat transfer follows ordinary relations for fully developed turbulent pipe flow, is usually expected to give a satisfactory agreement near and downstream of the nozzle throat. However, examination of the four graphs shows that the predicted heat fluxes were, in each case, higher (by 20 to 50 percent) than the measured fluxes at the nozzle throat. The agreement was also poor in the nozzle region downstream of the throat. In the combustion chamber, the simplified Bartz relation predicted heat fluxes that were lower than measured for the tests without film cooling but higher than were actually measured for those tests with film cooling. The simplified Bartz relation cannot correlate the tendency of experimental heat flux data to peak approximately 2 to 3 inches downstream of the injector and then decrease in the axial direction over the constant area portion of the chamber.

Figures 41 and 43 also compare the experimental heat fluxes to the predictions of the computerized Rocketdyne version of the Elliott-Bartz-Silver analysis.

$$h_g = 0.012\rho_\infty C_p U_\infty \left(\frac{T_\infty}{T_R}\right)\left(\frac{\rho_\infty}{\rho_R}\right)^{.25}\left(\frac{\mu_R}{\mu_\infty}\right)^{.25} \frac{1}{\left(Re_\theta\right)^{.25}\left(Pr\right)^{.67}} \qquad (7)$$

The Elliott-Bartz-Silver analysis (Ref. 7), and its modifications, are based upon the development of the energy boundary layer from an attachment point in the combustion chamber downstream through the nozzle. Velocity and temperature profiles are defined by 1/7 power law profile in the boundary layer. For the short L^* combustion chamber used with an efficient injector,

the boundary layer is usually in a developing stage for a considerable distance beyond the nozzle throat; consequently, Eq. 7 would be expected to give a substantially better correlation than Eq. 6 . Figures 41 and 43 show this to be the case. Similar comparisons with data from other tests indicate that the developing boundary layer model gives a better correlation than the fully developed pipe flow model.

Test 238, with results shown in Fig. 45, and Test 547, with results shown in Fig. 41, were made at essentially the same chamber pressure; consequently, differences between measured heat flux profiles in these firings can be attributed to the effects of mixture ratio bias and film cooling. Comparison of the experimental fluxes for the two tests indicates that the heat transfer was reduced by approximately 25 percent throughout the chamber and nozzle.

Tests 250, 251, and 252 were made at similar chamber pressure. Combining the data points for these three runs on Fig. 46 therefore serves to compare the effectiveness of reduced outer zone mixture ratio without film cooling (Test 252) and film cooling without mixture ratio bias (Test 250) in reducing the wall heat flux from that observed in Test 251 made without either bias or film cooling. Examination of Fig. 46 indicates that both mixture ratio bias and film cooling gave comparable reductions in heat transfer (10 to 15 percent over most of the chamber). Neither cooling scheme alone was demonstrated to be as effective as their combined use as noted above with Tests 238 and 547.

Correlation of the effects of reduced outer zone mixture ratio and/or film cooling upon wall heat transfer was based upon the assumption that the mixture ratio bias introduced at the injector between the inner and outer zones of the main flow was maintained throughout the combustor and nozzle, but that at least a partial mixing of the film coolant and outer zone flows occurred. This assumption is in agreement with the results of Hartnett et al (Ref. 8) and others, which show that gas phase mixing between parallel streams is inversely proportional to the thickness of the thinner gas layer raised to

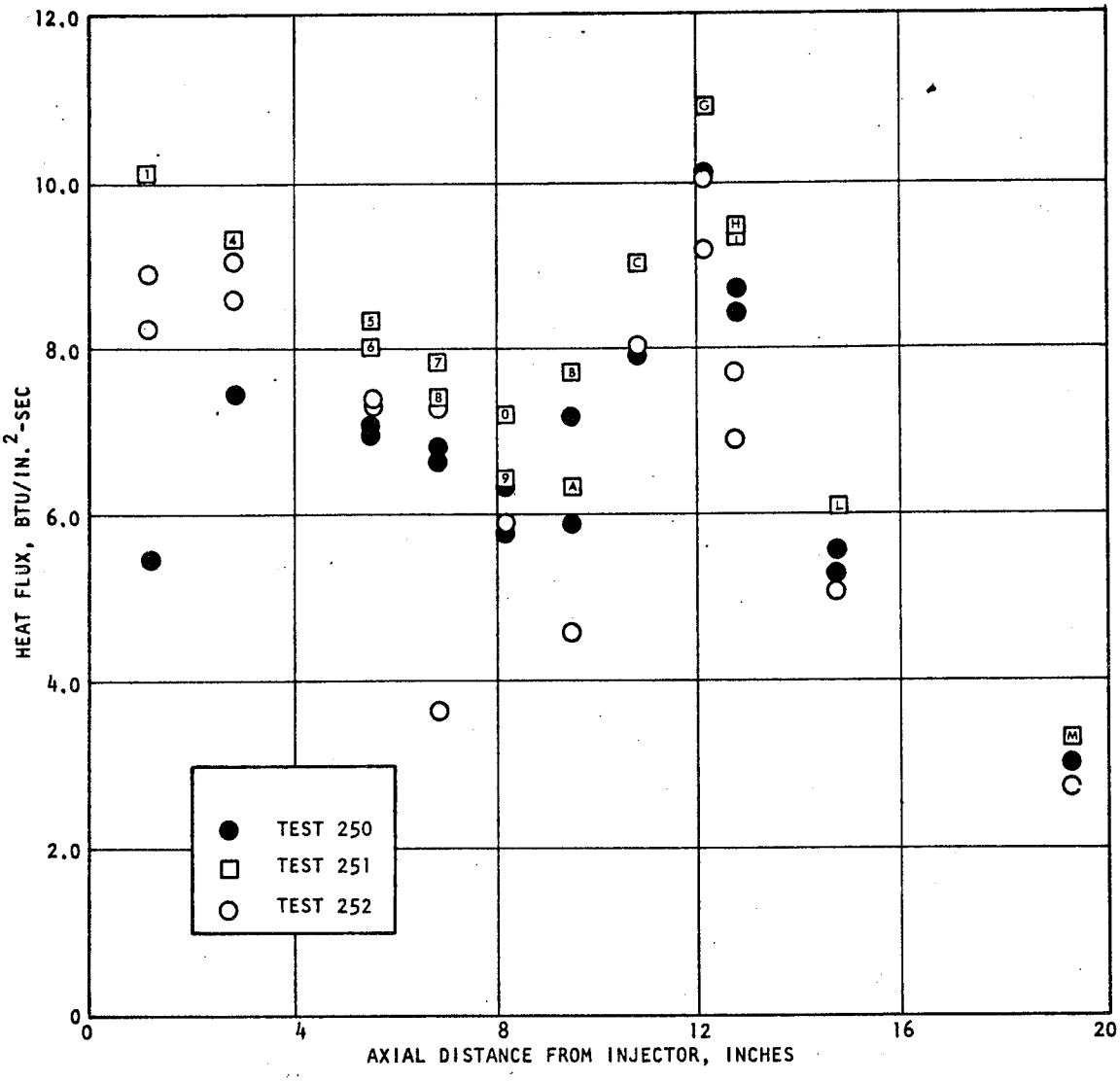

Figure 46. Comparison of Experimental Wall Heat Flux Profiles for Tests 250, 251, and 252

the 0.8 power. The functional dependence of mixing upon stream thickness is expected to be different for the present problem, in which a substantial portion of the mixing is probably accomplished by transverse spray velocities before combustion. However, it is certainly reasonable for the mixing of the film coolant stream (having a calculated initial thickness of only 0.015 to 0.020 inch) with the outer zone flow to be more complete at any axial station than the mixing of the outer zone (having a thickness of approximately 0.8 inch) with the inner core flow.

With the above assumption, the effect of film cooling and stratified flow upon heat transfer is determined by their effects upon the mixture ratio at the wall and the subsequent effects of the wall mixture ratio upon heat flux. The effect of mixture ratio upon convective heat transfer can be described in terms of a function, f(MR), which, from the simplified Bartz relation, Eq. 6, is defined as

$$f(MR) = \frac{\mu^{\cdot 2} C_p \left(T_0 - T_w \right)}{c^{*.8}} \qquad (8)$$

A similar relation can be derived for the Elliott-Bartz-Silver type of relation (Eq. 7). For the H_2/O_2 propellant combination, a chamber pressure of 260 psia, a nominal wall temperature of 800 F, and the dimensions of the stratified flow engine of this program, the variation of f(MR) with mixture ratio produces the variation in throat heat flux shown by the solid curve in Fig. 47. The relation shown in Fig. 47 is particularly significant because it shows that a useful reduction in heat flux is achieved only when the mixture ratio near the wall is reduced to a level below 3.0.

The relation between mixture ratio and heat transfer defined by Eq. 8 is particularly useful when it is employed to predict the effect of film cooling upon wall heat flux. If complete mixing between the injected film coolant and outer zone flows is assumed, then the effect of using 10 percent of the fuel on nozzle throat heat flux depends on the injected mixture ratio of the outer zone as shown by the broken curved line of Fig. 47. The results in

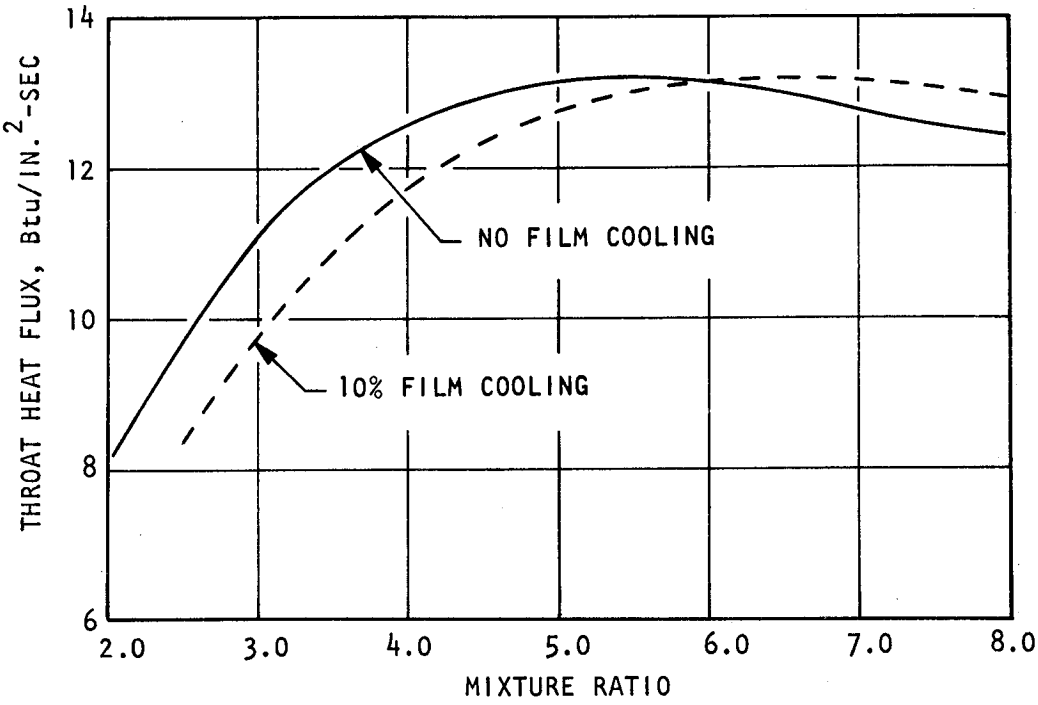

Figure 47. Predicted Effect of Mixture Ratio upon Throat Heat Flux in Stratified Flow Engine, P_C= 260

Fig. 47 are important because they show that the same percent of the overall fuel employed as a film coolant produces the following effects:

Outer Zone Mixture Ratio	Reduction in Throat Heat Flux
3.0	15 percent
4.5	5 percent
6.0	no reduction
>6.0	increases heat flux

The simplest assumption, i.e., complete mixing of the outer zone flow with the film coolant at the nozzle throat, is equivalent to assuming that the mixed layer, ΔR, is approximately one-fourth the chamber radius, R_w, the width of the wall of the annular space occupied by the outer zone. But if the mixed layer is assumed to be less than $R_w/4$, then the fraction of the outer zone flow mixed with the film coolant, F_M, can be defined as

$$F_M \cong \frac{4\Delta R}{R_w}$$

Obviously, if F_M is less than 1.0, the wall mixture ratio will be lower than would be the case with complete mixing, and the heat flux will be lower. A correlation of the combined effects of film cooling and stratified flow, therefore, includes a determination of the mixing constant, F_M.

The mixing coefficient was determined by correlation of two sets of nozzle throat heat flux data, each set of which included tests both with and without film cooling. The throat heat flux data for the first set, Tests 542 through 552, were standardized to an equivalent value at the average chamber pressure, 223 psia, by the relation

$$\frac{q/A\big|_{P_c}^{223}}{q/A\big|_{P_c}} = \left(\frac{223}{P_c}\right)^{.8}$$

The data for the second set, Tests 246 through 253, were likewise standardized to an equivalent value at the average chamber pressure, 262 psia, by

$$\frac{q/A\big|^{262}}{q/A\big|_{P_C}} = \left(\frac{262}{P_C}\right)^{.8}$$

Then the pressure standardized data were fitted to the equations

$$\begin{aligned} q/A\big|^{*} &= K_{223}\frac{\dot{\mu}^{.2}C_p}{c^{*.8}}(T_0 - 800) = K_{223}f(MR) \\ q/A\big|^{*} &= K_{262}\frac{\dot{\mu}^{.2}C_p}{c^{*.8}}(T_0 - 800) = K_{262}f(MR) \end{aligned} \tag{9}$$

where f(MR) was first evaluated assuming a complete mixing of film coolant with the outer zone combustion gas flow. For values of $K_{223} = 18.5$ and $K_{262} = 20.8$, the correlation of data to the proposed model gave the results shown in Fig. 48 and 49. It is significant that the best correlation in Fig. 48 and 49 occurs for the tests in which no film cooling was employed. This suggests that the model is correct but that there is incomplete mixing of the film coolant and outer zone flow. From the definition of the mixing coefficient F_M, it can be shown that

$$MR_f = \frac{F_M\left(\frac{MR_{OZ}}{MR_{OZ}+1}\right)}{\frac{\dot{w}_{FC}}{\dot{w}_{OZ}} + F_M\left(\frac{1}{MR_{OZ}+1}\right)} \tag{10}$$

The value of the mixing coefficient can then be determined from Eq. 10 by choosing the value which produces the best fit of the experimental data to Eq. 9. The value of F_M which produced the best overall fit of data and equation was 0.4. Correlation of the effect of film cooling and injected outer zone mixture ratio with $F_M = 0.4$ is presented in Fig. 50 and 51. The

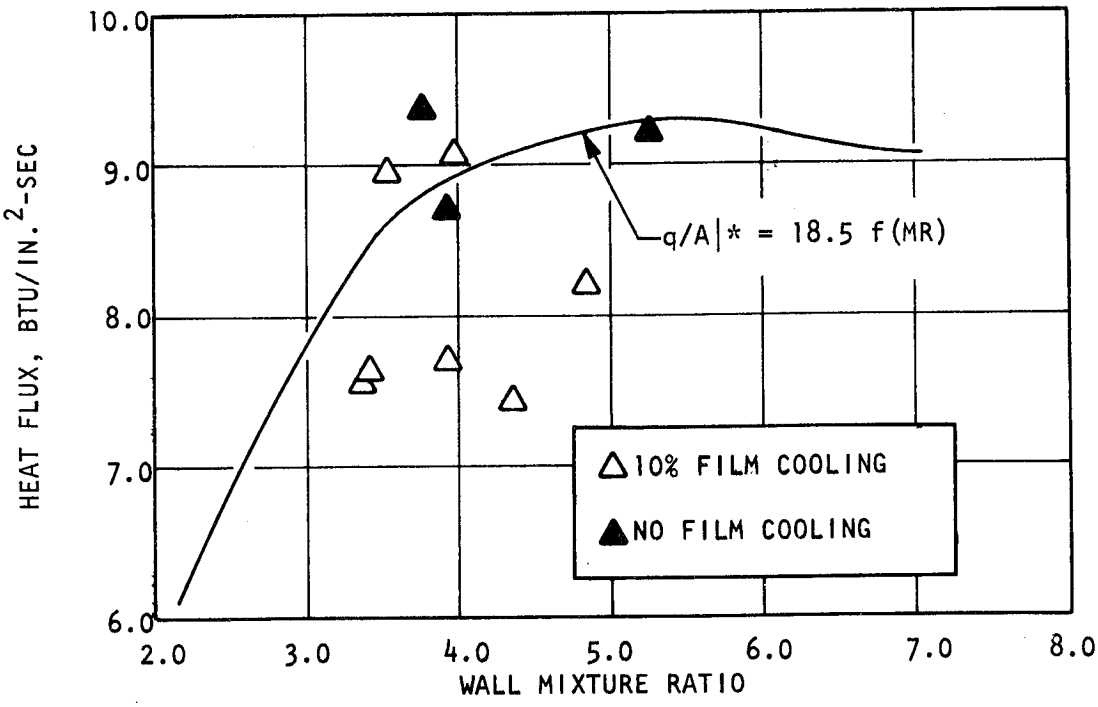

Figure 48. Correlation of Throat Heat Flux in Tests 542-552 for Complete Mixing of Film Coolant and Outer Zone Flow

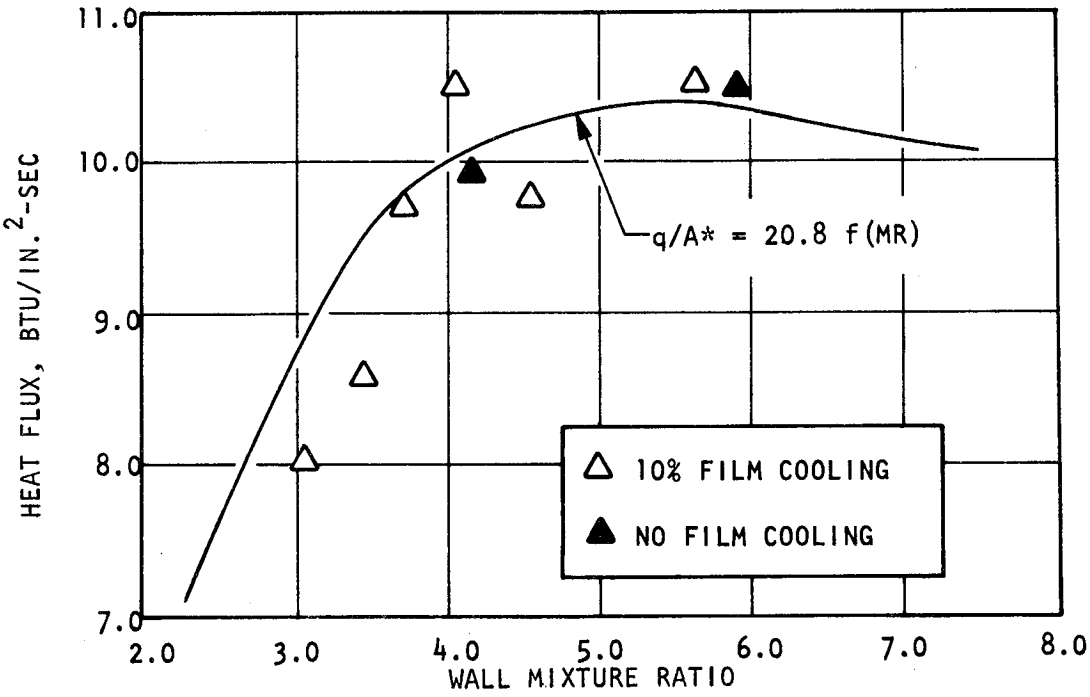

Figure 49. Correlation of Throat Heat Flux in Tests 246-253 for Complete Mixing of Film Coolant and Outer Zone Flow

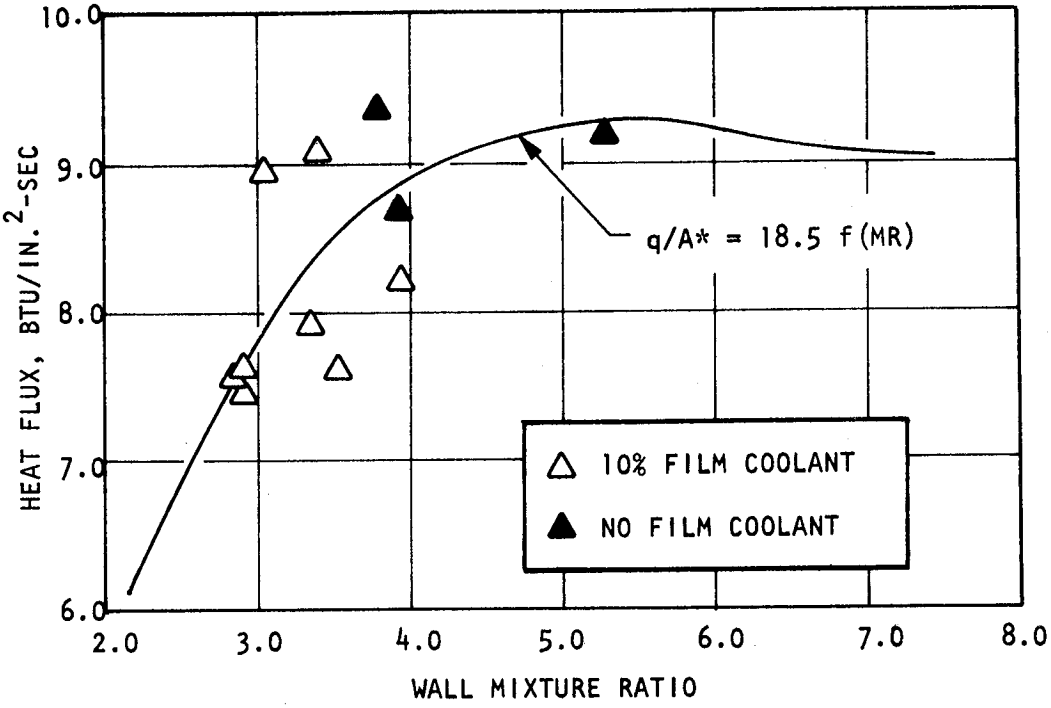

Figure 50. Correlation of Throat Heat Flux in Tests 542-552 for Partial Mixing of Film Coolant and Outer Zone Flow, $F_M = 0.4$

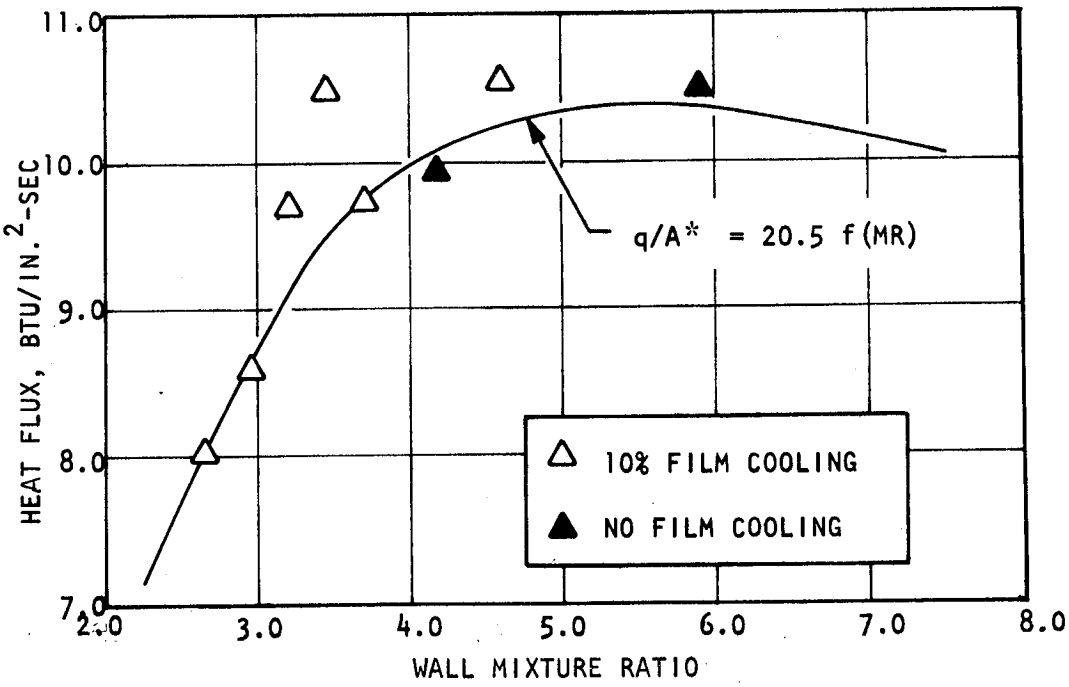

Figure 51. Correlation of Throat Heat Flux in Tests 246-253 for Partial Mixing of Film Coolant and Outer Zone Flow, $F_M = 0.4$

scatter of the experimental heat flux around the correlation curve is generally below the ±10 percent consistent with the estimated accuracy of the data on page 94.

The data correlation presented in Fig. 48 through 51 indicates that the combined effects of film cooling and stratification of the main combustion gas streams can be adequately described by a model which predicts that, at the nozzle throat, the film coolant is effectively mixed with slightly less than one-half the flow from the outer ring of injector elements. A review of the injector element layout in Fig. 1 and the single element mass flux profiles in Fig. 18 through 21 suggests that this degree of mixing is not coincidental: one-half the oxidizer spray in the outer triplet circle has a velocity component toward the wall and, therefore, into the film coolant layer. Therefore, a substantial portion of the mixing is probably accomplished either by direct spray penetration close to the injector or by the transverse gas velocities and turbulance which are induced by the transverse spray momentum even after evaporation. Consequently, it may be inferred that design of liquid-liquid or gas-liquid propellant, film-cooled thrust chambers (and any supporting applied research) should not be based directly upon the results of film cooling investigations made with parallel gas streams. The preferable analytical procedure should be to evaluate the mixing from a detailed analysis of the injector configuration, perhaps by means of the LISP computer program of the JANNAF analytical procedure (Ref. 3).

Exhaust Sampling

During firings, gas samples were withdrawn from the exhaust stream at either two or three of the probe locations shown in Fig. 52. The sample probes were aligned such that their angular direction corresponded with the direction of the theoretical streamlines of the expanding gas; their radial locations corresponded to the estimated centers of the concentric gas streams from the three separately controlled injector zones.

During a sequence of firings, the sample block was maintained at a temperature of approximately 300 F to prevent condensation of water vapor. Between the individual tests of the sequence, the sample block manifolds were evacuated and maintained at a nominal vacuum. After completion of the entire sequence of firings, the manifolds were again evacuated and maintained at a vacuum until the inlet line of the gas analyzer unit could be connected to the back of the manifold (a period of approximately 10 to 30 minutes).

The analysis for hydrogen, oxygen, and water was accomplished by a combination of PVT measurements and gas chromatography (gc). The total moles of gas in each sample vessel were first determined from the recorded pressure and temperature in the heated block together with the known sample bottle volume. The samplers next were cooled to condense all water, and the remaining gases from each sample were expanded into the precalibrated analyzer system. A portion of the expanded gas was injected into the gas chromatograph for determination of hydrogen, oxygen, and/or air. Using PVT data, the total moles of hydrogen and/or oxygen and nitrogen in the sample were calculated. If nitrogen was detected it was initially assumed to represent air leakage into the system. In that case, the moles of oxygen representing the air equivalent of the detected nitrogen were subtracted from the total moles of oxygen. Only the excess oxygen was subsequently used to calculate the exhaust gas composition. Water was determined from the difference between the total sample moles initially measured in the hot condition and the subsequently measured total moles in the cold expanded condition. Mixture ratios $\frac{\text{(mass oxygen)}}{\text{(mass hydrogen)}}$ were then calculated for each of the samples.

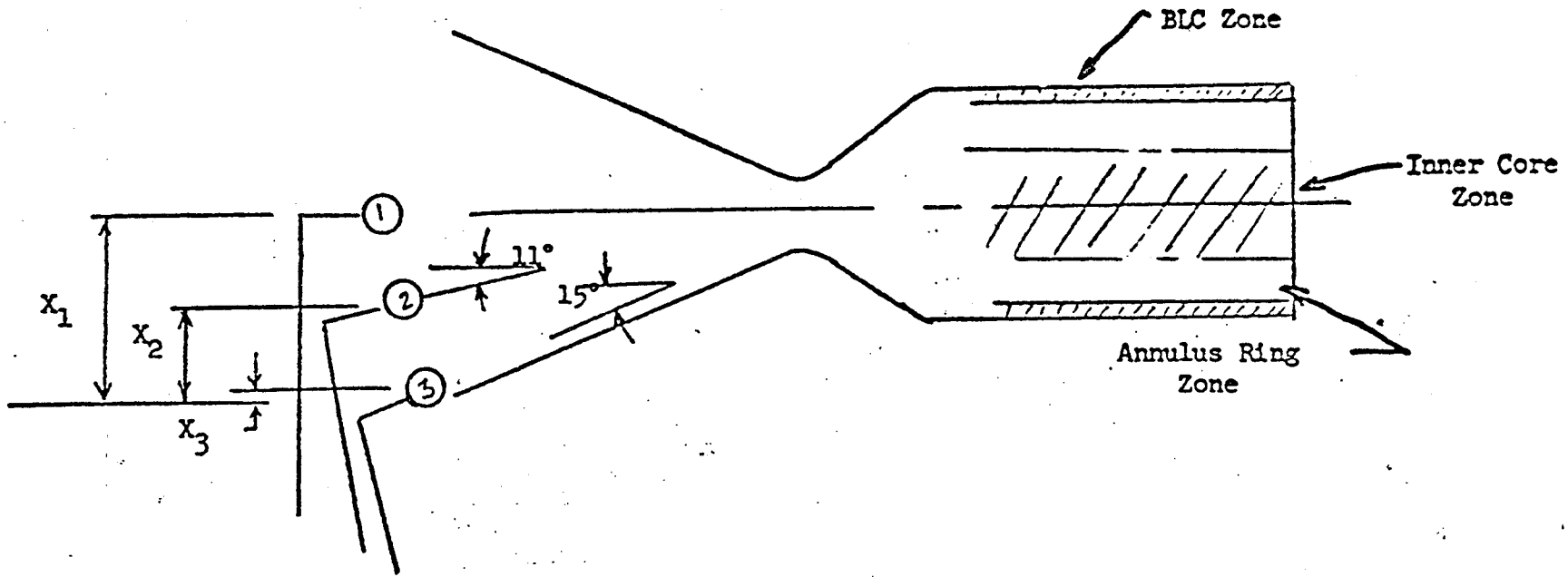

ϵ_c	X^*_1	X^*_2	X^*_3
25:1	12.1	2.07	1.20
4:1	8.40	.82	.48

* Nozzle Exit Radius

Figure 52. Location of Sample Probes in Nozzle Exhaust

The gc analyses were begun within 40 minutes after the test firings using a Varian Aerograph Series 200 gas chromatograph with a thermal conductivity detector. They were completed within six hours. Calibrations using known quantities of air were performed three times; before, during, and after sample analyses.

The following equations were used to calculate results

$$\text{Total moles, sample} = \frac{V_{\text{sampler,cc}}}{22.4 \text{ cc/mM}} \times \frac{P}{14.7} \times \frac{492}{T,R}$$

Using the linear coefficient of heat expansion of aluminum of 23.6 in./in./c x 10^{-6}, the volumes of the samplers were corrected from 76 to 300 F. This was a one percent increase in volume.

$$\text{mm } H_2 \text{ (or } 0_2\text{) in sample} = \text{mm } H_2 \text{ in gc} \times \frac{\text{Total V}}{V_{\text{sampler}}}$$

$$\text{mm } H_2 \text{ in gc} = \text{Calculated mm } H_2 \text{ (obtained from the gc curves)}$$

$$\text{Total V} = \text{Volume}_{\text{sampler}} + \text{Volume}_{\text{manifold}} + \text{Volume}_{\text{gc inlet and line}}$$

$$\text{moles } H_2 \text{ (or } 0_2\text{)} = \frac{V_{\text{sampler (76 F)}}}{22.4} \times \frac{\text{mm } H_2}{760} \times \frac{273}{T}$$

During the initial series of firings performed in 1971 (Tests 538 to 552 as shown in Table 13), samples were obtained at probe location X_1 along the thrust chamber axis and at probe location X_2 at the middle of the outer zone (see Fig. 52). The calculated results of these sampling experiments are presented in Table 17. Examination of the tabulated data indicates that the reliability of the defined gas composition is poor. As shown in the second from the last column, the samples from the probe located along the nozzle centerline were contaminated with 4 to 32 percent air while the samples from the outer zone probe contained 42 to 85 percent air. The relative contamination appears logical, if all the sample bottles are assumed to leak, because the initial pressures of the outer zone samples were only 1/3 as high as the chamber centerline samples (see the third column of Table 17); consequently the Δp from the

TABLE 17. SUMMARY OF SAMPLING TEST DATA OBTAINED DURING INITIAL FIRINGS (TESTS 538-552)

Probe Location	Test Number	Initial Pressure, psia	Block Temperature, F	V_{Block} cc/76 F	Total mMoles Gas	H_2 mMoles	XS O_2 mMoles	H_2O mMoles	Percent Air in Sample	Equivalent Mixture Ratio
X_1*	542	13.2	285	229	6.11	4.76	--	1.35	10	1.76
	543	--	--	224						
	544	12.1	266	215	5.40	1.89	0.015	3.49	32	5.18
	545	13.3	318	229	5.90	4.68	0.015	1.20	7	1.64
	546	14.5	314	230	6.49	5.37	--	1.12	14	1.37
	547	16.1	309	228	7.20	5.30	--	1.90	11	2.10
	548	15.0	306	230	6.79	3.77	--	3.02	4	3.53
	549	16.0	303	228	7.21	1.82	--	5.39	32	5.93
	550	14.1	300	228	6.38	6.04	--	0.34	8	0.42
	551	16.2	296	230	7.43	0.30	--	7.13	20	7.62
X_2**	542	4.93	2.93	230	2.27	0.08	0.46	1.73	72	9.62
	543	--	--	226	--					
	544	4.29	275	225	1.98	0.09	0.71	1.18	66	11.8
	545	5.53	332	232	2.44	0.06	1.34	1.04	42	17.1
	546	7.95	328	230	3.50	Lost Sample		--	--	
	547	3.37	323	228	1.48	0.28	0.28	0.92	82	7.97
	548	3.63	320	242	1.70	0.11	0.28	1.31	74	8.92
	549	4.48	316	232	2.02	0.02	1.39	0.61	70	25.2
	550	2.70	314	230	1.21	0.03	0.41	0.77	85	11.7
	551	4.80	310	229	2.13	--	--	2.13	N.A.	7.95

*Probe located on centerline of nozzle (see Fig. 52)
**Probe located on centerline of outer zone

outside atmosphere (which drives the contamination) was correspondingly higher for the outer zone samples. A potential error in calculated hydrogen composition and eventually in calculated mixture ratio may result because the computations must be based upon an assumed time at which most of the air contamination occurred (either prior to or after the sample was introduced to the bottle). The calculated results in Table 17 assume that all measured air contamination occurred after the test. However, in addition to the errors directly associated with air contamination, others probably occurred because the calculations were necessarily performed without allowance for the sample loss that must have occurred whenever the manifold was evacuated between individual firings. Because of the errors associated with the sample bottle valve leakage, it is not surprising that the calculated equivalent exhaust gas mixture ratios shown in the last column of Table 17 show no correlation to the injected mixture ratios of the various firings as presented in Table 13. Instead, the data from the first experiments only demonstrate the need to eliminate or, at least, reduce the valve leaks before attempting any further gas sampling. Consequently the original sample bottle valves were replaced, their sealing integrity was verified, and an additional demonstration of the overall PVT concept of determining condensible/non-condensible mole fractions in a gas mixture was made befor the motor firing program was resumed (see the Task III discussion.)

The second series of firings included eight tests at an expansion ratio of 25:1 (tests 238 to 245) and eight more tests at an expansion ratio of 4:1 (tests 246 to 249). Gas samples were obtained from two of the three probes in seven of the tests at the 25:1 area ratio; the third probe, located in the outer zone stream tube, was inoperative due to a small water leak. This probe was repaired before the next firing. During tests 246 to 249, all probes were in operation; however, in tests 250 to 253, the probe at the chamber center developed a visible leak and was removed from service.

The calculated results from tests 238 to 253 are presented in Table 18. Comparison of the data in the second from the last column with the corresponding data for the initial firings in Table 17 indicates that the substitution of improved valves markedly reduced but did not completely eliminate the contamination assigned to the outside atmosphere according to the data reduction

TABLE 18. SUMMARY OF SAMPLING TEST DATA OBTAINED DURING LATER FIRINGS (TESTS 238-253)

Probe Location	Test Number	Initial Pressure, psia	Block Temperature, F	V_{Block} cc/76 F	P_{H_2} mm Hg	P_{XSO_2} mm Hg	P_{H_2O} mm Hg	Percent Air in Sample	Equivalent Mixture Ratio
X_1*	238	4.95	339	215	0	130	126	14	24.5
	239	3.31	324	222	34	15	122	18	7.79
	240	3.94	312	216	70	12	122	15	6.08
	241	3.74	303	225	17	26	150	14	9.68
	242	4.80	296	220	9	95	144	13	17.5
	243	5.90	340	220	147	6	152	13	4.39
	244	---	---	---	---	---	---	---	---
	245	8.21	331	207	352	6	113	9	2.15
	246	20.9	360	215	0	888	191	0	82.4
	247	13.1	333	222	0	499	163	2	57.0
	248	21.0	375	216	0	892	179	2	87.7
	249	17.3	360	225	0	354	524	2	18.8
	250	---	---	---	---	---	---	---	---
	251	---	---	---	---	---	---	---	---
	252	---	---	---	---	---	---	---	---
	253	---	---	---	---	---	---	---	---
X_2**	238	---	---	---	---	---	---	---	---
	239	---	---	---	---	---	---	---	---
	240	---	---	---	---	---	---	---	---
	241	---	---	---	---	---	---	---	---
	242	---	---	---	---	---	---	---	---
	243	---	---	---	---	---	---	---	---
	244	---	---	---	---	---	---	---	---
	245	---	---	---	---	---	---	---	---
	246	19.1	357	220	427	321	210	3	10.7
	247	25.7	328	222	902	7	391	2	2.5
	248	26.6	370	225	0	348	742	3	14.8
	249	18.9	356	220	0	276	685	2	14.4
	250	---	---	---	---	---	---	---	---
	251	34.7	371	233	1172	6	536	4	2.6
	252	24.7	349	233	817	4	430	2	2.8
	253	10.0	343	225	69	53	373	4	8.7
X_3***	238	14.0	327	220	744	0	0	0	0
	239	10.5	311	227	510	0	31	0	0.46
	240	7.16	298	225	302	0	68	0	1.47
	241	6.74	290	226	279	0	69	0	1.59
	242	---	---	---	---	---	---	---	---
	243	6.77	327	234	225	0	125	0	2.86
	244	---	---	---	---	---	---	---	---
	245	6.55	319	226	251	0	88	0	2.08
	246	65.6	358	220	56.9†	0.36†	0.90†	11††	0.16
	247	94.1	328	227	84.9	0.54	0.50	9	0.15
	248	52.0	368	225	42.4	0.15	0	21	0.06
	249	98.1	352	226	95.3	0.65	1.5	1	0.23
	250	31.2	320	220	26.9	0.16	0	18	0.10
	251	18.2	361	231	6.7	0.99	1.12	51	3.1
	252	41.4	348	224	39.7	0.26	0	4	0.10
	253	47.3	334	226	45.8	0	0.20	3	0.03

*Located along chamber centerline (see Fig. 52)
**Located at center of outer zone
***Located in nominal location of film coolant streamtube
†Partial pressures for tests 246-253 in psia
††Percentage of N_2 contamination for tests 246-253 where sample system is at pressures above atmospheric

scheme used for tests 542 and 552. Moreover, the correlation of the data of tests 238 to 253 to the injected mixture ratios of Table 13 was still not considered satisfactory. In particular, examination of Table 18 reveals that high concentrations of unburned oxygen were measured in the noncondensible fraction, particularly in tests 246 to 250 where they were measured by the probes at both the chamber axis and in the outer zone. If these high concentrations of uncombined oxidizer at two separate locations are indicative of conditions elsewhere in the exhaust stream, then the low efficiencies for both combustion and mixing which they represent are completely incompatible with the high values of η_{c*} shown in Table 13 for the particular firings. Consequently, the measurement of substantial unburned oxygen in the 200 series firings is attributed to liquid oxygen entrapped in the probes at engine start as supported below. When the sampling data are corrected on that basis, reasonable correlation between injected and collected zonal mixture ratios are obtained.

The explanation for the presence both of unburned oxygen and of nitrogen arises from the use of a necessarily short combustion gas purge in the sample lines between the probe opening and the bypass valves (A_1, A_2, and A_3, of Fig. As noted in the sampling and firing sequences on page 76 and 77, respectively, the sample lines were vented to the diffuser for the first 850 milliseconds of a typical test* before being opened to the sample bottle manifolds for a 1.0 second period, while the LOX main valve was opened at 200 milliseconds. This apparently amounts to a 650-millisecond period in which sampling lines are purged by combustion gases to allow a typical steady-state sample to be obtained. However, if the valve sequences are compared to the typical LOX flowrate and chamber pressure histories shown in Fig. 36 and 37, it may be noted that the nominal purge period actually represents a period of high LOX flowrate and low chamber pressure, i.e., a period in which unburned liquid oxygen can be carried through the combustion chamber and nozzle directly into a probe inlet.

*Although the sequence discussed was actually used in the initial firings, (Tests 542 to 552), the same considerations apply to the later 200 series firings.

Although postulating such a mechanism for the presence of unburned oxygen is necessarily speculative, it is significant that the data in Table 18 show that:

1. The highest concentrations of oxygen were measured at probe location X_1 along the chamber centerline, which is in a direct line of sight with the injector
2. Lower concentrations of oxygen were measured at probe location X_2, which had a less direct view of the injector
3. There was very little free oxygen detected at probe location X_3, along the nozzle wall.* This location has the least direct view of the injector for liquid oxygen capture. Instead, it would preferentially receive the unburned hydrogen and remaining nitrogen purge gas during engine startup because these gaseous species would completely fill the nozzle
4. The free oxygen detected at probe location X_1 and the overall apparent contamination at probe location X_3 increased sharply during Tests 246 to 253 (nozzle expansion ratio of 4:1) as compared to Tests 238 to 245 (expansion ratio of 25:1). The increases are exactly what would be expected as the probes are moved closer to the injector with a correspondingly higher view factor for liquid capture and a higher pressure for gaseous capture.

Based upon the above four observations, it is hypothesized that data listed in Table 18 represent effects of an insufficient purge of sample lines by the desired combustion gas at engine startup rather than excessive leakage in the sampling system. Eliminating this problem will require initial purges of 2 to 5 seconds at start, and the correspondingly longer firing durations. Unfortunately, firing durations greater than 5 seconds were impossible with the uncooled heat sink chamber used in the program.

*Note in Table 18 that the "air" contamination listed for probe X_3 is nitrogen rather than the 4:1 nitrogen/oxygen mixture.

The last columns of Tables 17 and 18 present the equivalent mixture ratio for the gas samples calculated from the measured hydrogen, water, and the calculated excess oxygen, assuming atmospheric contamination, but no startup LOX entrapment. They represent, therefore, a calculation based on the two assumptions:

1. That air leaked into the samples as defined by the measured nitrogen
2. That unburned oxygen and hydrogen could exist in the same sample under steady-state conditions

The mixture ratios calculated on this basis are compared to the injected zonal mixture ratios in Table 19. The injected wall mixture ratio includes mixing between film coolant and outer zone in accordance with Eq. 10. Examination of the data reveals no correlation between injected and collected mixture ratios. The high leak rate during the initial 500 series firings provides the explanation for the lack of agreement in those tests. However, in the later 200-series firings, the system leakage was reduced; therefore the insufficient purge of sample lines discussed above is offered as the explanation. To further investigate this possibility, an alternate calculation of equivalent mixture ratio was made for the samples based on the assumption that all oxygen and nitrogen in the samples represented startup contamination and should, therefore, be excluded. The resultant mixture ratio is based only on the hydrogen and water in the sample. The sample mixture ratios calculated for the 200 series firings in accordance with the latter assumption are compared to injected mixture ratios in Table 20. Although the correlation is still not conclusive, the agreement between injected and collected mixture ratio is considerably improved; moreover, both sets show the same trends from the core through the outer zone to the wall. Based on the results shown in Table 20 it was therefore concluded that a limited demonstration had been made of exhaust flow stratification corresponding to injected mixture ratio bias. It was similarly concluded that improved exhaust gas sampling will require not only leak proof systems, but also adequate firing durations and carefully programmed sample line purges.

TABLE 19. COMPARISON OF EXHAUST GAS SAMPLES WITH INJECTED ZONAL MIXTURE RATIOS ASSUMING ATMOSPHERIC CONTAMINATION

Test	Expansion Ratio	Injected Into Core Zone	Sample Probe 1	Injected Into Outer Zone	Sample Probe 2	Mixed Wall Zone*	Sample Probe 3	Percent Film Coolant
542	25:1	7.98	1.76	4.71	---	3.39	9.62	9.65
543		---	---	---	---	---	---	---
544		6.94	5.18	6.17	---	3.93	11.8	11.97
545		7.70	1.64	4.20	---	3.01	17.1	10.02
546		6.90	1.37	3.76	---	3.76	---	0.00
547		6.00	2.10	5.28	---	5.28	7.97	0.00
548		7.28	3.53	4.04	---	2.90	8.92	9.82
549		6.16	5.93	5.59	---	3.52	25.2	12.09
550		6.89	0.42	3.97	---	2.85	11.7	9.71
551		7.83	7.62	4.65	---	3.33	7.95	9.70
552		7.29	---	3.92	---	3.92	---	0.00
238	25:1	7.02	24.5	3.94	---	2.50	0.0	9.70
239		8.75	7.79	5.15	---	5.15	0.46	0.00
240		6.16	6.08	5.67	---	3.34	1.47	11.79
241		6.33	9.68	5.27	---	3.31	1.59	11.80
242		7.13	17.5	3.89	---	2.58	---	9.70
243		5.69	4.39	4.81	---	4.81	2.86	0.00
244		7.18	---	3.94	---	2.66	---	9.70
245		7.38	2.15	4.05	---	2.72	2.08	9.69
246	4:1	8.08	82.4	4.80	10.7	3.45	0.16	9.70
247		6.67	57.0	3.66	2.5	2.65	0.15	9.72
248		8.04	87.7	7.21	14.8	4.59	0.06	11.81
249		7.35	18.8	4.09	14.4	2.96	0.23	9.73
250		6.45	---	5.81	---	3.69	0.10	11.82
251		6.55	---	5.90	2.6	5.90	3.1	0.00
252		6.00	---	4.18	2.8	4.18	0.10	0.00
253		7.53	---	4.40	8.7	3.17	0.03	9.71

*Based on incomplete mixing as defined by Eq. 10.

TABLE 20. COMPARISON OF EXHAUST GAS SAMPLES WITH INJECTED ZONAL MIXTURE RATIOS ASSUMING INSUFFICIENT PURGE OF STARTUP CONTAMINATION

Test	Expansion Ratio	Injected Into Core Zone	Sample Probe 1	Injected Into Outer Zone	Sample Probe 2	Mixed Wall Zone*	Sample Probe 3	Percent Film Coolant
238	25:1	7.02	7.95	3.94	---	2.50	0	9.70
239	↓	8.75	6.20	5.15	---	5.15	0.46	0.0
240	↓	6.16	5.05	5.67	---	3.34	1.47	11.79
241	↓	6.33	7.15	5.27	---	3.31	1.59	11.80
242	↓	7.13	7.50	3.89	---	2.58	---	9.70
243	↓	5.69	4.05	4.81	---	4.81	2.86	0.00
244	↓	7.18	---	3.94	---	2.66	---	9.70
245	↓	7.38	1.95	4.05	---	2.72	2.08	9.69
246	4:1	8.08	7.95	4.80	2.65	3.45	0.12	9.70
247	↓	6.67	7.95	3.66	2.40	2.65	0.05	9.72
248	↓	8.04	7.95	7.21	7.95	4.59	0	11.81
249	↓	7.35	7.95	4.09	7.95	2.96	0.12	9.73
250	↓	6.45	---	5.81	---	3.69	0	11.82
251	↓	6.55	---	5.90	2.50	5.90	1.15	0.00
252	↓	6.00	---	4.18	2.75	4.18	0	0.00
253	↓	7.23	---	4.40	6.65	3.17	0.03	9.71

*Based on incomplete mixing as defined by Eq. 10.

TASK V - THEORETICAL ANALYSES USING JANNAF PROGRAMS AND METHODOLOGY

A selection of the stratified flow engine firings was analyzed using the system of computer programs under development by the JANNAF Performance Standardization Working Group. The overall objective of the analysis was to determine the effectiveness of the present family of programs in predicting thrust chamber performance and heat transfer. The test program was designed to provide the input information required by the various model programs. Due to practical and physical limitations, experimental definition of all of the required input was not possible. The parameters that could not be directly prescribed by the experimental test conditions included:

1. The LOX spray dropsize distribution
2. The mixing between the core, outer zone, and film coolant layers
3. The best starting plane (in terms of distance from the injector) for the STC computer program calculation, together with the appropriate degree of LOX vaporization upstream of this starting plane
4. The proper starting location on the wall for the BLIMP program calculation, i.e., the single phase boundary layer attachment point.

As discussed below, several techniques for choosing the computer program input data in conjunction with available theoretical and empirical information were used to specify the necessary parameters. The validity of assumptions associated with these techniques determines the accuracy of the subsequent computer analyses.

The theoretical analysis was made with the same four stratified flow engine tests selected to typify experimental results in the preceding Task IV discussion (see Fig. 41 through 45). The conditions specified for the four

tests are listed in the upper portion of Table 21; these tests include both stratified and effectively uniform combustion gas core flows, made with and without film cooling at the chamber wall.

ANALYTICAL PROCEDURES

The analysis of the combustion gas flow field was made using the STC (Stream Tube Combustion) program block of the DER (Distributed Energy Release) model to calculate the spray combustion and resultant flow to the nozzle throat. The TDK program was used to calculate the subsequent expansion of the combustion gas from the throat to the nozzle exit. The boundary layer between the main flow field (assumed to be inviscid by STC and TDK) and the thrust chamber walls, together with the resultant wall heat transfer rates, were calculated by the BLIMP program, which is the accepted JANNAF computer program for bell nozzle rocket engines.

STC Program

The STC (Stream Tube Conbustion) program block of the DER model calculates the two-phase flow field associated with the burning of the propellant spray in a liquid-liquid or gas-liquid combustor from a specified starting plane to the nozzle throat. The flow field consists of an array of one to forty stream tubes of varying total mass and mixture ratio. Propellant flows (both sprays and gases) which enter a given stream tube are thereafter constrained to flow in that tube without exchange of mass, momentum, or energy with its neighboring stream tubes. The flow and combustion in each stream tube are analyzed by a one-dimensional formulation, with the local stream tube path as the independent variable. The formulation is based upon the conservation equations for mass, momentum, and energy within the stream, with the rate of mass and momentum exchange between liquid and gas phases defined by spray vaporization and drag formulae. Calculations are made by a marching procedure from the starting plane to the nozzle throat in which the individual stream tube solutions are coupled by constraints on total cross-sectional area and on the pressure profile. Pressure is assumed to be constant across each z (axial

TABLE 21. OPERATING CONDITIONS AND COMBUSTION PARAMETERS SPECIFIED FOR FOUR TEST CASES ANALYZED BY JANNAF PROGRAMS

	Stratified Flow Run Number			
	238	250	252	547
Conditions Specified by Experimental Measurement				
Total Propellant Flow, lbm/sec	17.31	21.73	21.25	17.79
Overall Mixture Ratio	4.78	5.36	4.93	5.76
Inner Core Flow, lbm/sec	9.13	11.36	11.30	9.59
Inner Core Mixture Ratio	7.02	6.39	6.00	6.00
Outer Zone Flow, lbm/sec	7.89	9.97	9.95	8.20
Outer Zone Mixture Ratio	3.93	5.75	4.18	5.28
Film Coolant Flow, lbm/sec	0.291	0.400	0.00	0.00
Fuel Injection Temperature, R	537	537	537	537
Oxidizer Injection Temperature, R	162	162	162	162
Conditions Specified by Preliminary Calculation				
Wall Mixture Ratio	2.50	3.69	4.18	5.28
$\overline{D}$, Inner Core, micron	115	104	109	104
$\overline{D}$, Outer Zone, micron	80	99	103	84

coordinate) plane until, at some point in the nozzle convergent section, curvature due to transonic flow effects is taken into account. At this point, rather than continuing to solve for a pressure which satisfies area continuity, an absolute pressure calculated by an auxiliary subprogram TRANS for an equivalent homogeneous flow is imposed upon the marching solution. The deviation of the sum of the computed areas at the nozzle throat from the actual geometric area is used to adjust the total pressure back at the starting plane, and the marching calculation is then repeated. Iteration of initial pressure computations is continued until satisfactory convergence of calculated and real throat areas is obtained.

The required input data to the STC program includes the chamber geometry, the propellant properties, the combustion gas properties as functions of mixture ratio, the initial plane gaseous flowrate and mixture ratio, together with the droplet diameters, velocities, and weight flowrates of the spray entering each of the stream tubes. These data may be provided by calculations of the LISP (Liquid Injector Spray Patterns) subprogram block of the DER model.

The subprogram TRANS, obtained from the TDK model, provides a family of as many as 20 isobaric lines in the nozzle throat region. The program is structured so that the intersection of the fifth isobar with the chamber wall occurs at the geometric nozzle throat and provides a start line for the subsequent use of the TDK program.

Further details of the STC program are available in Ref. 3.

TDK Program

The TDK program calculates the inviscid axisymmetric non-equilibrium supersonic nozzle expansion of non-uniform gaseous mixtures. The program constructs a finite difference mesh by tracing gas streamlines and left running characteristic surfaces. As many as 50 striations in the flow may be considered; there is no intermixing of the separate streams. The start line for the calculation by the method of characteristics can be provided directly as

input or supplied by the transonic analysis from the TRANS subprogram. The characteristics equations governing inviscid fluid dynamics are integrated using a second-order explicit integration method, while the chemical relaxation equations are integrated using a first-order implicit method to ensure numerical stability for the near thermodynamic equilibrium flow. As utilized in the DER model, the TDK program block accounts for the effect of incomplete combustion on specific impulse and ignores the effect of chemical kinetics. Thermochemical data used by TDK are available for 415 species. Further details of the TDK program are available in Ref. 9.

BLIMP Program

The BLIMP (Boundary Layer Integral Matrix Procedure) program uses a strip-integral numerical procedure to solve a comprehensive set of equations describing fluid flow in laminar or turbulent boundary layers at planar or axisymmetric bodies. The governing equations apply to general, multi-component, ionized species in local chemical equilibrium. Unequal mass or thermal diffusion coefficients for each specie may be considered through use of convenient approximations.

For turbulent flows, the time-averaged equations of motion are solved utilizing an eddy viscosity model to describe the "Reynolds stress" term, plus constant turbulent Prandtl and Schmidt numbers in the energy and species conservation equations. Eddy viscosity is related to a variable mixing length in the region very near the wall and to global parameters of the flow in the outer portion of the boundary layer. In this regard, the BLIMP formulation differs from that of the Elliott-Bartz-Silver type of models. In the former, the boundary layer velocity and temperature profiles result from an integration of the differential specification of the eddy diffusivity; in the latter formulation, a power law specification of the boundary layer velocity and temperature profiles is made. Turbulent transport terms in the equations of motion of BLIMP are considered only after the transition criterion, an input transition Reynolds number based on momentum thickness, has been satisfied.

The boundary layer edge gas is assumed to be adiabatic, but it may be non-isentropic. For boundary layer edge conditions, the user need supply only the composition of the edge gas, stagnation pressure and enthalpy, and the distributions of pressure, entropy, and radiant heat flux along the body. The radiation (if any) is assumed to pass through the boundary layer and into the wall.

The required input data to the BLIMP program include the gas composition and thermodynamic properties, the body geometry, and the aforementioned boundary layer edge conditions. The calculated output at a desired set of axial stations includes:

1. Velocity, enthalpy, shear, and temperature profiles in the boundary layer
2. Velocity, pressure, and temperature conditions at the edge of the boundary layer
3. Displacement, momentum, and energy thicknesses of the boundary layer
4. Heat flux into the surface of the body.

Specification of Initial Conditions for Combustor Flow Field

The conditions at the starting plane for the STC computer program calculation of the combustion chamber flow field are usually specified by prior calculations made with the LISP injector design computer program. In the present investigation, the particular injector design made an alternate specification more appropriate. The injector (see Fig. 1) employed separate manifolds to divide the propellant feed into three distinct zones with individually measured flows and utilized a face pattern which made the flow within each zone as homogeneous in mass and mixture ratio as possible close to the injector. Consequently, it was convenient to formulate the STC combustion flow field directly into three stream tubes based upon these zones.

Although the flow for the three zones (which will be referred to as the inner core, outer zone, and BLC region) represent distinct entities at the injector face, some of the spray fans out and mixes with spray and gas flows from neighboring zones as the two-phase flow travels downstream. The extent to which this mixing alters the mixture ratio defined at the injector is particularly important in the BLC region because of its relatively low flowrate (approximately 1.5 to 2.0 percent of the total propellant flow) and thin radial dimension (approximately 0.02 to 0.03 inch). Consequently, a revised definition of the BLC region stream tube mass flow and mixture ratio was made. This revised definition was obtained from a preliminary set of calculations with the BLIMP boundary layer program for a range of assumed gas mixture ratios from 1.5 to 3.5, followed by comparison of the calculated wall heat flux profile with experimental data from Test 238. The results, which are shown in Fig. 53, indicated that the best agreement between the calculated and measured heat transfer was obtained when the mixture ratio was defined as 2.5. This mixture ratio in the boundary layer was assumed to exist because of a complete mixing of a certain fraction of the outer zone flow with the BLC layer. Moreover, the extent of this mixing was assumed to be comparable in all tests made with the given injector/thrust chamber combination and film coolant rates near the nominal 10 percent of the total fuel flowrate. The predicted mixing was based upon the criterion

$$MR_{FC} = \frac{F_M\left(\frac{MR_{OZ}}{MR_{OZ}+1}\right)}{\frac{\dot{W}_{FC}}{\dot{W}_{OZ}} + F_M\left(\frac{1}{MR_{OZ}+1}\right)}$$

which is derived in Appendix C and has been discussed in the Task IV correlation of experimental data. The value of the mixing coefficient F_M, as determined in Task IV, ranged from 0.3 to 0.6, with the lower range of the coefficient providing the best fit shown in Fig. 53. Application of the assumed mixing criterion to get an initial prediction of wall region mixture ratio, followed by successive comparisons with the wall heat transfer calculated by

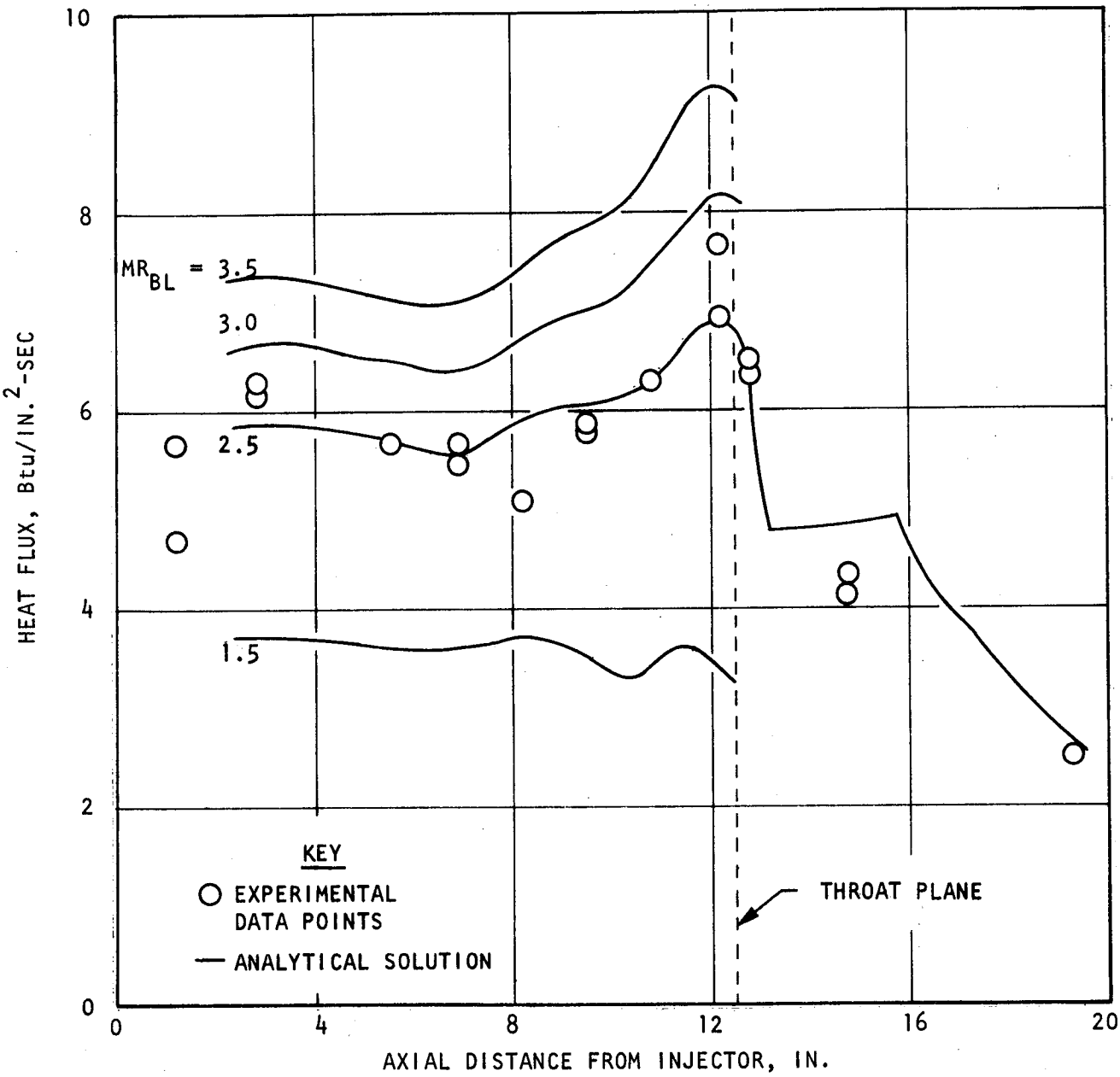

Figure 53. Comparison of Analytical Heat Flux Profiles and Experimental Data with Boundary Layer Edge Gas Mixture Ratio as a Parameter - Run 238

BLIMP at the defined mixture ratios, finally resulted in the assignment of the values shown in the lower portion of Table 21 for the two tests made with film cooling.

In addition to specifying the mixture ratios of the three defined STC stream tubes, it was also necessary to define a spectrum of droplet sizes for the oxygen spray entering the stream tubes. Although it was desired to relate the dropsize as closely as possible to the data obtained in the Task II hot wax atomization tests, the direct definition of a liquid oxygen diameter under combustion conditions from the experimental data for a liquid with markedly different physical properties is still beyond the state of the art. In order to determine whether an adequate prediction of LOX dropsize could be made, a preliminary calculation, based solely on the property correction criteron recommended by Falk and Burick (Ref. 10), was performed. Using this criterion, the mean droplet diameter of the LOX spray, $\overline{D}_{LOX}$, is related to the mean wax diameter, $\overline{D}_{WAX}$, by

$$\frac{\overline{D}_{LOX}}{\overline{D}_{WAX}} = \left[\frac{\mu_{LOX}}{\mu_{WAX}} \; \frac{\sigma_{LOX}}{\sigma_{WAX}} \; \frac{\rho_{WAX}}{\rho_{LOX}}\right]^{1/4}$$

$$\overline{D}_{LOX} \cong 0.43 \cdot \overline{D}_{WAX}$$

If this scale factor is applied to the dropsize correlation represented by the solid curve of Fig. 11, the functional relationship of $\overline{D}_{LOX}$ with hot fire mixture ratio is defined by the broken curve in the same figure.

When this prediction of mean droplet diameter was input to the STC program for the test cases, the subsequently calculated rapid burning rate produced static pressure profiles which did not agree with the experimentally measured profiles in the combustion chamber. However, an acceptable agreement between computer-calculated and experimental pressure profiles for Test 238 was obtained for a mean oxidizer spray droplet diameter of 100 microns;

moreover, the calculated and measured c* efficiencies were also in agreement within experimental accuracy. Consequently, the hot wax atomization data of Fig. 11 and the results of the preliminary STC calculations were combined by defining a scale factor from the ratio between the 100-micron $\overline{D}_{LOX}$ defined by the STC calculations made with Test 238 and the 183-micron $\overline{D}_{WAX}$ defined by the hot wax atomization studies for the same hot fire mixture ratio*. When this scale factor

$$\frac{100}{183} = 0.54$$

is applied to the hot wax correlation, the resultant relationship is that shown by the dotted curve of Fig. 13. Mean LOX droplet diameters were then defined for the inner core and outer zones during each of the four test cases from this graphic correlation at the respective mixture ratios of the various zones. The resulting definitions employed in the final round of STC calculations are shown in the lower portion of Table 21.

Based upon previous experience in using the JANNAF program with high performing injectors, the starting plane for the STC calculation was selected as 0.80 inch from the injector face. At this location, the injected oxidizer spray was assumed to be 3.0 percent vaporized. Because the LOX spray was calculated to be almost completely vaporized in the first 6 inches downstream of the injector, minor changes in either assumption have no appreciable effect on performance.

Combustion Gas Properties

The physical properties of the combustion gas mixture (which result from the burning of the gaseous-hydrogen/liquid-oxygen propellant combination) used by the STC program were based upon the calculations of the Rocketdyne N-element

*The mean hot fire mixture ratio of 5.29 for Test 238 did not include the fuel used as film coolant.

thermodynamic equilibrium computer program (Ref. 11). Initial calculations were made with the program for an assumed hydrogen inlet temperature of 537 R and a LOX inlet temperature of 162 R for a wide range of mixture ratios. The resultant property data used in STC are listed in Table 22.

Performance Correction Methods

The c* and I_s losses expected for the engine and propellant combination were calculated using methods recommended by Powell (Ref. 12), which reflect the recommended procedures of the JANNAF Performance Standardization Working Group. For the particular engine, the principal corrections to c* are defined by the energy release efficiency $\eta_{c^*_{ER}}$, the injector region heat loss, and the throat boundary layer loss. The energy release efficiency is the product of the mixing and vaporization efficiencies which are calculated by the STC program. The boundary layer loss is defined by

$$\eta_{c^*_{BL}} = \frac{1}{C_D\left(1 - \frac{2\delta^*_t}{r_t}\right)}$$

which represents an adjustment to the inviscid one-dimensional c* efficiency calculated by STC. The value of δ^*_t is calculated by the BLIMP program. Injector region heat loss efficiency was evaluated by removing the integrated heat loss to the chamber upstream of the start of the BLIMP boundary layer from the available enthalpy of the combustion gas. A crude calculation indicated that the maximum performance decrement by this mechanism was less than 0.2 percent of either the available I_s or c*; consequently, a more detailed calculation was not attempted.

The principal losses expected from the TDK calculation of inviscid I_s performance in a two-dimensional nozzle are the energy release loss and the

TABLE 22. COMBUSTION GAS PROPERTIES FOR THE LOX/GASEOUS HYDROGEN PROPELLANT COMBINATION AT A PRESSURE OF 300 PSIA (T_{LOX} = 162 R, T_{H_2} = 537 R)

Mixture Ratio	Stagnation Temperature	Molecular Weight	Specific Heat Ratio	Viscosity lbm/ft sec	c* ft/sec
0.0	537 R	2.016	1.405	5.97×10^{-6}	6300
0.5	1435 R	3.024	1.38	7.34×10^{-5}	7126
1.0	2264 R	4.032	1.338	2.09	7655
2.0	3661 R	6.047	1.274	3.49	8272
2.5	4248 R	7.049	1.255	4.11	8335
3.0	4754 R	8.03	1.240	4.66	8302
4.0	5517 R	9.921	1.221	5.52	8159
5.0	5996 R	11.649	1.210	6.11	7924
5.5	6151 R	12.447	1.207	6.32	7783
6.0	6260 R	13.200	1.204	6.47	7641
7.0	6370 R	14.569	1.201	6.57	7351
8.0	6385 R	15.769	1.200	6.77	7078

boundary layer loss. The I_s efficiency, defined as

$$\eta_{I_s} = \frac{I_s}{I_{s_{TDK}}}$$

was calculated from

$$\eta_{I_s} = \eta_{c^*_{ER}} \left[1 - \frac{\Delta I_{s_{BL}} + \Delta I_{s_{HL}}}{I_{s_{TDK}}} \right]$$

which simplifies to

$$\eta_{I_s} = \eta_{c^*_{ER}} \left[1 - \frac{\Delta I_{s_{BL}}}{I_{s_{TDK}}} \right]$$

because $\Delta I_{s_{HL}}$, the injector region heat loss, was estimated conservatively at less than 0.2 percent of I_s (as indicated in the previous paragraph) and therefore could be ignored.

The boundary layer loss, $\Delta I_{s_{BL}}$, was calculated using the formulae presented by Powell (Ref. 12).

$$\Delta I_{s_{BL}} = \left\{ \frac{2A_E P_E \cos \alpha_E}{\dot{w}} \left[\left(\frac{\rho_E u_E^2}{P_E} \right) \left(\frac{\theta_E}{r_E} \right) - \frac{\delta_E^*}{r_E} \right] \right\}$$

$$+ \frac{\partial}{\partial \varepsilon} \left\{ \frac{2A_E P_E \cos \alpha_E}{\dot{w}} \left[\left(\frac{\rho_E u_E^2}{P_E} \right) \left(\frac{\theta_E}{r_E} \right) - \frac{\delta_E^*}{r_E} \right] \right\} \times (\varepsilon' - \varepsilon)$$

$$- \frac{\partial}{\partial \varepsilon} \left[\Sigma I_{s_{\substack{\text{stream} \\ \text{tubes}}}} \frac{\dot{w}_{VAP}}{\dot{w}} \right] (\varepsilon' - \varepsilon)$$

and

$$(\varepsilon' - \varepsilon) = -2\varepsilon \frac{\left[\frac{\delta_E^*}{r_E} \cos \alpha_E - \left(\frac{\delta_t^*}{r_t}\right)\right]}{1 - \left(2 \frac{\alpha_t^*}{r_t}\right)}$$

The required boundary layer thicknesses, free stream flowrates, and vaporizations are obtained from the STC and BLIMP program printouts.

No allowance was made for either increase in nozzle throat and exit plane area from pressure stresses or thermal expansion or for nozzle discharge coefficient.

ANALYTICAL RESULTS

The four sample cases, Tests 238, 250, 252, and 547, were processed with the STC, TDK, and BLIMP programs for the conditions listed in Table 21. Pressure profiles in the combustion chamber and local heat fluxes to the chamber and nozzle walls were calculated directly from the STC and BLIMP programs, respectively. The c* and I_s efficiencies were first calculated on an inviscid basis with STC and TDK and then adjusted for boundary layer losses. The results are presented and discussed in the following paragraphs.

Performance

The calculated c* and I_s performance parameters are presented in Table 23. The upper portion of the table lists performance data for the equivalent inviscid flow field as calculated by STC and TDK. The efficiencies represent the difference between an inviscid stratified flow in a 2-dimensional limited expansion nozzle as compared to a uniform flow expanded to vacuum conditions in an ideal nozzle. The lower portion of the table lists performance data for a stratified flow in a 2-dimensional nozzle as corrected for boundary

TABLE 23. CALCULATED PERFORMANCE PARAMETERS FOR STRATIFIED FLOW ENGINE FIRINGS

Parameter	Test Number			
	238	250	252	547
Inviscid Flow Performance				
Energy Release η_{c^*}	0.971	0.990	0.993	0.996
Mixing Limited η_{c^*}	0.972	0.991	0.9937	0.9996
Vaporization Limited η_{c^*}	0.999	0.999	0.9997	0.996
C_D	0.994	0.994	0.994	0.994
TDK Specific Impulse, sec	424.3	374.7	379.5	431.1
Specific Impulse, Max, sec	466.5	462.9	466.2	460.9
η_{I_s} (inviscid, adiabatic)	0.909	0.809	0.814	0.937
Boundary Layer Correction Parameters				
δ^* (throat), feet	-7.74×10^{-4}	-8.74×10^{-4}	-8.87×10^{-4}	-7.90×10^{-4}
δ^* (exit), feet	12.8×10^{-3}	-7.29×10^{-4}	-15.5×10^{-4}	4.24×10^{-3}
θ (exit), feet	10.6×10^{-3}	4.52×10^{-3}	5.27×10^{-3}	19.3×10^{-2}
P (exit), psia	1.09	13.83	13.83	0.83
ρ (exit), lbm/ft^3	5.14×10^{-4}	2.69×10^{-3}	2.59×10^{-3}	3.67×10^{-4}
u (exit), ft/sec	1.39×10^{4}	1.19×10^{4}	1.18×10^{4}	1.39×10^{4}
$\dot{w}$, lbm/sec	17.31	17.79	21.73	21.25
r (throat), ft	0.1992	0.1992	0.1992	0.1992
r (exit), ft	0.9962	0.4102	0.4102	0.9962
$\eta_{c^*_{BL}}$	0.998	0.997	0.997	0.998
$\Delta I_{s_{BL}}$, sec	11.0	6.5	6.7	12.1
$\eta_{I_{s_{BL}}}$	0.974	0.982	0.982	0.972

TABLE 23. (Concluded)

Parameter	Test Number			
	238	250	252	547
Injector Region Heat Loss Correction				
Heat Loss, Btu/sec	224	224	224	224
$\Delta I_{s_{HL}}$	0.42	0.46	0.38	0.35
Delivered Performance Parameters				
Corrected η_{c^*}	0.969	0.987	0.990	0.994
Corrected Specific Impulse, sec	412.9	367.7	372.4	418.6
Calculated η_{I_s} (Heat loss & boundary layer for stratified flow)	0.973	0.981	0.981	0.971
Experimental Performance				
Measured η_{c^*}	0.983	1.007	0.982	1.012
Measured Specific Impulse, sec	407.4	366.0	359.6	414.1
Measured η_{I_s}	0.960	0.977	0.948	0.961

layer effects and injector region heat transfer, and also compares these results to the corresponding experimental data. Except for the case of Test 252, the experimental values of η_{c*} are approximately 1.5 percent higher than the calculated values; while the experimental values of I_s are approximately 1 percent lower than the calculated values for the corresponding striated flow, expansion ratio, and 2-dimensional nozzle. In Test 252, the relation between the measured and calculated values of both η_{c*} and η_{I_s} is approximately 2 percent lower than for the other three cases.

The data in Table 23 indicate that essentially all the calculated specific impulse efficiency loss is associated with the boundary layer losses; the injector region heat losses only contribute approximately 1/10 percent.

Because the measured values of η_{c*} in Tests 250 and 547 were both greater than the limiting values of unity by approximately 1 percent, it is reasonable to assume that a systematic error of the same magnitude is present in the experimental c* performance values. Such an error would probably be associated with either a difference in the real throat area under hot fire conditions from that employed in the calculations or an error in the measurement of chamber pressure, rather than from an error in the propellant flowrate. (This assumption is made because a small systematic error in either pressure or throat area would not affect the calculated I_s; but an error in weight flow must cause experimental values of both c* and I_s to deviate in the same direction from theoretical values. Therefore, because the deviations were in opposite directions for both η_{c*} and I_s, a systematic error in weight flow cannot be offered as the explanation.)

Because of the number of effects for which corrections of from 1/2 to 3 percent are applied, the agreement between experimental and analytical results is remarkably good for all the tests. An exception is the I_s value for Run 252. It appears that the thrust measurement may have been in error, since η'_{c*} compares very well. The overall agreement between measured and

predicted performance can be considered to be a satisfactory demonstration of the performance prediction capability of the JANNAF system of computer programs.

Pressure Distribution

The pressure distributions calculated by STC in the constant area combustion chamber are compared to experimental data for the four test cases in Fig. 54. The distributions are normalized according to the ratio (P_{static}/P_0) for easy comparison. The graphic results indicate that the agreement between the shape of the experimental and calculated profiles is excellent in Tests 238 and 547, although it is not quite as good in Tests 250 and 252. In all four cases, the difference between experimental and theoretical reduced pressures is less than 2 percent. Some of the small difference between the calculated and empirical data can be attributed to experimental error; however, based on the scatter in the data, the magnitude of the possible error in local pressure measurement is estimated to be less than 1 percent. With this limit on measurement error, a small but definite deviation between experimental and calculated pressure ratios in Tests 250 and 252 is clear. Since the pressure ratio at a given axial station is a measure of the degree of vaporization and, therefore, of initial drop size distribution, it appears that the method employed for specifying drop size from cold flow data and hot fire injection conditions (as described previously) needs to be refined before it can be recommended for exact calculations in the upstream portion of the combustion chamber.

A second source of the minor differences in calculated and experimental profiles arises from the definitions of the gas and spray velocities in the starting plane of the STC marching calculation. The gas velocity is defined wholly in terms of the continuity requirements set by the injected gas flowrate, the degree of spray vaporization at the starting plane, the cross-sectional area of the combustion chamber, and the stagnation pressure. Similarly, the spray velocity is defined as equal to the liquid injection velocity. These assumptions introduce no deviations from physical reality with

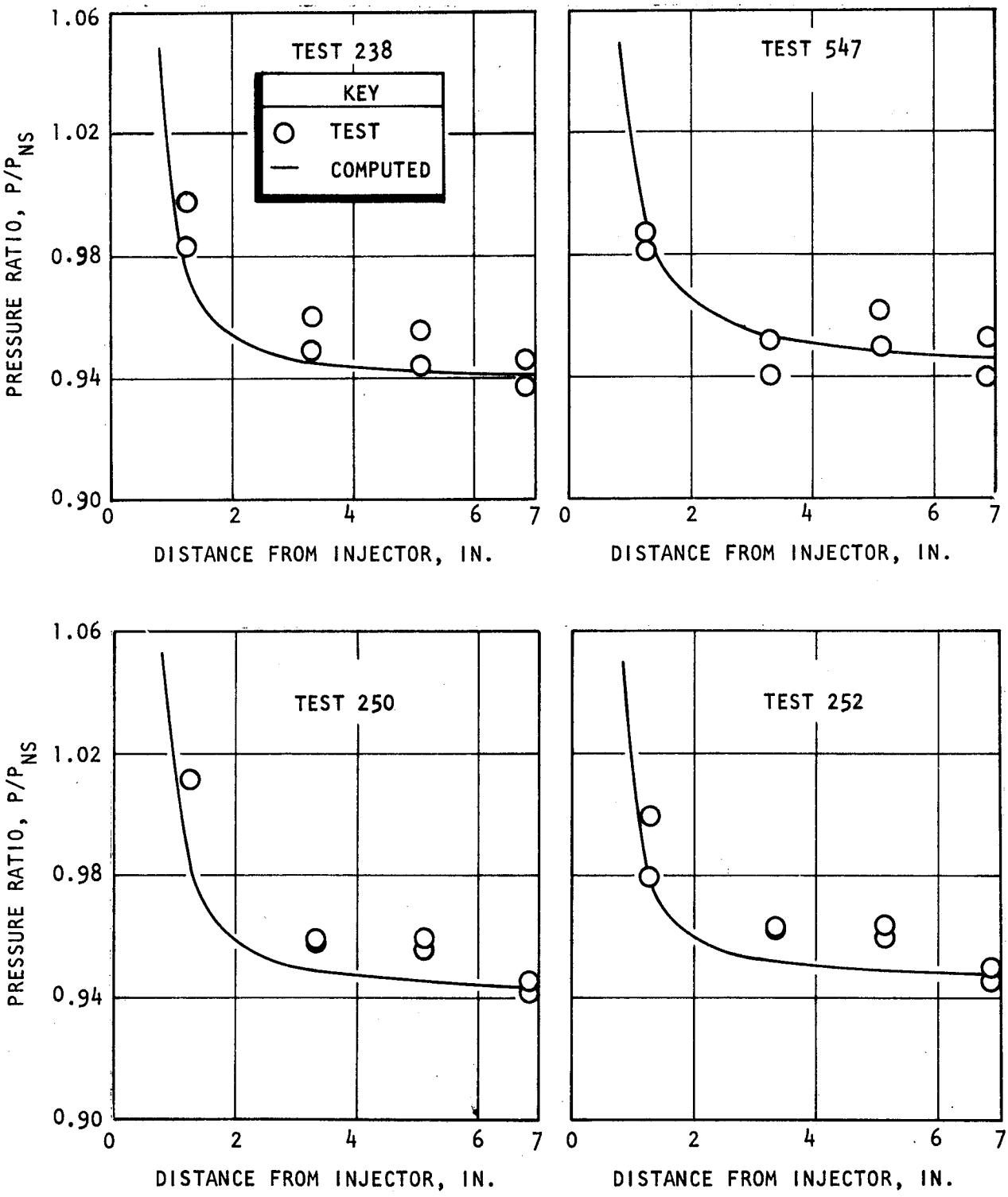

Figure 54. Comparison of Computed and Measured Pressure Ratio -Profiles of Tests 238, 547, 250, and 252

liquid/liquid injection systems. However, with the gas/liquid injector, these starting conditions ignore the significant momentum carried by the injected gaseous propellant. Some of this momentum must go to accelerate the spray very close to the element impingement points; the remainder is associated with non-uniform axial gas velocities. The net effect of high injected gas momentum is to reduce the axial pressure gradient required close to the injector; consequently, the analytical pressure profile of the STC computer program is expected to show a steeper slope than the experimental profile. Figure 54 definitely shows this trend. However, despite this oversimplification in the analytical model, the overall agreement between the theoretically calculated and empirical pressure profiles must be considered an extremely encouraging demonstration of the effectiveness of the JANNAF performance prediction methods.

Heat Transfer

The wall heat flux profiles, calculated by the BLIMP computer program for the four test cases, are compared to experimental heat flux data for the respective tests in Fig. 55 through 57. The heat transfer distributions which were calculated for a range of wall mixture ratios are presented for Test 238 in Fig. 53. As discussed on page 127, a matching of the experimental data to the best-fitting analytical distribution (the curve for a mixture ratio of 2.5 was chosen for Run 238) was utilized to establish a criterion for the mixing of the film coolant (when used) with the adjacent outer zone combustion gas flow. Figures 55 through 57 show the BLIMP-calculated heat transfer only for the established wall mixture ratio.

The overall agreement between the experimental and analytical results is excellent for Tests 238 and 250. The average deviations between measured and calculated heat fluxes in the two tests are only 6 percent and 10 percent, respectively; moreover, the deviations of the experimental points are uniformly distributed about the analytical curve. However, the agreement is not nearly as good in Tests 252 and 547. In these two firings, the average deviations between measured and calculated local heat fluxes are 18 percent and

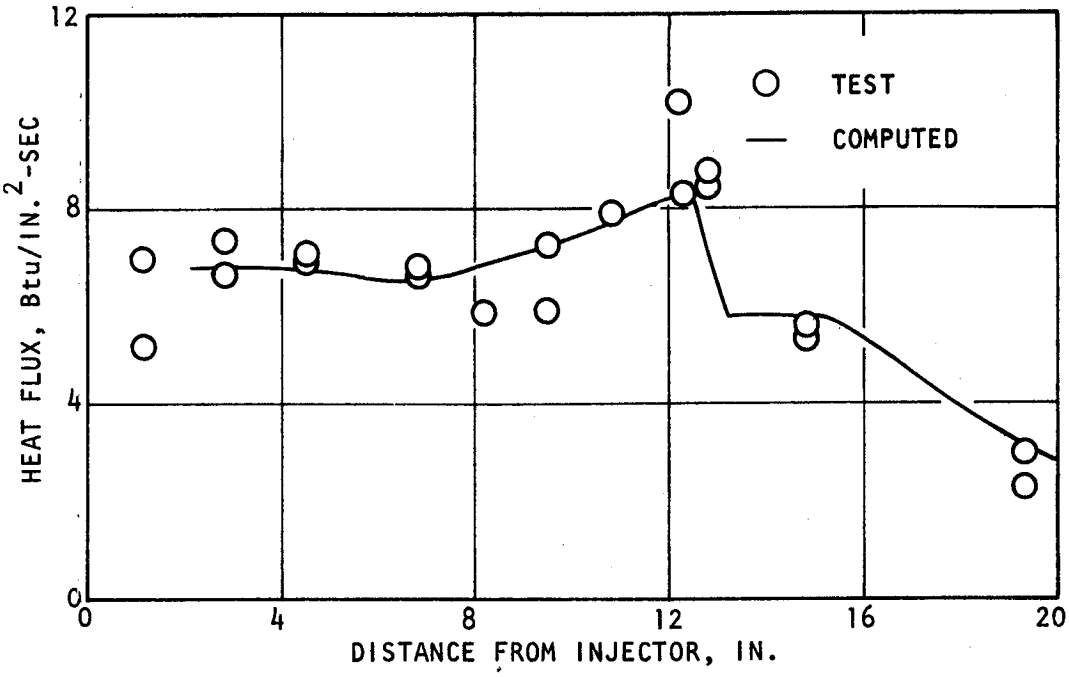

Figure 55. Comparison of Analytical Heat Flux Profile with Experimental Data for Test 250

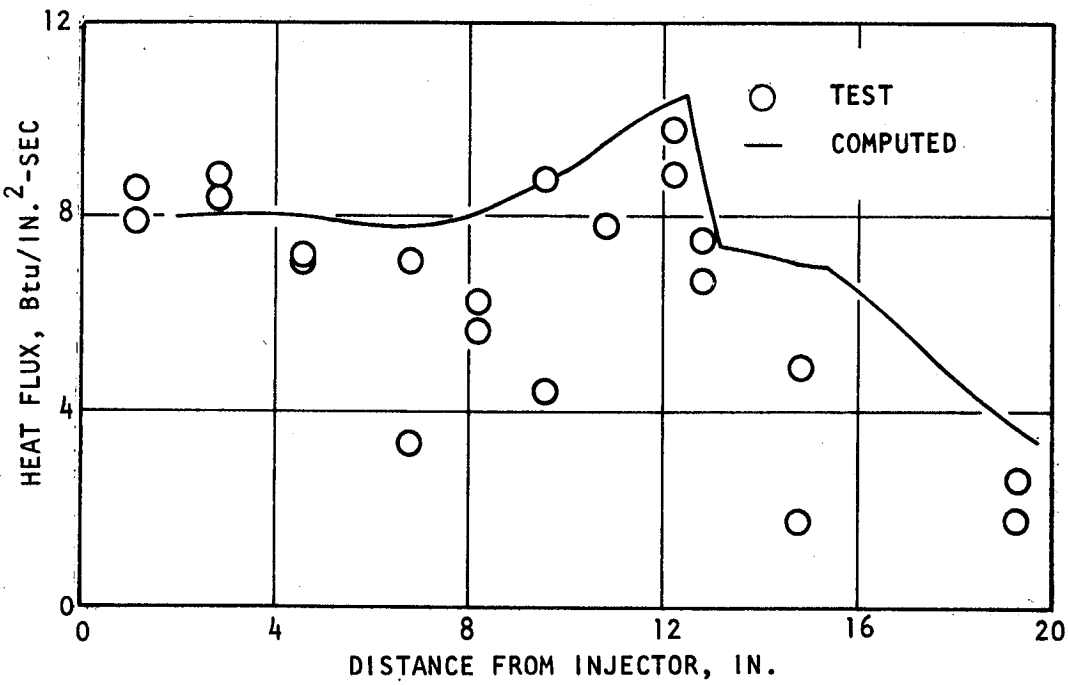

Figure 56. Comparison of Analytical Heat Flux Profile with Experimental Data for Test 252

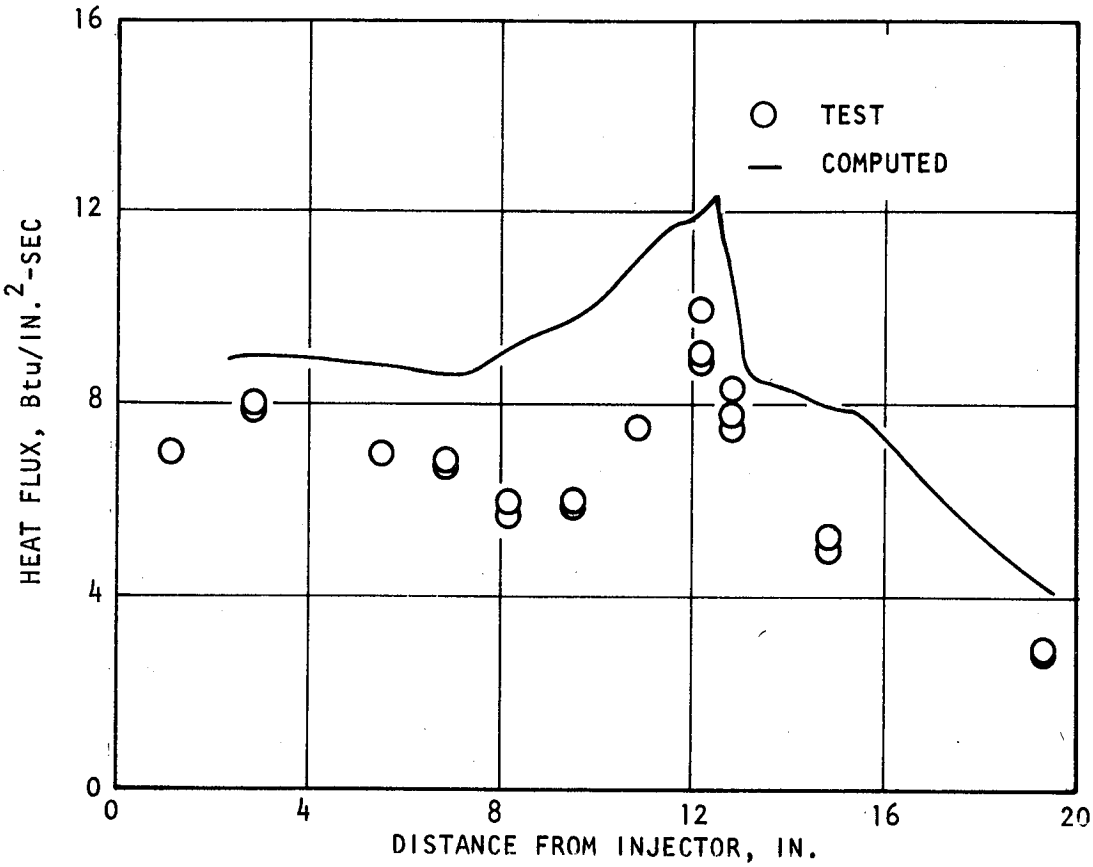

Figure 57. Comparison of Analytical Heat Flux Profile with Experimental Data for Test 547

26 percent, respectively, and the experimental data points are consistently well below the analytical curve except at the boundary layer attachment point.

The difference between the predictions of BLIMP and the measured heat transfer may result from the failure of dissociation-recombination chemical reactions such as

$$H + H \rightleftharpoons H_2$$

$$H + OH \rightleftharpoons H_2O$$

to occur in the nozzle boundary layer with subsequent enhancement of the convective heat transport. The BLIMP equations* describing the turbulent transport of energy in the boundary layer contain the terms

$$\varepsilon \frac{\overline{C_{p_F}}}{Pr_t} \frac{\partial T}{\partial \eta} + \frac{\varepsilon}{Sch_t} \frac{\partial H}{\partial \eta} - \frac{\varepsilon \overline{C_{p_F}}}{Sch_t} \frac{\partial T}{\partial \eta}$$

where

ε = the eddy diffusivity for mass, momentum, and energy

$\overline{C_{p_F}}$ = the frozen specific heat of the gas mixture

Pr_t = the turbulent Prandtl number

Sch_t = the turbulent Schmidt number

$\frac{\partial H}{\partial \eta}, \frac{\partial T}{\partial \eta}$ = the respective static enthalpy and static temperature gradients with respect to η, the boundary layer coordinate normal to the wall

When, as normally assumed for gas mixtures, the turbulent Prandtl and Schmidt numbers are equal, the heat transport across a turbulent boundary layer for a chemically reacting system in local thermodynamic equilibrium becomes proportional to the term

$$\varepsilon \overline{C_{p_s}} \frac{\partial T}{\partial \eta}$$

*See Eq. 85, p 3-20, in Ref. 13.

(where $\overline{C_{p_s}}$ is the shifting specific heat of the gas mixture) rather than

$$\varepsilon \overline{C_{p_F}} \frac{\partial T}{\partial \eta}$$

as is the case for a nonreacting system. The ratio between a reacting system in thermodynamic equilibrium and the corresponding nonreactive system is a function of the ratio $(\overline{C_{p_s}}/\overline{C_{p_F}})$. From the usual convection relations, the heat transfer coefficient for a gas of constant thermal conductivity is defined by

$$h \sim C_p^{1/3}$$

Consequently, the ratio of heat transfer with chemical reactions to the non-reacting system is defined by

$$\frac{(q/A)_s}{(q/A)_F} = \left(\frac{\overline{C_{p_s}}}{\overline{C_{p_F}}} \right)^{1/3}$$

The dissociation of water and molecular hydrogen (and therefore of the $\overline{C_{p_s}}/\overline{C_{p_F}}$ ratio) is favored by high temperature and consequently by increasing mixture ratio up to the stoichiometric ratio of 8. The variation of both $(\overline{C_{p_s}}/\overline{C_{p_F}})$ and of $(C_{p_s}/C_{p_F})^{1/3}$ with mixture ratio is shown for the H_2/O_2 propellant combination in Fig. 58. The values of the $(C_{p_s}/C_{p_F})^{1/3}$ ratio for the four test cases at their respective wall mixture ratios are compared to the ratio of the computed to the experimental average heat fluxes in Table 24. The comparison suggests strongly that the deviation between the BLIMP predictions and the corresponding experimental data may result because recombination reactions are too slow to occur (or at least to proceed to thermodynamic equilibrium) in the short time the individual molecules spend in the boundary layer.

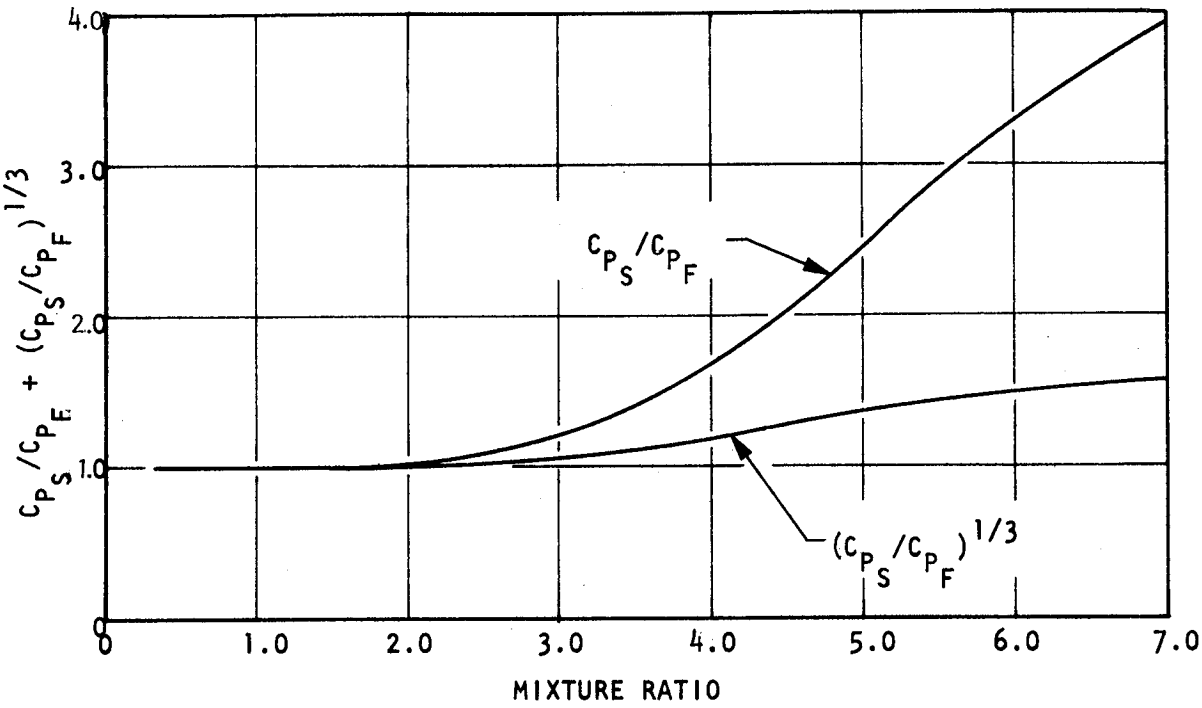

Figure 58. Effect of Mixture Ratio Upon the Ratios Between Shifting and Frozen Specific Heat of the H_2/O_2 Combustion Products and Upon the 1/3 Power of This Ratio

TABLE 24. COMPARISON OF $(C_{p_s}/C_{p_F})^{1/3}$ WITH THE RATIO BETWEEN HEAT TRANSFER COMPUTED BY BLIMP TO EXPERIMENTAL HEAT TRANSFER

Test	Wall Mixture Ratio	$\frac{(q/A)_{BLIMP}}{(q/A)_{EXP}}$	$\left(\frac{C_{p_s}}{C_{p_F}}\right)^{1/3}$
238	2.50	1.0	1.0
250	3.07	1.0	1.06
252	4.18	1.18	1.20
547	5.28	1.26	1.40

A simplified calculation of the residence time of a reactive molecule in the turbulent boundary layer at the nozzle throat results in an estimate of 5 to 10 microseconds for an assumed mixing length of 0.01 inch and assumed transverse velocity components of 100 to 200 ft/sec. Similarly, simplified estimates of the time required for the recombination of half the mainstream concentrations of atomic hydrogen with itself and the OH radical result in estimations of 1 to 5 microseconds for this process at a comparatively high temperature of 4500 R, with much slower reaction rates at lower temperatures. With both times being of the same order of magnitude, it is very reasonable to assume that the calculated heat transfer associated with boundary layer recombination can be in substantial error if the reactions are assumed to follow thermodynamic equilibria.

The significance of the differences between the BLIMP-calculated and the experimental trends in heat transfer with mixture ratio can become significant in the design of thrust chambers which utilize either film cooling, mixture ratio bias, or a combination of both in protecting thrust chamber walls. Although the advantages of a low wall mixture ratio in reducing heat transfer were demonstrated in the analysis of experimental results made in Task IV, it appears that requirements for such cooling might be overestimated in design calculations made with the BLIMP computer program.

CONCLUSIONS AND RECOMMENDATIONS

The analytical and experimental results of the program have demonstrated that:

1. Mixture ratio bias introduced at the injector persists through the combustion chamber and nozzle with quantitatively predictable effects upon performance and wall heat transfer
2. Controlled levels of combustion gas mixture ratio striation can be built into high performing rocket engine injectors
3. Cold flow atomization studies provide a useful tool for predicting the dropsize characteristics of injector elements; however, additional work is needed to completely relate cold flow droplet size to equivalent propellant and operating conditions of the hot fire application
4. The predictions of the computer programs (STC, TDK and BLIMP) developed under the JANNAF Performance Standardization Working Group correlate the experimental performance and heat transfer results when appropriate spray dropsizes and mixing between adjacent fluid layers are defined
5. Quantitative samples of rocket exhaust composition can be obtained only when adequate precautions are taken to prevent heat transfer failure, condensation, and contamination, both from the atmosphere and from the species introduced during engine startup and shutdown transients
6. For the H_2/LOX propellant combination, the use of film cooling and/or mixture ratio bias becomes an effective method of reducing wall heat transfer only when the wall mixture ratio is reduced below approximately 3.0.

It is recommended that the current program of investigations of H_2/LOX propellant combination be extended to other propellant combinations and injectors,

and in particular to a typical liquid/liquid system, to generalize the data and conclusions obtained. It is further recommended that such an investigation:

1. Be made with hardware which permits firing durations of at least 5 seconds to enable exhaust gas sampling to be performed
2. Include thorough cold flow characterization of the complete injector for subsequent correlation of hot-fire results
3. Include a thorough correlation of all results using the accepted JANNAF methodology.

REFERENCES

1. Mehegan, P. F., D. T. Campbell and C. H. Scheurman, Investigation of Gas-Augmented Injectors, Final Report, Rocketdyne, a Division of Rockwell International, Canoga Park, California,

2. Burick, R. J., Atomization and Mixing Characteristics of Gas Liquid Coaxial Injector Elements, AIAA Paper 71-672, 14 June 1971.

3. Combs, L. P., Liquid Rocket Performance Computer Model with Distributed Energy Release, Final Report, NASA CR-114462, Rocketdyne, a Division of Rockwell International, Canoga Park, California, 10 June 1972.

4. Sutton, G. P., Rocket Propulsion Elements, 3rd Edition, John Wiley and Sons, Inc., New York, 1963.

5. Witte, A. B. and E. Y. Harper, "Experimental Investigation of Heat Transfer Rates in Rocket Thrust Chambers," AIAA Journal, Vol. 1, 2 February 1963, pp. 443-451.

6. Bartz, D. R., "A Simple Equation for Rapid Estimation of Rocket-Nozzle Convective Heat Transfer Coefficients," Jet Propulsion, January 1957, pp. 49-51.

7. Elliott, D. G., D. R. Bartz and S. Silver, Calculation of Turbulent Boundary Layer Growth and Heat Transfer in Axi-Symmetric Nozzles, TR 32-387, Jet Propulsion Laboratory, Pasadena, California, 15 February 1963.

8. Hartnett, J. P., R. C. Birkebak and E. R. G. Eckert, "Velocity Distributions, Temperature Distributions, Effectiveness and Heat Transfer for Air Injected Through a Tangential Slot into a Turbulent Boundary Layer," Journal of Heat Transfer, August 1961, pp. 293-306.

9. Kliegel, J. R. et al, ICRPG Two Dimensional Kinetic Reference Program, Dynamic Science, a Division of Marshall Industries, Irvine, California, July 1968.

10. Burick, R. J. and A. Y. Falk, Injector Design Guidelines for Gas Liquid Propellant Systems, NASA CR-120968, Rocketdyne, a Division of Rockwell International, Canoga Park, California, May 1973.

11. Thompson, R. J., Jr., The Chemistry of Propellants, Pergamon Press, New York, 1960, pp. 25-120.

12. Powell, W. B., Simplified Procedures for Correlation of Experimentally Measured and Predicted Thrust Chamber Performance, TM 33-548, Jet Propulsion Laboratory, Pasadena, California, 1 April 1973.

13. Aeotherm Report No. UM-70-20, User's Manual Boundary Layer Integral Matrix Procedure, Version C (BLIMPC), NASA Contract NAS9-9494, Lyndon B. Johnson Spacecraft Center, Houston, Texas, 22 June 1970.

APPENDIX A

RESULTS OF EXPERIMENTAL STRATIFIED FLOW H_2/LOX ENGINE FIRINGS

Note:

For Runs 542 to 552 and 238 to 244. . . . . = 25:1

For Runs 245 to 253. . . . . = 4:1

TEST NUMBER 869- 542
TEST DATE 1103/70/ 0
IBM DATE 11/10/71
TEST CELL CTL4-29B

		SITE PERFORMANCE
LOCAL AMBIENT PRESSURE	(PSIA)	13.886
ENVIRONMENTAL PRESSURE	(PSIA)	1.051
THRUST (SITE)	(LB)	7218.6
THRUST (VACUUM)	(LB)	7701.8
CHAMBER PRESSURE 7,8 AVG	(PSIA)	231.66
MIXTURE RATIO (OVERALL)	(O/F)	5.482
MIXTURE RATIO (CORE)	(O/F)	7.976
MIXTURE RATIO (OUTER RING)	(O/F)	4.711
SPECIFIC IMPULSE	(SEC)	407.6
C-STAR (NOZ STAG)	(FT/SEC)	7481.
C-SUB-F (NOZ STAG)		1.6429
C-SUB-F VACUUM (NOZ STAG)		1.7528
THEORETICAL C-STAR (NOZ STAG)	(FT/SEC)	7617.
THEORETICAL C-SUB-F (NOZ STAG)		1.8710
THEORETICAL SPECIFIC IMPULSE	(SEC)	442.9
C-STAR EFFICIENCY		0.9821
C-SUB-F EFFICIENCY		0.9368
ISP EFFICIENCY		0.9202
FUEL WEIGHT FLOWRATE (TOTAL)	(LB/SEC)	2.915
BLC WEIGHT FLOWRATE	(LB/SEC)	(.281
RELATIVE OXID F/M AGREEMENT	(%)	-1.31
PERCENT BLC OF FUEL	(%)	9.651
OXID WEIGHT FLOWRATE	(LB/SEC)	15.981
TOTAL WEIGHT FLOWRATE	(LB/SEC)	18.897
THROAT AREA	(SQ IN)	17.92
EXIT AREA	(SQ IN)	459.85
LOX OUTER DELTA P	(PSID)	112.46
LOX CORE DELTA P	(PSID)	204.61
GH2 OUTER DELTA P	(PSID)	91.17
GH2 CORE DELTA P	(PSID)	49.61
GH2 BLC DELTA P	(PSID)	86.11

TEST NUMBER 869- 544
TEST DATE 1103/70/ 0
IBM DATE 11/10/71
TEST CELL CTL4-29R

		SITE PERFORMANCE
LOCAL AMBIENT PRESSURE	(PSIA)	13.886
ENVIRONMENTAL PRESSURE	(PSIA)	0.891
THRUST (SITE)	(LB)	7391.5
THRUST (VACUUM)	(LB)	7861.2
CHAMBER PRESSURE 7,8 AVG	(PSIA)	232.44
MIXTURE RATIO (OVERALL)	(O/F)	5.778
MIXTURE RATIO (CORE)	(O/F)	6.941
MIXTURE RATIO (OUTER RING)	(O/F)	6.165
SPECIFIC IMPULSE	(SEC)	413.3
C-STAR (NOZ STAG)	(FT/SEC)	7528.
C-SUB-F (NOZ STAG)		1.6737
C-SUB-F VACUUM (NOZ STAG)		1.7664
THEORETICAL C-STAR (NOZ STAG)	(FT/SEC)	7539.
THEORETICAL C-SUB-F (NOZ STAG)		1.8830
THEORETICAL SPECIFIC IMPULSE	(SEC)	441.2
C-STAR EFFICIENCY		0.9986
C-SUB-F EFFICIENCY		0.9381
ISP EFFICIENCY		0.9368
FUEL WEIGHT FLOWRATE (TOTAL)	(LB/SEC)	2.785
BLC WEIGHT FLOWRATE	(LB/SEC)	0.333
RELATIVE OXID F/M AGREEMENT	(%)	-1.13
PERCENT BLC OF FUEL	(%)	11.968
OXID WEIGHT FLOWRATE	(LB/SEC)	16.090
TOTAL WEIGHT FLOWRATE	(LB/SEC)	18.875
THROAT AREA	(SQ IN)	17.95
EXIT AREA	(SQ IN)	459.85
LOX OUTER DELTA P	(PSID)	360.56
LOX CORE DELTA P	(PSID)	470.51
GH2 OUTER DELTA P	(PSID)	304.61
GH2 CORE DELTA P	(PSID)	307.88
GH2 BLC DELTA P	(PSID)	359.51

TEST NUMBER 869- 545
TEST DATE 1103/70/ 0
IBM DATE 11/10/71
TEST CELL CTL4-298

		SITE PERFORMANCE
LOCAL AMBIENT PRESSURE	(PSIA)	13.886
ENVIRONMENTAL PRESSURE	(PSIA)	1.161
THRUST (SITE)	(LB)	6574.8
THRUST (VACUUM)	(LB)	7108.7
CHAMBER PRESSURE 7,8 AVG	(PSIA)	216.65
MIXTURE RATIO (OVERALL)	(O/F)	5.089
MIXTURE RATIO (CORE)	(O/F)	7.702
MIXTURE RATIO (OUTER RING)	(O/F)	4.196
SPECIFIC IMPULSE	(SEC)	404.2
C-STAR (NOZ STAG)	(FT/SEC)	7528.
C-SUB-F (NOZ STAG)		1.5979
C-SUB-F VACUUM (NOZ STAG)		1.7278
THEORETICAL C-STAR (NOZ STAG)	(FT/SEC)	7712.
THEORETICAL C-SUB-F (NOZ STAG)		1.8547
THEORETICAL SPECIFIC IMPULSE	(SEC)	444.6
C-STAR EFFICIENCY		0.9761
C-SUB-F EFFICIENCY		0.9315
ISP EFFICIENCY		0.9093
FUEL WEIGHT FLOWRATE (TOTAL)	(LB/SEC)	2.888
BLC WEIGHT FLOWRATE	(LB/SEC)	0.290
RELATIVE OXID F/M AGREEMENT	(%)	-1.47
PERCENT BLC OF FUEL	(%)	10.025
OXID WEIGHT FLOWRATE	(LB/SEC)	14.697
TOTAL WEIGHT FLOWRATE	(LB/SEC)	17.586
THROAT AREA	(SQ IN)	17.94
EXIT AREA	(SQ IN)	459.85
LOX OUTER DELTA P	(PSID)	88.77
LOX CORE DELTA P	(PSID)	158.86
GH2 OUTER DELTA P	(PSID)	95.01
GH2 CORE DELTA P	(PSID)	52.02
GH2 BLC DELTA P	(PSID)	91.68

TEST NUMBER 869- 546
TEST DATE 1103/70/ 0
IBM DATE 11/10/71
TEST CELL CTL4-29B

		SITE PERFORMANCE
LOCAL AMBIENT PRESSURE	(PSIA)	13.886
ENVIRONMENTAL PRESSURE	(PSIA)	0.909
THRUST (SITE)	(LB)	6697.9
THRUST (VACUUM)	(LB)	7116.0
CHAMBER PRESSURE 7,8 AVG	(PSIA)	217.20
MIXTURE RATIO (OVERALL)	(O/F)	5.064
MIXTURE RATIO (CORE)	(O/F)	6.896
MIXTURE RATIO (OUTER RING)	(O/F)	3.756
SPECIFIC IMPULSE	(SEC)	408.4
C-STAR (NOZ STAG)	(FT/SEC)	7625.
C-SUB-F (NOZ STAG)		1.6220
C-SUB-F VACUUM (NOZ STAG)		1.7233
THEORETICAL C-STAR (NOZ STAG)	(FT/SEC)	7718.
THEORETICAL C-SUB-F (NOZ STAG)		1.8535
THEORETICAL SPECIFIC IMPULSE	(SEC)	444.6
C-STAR EFFICIENCY		0.9879
C-SUB-F EFFICIENCY		0.9297
ISP EFFICIENCY		0.9185
FUEL WEIGHT FLOWRATE (TOTAL)	(LB/SEC)	2.874
BLC WEIGHT FLOWRATE	(LB/SEC)	0.0
RELATIVE OXID F/M AGREEMENT	(%)	-2.17
PERCENT BLC OF FUEL	(%)	0.0
OXID WEIGHT FLOWRATE	(LB/SEC)	14.551
TOTAL WEIGHT FLOWRATE	(LB/SEC)	17.425
THROAT AREA	(SQ IN)	17.96
EXIT AREA	(SQ IN)	459.85
LOX OUTER DELTA P	(PSID)	97.03
LOX CORE DELTA P	(PSID)	173.22
GH2 OUTER DELTA P	(PSID)	118.40
GH2 CORE DELTA P	(PSID)	62.82
GH2 BLC DELTA P	(PSID)	2.06

TEST NUMBER 869- 547
TEST DATE 1103/70/ 0
IBM DATE 11/10/71
TEST CELL CTL4-29B

			SITE PERFORMANC
	LOCAL AMBIENT PRESSURE	(PSIA)	13.886
	ENVIRONMENTAL PRESSURE	(PSIA)	0.833
	THRUST (SITE)	(LB)	6985.3
	THRUST (VACUUM)	(LB)	7368.3
	CHAMBER PRESSURE 7,8 AVG	(PSIA)	222.89
	MIXTURE RATIO (OVERALL)	(O/F)	5.645
	MIXTURE RATIO (CORE)	(O/F)	5.995
	MIXTURE RATIO (OUTER RING)	(O/F)	5.276
	SPECIFIC IMPULSE	(SEC)	414.1
	C-STAR (NOZ STAG)	(FT/SEC)	7665.
	C-SUB-F (NOZ STAG)		1.6480
	C-SUB-F VACUUM (NOZ STAG)		1.7384
	THEORETICAL C-STAR (NOZ STAG)	(FT/SEC)	7572.
	THEORETICAL C-SUB-F (NOZ STAG)		1.8777
	THEORETICAL SPECIFIC IMPULSE	(SEC)	441.9
	C-STAR EFFICIENCY		1.012
	C-SUB-F EFFICIENCY		0.9258
	ISP EFFICIENCY		0.9372
	FUEL WEIGHT FLOWRATE (TOTAL)	(LB/SEC)	2.678
	BLC WEIGHT FLOWRATE	(LB/SEC)	0.0
	RELATIVE OXID F/M AGREEMENT	(%)	-2.13
	PERCENT BLC OF FUEL	(%)	0.0
	OXID WEIGHT FLOWRATE	(LB/SEC)	15.115
	TOTAL WEIGHT FLOWRATE	(LB/SEC)	17.792
	THROAT AREA	(SQ IN)	17.96
	EXIT AREA	(SQ IN)	459.85
	LOX OUTER DELTA P	(PSID)	122.43
	LOX CORE DELTA P	(PSID)	184.91
	GH2 OUTER DELTA P	(PSID)	77.03
	GH2 CORE DELTA P	(PSID)	82.11
	GH2 BLC DELTA P	(PSID)	7.49

TEST NUMBER 869- 548
TEST DATE 1103/70/ 0
IBM DATE 11/10/71
TEST CELL CTL4-29B

		SITE PERFORMANCE
LOCAL AMBIENT PRESSURE	(PSIA)	13.886
ENVIRONMENTAL PRESSURE	(PSIA)	1.010
THRUST (SITE)	(LB)	6475.8
THRUST (VACUUM)	(LB)	6940.1
CHAMBER PRESSURE 7,8 AVG	(PSIA)	211.63
MIXTURE RATIO (OVERALL)	(O/F)	4.854
MIXTURE RATIO (CORE)	(O/F)	7.281
MIXTURE RATIO (OUTER RING)	(O/F)	4.042
SPECIFIC IMPULSE	(SEC)	403.9
C-STAR (NOZ STAG)	(FT/SEC)	7537.
C-SUB-F (NOZ STAG)		1.6087
C-SUB-F VACUUM (NOZ STAG)		1.7241
THEORETICAL C-STAR (NOZ STAG)	(FT/SEC)	7766.
THEORETICAL C-SUB-F (NOZ STAG)		1.8448
THEORETICAL SPECIFIC IMPULSE	(SEC)	445.3
C-STAR EFFICIENCY		0.9706
C-SUB-F EFFICIENCY		0.9345
ISP EFFICIENCY		0.9071
FUEL WEIGHT FLOWRATE (TOTAL)	(LB/SEC)	2.935
BLC WEIGHT FLOWRATE	(LB/SEC)	0.288
RELATIVE OXID F/M AGREEMENT	(%)	-2.46
PERCENT BLC OF FUEL	(%)	9.821
OXID WEIGHT FLOWRATE	(LB/SEC)	14.248
TOTAL WEIGHT FLOWRATE	(LB/SEC)	17.183
THROAT AREA	(SQ IN)	17.97
EXIT AREA	(SQ IN)	459.85
LOX OUTER DELTA P	(PSID)	119.81
LOX CORE DELTA P	(PSID)	261.19
GH2 OUTER DELTA P	(PSID)	105.37
GH2 CORE DELTA P	(PSID)	54.78
GH2 BLC DELTA P	(PSID)	107.57

TEST NUMBER 869- 549
TEST DATE 11/3/70/ 0
IBM DATE 11/10/71
TEST CELL CTL4-29B

		SITE PERFORMANCE
LOCAL AMBIENT PRESSURE	(PSIA)	12.884
ENVIRONMENTAL PRESSURE	(PSIA)	[illegible]
THRUST (SITE)	(LB)	6548.6
THRUST (VACUUM)	(LB)	[illegible]
CHAMBER PRESSURE 7,8 AVG	(PSIA)	214.42
MIXTURE RATIO (OVERALL)	(O/F)	5.171
MIXTURE RATIO (CORE)	(O/F)	5.163
MIXTURE RATIO (OUTER RING)	(O/F)	5.586
SPECIFIC IMPULSE	(SEC)	402.9
C-STAR (NOZ STAG)	(FT/SEC)	7621.
C-SUB-F (NOZ STAG)		1.5906
C-SUB-F VACUUM (NOZ STAG)		1.7009
THEORETICAL C-STAR (NOZ STAG)	(FT/SEC)	7692.
THEORETICAL C-SUB-F (NOZ STAG)		1.6038
THEORETICAL SPECIFIC IMPULSE	(SEC)	444.2
C-STAR EFFICIENCY		0.9907
C-SUB-F EFFICIENCY		0.9155
ISP EFFICIENCY		0.9070
FUEL WEIGHT FLOWRATE (TOTAL)	(LB/SEC)	2.817
BLC WEIGHT FLOWRATE	(LB/SEC)	0.341
RELATIVE OXID F/M AGREEMENT	(%)	-2.52
PERCENT BLC OF FUEL	(%)	12.089
OXID WEIGHT FLOWRATE	(LB/SEC)	14.565
TOTAL WEIGHT FLOWRATE	(LB/SEC)	17.382
THROAT AREA	(SQ IN)	17.97
EXIT AREA	(SQ IN)	459.85
LOX OUTER DELTA P	(PSID)	136.77
LOX CORE DELTA P	(PSID)	340.73
GH2 OUTER DELTA P	(PSID)	68.45
GH2 CORE DELTA P	(PSID)	72.74
GH2 BLC DELTA P	(PSID)	136.89

TEST NUMBER 869- 550
TEST DATE 1103/70/ 0
IBM DATE 11/10/71
TEST CELL CTL4-29B

		SITE PERFORMANCE
LOCAL AMBIENT PRESSURE	(PSIA)	13.886
ENVIRONMENTAL PRESSURE	(PSIA)	1.458
THRUST (SITE)	(LB)	6246.1
THRUST (VACUUM)	(LB)	6916.5
CHAMBER PRESSURE 7,8 AVG	(PSIA)	207.29
MIXTURE RATIO (OVERALL)	(O/F)	4.682
MIXTURE RATIO (CORE)	(O/F)	6.886
MIXTURE RATIO (OUTER RING)	(O/F)	3.972
SPECIFIC IMPULSE	(SEC)	414.6
C-STAR (NOZ STAG)	(FT/SEC)	7608.
C-SUB-F (NOZ STAG)		1.5386
C-SUB-F VACUUM (NOZ STAG)		1.7536
THEORETICAL C-STAR (NOZ STAG)	(FT/SEC)	7802.
THEORETICAL C-SUB-F (NOZ STAG)		1.8376
THEORETICAL SPECIFIC IMPULSE	(SEC)	445.6
C-STAR EFFICIENCY		0.9751
C-SUB-F EFFICIENCY		0.9543
ISP EFFICIENCY		0.9305
FUEL WEIGHT FLOWRATE (TOTAL)	(LB/SEC)	2.936
BLC WEIGHT FLOWRATE	(LB/SEC)	0.285
RELATIVE OXID F/M AGREEMENT	(%)	-2.24
PERCENT BLC OF FUEL	(%)	9.711
OXID WEIGHT FLOWRATE	(LB/SEC)	13.745
TOTAL WEIGHT FLOWRATE	(LB/SEC)	16.681
THROAT AREA	(SQ IN)	17.97
EXIT AREA	(SQ IN)	459.85
LOX OUTER DELTA P	(PSID)	138.93
LOX CORE DELTA P	(PSID)	311.40
GH2 OUTER DELTA P	(PSID)	108.92
GH2 CORE DELTA P	(PSID)	56.32
GH2 BLC DELTA P	(PSID)	107.09

TEST NUMBER 869- 551
TEST DATE 1103/70/ 0
IBM DATE 11/10/71
TEST CELL CTL4-29B

		SITE PERFORMANCE
LOCAL AMBIENT PRESSURE	(PSIA)	13.886
ENVIRONMENTAL PRESSURE	(PSIA)	0.941
THRUST (SITE)	(LB)	7019.4
THRUST (VACUUM)	(LB)	7452.0
CHAMBER PRESSURE 7,8 AVG	(PSIA)	229.18
MIXTURE RATIO (OVERALL)	(O/F)	5.394
MIXTURE RATIO (CORE)	(O/F)	7.831
MIXTURE RATIO (OUTER RING)	(O/F)	4.651
SPECIFIC IMPULSE	(SEC)	396.4
C-STAR (NOZ STAG)	(FT/SEC)	7463.
C-SUB-F (NOZ STAG)		1.6100
C-SUB-F VACUUM (NOZ STAG)		1.7092
THEORETICAL C-STAR (NOZ STAG)	(FT/SEC)	7639.
THEORETICAL C-SUB-F (NOZ STAG)		1.8471
THEORETICAL SPECIFIC IMPULSE	(SEC)	443.3
C-STAR EFFICIENCY		0.9769
C-SUB-F EFFICIENCY		0.9155
ISP EFFICIENCY		0.8943
FUEL WEIGHT FLOWRATE (TOTAL)	(LB/SEC)	2.940
BLC WEIGHT FLOWRATE	(LB/SEC)	0.285
RELATIVE OXID F/M AGREEMENT	(%)	-1.67
PERCENT BLC OF FUEL	(%)	9.702
OXID WEIGHT FLOWRATE	(LB/SEC)	15.857
TOTAL WEIGHT FLOWRATE	(LB/SEC)	18.797
THROAT AREA	(SQ IN)	17.97
EXIT AREA	(SQ IN)	459.55
LOX OUTER DELTA P	(PSID)	134.73
LOX CORE DELTA P	(PSID)	162.42
GH2 OUTER DELTA P	(PSID)	86.16
GH2 CORE DELTA P	(PSID)	51.98
GH2 BLC DELTA P	(PSID)	96.84

TEST NUMBER 869- 552
TEST DATE 1103/70/ 0
IBM DATE 11/10/71
TEST CELL CTL4-29B

		SITE PERFORMANCE
LOCAL AMBIENT PRESSURE	(PSIA)	13.886
ENVIRONMENTAL PRESSURE	(PSIA)	1.007
THRUST (SITE)	(LB)	4806.2
THRUST (VACUUM)	(LB)	5269.0
CHAMBER PRESSURE 7,8 AVG	(PSIA)	224.10
MIXTURE RATIO (OVERALL)	(O/F)	5.315
MIXTURE RATIO (CORE)	(O/F)	7.291
MIXTURE RATIO (OUTER RING)	(O/F)	3.918
SPECIFIC IMPULSE	(SEC)	290.0
C-STAR (NOZ STAG)	(FT/SEC)	7552.
C-SUB-F (NOZ STAG)		1.1273
C-SUB-F VACUUM (NOZ STAG)		1.2358
THEORETICAL C-STAR (NOZ STAG)	(FT/SEC)	7658.
THEORETICAL C-SUB-F (NOZ STAG)		1.8639
THEORETICAL SPECIFIC IMPULSE	(SEC)	443.6
C-STAR EFFICIENCY		0.9860
C-SUB-F EFFICIENCY		0.6630
ISP EFFICIENCY		0.6538
FUEL WEIGHT FLOWRATE (TOTAL)	(LB/SEC)	2.877
BLC WEIGHT FLOWRATE	(LB/SEC)	0.0
RELATIVE OXID F/M AGREEMENT	(%)	-1.77
PERCENT BLC OF FUEL	(%)	0.0
OXID WEIGHT FLOWRATE	(LB/SEC)	15.290
TOTAL WEIGHT FLOWRATE	(LB/SEC)	18.166
THROAT AREA	(SQ IN)	17.97
EXIT AREA	(SQ IN)	459.85
LOX OUTER DELTA P	(PSID)	118.94
LOX CORE DELTA P	(PSID)	165.14
GH2 OUTER DELTA P	(PSID)	118.25
GH2 CORE DELTA P	(PSID)	58.56
GH2 BLC DELTA P	(PSID)	0.16

TEST NUMBER	869- 239	TEST DURATION	2.40
TEST DATE	8/18/72	SLICE DURATION	0.20
IBM DATE	C8/31/72	SLICE START TIME	0.0
TEST CELL	CTL4-29B		

		SITE PERFORMANCE
LOCAL AMBIENT PRESSURE	(PSIA)	13.788
ENVIRONMENTAL PRESSURE	(PSIA)	1.738
THRUST (SITE)	(LB)	5364.0
THRUST (VACUUM)	(LB)	6163.1
CHAMBER PRESSURE 7,8 AVG	(PSIA)	136.50
MIXTURE RATIO (OVERALL)	(O/F)	6.639
MIXTURE RATIO (CORE)	(O/F)	8.747
MIXTURE RATIO (OUTER RING)	(O/F)	5.148
SPECIFIC IMPULSE	(SEC)	483.1
C-STAR (NOZ STAG)	(FT/SEC)	6540.
C-SUB-F (NOZ STAG)		2.0686
C-SUB-F VACUUM (NOZ STAG)		2.3768
THEORETICAL C-STAR (NOZ STAG)	(FT/SEC)	7253.
THEORETICAL C-SUB-F (NOZ STAG)		1.9216
THEORETICAL SPECIFIC IMPULSE	(SEC)	433.2
C-STAR EFFICIENCY		0.9017
C-SUB-F EFFICIENCY		1.2369
ISP EFFICIENCY		1.1153
FUEL WEIGHT FLOWRATE (TOTAL)	(LB/SEC)	1.670
BLC WEIGHT FLOWRATE	(LB/SEC)	0.0
RELATIVE OXID F/M AGREEMENT	(%)	0.42
PERCENT BLC OF FUEL	(%)	0.0
OXID WEIGHT FLOWRATE	(LB/SEC)	11.087
TOTAL WEIGHT FLOWRATE	(LB/SEC)	12.757
THROAT AREA	(SQ IN)	17.95
EXIT AREA	(SQ IN)	459.85
LOX OUTER DELTA P	(PSID)	120.29
LOX CORE DELTA P	(PSID)	132.39
GH2 OUTER DELTA P	(PSID)	41.31
GH2 CORE DELTA P	(PSID)	3.08
GH2 BLC DELTA P	(PSID)	4.47

TEST NUMBER	869- 240	TEST DURATION	2.40
TEST DATE	8/18/72	SLICE DURATION	0.20
IBM DATE	08/31/72	SLICE START TIME	0.0
TEST CELL	CTL4-29B		

		SITE PERFORMANCE
LOCAL AMBIENT PRESSURE	(PSIA)	13.788
ENVIRONMENTAL PRESSURE	(PSIA)	1.077
THRUST (SITE)	(LB)	6934.1
THRUST (VACUUM)	(LB)	7429.5
CHAMBER PRESSURE 7,8 AVG	(PSIA)	219.14
MIXTURE RATIO (OVERALL)	(O/F)	5.313
MIXTURE RATIO (CORE)	(O/F)	6.161
MIXTURE RATIO (OUTER RING)	(O/F)	5.667
SPECIFIC IMPULSE	(SEC)	424.2
C-STAR (NOZ STAG)	(FT/SEC)	7653.
C-SUB-F (NOZ STAG)		1.6645
C-SUB-F VACUUM (NOZ STAG)		1.7834
THEORETICAL C-STAR (NOZ STAG)	(FT/SEC)	7657.
THEORETICAL C-SUB-F (NOZ STAG)		1.8640
THEORETICAL SPECIFIC IMPULSE	(SEC)	443.6
C-STAR EFFICIENCY		0.9994
C-SUB-F EFFICIENCY		0.9568
ISP EFFICIENCY		0.9562
FUEL WEIGHT FLOWRATE (TOTAL)	(LB/SEC)	2.774
BLC WEIGHT FLOWRATE	(LB/SEC)	0.327
RELATIVE OXID F/M AGREEMENT	(%)	1.69
PERCENT BLC OF FUEL	(%)	11.788
OXID WEIGHT FLOWRATE	(LB/SEC)	14.740
TOTAL WEIGHT FLOWRATE	(LB/SEC)	17.515
THROAT AREA	(SQ IN)	17.96
EXIT AREA	(SQ IN)	459.85
LOX OUTER DELTA P	(PSID)	135.07
LOX CORE DELTA P	(PSID)	168.15
GH2 OUTER DELTA P	(PSID)	67.29
GH2 CORE DELTA P	(PSID)	72.83
GH2 BLC DELTA P	(PSID)	141.97

TEST NUMBER	869- 241	TEST DURATION	2.40
TEST DATE	8/18/72	SLICE DURATION	0.20
IBM DATE	08/31/72	SLICE START TIME	0.0
TEST CELL	CTL4-29B		

		SITE PERFORMANCE
LOCAL AMBIENT PRESSURE	(PSIA)	13.788
ENVIRONMENTAL PRESSURE	(PSIA)	1.047
THRUST (SITE)	(LB)	7131.8
THRUST (VACUUM)	(LB)	7613.4
CHAMBER PRESSURE 7,8 AVG	(PSIA)	215.14
MIXTURE RATIO (OVERALL)	(O/F)	5.209
MIXTURE RATIO (CORE)	(O/F)	6.331
MIXTURE RATIO (OUTER RING)	(O/F)	5.268
SPECIFIC IMPULSE	(SEC)	442.3
C-STAR (NOZ STAG)	(FT/SEC)	7647.
C-SUB-F (NOZ STAG)		1.7434
C-SUB-F VACUUM (NOZ STAG)		1.8611
THEORETICAL C-STAR (NOZ STAG)	(FT/SEC)	7682.
THEORETICAL C-SUB-F (NOZ STAG)		1.8597
THEORETICAL SPECIFIC IMPULSE	(SEC)	444.0
C-STAR EFFICIENCY		0.9953
C-SUB-F EFFICIENCY		1.0008
ISP EFFICIENCY		0.9962
FUEL WEIGHT FLOWRATE (TOTAL)	(LB/SEC)	2.772
BLC WEIGHT FLOWRATE	(LB/SEC)	0.327
RELATIVE OXID F/M AGREEMENT	(%)	1.55
PERCENT BLC OF FUEL	(%)	11.798
OXID WEIGHT FLOWRATE	(LB/SEC)	14.440
TOTAL WEIGHT FLOWRATE	(LB/SEC)	17.212
THROAT AREA	(SQ IN)	17.96
EXIT AREA	(SQ IN)	459.85
LOX OUTER DELTA P	(PSID)	126.16
LOX CORE DELTA P	(PSID)	172.65
GH2 OUTER DELTA P	(PSID)	68.66
GH2 CORE DELTA P	(PSID)	74.31
GH2 BLC DELTA P	(PSID)	145.10

TEST NUMBER	869- 242	TEST DURATION	2.40
TEST DATE	8/18/72	SLICE DURATION	0.20
IBM DATE	08/31/72	SLICE START TIME	0.0
TEST CELL	CTL4-29B		

		SITE PERFORMANCE
LOCAL AMBIENT PRESSURE	(PSIA)	13.788
ENVIRONMENTAL PRESSURE	(PSIA)	1.014
THRUST (SITE)	(LB)	7294.8
THRUST (VACUUM)	(LB)	7761.2
CHAMBER PRESSURE 7,8 AVG	(PSIA)	212.60
MIXTURE RATIO (OVERALL)	(O/F)	4.789
MIXTURE RATIO (CORE)	(O/F)	7.126
MIXTURE RATIO (OUTER RING)	(O/F)	3.885
SPECIFIC IMPULSE	(SEC)	453.3
C-STAR (NOZ STAG)	(FT/SEC)	7596.
C-SUB-F (NOZ STAG)		1.8046
C-SUB-F VACUUM (NOZ STAG)		1.9200
THEORETICAL C-STAR (NOZ STAG)	(FT/SEC)	7780.
THEORETICAL C-SUB-F (NOZ STAG)		1.8421
THEORETICAL SPECIFIC IMPULSE	(SEC)	445.4
C-STAR EFFICIENCY		0.9763
C-SUB-F EFFICIENCY		1.0423
ISP EFFICIENCY		1.0176
FUEL WEIGHT FLOWRATE (TOTAL)	(LB/SEC)	2.958
BLC WEIGHT FLOWRATE	(LB/SEC)	0.287
RELATIVE OXID F/M AGREEMENT	(%)	1.37
PERCENT BLC OF FUEL	(%)	9.695
OXID WEIGHT FLOWRATE	(LB/SEC)	14.165
TOTAL WEIGHT FLOWRATE	(LB/SEC)	17.123
THROAT AREA	(SQ IN)	17.96
EXIT AREA	(SQ IN)	459.85
LOX OUTER DELTA P	(PSID)	136.90
LOX CORE DELTA P	(PSID)	171.06
GH2 OUTER DELTA P	(PSID)	111.89
GH2 CORE DELTA P	(PSID)	57.98
GH2 BLC DELTA P	(PSID)	114.89

TEST NUMBER	869- 243	TEST DURATION	2.40
TEST DATE	8/18/72	SLICE DURATION	0.20
IBM DATE	08/31/72	SLICE START TIME	0.0
TEST CELL	CTL4-29B		

		SITE PERFORMANCE
LOCAL AMBIENT PRESSURE	(PSIA)	13.788
ENVIRONMENTAL PRESSURE	(PSIA)	0.880
THRUST (SITE)	(LB)	7456.3
THRUST (VACUUM)	(LB)	7861.1
CHAMBER PRESSURE 7,8 AVG	(PSIA)	211.89
MIXTURE RATIO (OVERALL)	(O/F)	5.326
MIXTURE RATIO (CORE)	(O/F)	5.689
MIXTURE RATIO (OUTER RING)	(O/F)	4.810
SPECIFIC IMPULSE	(SEC)	468.0
C-STAR (NOZ STAG)	(FT/SEC)	7717.
C-SUB-F (NOZ STAG)		1.8508
C-SUB-F VACUUM (NOZ STAG)		1.9513
THEORETICAL C-STAR (NOZ STAG)	(FT/SEC)	7652.
THEORETICAL C-SUB-F (NOZ STAG)		1.8647
THEORETICAL SPECIFIC IMPULSE	(SEC)	443.5
C-STAR EFFICIENCY		1.0085
C-SUB-F EFFICIENCY		1.0464
ISP EFFICIENCY		1.0553
FUEL WEIGHT FLOWRATE (TOTAL)	(LB/SEC)	2.655
BLC WEIGHT FLOWRATE	(LB/SEC)	0.0
RELATIVE OXID F/M AGREEMENT	(%)	1.19
PERCENT BLC OF FUEL	(%)	0.0
OXID WEIGHT FLOWRATE	(LB/SEC)	14.142
TOTAL WEIGHT FLOWRATE	(LB/SEC)	16.797
THROAT AREA	(SQ IN)	17.96
EXIT AREA	(SQ IN)	459.85
LOX OUTER DELTA P	(PSID)	183.88
LOX CORE DELTA P	(PSID)	182.79
GH2 OUTER DELTA P	(PSID)	82.01
GH2 CORE DELTA P	(PSID)	89.04
GH2 BLC DELTA P	(PSID)	1.97

TEST NUMBER 869- 244
TEST DATE 8/18/72
IBM DATE 08/31/72
TEST CELL CTL4-203

TEST DURATION 2.40
SLICE DURATION 0.20
SLICE START TIME 0.0

		SITE PERFORMANCE
LOCAL AMBIENT PRESSURE	(PSIA)	13.788
ENVIRONMENTAL PRESSURE	(PSIA)	2.558
THRUST (SITE)	(LB)	6018.4
THRUST (VACUUM)	(LB)	7194.5
CHAMBER PRESSURE 7,8 AVG	(PSIA)	204.87
MIXTURE RATIO (OVERALL)	(O/F)	4.713
MIXTURE RATIO (CORE)	(O/F)	7.175
MIXTURE RATIO (OUTER RING)	(O/F)	3.944
SPECIFIC IMPULSE	(SEC)	430.8
C-STAR (NOZ STAG)	(FT/SEC)	7504.
C-SUB-F (NOZ STAG)		1.5451
C-SUB-F VACUUM (NOZ STAG)		1.8471
THEORETICAL C-STAR (NOZ STAG)	(FT/SEC)	7795.
THEORETICAL C-SUB-F (NOZ STAG)		1.8390
THEORETICAL SPECIFIC IMPULSE	(SEC)	445.5
C-STAR EFFICIENCY		0.9626
C-SUB-F EFFICIENCY		0.0044
ISP EFFICIENCY		0.9669
FUEL WEIGHT FLOWRATE (TOTAL)	(LB/SEC)	2.923
BLC WEIGHT FLOWRATE	(LB/SEC)	0.284
RELATIVE OXID F/M AGREEMENT	(%)	-1.27
PERCENT BLC OF FUEL	(%)	9.699
OXID WEIGHT FLOWRATE	(LB/SEC)	13.778
TOTAL WEIGHT FLOWRATE	(LB/SEC)	16.701
THROAT AREA	(SQ IN)	17.96
EXIT AREA	(SQ IN)	459.85
LOX OUTER DELTA P	(PSID)	281.61
LOX CORE DELTA P	(PSID)	223.06
GH2 OUTER DELTA P	(PSID)	115.41
GH2 CORE DELTA P	(PSID)	59.20
GH2 BLC DELTA P	(PSID)	118.24

TEST NUMBER	869- 245	TEST DURATION	2.40
TEST DATE	8/18/72	SLICE DURATION	0.20
IBM DATE	08/31/72	SLICE START TIME	0.0
TEST CELL	CTL4-298		

		SITE PERFORMANCE
LOCAL AMBIENT PRESSURE	(PSIA)	13.788
ENVIRONMENTAL PRESSURE	(PSIA)	0.935
THRUST (SITE)	(LB)	6784.1
THRUST (VACUUM)	(LB)	7213.9
CHAMBER PRESSURE 7,8 AVG	(PSIA)	209.57
MIXTURE RATIO (OVERALL)	(O/F)	4.942
MIXTURE RATIO (CORE)	(O/F)	7.375
MIXTURE RATIO (OUTER RING)	(O/F)	4.048
SPECIFIC IMPULSE	(SEC)	423.9
C-STAR (NOZ STAG)	(FT/SEC)	7533.
C-SUB-F (NOZ STAG)		1.7027
C-SUB-F VACUUM (NOZ STAG)		1.8107
THEORETICAL C-STAR (NOZ STAG)	(FT/SEC)	7745.
THEORETICAL C-SUB-F (NOZ STAG)		1.8485
THEORETICAL SPECIFIC IMPULSE	(SEC)	445.0
C-STAR EFFICIENCY		0.9726
C-SUB-F EFFICIENCY		0.9794
ISP EFFICIENCY		0.9527
FUEL WEIGHT FLOWRATE (TOTAL)	(LB/SEC)	2.864
BLC WEIGHT FLOWRATE	(LB/SEC)	0.277
RELATIVE OXID F/M AGREEMENT	(%)	0.77
PERCENT BLC OF FUEL	(%)	9.686
OXID WEIGHT FLOWRATE	(LB/SEC)	14.153
TOTAL WEIGHT FLOWRATE	(LB/SEC)	17.017
THROAT AREA	(SQ IN)	17.96
EXIT AREA	(SQ IN)	459.85
LOX OUTER DELTA P	(PSID)	218.29
LOX CORE DELTA P	(PSID)	206.30
GH2 OUTER DELTA P	(PSID)	107.09
GH2 CORE DELTA P	(PSID)	55.26
GH2 BLC DELTA P	(PSID)	107.76

TEST NUMBER	869- 246	TEST DURATION	3.10
TEST DATE	9/ 8/72	SLICE DURATION	0.20
IBM DATE	09/12/72	SLICE START TIME	0.0
TEST CELL	CTL4-29B		

		SITE PERFORMANCE
LOCAL AMBIENT PRESSURE	(PSIA)	13.822
ENVIRONMENTAL PRESSURE	(PSIA)	13.834
THRUST (SITE)	(LB)	6363.5
THRUST (VACUUM)	(LB)	7365.1
CHAMBER PRESSURE 7,8 AVG	(PSIA)	254.25
MIXTURE RATIO (OVERALL)	(O/F)	5.562
MIXTURE RATIO (CORE)	(O/F)	8.004
MIXTURE RATIO (OUTER RING)	(O/F)	4.751
SPECIFIC IMPULSE	(SEC)	355.0
C-STAR (NOZ STAG)	(FT/SEC)	7481.
C-SUB-F (NOZ STAG)		1.3191
C-SUB-F VACUUM (NOZ STAG)		1.5266
THEORETICAL C-STAR (NOZ STAG)	(FT/SEC)	7602.
THEORETICAL C-SUB-F (NOZ STAG)		1.8737
THEORETICAL SPECIFIC IMPULSE	(SEC)	442.7
C-STAR EFFICIENCY		0.9841
C-SUB-F EFFICIENCY		0.8147
ISP EFFICIENCY		0.802
FUEL WEIGHT FLOWRATE (TOTAL)	(LB/SEC)	3.162
BLC WEIGHT FLOWRATE	(LB/SEC)	0.307
RELATIVE OXID F/M AGREEMENT	(%)	1.01
PERCENT BLC OF FUEL	(%)	9.704
OXID WEIGHT FLOWRATE	(LB/SEC)	17.585
TOTAL WEIGHT FLOWRATE	(LB/SEC)	20.747
THROAT AREA	(SQ IN)	17.92
EXIT AREA	(SQ IN)	459.85
LOX OUTER DELTA P	(PSID)	299.87
LOX CORE DELTA P	(PSID)	330.11
GH2 OUTER DELTA P	(PSID)	244.69
GH2 CORE DELTA P	(PSID)	174.34
GH2 BLC DELTA P	(PSID)	-51.43

TEST NUMBER	869- 247	TEST DURATION	3.10
TEST DATE	9/ 8/72	SLICE DURATION	0.20
IBM DATE	C9/12/72	SLICE START TIME	0.0
TEST CELL	CTL4-29B		

		SITE PERFORMANCE
LOCAL AMBIENT PRESSURE	(PSIA)	13.822
ENVIRONMENTAL PRESSURE	(PSIA)	13.834
THRUST (SITE)	(LB)	6728.2
THRUST (VACUUM)	(LB)	7718.9
CHAMBER PRESSURE 7,8 AVG	(PSIA)	268.78
MIXTURE RATIO (OVERALL)	(O/F)	4.422
MIXTURE RATIO (CORE)	(O/F)	6.600
MIXTURE RATIO (OUTER RING)	(O/F)	3.616
SPECIFIC IMPULSE	(SEC)	366.9
C-STAR (NOZ STAG)	(FT/SEC)	7803.
C-SUB-F (NOZ STAG)		1.3184
C-SUB-F VACUUM (NOZ STAG)		1.5125
THEORETICAL C-STAR (NOZ STAG)	(FT/SEC)	7862.
THEORETICAL C-SUB-F (NOZ STAG)		1.8267
THEORETICAL SPECIFIC IMPULSE	(SEC)	446.3
C-STAR EFFICIENCY		0.9926
C-SUB-F EFFICIENCY		0.8281
ISP EFFICIENCY		0.822
FUEL WEIGHT FLOWRATE (TOTAL)	(LB/SEC)	3.881
BLC WEIGHT FLOWRATE	(LB/SEC)	0.377
RELATIVE OXID F/M AGREEMENT	(%)	0.93
PERCENT BLC OF FUEL	(%)	9.723
OXID WEIGHT FLOWRATE	(LB/SEC)	17.161
TOTAL WEIGHT FLOWRATE	(LB/SEC)	21.042
THROAT AREA	(SQ IN)	17.94
EXIT AREA	(SQ IN)	459.85
LOX OUTER DELTA P	(PSID)	285.58
LOX CORE DELTA P	(PSID)	335.90
GH2 OUTER DELTA P	(PSID)	304.45
GH2 CORE DELTA P	(PSID)	211.18
GH2 BLC DELTA P	(PSID)	-59.69

TEST NUMBER	869- 248	TEST DURATION	3.10
TEST DATE	9/ 8/72	SLICE DURATION	0.20
IBM DATE	C9/12/72	SLICE START TIME	0.0
TEST CELL	CTL4-298		

		SITE PERFORMANCE
LOCAL AMBIENT PRESSURE	(PSIA)	13.822
ENVIRONMENTAL PRESSURE	(PSIA)	13.834
THRUST (SITE)	(LB)	6242.7
THRUST (VACUUM)	(LB)	7224.6
CHAMBER PRESSURE 7,8 AVG	(PSIA)	250.45
MIXTURE RATIO (OVERALL)	(O/F)	6.732
MIXTURE RATIO (CORE)	(O/F)	7.956
MIXTURE RATIO (OUTER RING)	(O/F)	7.135
SPECIFIC IMPULSE	(SEC)	345.7
C-STAR (NOZ STAG)	(FT/SEC)	7326.
C-SUB-F (NOZ STAG)		1.3119
C-SUB-F VACUUM (NOZ STAG)		1.5185
THEORETICAL C-STAR (NOZ STAG)	(FT/SEC)	7281.
THEORETICAL C-SUB-F (NOZ STAG)		1.9195
THEORETICAL SPECIFIC IMPULSE	(SEC)	434.4
C-STAR EFFICIENCY		1.0061
C-SUB-F EFFICIENCY		1.3799
ISP EFFICIENCY		0.796
FUEL WEIGHT FLOWRATE (TOTAL)	(LB/SEC)	2.703
BLC WEIGHT FLOWRATE	(LB/SEC)	0.319
RELATIVE OXID F/M AGREEMENT	(%)	1.00
PERCENT BLC OF FUEL	(%)	11.806
OXID WEIGHT FLOWRATE	(LB/SEC)	18.196
TOTAL WEIGHT FLOWRATE	(LB/SEC)	20.899
THROAT AREA	(SQ IN)	17.95
EXIT AREA	(SQ IN)	459.85
LOX OUTER DELTA P	(PSID)	300.11
LOX CORE DELTA P	(PSID)	330.28
GH2 OUTER DELTA P	(PSID)	190.89
GH2 CORE DELTA P	(PSID)	183.29
GH2 BLC DELTA P	(PSID)	-20.24

TEST NUMBER	869- 249	TEST DURATION	3.10
TEST DATE	9/ 8/72	SLICE DURATION	0.20
IBM DATE	C9/12/72	SLICE START TIME	0.0
TEST CELL	CTL4-29B		

		SITE PERFORMANCE
LOCAL AMBIENT PRESSURE	(PSIA)	13.822
ENVIRONMENTAL PRESSURE	(PSIA)	13.834
THRUST (SITE)	(LB)	6630.1
THRUST (VACUUM)	(LB)	7628.6
CHAMBER PRESSURE 7,8 AVG	(PSIA)	264.06
MIXTURE RATIO (OVERALL)	(O/F)	4.916
MIXTURE RATIO (CORE)	(O/F)	7.283
MIXTURE RATIO (OUTER RING)	(O/F)	4.053
SPECIFIC IMPULSE	(SEC)	360.9
C-STAR (NOZ STAG)	(FT/SEC)	7650.
C-SUB-F (NOZ STAG)		1.3193
C-SUB-F VACUUM (NOZ STAG)		1.5177
THEORETICAL C-STAR (NOZ STAG)	(FT/SEC)	7762.
THEORETICAL C-SUB-F (NOZ STAG)		1.8467
THEORETICAL SPECIFIC IMPULSE	(SEC)	445.5
C-STAR EFFICIENCY		0.9855
C-SUB-F EFFICIENCY		0.8218
ISP EFFICIENCY		0.810
FUEL WEIGHT FLOWRATE (TOTAL)	(LB/SEC)	3.573
BLC WEIGHT FLOWRATE	(LB/SEC)	0.348
RELATIVE OXID F/M AGREEMENT	(%)	0.99
PERCENT BLC OF FUEL	(%)	9.726
OXID WEIGHT FLOWRATE	(LB/SEC)	17.565
TOTAL WEIGHT FLOWRATE	(LB/SEC)	21.138
THROAT AREA	(SQ IN)	17.98
EXIT AREA	(SQ IN)	459.85
LOX OUTER DELTA P	(PSID)	164.20
LOX CORE DELTA P	(PSID)	221.35
GH2 OUTER DELTA P	(PSID)	145.57
GH2 CORE DELTA P	(PSID)	70.31
GH2 BLC DELTA P	(PSID)	137.39

TEST NUMBER	86P- 250	TEST DURATION	3.10
TEST DATE	9/ 8/72	SLICE DURATION	0.20
IBM DATE	09/28/72	SLICE START TIME	0.0
TEST CELL	CTL4-295		

		SITE PERFORMANCE
LOCAL AMBIENT PRESSURE	(PSIA)	13.622
ENVIRONMENTAL PRESSURE	(PSIA)	13.834
THRUST (SITE)	(LB)	6958.5
THRUST (VACUUM)	(LB)	7952.4
CHAMBER PRESSURE 7,8 AVG	(PSIA)	274.05
MIXTURE RATIO (OVERALL)	(O/F)	5.414
MIXTURE RATIO (CORE)	(O/F)	6.388
MIXTURE RATIO (OUTER RING)	(O/F)	5.754
SPECIFIC IMPULSE	(SEC)	366.0
C-STAR (NOZ STAG)	(FT/SEC)	7707.
C-SUB-F (NOZ STAG)		1.3368
C-SUB-F VACUUM (NOZ STAG)		1.5277
THEORETICAL C-STAR (NOZ STAG)	(FT/SEC)	7645.
THEORETICAL C-SUB-F (NOZ STAG)		1.3187
THEORETICAL SPECIFIC IMPULSE	(SEC)	384.6
C-STAR EFFICIENCY		1.0082
C-SUB-F EFFICIENCY		0.9438
ISP EFFICIENCY		0.9515
FUEL WEIGHT FLOWRATE (TOTAL)	(LB/SEC)	3.388
BLC WEIGHT FLOWRATE	(LB/SEC)	0.400
RELATIVE OXID F/M AGREEMENT	(%)	0.97
PERCENT BLC OF FUEL	(%)	11.818
OXID WEIGHT FLOWRATE	(LB/SEC)	18.342
TOTAL WEIGHT FLOWRATE	(LB/SEC)	21.730
THROAT AREA	(SQ IN)	17.94
EXIT AREA	(SQ IN)	71.84
LOX OUTER DELTA P	(PSID)	309.57
LOX CORE DELTA P	(PSID)	340.66
GH2 OUTER DELTA P	(PSID)	228.58
GH2 CORE DELTA P	(PSID)	228.76
GH2 BLC DELTA P	(PSID)	-36.29

TEST NUMBER	869- 251	TEST DURATION	3.10
TEST DATE	9/ 8/72	SLICE DURATION	0.20
IBM DATE	C9/12/72	SLICE START TIME	0.0
TEST CELL	CTL4-298		

		SITE PERFORMANCE
LOCAL AMBIENT PRESSURE	(PSIA)	13.822
ENVIRONMENTAL PRESSURE	(PSIA)	13.834
THRUST (SITE)	(LB)	6816.4
THRUST (VACUUM)	(LB)	7815.7
CHAMBER PRESSURE 7,8 AVG	(PSIA)	269.26
MIXTURE RATIO (OVERALL)	(O/F)	6.238
MIXTURE RATIO (CORE)	(O/F)	6.490
MIXTURE RATIO (OUTER RING)	(O/F)	5.837
SPECIFIC IMPULSE	(SEC)	360.8
C-STAR (NOZ STAG)	(FT/SEC)	7601.
C-SUB-F (NOZ STAG)		1.3322
C-SUB-F VACUUM (NOZ STAG)		1.5274
THEORETICAL C-STAR (NOZ STAG)	(FT/SEC)	7424.
THEORETICAL C-SUB-F (NOZ STAG)		1.9001
THEORETICAL SPECIFIC IMPULSE	(SEC)	438.4
C-STAR EFFICIENCY		1.0238
C-SUB-F EFFICIENCY		0.8038
ISP EFFICIENCY		0.823
FUEL WEIGHT FLOWRATE (TOTAL)	(LB/SEC)	2.993
BLC WEIGHT FLOWRATE	(LB/SEC)	0.0
RELATIVE OXID F/M AGREEMENT	(%)	1.04
PERCENT BLC OF FUEL	(%)	0.0
OXID WEIGHT FLOWRATE	(LB/SEC)	18.666
TOTAL WEIGHT FLOWRATE	(LB/SEC)	21.659
THROAT AREA	(SQ IN)	17.95
EXIT AREA	(SQ IN)	459.85
LOX OUTER DELTA P	(PSID)	333.91
LOX CORE DELTA P	(PSID)	364.34
GH2 OUTER DELTA P	(PSID)	227.17
GH2 CORE DELTA P	(PSID)	227.91
GH2 BLC DELTA P	(PSID)	-0.90

TEST NUMBER	869- 238
TEST DATE	8/18/72
IBM DATE	08/31/72
TEST CELL	CTL4-29B

TEST DURATION	2.40
SLICE DURATION	0.20
SLICE START TIME	0.0

		SITE PERFORMANCE
LOCAL AMBIENT PRESSURE	(PSIA)	13.788
ENVIRONMENTAL PRESSURE	(PSIA)	1.094
THRUST (SITE)	(LB)	6550.8
THRUST (VACUUM)	(LB)	7053.6
CHAMBER PRESSURE 7,8 AVG	(PSIA)	216.97
MIXTURE RATIO (OVERALL)	(O/F)	4.779
MIXTURE RATIO (CORE)	(O/F)	7.017
MIXTURE RATIO (OUTER RING)	(O/F)	3.935
SPECIFIC IMPULSE	(SEC)	407.4
C-STAR (NOZ STAG)	(FT/SEC)	7649.
C-SUB-F (NOZ STAG)		1.5917
C-SUB-F VACUUM (NOZ STAG)		1.7138
THEORETICAL C-STAR (NOZ STAG)	(FT/SEC)	7783.
THEORETICAL C-SUB-F (NOZ STAG)		1.8419
THEORETICAL SPECIFIC IMPULSE	(SEC)	445.6
C-STAR EFFICIENCY		0.9826
C-SUB-F EFFICIENCY		0.9305
ISP EFFICIENCY		0.9144
FUEL WEIGHT FLOWRATE (TOTAL)	(LB/SEC)	2.996
BLC WEIGHT FLOWRATE	(LB/SEC)	0.291
RELATIVE OXID F/M AGREEMENT	(%)	1.48
PERCENT BLC OF FUEL	(%)	9.703
OXID WEIGHT FLOWRATE	(LB/SEC)	14.317
TOTAL WEIGHT FLOWRATE	(LB/SEC)	17.313
THROAT AREA	(SQ IN)	17.92
EXIT AREA	(SQ IN)	459.85
LOX OUTER DELTA P	(PSID)	91.64
LOX CORE DELTA P	(PSID)	136.42
GH2 OUTER DELTA P	(PSID)	109.53
GH2 CORE DELTA P	(PSID)	59.98
GH2 BLC DELTA P	(PSID)	107.79

TEST NUMBER 369- 252
TEST DATE 9/ 8/72
IBM DATE 09/25/72
TEST CELL CTL4-29B

TEST DURATION 5.10
SLICE DURATION 0.20
SLICE START TIME 0.0

		SITE PERFORMANCE
LOCAL AMBIENT PRESSURE	(PSIA)	13.622
ENVIRONMENTAL PRESSURE	(PSIA)	13.634
THRUST (SITE)	(LB)	6648.9
THRUST (VACUUM)	(LB)	7642.7
CHAMBER PRESSURE 7,8 AVG	(PSIA)	264.79
MIXTURE RATIO (OVERALL)	(O/F)	4.934
MIXTURE RATIO (CORE)	(O/F)	6.822
MIXTURE RATIO (OUTER RING)	(O/F)	1.533
SPECIFIC IMPULSE	(SEC)	359.6
C-STAR (NOZ STAG)	(FT/SEC)	7622.
C-SUB-F (NOZ STAG)		1.3206
C-SUB-F VACUUM (NOZ STAG)		1.5181
THEORETICAL C-STAR (NOZ STAG)	(FT/SEC)	7758.
THEORETICAL C-SUB-F (NOZ STAG)		1.6121
THEORETICAL SPECIFIC IMPULSE	(SEC)	388.7
C-STAR EFFICIENCY		0.9823
C-SUB-F EFFICIENCY		0.9417
ISP EFFICIENCY		0.9251
FUEL WEIGHT FLOWRATE (TOTAL)	(LB/SEC)	3.582
ELC WEIGHT FLOWRATE	(LB/SEC)	0.0
RELATIVE OXID F/M AGREEMENT	(%)	20.17
PERCENT ELC OF FUEL	(%)	0.0
OXID WEIGHT FLOWRATE	(LB/SEC)	17.670
TOTAL WEIGHT FLOWRATE	(LB/SEC)	21.252
THROAT AREA	(SQ IN)	17.96
EXIT AREA	(SQ IN)	71.84
LOX OUTER DELTA P	(PSID)	189.16
LOX CORE DELTA P	(PSID)	247.03
GH2 OUTER DELTA P	(PSID)	218.39
GH2 CORE DELTA P	(PSID)	93.37
GH2 ELC DELTA P	(PSID)	3.24

TEST NUMBER	869- 253	TEST DURATION	3.10
TEST DATE	9/ 8/72	SLICE DURATION	0.20
IBM DATE	C9/12/72	SLICE START TIME	0.0
TEST CELL	CTL4-29B		

		SITE PERFORMANCE
LOCAL AMBIENT PRESSURE	(PSIA)	13.822
ENVIRONMENTAL PRESSURE	(PSIA)	13.834
THRUST (SITE)	(LB)	6499.7
THRUST (VACUUM)	(LB)	7496.7
CHAMBER PRESSURE 7,8 AVG	(PSIA)	258.52
MIXTURE RATIO (OVERALL)	(O/F)	5.140
MIXTURE RATIO (CORE)	(O/F)	7.465
MIXTURE RATIO (OUTER RING)	(O/F)	4.365
SPECIFIC IMPULSE	(SEC)	361.2
C-STAR (NOZ STAG)	(FT/SEC)	7618.
C-SUB-F (NOZ STAG)		1.3224
C-SUB-F VACUUM (NOZ STAG)		1.5251
THEORETICAL C-STAR (NOZ STAG)	(FT/SEC)	7709.
THEORETICAL C-SUB-F (NOZ STAG)		1.8561
THEORETICAL SPECIFIC IMPULSE	(SEC)	444.7
C-STAR EFFICIENCY		0.9882
C-SUB-F EFFICIENCY		0.8217
ISP EFFICIENCY		0.812
FUEL WEIGHT FLOWRATE (TOTAL)	(LB/SEC)	3.381
BLC WEIGHT FLOWRATE	(LB/SEC)	0.328
RELATIVE OXID F/M AGREEMENT	(%)	0.77
PERCENT BLC OF FUEL	(%)	9.712
OXID WEIGHT FLOWRATE	(LB/SEC)	17.377
TOTAL WEIGHT FLOWRATE	(LB/SEC)	20.758
THROAT AREA	(SQ IN)	17.96
EXIT AREA	(SQ IN)	459.85
LOX OUTER DELTA P	(PSID)	180.10
LOX CORE DELTA P	(PSID)	271.65
GH2 OUTER DELTA P	(PSID)	132.24
GH2 CORE DELTA P	(PSID)	67.92
GH2 BLC DELTA P	(PSID)	132.19

APPENDIX B

DETERMINATION OF CHAMBER WALL HEAT FLUX BY TRANSIENT TEMPERATURE RESPONSE

Values of heat flux to the combustion chamber and nozzle walls were calculated from the response of the thermocouples attached to the back surfaces of thermal isolation plugs similar to that shown in Fig. B-1. The technique involved the numerical solution of the transient conduction relation

$$\nabla(-k\nabla T) = \rho C_p \frac{\partial T}{\partial \tau} \qquad \text{(B-1)}$$

by the HEATING (Heat Engineering and Transfer in Nine Geometries) computer program (Ref. B-1). The definition of wall heat transfer was made under the assumption that both convective heat transfer coefficient and adiabatic wall temperature established themselves in a short time relative to the overall engine firing duration of 2 to 2.5 seconds.

To reduce the overall human labor and computer time required to reduce the multiple local heat flux measurements in the 27 engine firings analyzed, a trial calculation was first made on a two-dimensional basis to determine whether the calculation could be further simplified. This trial calculation was made using an axisymmetric cylindrical (r-z) coordinate system referenced to the thermal plug centerline for a 2-second heating period. The boundary conditions used were:

$$T_{aw} = 5700 \text{ R (mixture ratio of 4.5)}$$

$$h_g = 0.0010,\ 0.0020,\ 0.0030,\ \text{Btu/in.}^2\text{sec R}$$

These were selected as pertinent for the propellant combination and chamber pressures of the program. The calculated temperature distribution in the plug and adjacent copper wall at the end of the 2-second period are shown in Fig. B-2. The calculation was then repeated on a one-dimensional basis by

eliminating all but the thermal plug itself from the problem geometry. The back surface temperatures of the thermal plug measured by the two methods are compared in Fig. B-3. Although Fig. B-2 indicates that a substantial temperature difference exists between the isolation plug and surrounding chamber wall, the data in Fig. B-3 show that this gradient does not significantly change the plug back wall temperature from the value defined by completely one-dimensional conduction over a 2-second period. The equivalence of the one and two-dimensional, numerical solutions in the trial calculation allowed Eq. B-1 to be reduced to

$$\frac{\partial}{\partial z}\left(-k\frac{\partial T}{\partial z}\right) = -\rho C_p \frac{\partial T}{\partial z} \qquad \text{(B-2)}$$

Generalized solutions to Eq. B-2 are usually prepared as graphs of the unaccomplished temperature difference Ψ defined as

$$\Psi = \frac{T_{aw} - T_{(z,\tau)}}{T_{aw} - T_{(\tau=o)}}$$

at various values of τ and for a range of values of the non-dimensional Biot and Fourier parameters

$$Bi = ht/k$$

$$Fo = \frac{\alpha\tau}{t^2}$$

For the particular situation of a measured plug back transient temperature, $T(t,\tau)$, and for a particular geometry and material (copper), it was more convenient to prepare a graphical correlation of Ψ_t defined by

$$\Psi_t = \frac{T_{aw} - T_{(t,\tau)}}{T_{aw} - T_{(\tau=o)}}$$

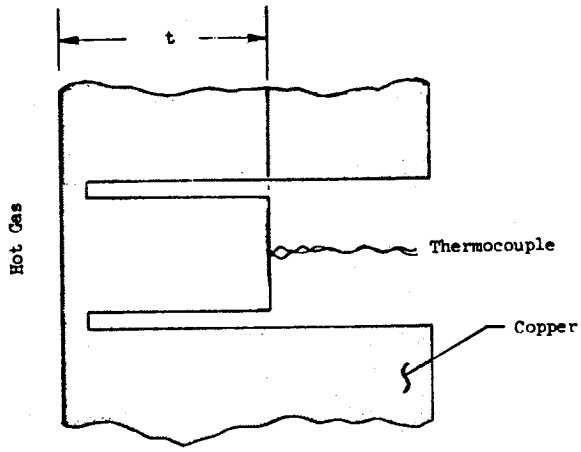

Figure B-1. Heat Transfer Plug

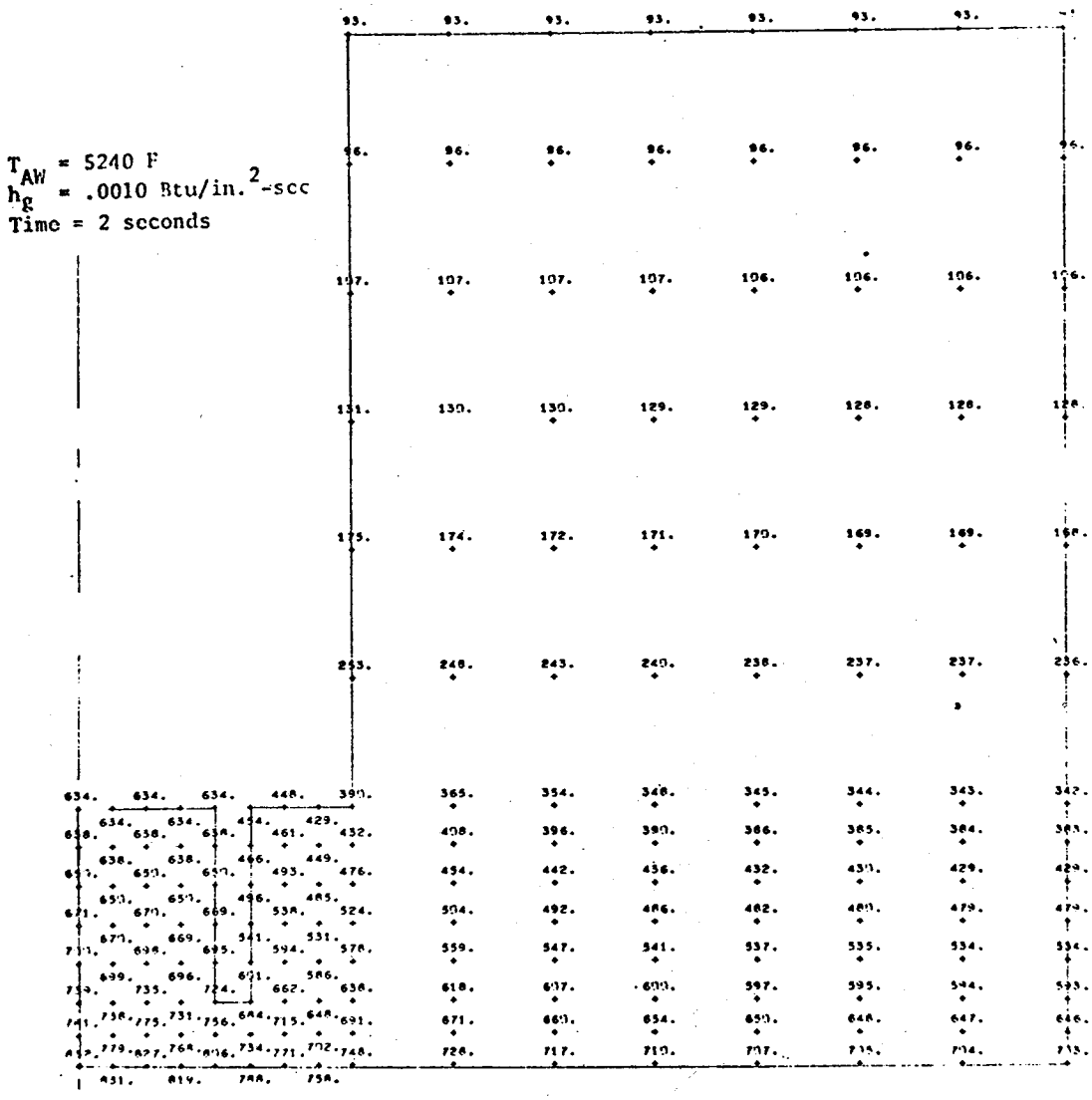

Figure B-2. Thermal Plug Temperature Distribution

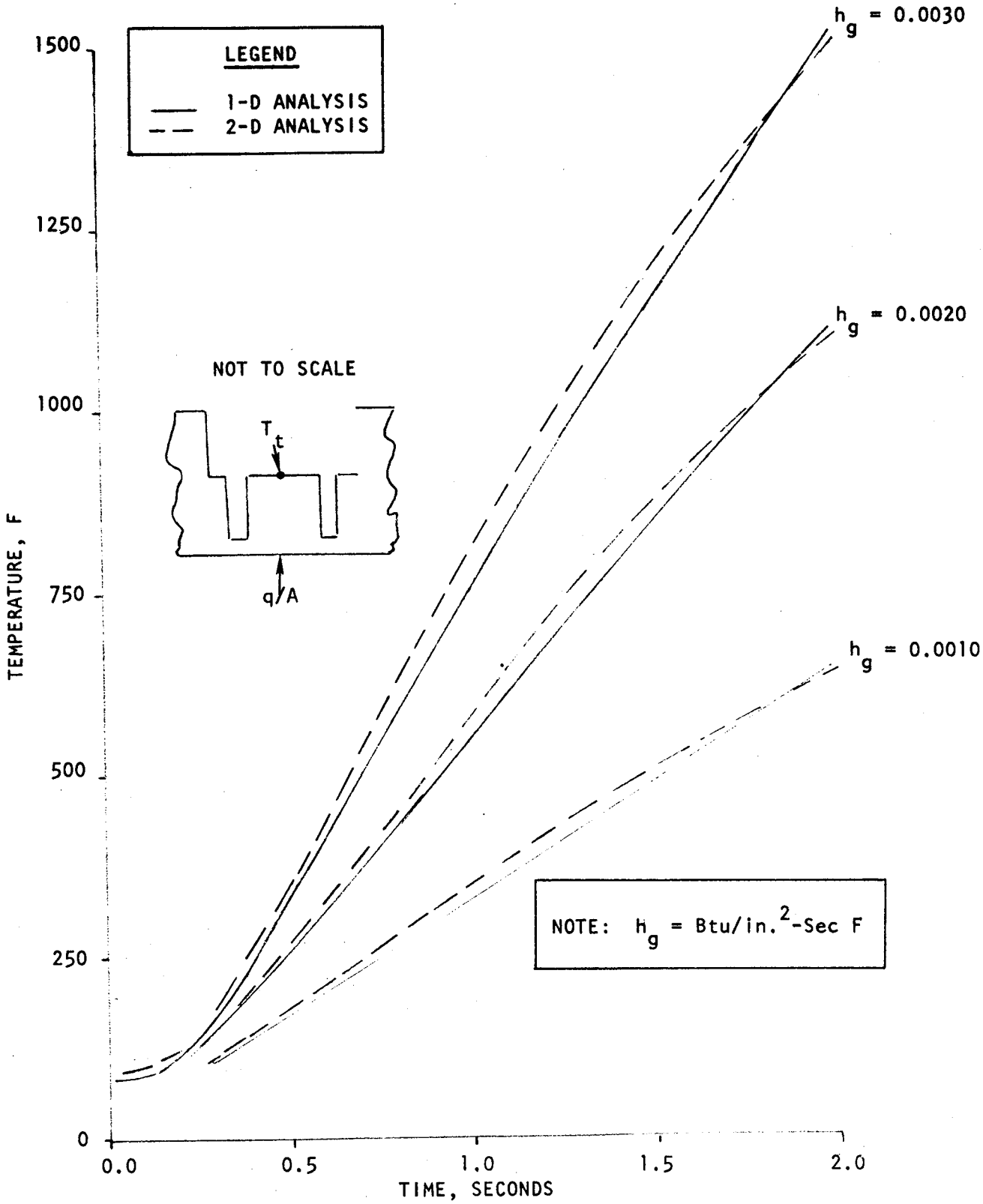

Figure B-3. Theoretical Temperature Response of Thermal Isolation Plug

versus time for a range of values of heat transfer coefficient as shown in Fig. B-4. The calculation was made by successive applications of the HEATING program and a similar Rocketdyne program, DEAP (Differential Equation Analyzer Program). DEAP permitted the instantaneous value of heat transfer coefficient to be related to the steady-state value in accordance with the relation

$$\frac{h(\tau)}{h_{\text{steady state}}} = \left[\frac{P_c\ (\tau)}{P_{c\ \text{steady state}}}\right]^{0.8} = f(P_c)$$

The chamber pressure correction $f(P_c)$ was defined by fitting a series of P_c curves similar to that shown in Fig. 37; its use provides a more rigorous boundary condition on the hot gas side than the usual step function value of heat transfer coefficient usually employed in transient conduction problems.

The initial values of the measured back-wall temperatures of the plugs were in the range 800-1200 F. Both are well below the H_2/O_2 combustion gas flame temperature which ranged from 4200 F to 5900 F for the mixture ratios of the engine firings; consequently the ratio Ψ changed a maximum of 30 percent during a firing. Similarly, the measured back-wall temperatures usually exhibited the linear variation with time shown in Fig. 39, a relationship which is indicative of a moderate percentage change in Ψ. Such a moderate change is fortuitous for heat transfer calculations. It permitted a reasonable value of T_{aw} to be chosen arbitrarily and the resultant value of $\Psi(t,\tau)$, obtained by combining the defined T_{aw} with the measured $T(t,\tau)$ and $T(\tau=o)$, could then be used to define an experimental heat transfer coefficient, h_g, from the graphical correlation shown in Fig. B-4. The value of h_g defined by this procedure is particular to the choice of both T_{aw} and τ. However, when the same value of h_g is obtained at two values of τ for a given value of T_{aw}, then this combination of T_{aw} and h_g can be used to calculate wall heat flux according to

$$q/A = h_g\ (T_{aw} - T_w) \qquad \text{(B-3)}$$

over essentially the entire range $T(t=o)<T_w<T(t,\tau_{max})$. The resultant heat flux is relatively insensitive to the exact value of T_{aw} chosen.

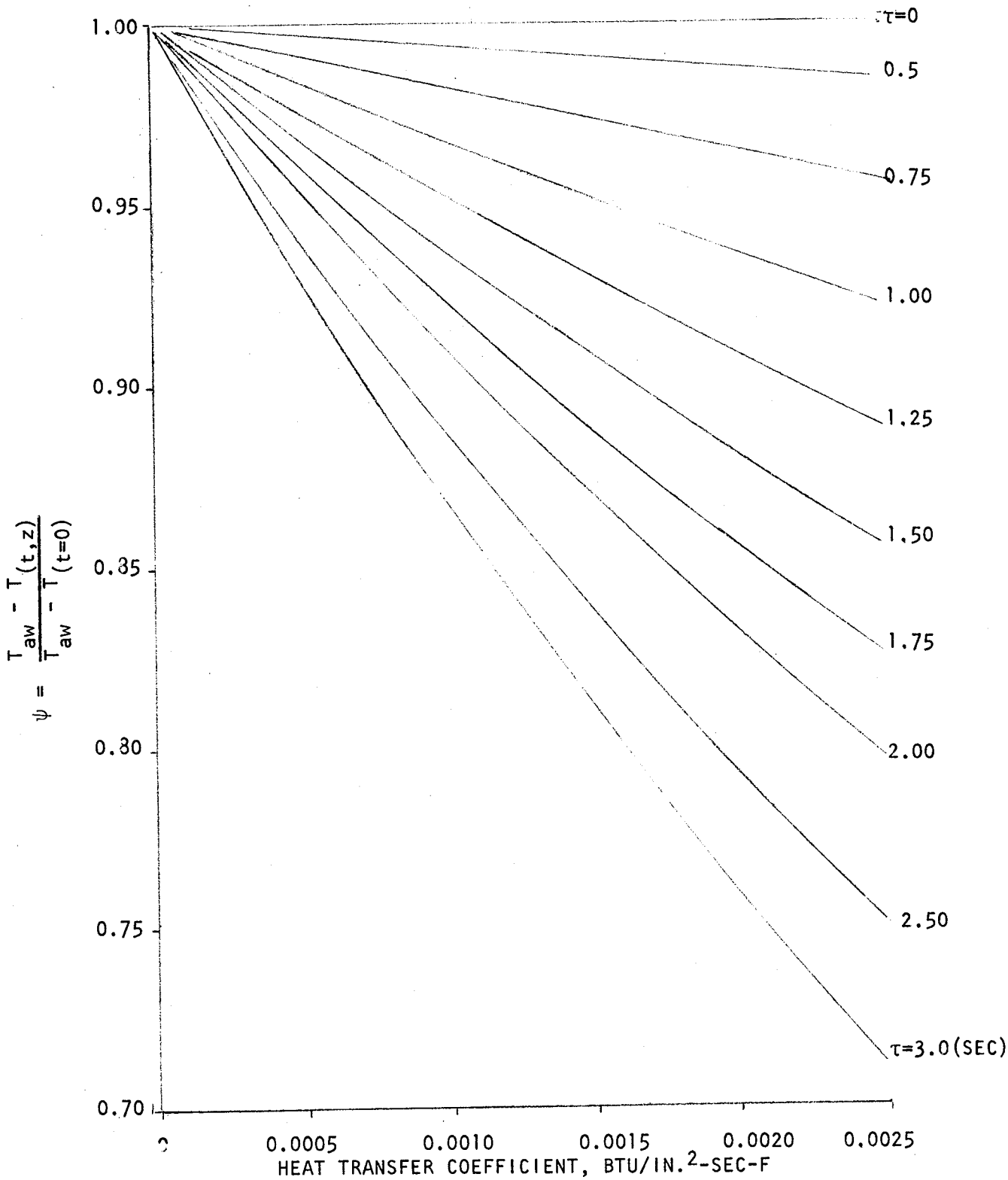

Figure B-4. Variation of Unaccomplished Temperature Ratio With Time and Film Coefficient for Heat Transfer Plugs

The experimental wall heat fluxes presented in Table 16 were calculated by (1) defining a value of T_{aw} in terms of the combustion gas flame temperature, (2) using this value of T_{aw} together with the back-wall temperature history to define a correlation of Ψ_t with time, (3) matching this correlation with the curves of Fig. B-4 to obtain the value of h_g adjoint to the assumed T_{aw}, and (4) calculating a wall heat flux from Eq. B-3 for a value of T_w defined as 800 F.

REFERENCE

B-1. The Heating Program, Report 417-5.0, Astra, Inc., Raleigh, North Carolina, 1 January 1961.

NOMENCLATURE

Bi	=	Biot number, h t/k
C_p	=	Specific heat
$F\sigma$	=	Fourier number, $\alpha\ \tau/t^2$
h	=	Heat transfer coefficient
k	=	Thermal conductivity
P_c	=	Chamber pressure
q/A	=	Heat flux
T	=	Temperature
t	=	Thickness
z	=	Coordinate along plug centerline
ρ	=	Density
ψ	=	Unaccomplished temperature difference
τ	=	Time

Subscripts

aw	=	Adiabatic wall
g	=	Gas
w	=	Wall
max	=	Maximum
steady state	=	Steady state conditions
t	=	At back wall
τ	=	At time τ

APPENDIX C

DEFINITION OF WALL MIXTURE RATIO

The model employed to correlate the wall mixture ratio in the stratified flow engine firings is shown in the sketch below.

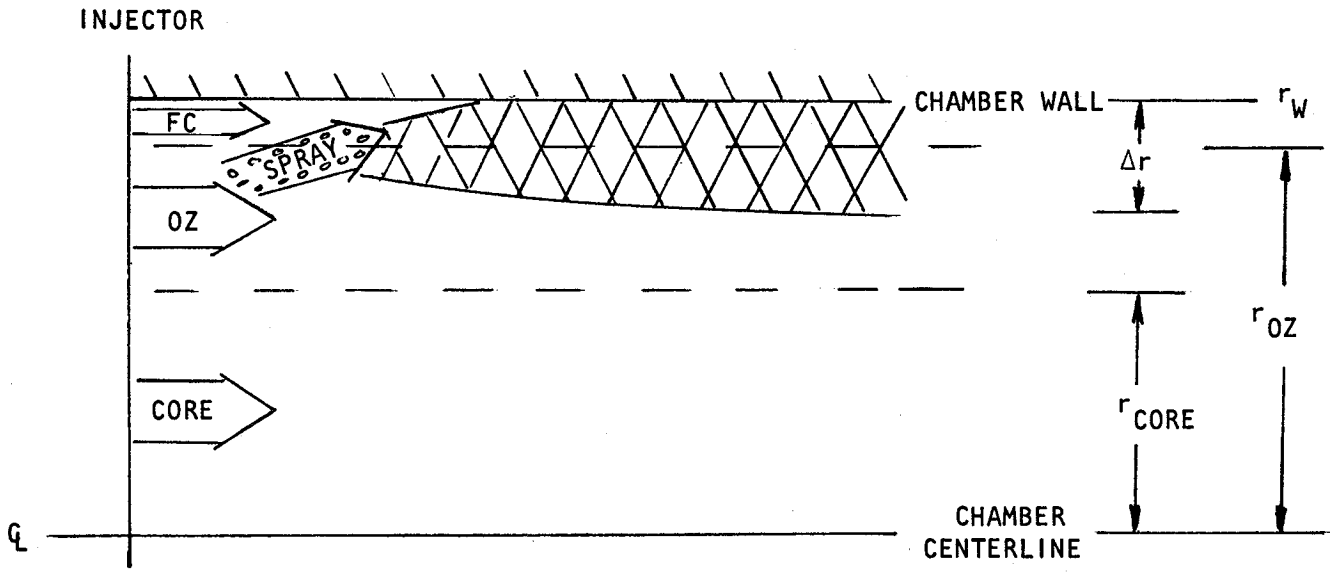

If no mixing occurred, the three injected streams designated CORE, OZ (outer zone), and FC (film coolant) would flow as shown by the three parallel layers separated by the broken lines, with a uniform mass flux and mixture ratio in each layer. However, because of the transverse velocity components associated with an impinging stream injector of the type used in the stratified flow engine, and also because of gas turbulence, mixing between streams will occur. The resultant mixed zone is shown by the cross-hatched region Δr of the sketch. This mixed zone will grow most rapidly near the injector where spray penetration is the primary mechanism; it will then expand much more slowly in the downstream region where all the spray has evaporated. For simplicity in model formulation, it is therefore possible to assign a constant thickness Δr, with the restriction that resultant heat transfer correlations will apply only to the region where spray evaporation is relatively complete and the flow assumes stream tube characteristics. Additionally, it is assumed that the mixed zone includes the entire

film coolant layer, a simplification that applies when moderate percentages of the fuel are used as a gaseous film coolant.

From the sketch, the portion of the outer zone flow, $\dot{w}_{ML}$, that is swallowed by the mixing layer is related to the total injected outer zone flow by

$$\frac{\dot{w}_{ML}}{\dot{w}_{OZ}} = \frac{2\pi \bar{r}_{ML}\, \Delta r\, \rho_{ML}\, U_{ML}}{\pi(r_{OZ}^2 - r_{CORE}^2)\rho_{OZ}\, U_{OZ}} \tag{C-1}$$

Because a separately injected film coolant serves no useful purpose unless the mixed layer thickness Δr is much less than the thickness of the outer zone, Eq. C-1 can be approximated by

$$\frac{\dot{w}_{ML}}{\dot{w}_{OZ}} \cong \frac{2\Delta r}{r_{OZ}\left(1 - \frac{r_{CORE}^2}{r_{OZ}^2}\right)} \simeq \frac{2\Delta r}{r_w\left(1 - \frac{r_{CORE}^2}{r_w^2}\right)} \tag{C-2}$$

When (as in the stratified flow engine) the outer zone is defined to consist of the outer ring of injector elements, the ratio $\dot{w}_{ML}/\dot{w}_{OZ}$ can be expected to approach a constant, i.e.,

$$\frac{\dot{w}_{ML}}{\dot{w}_{OZ}} \triangleq K \simeq \frac{2\Delta r}{r_w\left(1 - \frac{r_{CORE}^2}{r_w^2}\right)} \tag{C-3}$$

Finally, when (as in the case of the stratified flow system) the flow in the outer zone is equal to the flow in the core for a uniform mixture ratio, and the injection density is uniform across the injector face,

$$1 - \frac{r_{CORE}^2}{r_w^2} \simeq 1/2$$

so that

$$\frac{\dot{w}_{ML}}{\dot{w}_{OZ}} \triangleq K \simeq \frac{4\Delta r}{r_w} \tag{C-4}$$

The mixture ratio in the mixed layer is given by

$$MR_{ML} = \frac{\dot{w}_{ML}\left(\frac{MR_{OZ}}{MR_{OZ}+1}\right)}{\dot{w}_{FC} + \dot{w}_{ML}\left(\frac{1}{MR_{OZ}+1}\right)}$$

Dividing by $\dot{w}_{OZ}$ gives the wall mixture ratio in terms of the mixing coefficient

$$MR_{ML} = MR_w = \frac{K\left(\frac{MR_{OZ}}{MR_{OZ}+1}\right)}{\frac{\dot{w}_{FC}}{\dot{w}_{OZ}} + K\left(\frac{1}{MR_{OZ}+1}\right)} \tag{C-5}$$

If experimental heat transfer data are employed to define the effective wall mixture ratio for a given film coolant flow, then Eq. C-5 permits a calculation of the mixing coefficient.